国立真珠研究所報告

7

昭和36年(1961)7月

Bulletin of the National Pearl Research Laboratory

7

July 1961

CONTENTS

National Pearl Research Laboratory
Kashikojima, Ago-cho, Shima-gun,
Mie Prefecture, Japan

Crystal Growth of Molluscan Shells*, [1]

Kōji Wada

National Pearl Research Laboratory, Kashikojima, Mie Prefecture, Japan

Preface

From ancient times, the shell structure of molluscs has been studied by many workers from each viewpoints such as the evolution of species, the mechanism of calcification etc., which were very interesting problems to biologists, to geologists, to dentists, and to biochemists. In 1923, excellent work on the structure of shells has been done by Schmidt. Tsutsumi (1928) has first investigated the crystalline structure of the shell of a marine molluscan species, *Atrina japonica*, by taking the Laue photographs.

Shells of marine and fresh-water mussels are complex system, more than 80% of which consists of inorganic salts, mainly calcium carbonate, and less than 20% organic materials, commonly termed "conchiolin". Calcium carbonate crystals forming molluscan shells are divided into three following polymorphs; calcite, aragonite, varterite. At present, the organic material is thought to be a kind of the albuminoid, and to be closely related to calcification. The roles of alkaline phosphatase, carbonic anhydrase, sulphatase, and mucopolysaccharide in shell formation have also been reported in the last few years (Freeman *et al.* 1948, Kado 1953, 1954).

Recently, the problem of shell formation has been pursued by the techniques of the radioisotope, and the separation of organic and inorganic substances from the solution transported to the inner shell surface through the mantle tissue has been under discussion (Bevelander 1952, Jodrey 1953, Tanaka 1956). Crystal growth of shells has been investigated under the electron microscope, and a great deal of attention has been paid to the role of the shell-forming tissue and the organic matrix in the mineralization of shells (Wada 1958, 1960, Watabe 1959).

As above mentioned, each worker has studied only in his part, and as yet, the most of the studies on the crystal growth of shells was discussed only from crystallographic viewpoint. Therefore, strictly speaking, we are not given sufficient fundamental knowledge of the crystal growth of shells. The author has paid special attention to the growth and the dissolution phenomena of shell salts under the variable physiological conditions and the changes of environments throughout its development. Since the crystal growth of shells occurs only on the basis of

* Kōji Wada. Crystal growth of molluscan shells. Bull. Natl. Pearl Res. Lab. 7: 703 — 828. 1961.

[1] Contribution from the National Pearl Research Laboratory, Japan No. 87.

complex biological and biochemical factors, it is uneasy to control experimentally the conditions of the mother fluid surrounding growing crystals. However, the above mentioned attempts of the author must be carried out for resolving the problem of the shell formation even if some erroneous results are drawn out from the initial experiments.

This manuscript is composed of six chapters as follows:

Chapter I On the Characteristics of the Ground of Crystal Growth
Chapter II Mineral Constituents and Structure of Shell
Chapter III The Organic Matrix of Shell
Chapter IV Electron Diffraction and Electron Microscopic Investigations of the Calcification of Shell
Chapter V Crystal Growth of Shell
Chapter VI The Mechanism of Formation of the Spiral Growth Steps

These chapters will be divided into two sections. The first is concerned with the liquid and the solid phases around growing crystals; the grounds of crystal growth (chapters I~III), and the second is crystal growth itself of shells (chapters IV~VI).

Acknowledgements

The author expresses his sincere thanks to Mr. Katsuo Takayama, Director of National Pearl Research Laboratory, and Dr. Toshio Sudo, Professor of the Institute of Geology and Mineralogy, Tokyo University of Education for the kind directions and useful suggestions they gave throughout the whole work. Drs. Toshio Sudo, Hidekata Shibata, Masao Nakazima, and Kenichi Hirano carefully read this manuscript and give their helpful criticisms in each speciality. Thanks are also extended to Drs. Shoji Ijiri, Eiji Suito, Norimitsu Watabe, Jirō Senō, Masae Ōmori, and Hiroshi Nakahara for their useful discussions, and students in the Institute of Geology and Mineralogy, Tokyo University of Educations for their helps in X-ray and chemical analysis.

For accomplished this work, the author is in debt to Mrs. Shigeru Ōta, Tomio Ishihara, and Kyouji Okutani for several experimental materials.

CONTENTS

Chapter I

On The Characteristics of the Ground of Crystal Growth

1 Introduction

For the studies of shell growth, it had very early been attempted to represent the change in the weight or size of shells with the age as the growth of molluscan shells could be expressed quantitatively. And it has been evidently established that the growth in the weight or size of shells follows a S-shaped curve as the growth of an animal and plant usually exhibits. The general growth of shells in the weight or size throughout a year may also show a change in that fashion. The seasonal changes of shell growth appear to be caused by a great variety of biological systems, but the growth data examined in connection with these various biological conditions are almost absent. Until recent year, the studies on shell formation had shown a tendency to be carried out independently in the respective fields of workers by biologists and biochemists.

Histological and histochemical works on the shell-forming tissue, "mantle", have been done in regard to Ca metabolism in molluscs. The epithelium on the different areas of the mantle secretes characteristic layer of shells and is different in histological features from each other (Ojima 1952, Owen, Trueman and Yonge 1953, and Beedham 1958). But the shape of the epithelium is rather unstable under special conditions, and the variation of histological features is correlated with the secretion of various shell substances (Nakahara 1958). According to Kawakami's aspects (1952) on the regeneration of the grafted mantle tissue, the epithelium on the outer surface of the mantle rearranges through multiplication and develops into the epithelium of pearl-sac, whereas the epithelium on the inner surface of the mantle diminishes and disappears. The distribution of alkaline phosphatase and carbonic anhydrase in the mantle was examined histochemically by Greenberg (1947), Freeman and Wilbur (1948), Bevelander (1952), Kado (1954), and Kawai (1955). Wilbur and Jodrey (1955) have noticed that calcium deposition in the shell was spoiled by the effect of carbonic anhydrase inhibitors. These results have suggested that these enzymes play important roles in Ca metabolism of molluscs; the transportation of calcium in organic systems, the absorption of calcium from sea water, and the supply of shell carbonate. The distribution of the calcium granules in the mantle has been observed by microincineration and histochemical methods, and was discussed in relation to the activity of alkaline phosphatase or carbonic anhydrase (Bevelander 1952, Ojima 1952, Kado 1954, 1960 and Tsujii 1959, 1960).

On the other hand, the deposition of shell lime salts has also been studied particularly from physiological and biochemical viewpoints in applying isotope methods (Wilbur and Jodrey 1952, Jodrey 1953, Tanaka and Hatano 1957), and ecological, physiological and chemical works were made independently in each

special fields (Kokubo 1929, Mori 1948, Kobayashi and Tohata 1949, Ashikaga 1951 and Suzuki 1957). The author has usually taken into account the biological and physiological factors in the investigation of the mechanism of the growth and arrangement of inorganic crystals in the shell.

In the field of biocrystallography it is necessary to investigate synthetically the mutual relations among the secretive activity of the mantle, and the liquid and the solid phases surrounding growing crystals. The peculiarity of the ground of crystal growth in molluscs will be studied systematically in this chapter.

2 On the relationships between the ground of mineralization and the surrounding tissue

The materials used were the shells of 1 aged *Pinctada martensii* and *Mytilus edulis* which were collected from Ago Bay in 1958, and were fixed in neutral formalin. Being completely decalcified in 10% aqueous solution of ethylenediaminetetra-acetic acid disodium salt at pH 7.5 ~ 8.0, the materials were embedded in paraffin, and cut at 10μ. The sections were stained with Ehrlich's haematoxylin-eosin, or with Mallory's triple-stain. On the other hand, the fragments of the mantle removed from the pearl oyster taking up per a month during July 1958 to June 1959, were fixed with 95% alcohol, and were cut by the usual paraffin method. The sections were placed in the electric furnace at the controlled temperature of 550 ~ 600 °C for about one hour. Then the distribution of inorganic constituents in the mantle through the year was investigated under the dark field of the phase contrast microscope.

Since the ground of mineralization in Lamellibrachia is perfectly surrounded by the mantle, valves and organic matter, and is separated from its environment, as seen in figure 1, sea water does not go directly in and out of that ground under normal conditions. In living animals, the mantle spreads in contact with the inner shell surface, and the large space seen in figure 1 appears to be absent, though the mantle is free from the shell. In other words, the epithelial cells of the mantle do not join closely to unit prism or crystal of shell, and the mother fluid exists between both systems. Shell substances are crystallized out from the mother fluid which is introduced into the ground through the mantle, and are characterized by the different areas of the mantle.

General anatomy of the mantle in *Pinctada martensii* is illustrated in figure 2. The marginal region of the mantle is divided into three folds, and is covered by an epithelial layer. Mucous cells are found here and there among the epithelium or in the subepithelial connective tissue, and longitudinal and transverse muscular bundles run in the connective tissue, the latter running at direction tangent to the former. Organic matter secreted by the epithelium of the middle fold is connected with the periphery of the shell, and develops into the periostracum covering the outside of the shell. The outer layer, commonly termed as "prismatic layer", is formed by the epithelium on the outer surface of the shell fold, and

shows columnar structure. On the contrary, the inner layer (i.e., nacreous layer) is secreted by the epithelium on the outer surface of the mantle, and reveals laminary structure. Figures 3 and 4 are micrographs showing the distribution of inorganic components in the mantle. As was pointed out by Ojima (1952) and Tsujii (1959, 1960), calcium granules are smaller and more abundant in the epithelium on the outer surface than in that on the inner surface. Throughout the year, on the pallial zone the amount of the granules is usually more abundant in the epithelium of the outer surface than in that of the inner surface, and there is no change in the distribution of inorganic components. But seasonal change in the amount of calcium in the mantle is not quantitatively acertained from the results obtained by the microincineration method. Crystal growth and the ratio of calcium deposition are very different in various seasons (see chapter V), although the distribution of inorganic components in the mantle is constant, and the shape of the epithelial cells on the outer surface is similar throughout the year.

Outline of the inner shell surface in *Pinctada martensii* is shown in figure 5. The amount of calcium carbonate deposition in each local area of the same shell appears to be not uniformed in various developmental stages of a species and in various species. The mother fluid in shell formation is prepared by the secretive activity of the mantle, which varies with the change of the physiological conditions of animals. That amount is controlled by the above mentioned factors, but it is a common result that the amount is larger in marginal area than central one of shells in oyster and pearl oyster (Wilbur *et al.* 1952, Nakahara 1961). And the velocity and the mode of crystal growth will be characterized by the different calcium carbonate concentration and physicochemical conditions in the mother fluid as described following part.

3 Relations in the pearl oyster among calcium deposition, mother fluid, and physiology

For the understanding of the daily or seasonal variations of the metabolic activity in the bivalves, the pH value of the body fluid was determined by the pH meter. Adsorbed sea water on the body surface being removed with filter paper, two glass electrodes were inserted directly into the body, and thus pH value was measured. Ca ions in the mother fluid were determined in ten specimens which were taken up from sea water at 9 a.m. of each experimental days during the period from July 1959 to June 1960. The solution which was presented between shell and mantle was collected in beakers, and was treated as the mother fluid of shell salts. The concentration of Ca ions in 1 cc of that fluid was determined by the direct titration method of Holtz and Seekles for the quantitative analysis of calcium in blood serum. The sample was kept in more alkaline condition than pH 13. The titration was carried out with a 0.005 molar solution of ethylenediaminetetra-acetic acid disodium salt. The dye 2-hydroxy-1-(2-hydroxy-4-sulfo-1-

naphthylazo)-3-naphthoic acid (dotite 2N) was used instead of the dye mulexid as a calcium indicator.

Seasonal and daily variations of pH of the body fluid are examined from 1958 to 1959, and are plotted in text-figures 1 and 2. The pH curve in figure 1 rises

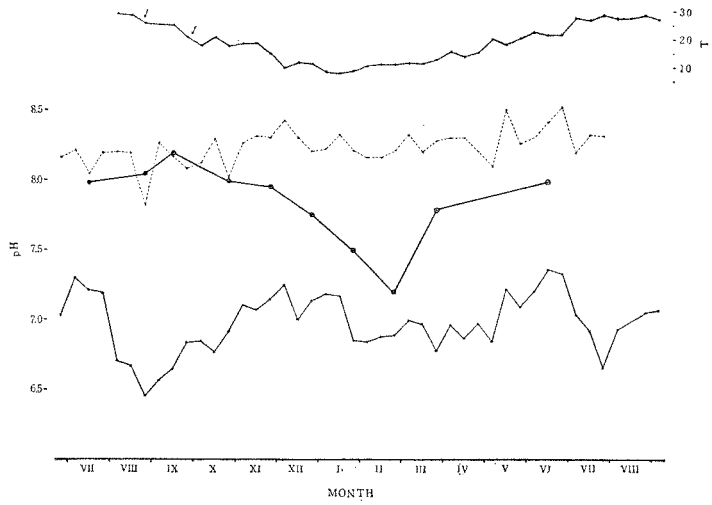

Text-fig. 1 Seasonal change of pH of the body and the mother fluids.
T; —•—•— sea water temperature. arrows indicate visit of typhoon.
pH; —•—•— the body fluid. —◉—◉— the mother fluid.
···•···•··· sea water.

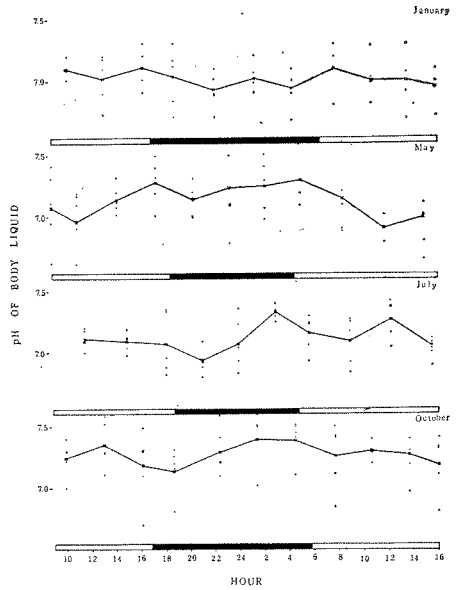

Text-fig. 2 Daily variation of pH of the body fluid in various seasons.

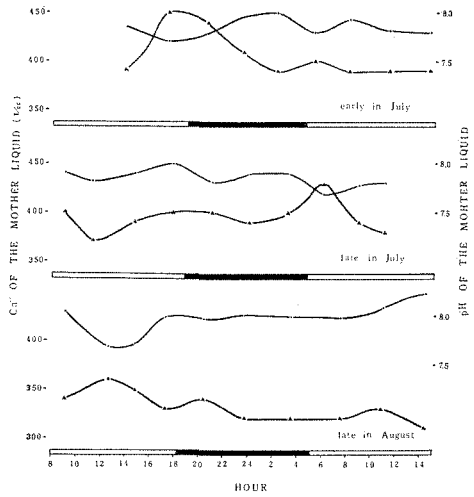

Text-fig. 3 Daily variation of pH and Ca ions of the mother fluid.
—·—·— pH, —▲—▲— Ca

Table I Daily variation of Ca ions in the mother fluid of *P. martensii* (measured in 1959).

No. of experiment								
1			2			3		
Time	pH	Concentration of Ca^{++} (γ/cc)	Time	pH	Concentration of Ca^{++} (γ/cc)	Time	pH	Concentration of Ca^{++} (γ/cc)
VII/9			VII/24			VIII/27		
13.55	7.85	390	09.00	7.91	400	09.10	8.04	340
17.15	7.71	450	11.25	7.82	370	12.35	7.68	360
20.30	7.79	440	14.45	7.90	390	14.55	7.71	350
23.20	7.96	410	17.50	8.00	400	17.15	7.98	330
VII/10			20.55	7.81	400	20.25	7.97	340
02.10	8.01	390	VII/25			23.40	8.01	320
05.10	7.79	400	00.00	7.88	390	VIII/28		
08.05	7.93	390	03.10	7.89	400	03.30	7.99	320
11.20	7.81	390	06.00	7.68	430	07.30	7.98	320
14.35	7.80	390	08.55	7.78	390	10.50	8.09	330
			11.00	7.80	380	14.20	8.23	310

gradually after hibernation (i.e., from late of January to early of May in Ago Bay) and reaches the maximum value of 7.4 during the period from June to July. Thereafter the minimum pH value of 6.5 is shown in July to August, the maximum value of 7.3 in October to November, and again the pH 6.7 when sea water temperature falls below 10°C. It is obvious, however, that the season from June to August coincides with the spawning period of the animal. The pH curve begins to fall after spawning, and thereafter it shows again the minimum value in hibernation. Although spawning and hibernation have the same effect on the seasonal pH value of the body fluid, daily variation of the pH curve is entirely different in

both periods as seen in text-figure 2. These results suggest that daily rhythmic activity is found in the pearl oyster in the spawning period, whereas its metabolic activities fall markedly and rhythmic changes are not found in hibernation. The pH curve of the body fluid is parallel to that of the mother fluid except for some

Table II Seasonal changes of $CaCO_3$ deposition, concentration of Ca ions and pH in the mother fluid of *P. martensii*.

Date of measurement	pH	Concentration of Ca^{++} (γ/cc)	Amount of $CaCO_3$ deposition in mg during a month previous to measurement
1959, VII / 18	7.98	390	—
VII / 28	7.69	390	11.1
VIII / 6	7.90	410	—
VIII / 28	8.04	340	19.98
IX / 9	8.19	360	—
IX / 26	—	—	21.32
X / 28	7.99	370	17.49
XI / 25	7.95	420	10.51
XII / 24	7.75	450	5.52
1960, I / 26	7.50	450	—
II / 18	7.19	480	—
III / 30	7.79	480	—
VI / 9	7.98	400	10.80
VIII / 12	—	380	—

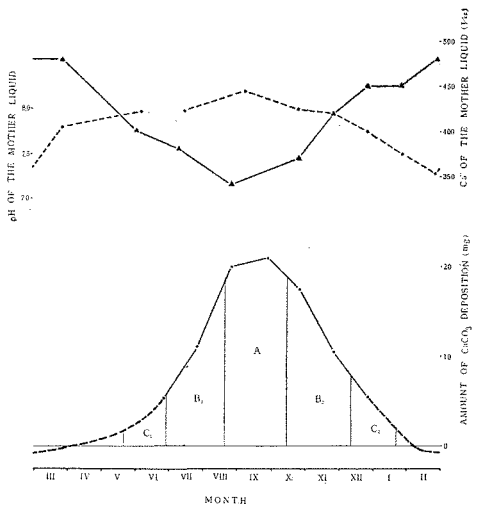

Text-fig. 4 General curve of $CaCO_3$ deposition (1959~1960).
— • — • — change in the rate of $CaCO_3$ deposition during the year.
—▲—▲— change of Ca ions in the mother fluid.
- - - • - - • - - change of pH of the mother fluid.

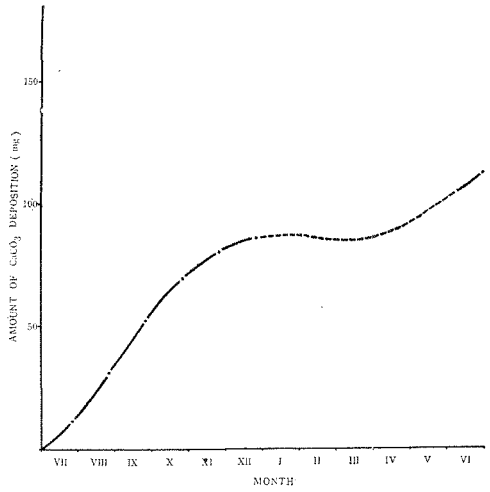

Text-fig. 5 General change of $CaCO_3$ deposition during a year.

time after spawning (Text-fig. 1). That is, opposite relations between the pH curves of the body and mother fluids are noted in spawning, while these curves run parallel with each other in hibernation. In hibernation, calcium deposition stops perfectly in almost all specimens, and general dissolution phenomena are frequently seen. In the spawning period, very much increase in calcium deposition is recognized irrespective of the dissolution of shell salts often occurring in that period. The increase and decrease of Ca ions in the mother fluid appear to be accompanied by pH changes, as shown in tables I and II, and text-figures 3 and 4. The observed concentration of Ca ions in the mother fluid is in inverse proportion to the pH value in daily and seasonal changes of calcium metabolism. Above mentioned Ca ions decrease in correlation with an increase of calcium deposition, and are somewhat more concentrated than those in the surrounding sea water (300~400 γ/cc in Ago Bay throughout the year). Calcium deposition throughout a year, on the other hand, is represented in S-shaped curve, rising sharply during the period from summer to early autumn (Text-figs. 4 and 5). From text-figure 4, the mother fluid is thought to be in a similar conditions when same amount of calcium is deposited; namely, the pH value, the concentration of Ca ions, and the amount of calcium deposition in the shell are similar between B_1 and B_2, or C_1 and C_2 (Text-fig. 4). However, somewhat different rhythmic curve is obtained in accordance with the change in various ages, environments, and years.

4 Discussion

It is considered that calcium and carbonate in shell constituents are transported into the ground of crystal growth by different pathways in the shell formation, and some enzymes will play important roles in calcium metabolism (Robertson 1941).

Carbonic anhydrase is one of these enzymes (Freeman and Wilbur 1948, Kawai 1954). According to Kawai's aspects (1955) with *Pinctada martensii*, the ratio of shell growth was affected by the carbonic anhydrase activity which was low in winter and reached the maximum during summer to autumn. He has stated furthermore that the enzyme activity decreases with an increase of age, weakening or spawning of the pearl oyster. The relationships between calcium deposition and sea water temperature were investigated by Watabe (1952). The present author has pointed out that crystal growth of shell reduces or stops in weakening oysters. However, carbonic anhydrase may be in close relation with calcium deposition, and similar growth of shell salts seems to occur under the same degrees of the enzyme activity which is influenced by the internal and external factors of the organism. This idea has been confirmed by the interesting experiments of Wilbur and Jodrey (1955), who have found in *Crassostrea virginica*, that the activity of calcium metabolism is greatly spoiled by carbonic anhydrase inhibitors. On the other hand, organic substances and alkaline phosphatase may be possible to play important roles in the calcium transportation through the mantle from its habitat to the ground of crystal growth, and the deposition of shell lime salts has been thought to occur by dissociation of calcium bicarbonate. It was reported by Kado (1960) that alkaline phosphatase may not be concerned with the percutaneous uptake of calcium from the surroundings, but may probably be a part of a system of enzymes involved in the secretion of the shell protein. Horiguchi (1960) has done the serial of the biochemical studies on the effects of organic acids on the calcium and phosphorus metabolism in regard to the calcium carbonate deposition, and attempted to read the mechanism of the selective excretion of calcium carbonate from the mantle. And he stated that the ionic concentration of Ca^{++}, HCO_3^- in blood and tissue fluids of shell-fishes was closely related to the calcium carbonate deposition. The mother fluid thus produced differs from that in inanimate objects by the presence of organic substances which are synthesized within the mucous cells, and varies with different physiological conditions of the organism during a year and its development. In the shell formation, the organic substance is first formed, and it seems to affect directly the deposition of mineral components. The shell substances are thought to be crystallized out after passing through the amorphous state when the solid phase separates from the liquid phases. That is, the shell mineralization in Pelecypoda and Gastropoda is assumed to pass through the following three processes: (1) The formation of organic matrix as the basis of shell material, (2) Fixation of calcium in this organic matrix, and (3) The deposition of calcium carbonate crystal. In these processes, a definite current occurring in the mother fluid by the movement of the mantle tissue must play the important factor in the crystal growth of molluscan shells. The nature of the mother fluid must be more or less different among the species with calcite or aragonite shell.

Since physical and chemical conditions of the mother fluid are varied with the differences in the secretive function of the mantle, as have already been mentioned,

crystallites of shells show different growth during the development of organisms and among different species (see chapters V and VI). The rate of crystallization is, general speaking, in proportion to the concentration of the solvent in a mother fluid. But the present result indicates that the observed concentration of Ca ions in the mother fluid decreases with the increased calcium deposition, suggesting two cases of crystal growth in shell-fishes. That is, in one case, the crystal growth occurring in unsuitable environments or in abnormal state of animals is assumed to be in the same condition as that in the closed system since the activity of calcium metabolism is low or stops in that case, and in other case, when the animals are in good condition, the crystal growth is considered to be in the opened system since the secretive activity of the mantle is high and the shell substances are constantly supplied into the mother fluid. Consequently, we meet with such an inconsistent result that the decrease in the amount of Ca ions is correlated with the increase of calcium carbonate deposition. The pH value of the mother fluid also affects the crystal growth and calcium deposition. It may be thought that biological factors play the important roles when calcium is supplied into the mother fluid by the mantle and mineral components are separated from the liquid phase. In particular, the crystallization of shells is carried out in the presence of organic substance and enzyme.

5 Summary

1) The ground of crystal growth in the shells of Lamellibranchia is perfectly separated from the surrounding sea water.
2) No change in the distribution of inorganic granules is found in the mantle during the year.
3) The mother fluid introduced throughout the mantle is characterized by the presence of organic substance.
4) The calcium deposition similarly increases and decreases in amount under the same conditions of the mother fluid in different seasons.

Chapter II

Mineral Constituents and Structure of Shell

1 Introduction

The purpose in this chapter is to describe the nature of the solid phase as the ground of crystal growth. It will be confirmed from the interesting experiment for the cultivation of the mantle tissue that the crystalline structure of the nacre is affected by the movement and the tension of the shell-forming tissue. Of course, it is needless to say that mineral constituents of the solid substance in the ground of crystal growth may depend upon the nature of the liquid phase and the biochemical reaction in Ca metabolism, and that the shell structure is influenced by the deposition of organic and mineral substances, which is varied by physicochemical conditions of the mother fluid. The shell growth of Pelecypoda is divided into the two directions which are vertical and horizontal to its inner surface. A shell increases in thickness in the former and in size in the latter. In *Pinctada martensii*, the shells thus formed consist of three elements, which are periostracum, prismatic and nacreous layers in the order from external to internal side of the shell, and a hypostracum lies in the nacre in addition to these elements separating the inner and outer nacreous layer. It has already been known that the periostracum is made only of organic substance, so-called conchiolin, without any crystal, and that the prismatic layer and hypostracum indicate polygonal prismatic structure with calcite in the former and aragonite in the latter, and moreover that the nacreous layer has laminary structure being constructed with alternately accumulated thin conchiolin membrane and aragonite crystals. But the shell consists of only porcellanous layer of aragonite in *Veneracea*, *Lucinacea*, etc., and calcitostracum and prismatic layer of calcite in *Ostreacea*. Further, vaterite was detected in some Gastropoda by Mayer (1931), Mayer and Weineck (1932), and Stolkowski (1950).

The crystalline structure of shells has been studied crystallographically by using the polarizing microscope and the X-ray techniques, and several numbers of papers concerning the above mentioned studies have been published until now. These results showed that the *c*-axis of crystallites of lime salts in molluscan shells was arranged in the direction perpendicular to the inner shell surface. According to the author's recent works, it has been obvious that the shell-forming tissue affects the elongation of crystallites of aragonite during growth.

2 X-ray powder diffraction analysis of shell materials

X-ray powder diffraction data is obtained by using X-ray diffractometer under such experimental conditions as copper $K\alpha$ radiation, 35KV, 15mA, scanning speed 2°/min., scale factor 8, multiplier 1, time constant 4 seconds, slit system 1° - 1° - 0.4°.

Table III Data for mineral constitutents of shell salt in different species.

Class	Species	calcite	aragonite
Amphineura	*Liolophura japonica* (Lisckke)		+
	Acanthochiton defilippi (Tapparone et Canefri)		+
Peleeypoda	*Anadara subcrenata* (Lisckke)		+
	Volsella nipponica Oyama	+	+
	Septifer bilocularis pilosus (Reeve)	+	+
	Pteria penguin (Röding)	+	+
	P. panasesae (Jameson)	+	+
	P. margaritifera Röding	+	+
	P. maxima (Jameson)	+	+
	Pinna attenuata Reeve	+	+
	Chlamys nobilis (Reeve)	+	
	Notovola albicans (Schröter)	+	
	Ostrea gigas (Thunberg)	+	
	Unio margaritifera (Linné)	+	+
	Hyriopsis schlegeli (v. Martens)	+	+
	Corbicula japonica Prime		+
	Saxidomus purpuratus (Sowerky)		+
	Meretrix meretrix lusoria Röding		+
	Tapes variegata Sowerky		+
	Paphia undulata (Born)		+
	Irus mitis (Deshayes)		+
	Chion semigranosum (Dunker)		+
	Macoma incongrua (v. Martens)		+
	Fabulina nitidula (Dunker)		+
	Solen gouldi Conrad		+
	Ensciculus philippianus (Dunker)		+
	Solidicorbule erythrodon (Lamerck)		+
Scaphopoda	*Dentalium octangulatum* Donovan		+
Gastropoda	*Haliotis discus* Reeve	+	+
	Patelloida saccharinaianx (Reeve)		+
	Pliosabia pilosa (Deshayes)		+
	Nerita albicilla Linné	+	+
	Crepidula gravispinosa Kuroda et Habe		+
	Hydatina physis (Linné)		+
	Tonna luteostoma (Küster)		+
	Nassarius linescens (Phillippi)		+
	Tritia festivus (Powys)		+
	Columbella versicolor Sowerby		+
	Semisulcospia libertina (Gould)		+
	Batilleria multiformis (Lischke)		+
	Lietorivaga brevicula (Phillippi)		+
	Monodonta labio (Linné)		+
	Neverita didyma (Röding)		+
	Umbonium costalum (Kiener)		+
	Evenaria japonica (Schilder)		+
Cephalopoda	*Sepia kobiensis* Hoyle		+
	Argonauta argo (Linné)	+	

Table III is X-ray powder data for several Pelecypoda, Gastropoda and other groups showing on the base of mineral constituents that the molluscan shells are possibly divided into three types as follows; *Meretrix* shell consisting of only aragonite, *Ostrea* shell of only calcite, and *Pinctada* shell consisting of both of these minerals. In addition to aragonite and calcite, calcium carbonate is crystallized out as the form of unstable vaterite in some species of Gastropoda (Mayer and Stolkowski). However, since histochemical reactions for the mantle are characteristic among various species, physicochemical and biochemical conditions in the mother fluid of each species are assumed to be different from one another and to be concerned with the polymorphism of calcium carbonate in each species. The mineral components of *Pinctada* type are different in local area of the same shell, as seen in table IV; for instance the shell salt of *Pinctada martensii* is calcite in the prismatic

Table IV Mineral consituents in different regions of the same shell in several species.

Species	Region	calcite	aragonite
Pinctada martensii (Dunker)	outer layer	+	
	inner layer		+
	ligament		+
Pinctada maxima (Jameson)	outer layer	+	
	inner layer		+
	ligament		+
Chlamys nobilis (Reeve)	shell	+	
	ligament		+
Ostrea gigas Thunberg	outer layer	+	
	inner layer	+	
	ligament		+
Patinopecten yessoensis Jay	shell	+	
	ligament		+
Hyriopsis schlegeli (v. Martens)	outer layer	+	
	inner layer		+
	ligament		+

layer and aragonite in the nacreous layer, respectively, although the cause of polymorphism of calcium carbonate crystal in living organisms is not elucidated. More interesting fact is that the ligament salt of the shells of all species given in that table is composed of aragonite alone irrespective of the shell valve salt is either aragonite or calcite. The ligament, prismatic and nacreous layers are secreted respectively by different areas of the mantle, the epithelium of which exhibits the variation in histological structure. Such polymorphism in organisms is presumed to depend upon biological factors as is demonstrated by means of grafting as follows: If the piece of epithelium from different regions of the mantle of the

pearl oyster is grafted into the gonad of another, the original functional difference of the epithelial cells is almost maintained through the multiplication of the graft even if the adjacent tissues somewhat influence it; for instance, the regenerated epithelium derived from the grafts of mantle edge will secrete generally prismatic substances. But the difference in the adjacent tissues in the grafting is expected to have various effect on regeneration of grafts. In text-figure 6, S-1, S-2 and S-3 are the reflexion patterns for the specimens from the different areas of the valve in *Pinctada martensii* and the ligament of *Pinctada maxima*. These patterns have a broad reflexion peak between 10 ~ 30° in 2θ besides the diffraction pattern of aragonite or calcite, as is marked by an arrow in text-figure 6. Here, the peak in the last S-3 is recognized obviously to consist of two broad ones. These peaks appear to be due to the organic substance in shell materials, and to enlarge with an increase in quantity (see chapter III).

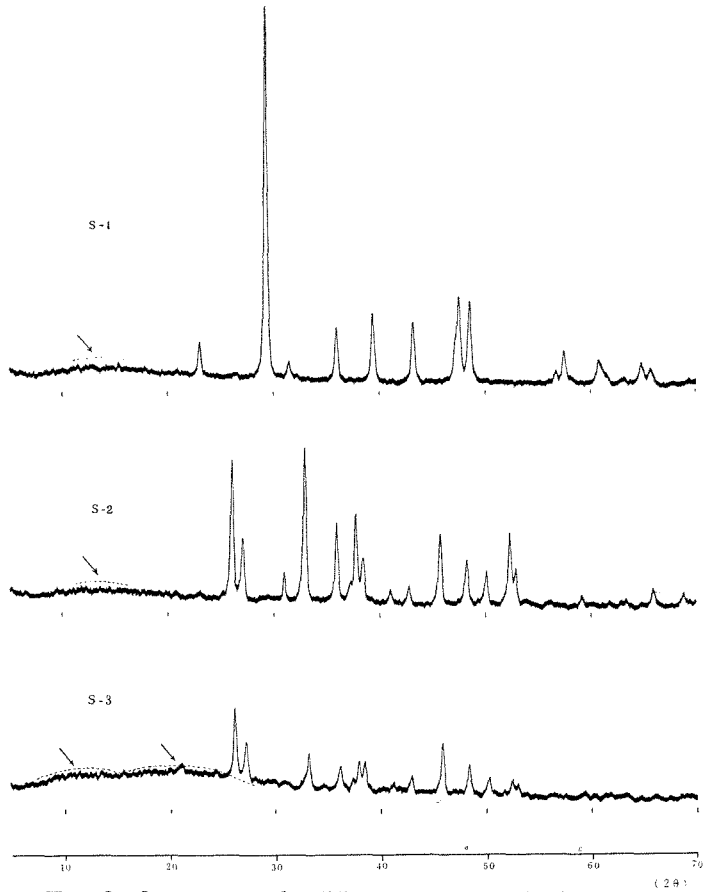

Text-fig. 6 X-ray powder diffraction of the shell substances.
S—1 prismatic substance of *P. martensii*
S—2 nacreous substance of *P. martensii*
S—3 ligament of *P. maxima*

In all cases, judging from the shape and the intensity of the reflexion patterns, the aragonite and calcite of the shell do not differ in their crystalline state from these of inanimate objects (Text-fig. 6), nevertheless the degree of calcification in various portions of the prismatic layer seems to be different from each other in its histochemical tests. Furthermore, it can be said that any other mineral is never contained in more amount than 10% except calcium carbonate.

3 Differential thermal analysis of shell materials

The differential thermal analysis curves for the shell materials of *Pinctada martensii* are recorded in text-figure 7 at the mean heating rate of approximately

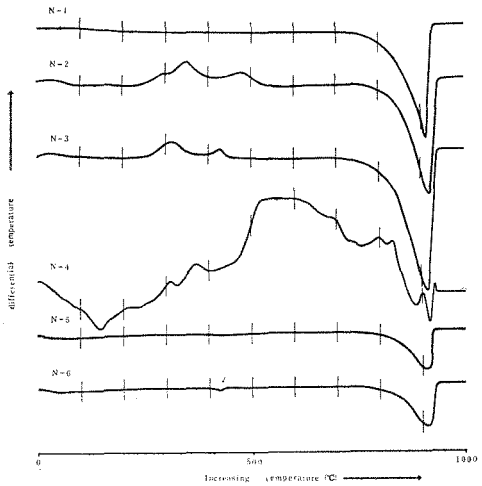

Text-fig. 7 Differential thermal analysis curves for molluscan shell substances and $CaCO_3$.

N—1 $CaCO_3$
N—2 prismatic substance of *P. martensii*
N—3 nacreous substance of *P. martensii*
N—4 ligament of *P. martensii*
N—5 prismatic substance treated with H_2O_2
N—6 nacreous substance treated with H_2O_2

10°C per minute until the heating temperature rises up to 1000°C. The first two and three curves N-2, N-3 are produced by the materials of the prismatic and nacreous layers, respectively, and show a broad double exothermic peak between 250°C and 550°C and a sharp endothermic break at about 920°C. The results are essentially identical between both materials, though calcium carbonate crystal is calcite in the former, and aragonite in the latter. However, since lime salts in inanimate objects have not any distinct exothermic peak at 250~550°C as seen in the curve N-1, the exothermic peak which begins at 250~260°C is believed to arise through the combustion of the organic substance in the shell. The curve N-4 is that for the ligament of *Pinctada martensii*, and suggests that the larger the

amount of contained organic substance, the greater the exothermic peak develops. Hence, if the organic substance can not be removed from the giving sample, it is obviously impossible to observe the small endothermic break, at near 450°C, which can be seen for aragonite. Curves N-5 and N-6 are those for the materials of the prismatic and nacreous layers treated with H_2O_2. In comparing the curves N-2 and N-3 with these just described curves, we will notice that the exothermic peaks disappear perfectly, and on the contrary, the new endothermic break takes place at 430°C in the curve for the nacre. This endothermic break occurs when aragonite is transformed into calcite.

Besides, a broad endothermic curve between 50°C and 200°C seems to be due to the loss of adsorbed water in the giving samples, and a sharp endothermic break at about 850~950°C takes place by the loss of carbon dioxide in calcium carbonate to the atmosphere. The thermal analysis of carbonate minerals has already been done by Kôzu and Kami (1934), Faust (1950), and Beck (1950), so for details the reader must be referred to their original papers. The results obtained from the differential thermal analysis are in good accordance with the those of X-ray powder analysis.

4 Chemical components of the shell substance

Materials used in this study were as follows:

class	species	location
Amphineura	*Liolophura japonica*	Enoshima
Pelecypoda	*Pinctada martensii*	Ago Bay
	Pinctada maxima	Arafura Sea
	Chlamys nobilis	Ago Bay
	Patinopecten yessoensis	Hokkaido
	Ostrea gigas	Ago Bay
	Hyriopsis schlegeli	Lake Biwa
	Corbicula japonica	River Tama
	Meretrix meretrix lusoria	Tokyo Bay
	Venerupis philippinarum	Tokyo Bay
Scaphopoda	*Dentalium octangulatum*	Sagami Bay
Gastropoda	*Haliotis discus*	Shima
Cephalopoda	*Sepia kobiensis*	Chiba
	Agronauta argo	Arafura Sea

It was hardly possible to carry out chemical analysis with many members of each class, so sixteen materials were selected taking into account the taxonomical, ecological, and mineralogical factors as follows: (1) Materials belong to various classes. (2) Mineral constituents of their shells are only aragonite, only calcite, or both minerals. (3) They are in fresh water or in marine. These materials were washed with fresh water and dried at room temperature, and then, were powdered by an agate mortor. After the material was separated into inner and

outer layers in the shells which consisted of both minerals of aragonite and calcite, it was grained by the same way. The samples were dissolved by about 20 ml of 6 N HCl with 30% H_2O_2, and dried up on a water bath. Then the inorganic elements of the shell substance were separated by means of ion exchange resins (Amberite IR-120 and Dowex IX-8). The procedure for fractionation is shown in text-figure 8. The elements separated by these resins were determined as

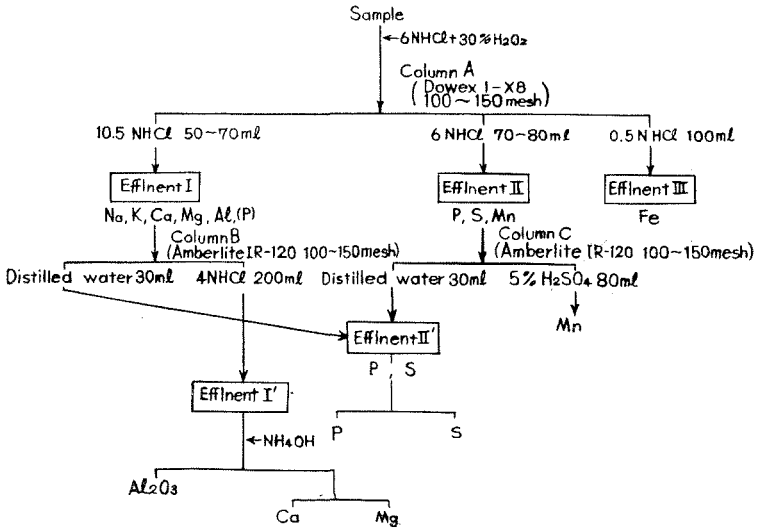

Text-fig. 8 Fractionation of inorganic elements from a shell.

follows: Calcium as CaO, magnesium as MgO, manganese as MnO_5, iron as Fe_2O_3, aluminum as Al_3O_5, sulfate as SO_4, and phosphate as P_2O_3, respectively. The amount of H_2O^+ was measured according to Penfield's method. The amount of the organic substance in the shells was not decided chemically, but with differential thermal analysis the endothermal peak of the organic one was made on 0.25 gr of several samples.

The chemical data on inorganic components of the shell substances are indicated in table V. It can be seen that the amount of calcium contents is nearly same in all species, though is somewhat low in the Cephalopod shells. On the contrary, that of the magnesium content in the Cephalopod shells shows to be higher than other classes. The mineral component of *Corbicular* shell is aragonite although it contains the larger amount of magnesium than other Pelecypod shells. Trace of manganese is found in nearly all species examined, but it is contained in the relatively large amount in *Hyriopsis* shell only. Iron is found about 0.2~0.3% in these shells, and aluminum is recognized too. Phosphate and sulfate are contained in only minute amounts in these shells as compared with those in the mineralized tissues of Vertebrata.

The chemical components of the shell substance seem to be characterized

Table V The chemical components of several shells.

Species	Part	Mineral Component	H_2O^- (%)	H_2O^+ (%)	CaO (%)	MgO (%)	MnO (%)	Fe_2O_3 (%)	P_2O_5 (%)	SO_4 (%)
Liolophura japonica	shell	aragonite	—	—	49.85	0.40	trace	0.14	0.01	0.74
Pinctada martensii	prismatic layer	calcite	—	—	52.36	1.22	trace	0.15	0.01	1.02
	nacreous layer	aragonite	0.68	—	53.38	0.20	trace	0.11	0.01	0.55
Pinctada maxima	prismatic layer	calcite	0.82	—	51.83	1.40	trace	0.26	0.01	1.14
	nacreous layer	aragonite	0.66	—	52.70	0.34	trace	0.29	0.01	0.76
Chlamys nobilis	shell	calcite	0.29	2.18	54.38	0.52	trace	0.09	0.03	1.97
Patinopecten yessoensis	shell	calcite	2.08		54.71	0.26	trace	0.12	0.04	1.97
Ostrea gigas	shell	calcite	0.52	1.36	52.16	0.28	trace	0.18	0.03	1.56
Hyriopsis schlegeli	inner layer	aragonite	0.60	—	53.50	0.45	0.04	0.13	0.02	1.63
Corbicula japonica	shell	aragonite	0.40	1.65	53.47	1.26	trace	0.18	0.01	1.54
Meretrix meretrix lusoria	shell	aragonite	0.70	1.29	54.50	0.12	trace	0.19	0.01	2.10
Venerupis philippinarum	shell	aragonite	0.70	2.13	51.32	0.13	trace	0.11	0.03	1.89
Dentalium octangulatum	shell	aragonite	—	—	54.10	0.60	trace	0.15	0.02	1.16
Haliotis discus	inner layer	aragonite	—	—	53.80	0.40	trace	0.27	0.01	0.83
Sepia kobiensis	shell	aragonite	1.75	2.23	49.09	1.20	trace	0.16	0.03	2.40
Argonauta argo	shell	calcite	1.70	2.88	48.15	2.00	trace	0.15	0.03	1.28

by various species even though they are under a similar environment. The amount of the divalent cations, in particular magnesium, considers to be related with the structure of calcium carbonate in molluscs. Generally speaking, magnesium content in calcite of the prismatic layer is larger than that in aragonite of the nacreous layer. But that relation between the magnesium content and mineral components is not always common in all molluscan shells. The relationships between the amount of $MgCO_3$, and mineral constituents of the mineralized tissues, or water temperature of the environment were investigated with several marine organisms by Chore (1954). He reported that the magnesium content in the mineralized tissues was controlled by mineralogical factor and varied in correlation with the water temperature of the environment. Of course, the content was different among various species. Similarly, the present results show that the chemical components of molluscan shells depend upon the taxonomical, the ecological, and the mineralogical factors. It has already been known that such divalent cations as magnesium, manganese, and iron, determin the structure of the anhydrous carbonate. In mollusca, those cations may also easily enter into the lattice of calcite rather than into that of aragonite, but they may not be the most important determining factor on the structure of the shell lime salt. Text-figure 9 is the differential thermal analysis curves on the shell substances. Since the area of the endothermal peak is larger in proportion to the increase of the amount of the organic substance, the amount can be discussed by the comparison of the relative area of the peak among the curves. The amount of the organic substance is not different between the aragonite and the calcite shells, and rather is different among various species.

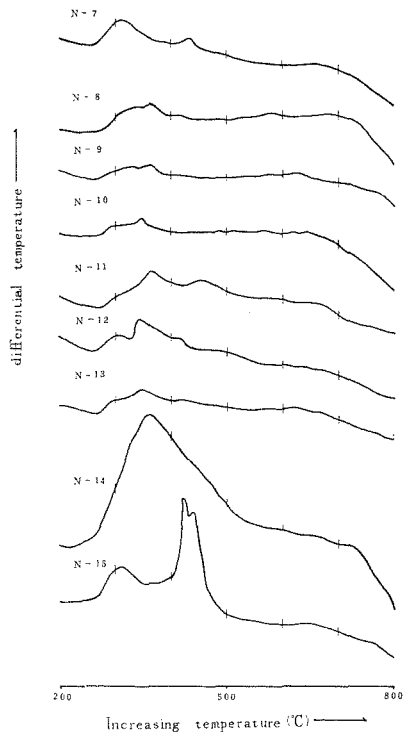

Text-fig. 9 Differential thermal analysis curves of several molluscan shells.
N— 7 *Liolophura japonica*
N— 8 *Chlamys nobilis*
N— 9 *Patinopecten yessoensis*
N—10 *Ostrea gigas*
N—11 *Corbicula japonica*
N—12 *Meretrix meretrix lusoria*
N—13 *Venerupis philippinarum*
N—14 *Argonauta argo*
N—15 *Sepia kobiensis*

The result suggests that the amount of the organic substance is independent of the structure of the shell lime salt. Besides, the Cephalopod shells seem to contain large amounts of crude fats with conchiolin.

5 Observations of shell structure with electron microscope

For electron microscopic observations, methylmethacryl-alminum replica method was used in this experiment. Replicas were prepared with the pre-polymeride of methylmethacrylate. The plastic was droped on the specimen surfaces, such as natural surface, fracture surface or polished surface etched with 0.1% HCl, and was polymerized in an incubator at controlled temperature 30~35°C. After the surface of replicas teared off from the specimens was shadowed with

chromium or germanium at approximately 26° angle from the definite orientation for increasing the contrast of the electron image, aluminum as backing film was evaporated vertically on the surface. The all evaporation was done in vacuum at about 5×10^{-5}mm Hg. The aluminum films were grided into 1×1mm squares and the plastics were dissolved in aceton. Then the fragments of the film in aceton were scooped with a mesh of copper. The electron microscopes used were the HS-2 and HU-10 types of Hitachi.

i) Prismatic layer

Generally speaking, the surface of the prismatic layers shows under optical microscopes a honeycomb pattern consisting of chambers, which are 5μ to $100\,\mu$ in diameter, though the pattern is more or less different from one portion to another in the layer. Figure 6 is an electron micrograph of the periphery of a growth process on the inner surface of the layer, showing that rounded crystals which are of all sizes grow in or on the thick organic membrane. The crystals of shell salts which are $0.01\,\mu$ to $4\,\mu$ in size, are deposited almost parallel in a definite orientation. The edges of the underlying prismatic chambers are seen as groove on the membrane, which reveals fibrous appearance. In some region of a growth process, main stems of growth of crystals run along the boundary between underlying prismatic chambers, and the deposited crystalline substances exhibit irregular forms (Fig. 7). On the edge of scaly lamellae (i.e., growth process) or on the prismatic surface at an early stage in the formation of the layer oolitic and rosette-shaped prisms were found to grow loosely fusing with one another, as shown in figures 8, 9, and 10. Each prism gradually increasing in size, comes to be closely compacted together and develops into a prismatic layer. Moreover, the prism itself is also divided, in general, into micro-chambers, thus exhibiting a polygonal prismatic chamber with micro-chambers, $2 \sim 20\,\mu$, as in figure 11. Prismatic chambers are separated from each other by conchiolin walls.

During growth of the layer, prismatic lamellae become to cover the surface of the lower lamella, already stopped its growth. And each prism on the marginal parts of the upper lamina grows in the directions vertical and horizontal to its surface. Its surface is curved and the growing point is the highest, as seen in figure 11. Occasionally, if the horizontal growth of the prism is in similar rates around the growing points, each prism exhibits a round shape, whereas, if a prism grows at unequal rate in different directions of the horizontal growth, it develops into various rosette-forms. A prismatic region near the nacre is shown in figures 12 and 14. The outline of crystal areas is round and the width of the conchiolin walls sandwiched between each chamber increases up to $6 \sim 17\,\mu$, being far wider than that in figure 16. In these parts, at the end of growth of the chambers, conchiolin walls forming shallow grooves climb up the crystal areas, which are finally covered perfectly with the thick organic membrane (Fig. 15). Almost all parts of the prismatic regions, except above mentioned areas, generally show networks of polygons. The boundaries of these networks are made of the conchiolin walls

running as grooves between the crystal portions (Fig. 16). Very fine calcite crystals, about 0.1 μ to 1 μ in size, grow inside the chamber, and aggregate in parallel or irregular. They exhibit rarely concentric and spiral patterns.

Figure 13 shows the regenerated prismatic layer of *Pinna attenuata* treated by von Kossa's silver method. Although the reaction is different from portion to portion of the layer, conchiolin wall is stained considerably and the center of each prismatic chamber is more deeply, in general. Decalcified specimens indicate negative reaction. The similar results are obtained in *Pinctada matrensii*. From these facts, it appears that mineral components react positively with this test and deposit in the organic matters, and mineralization of the prismatic layer may be different in each element and portion of the layer. Whole area of the chamber is seen to extinct at the same time or not in the horizontal section under crossed nicols. In the former, directions image of uniaxial crystals is indicated (Fig. 19), in the latter, windmill, flamboyant, or partial irregular extinction is revealed in general (Figs. 17 and 18).

In the vertical section, the prismatic layer indicates a columnar structure separated by thick conchiolin walls running roughly parpendicularly to the inner shell surface. Such portions of the walls exposed on the inner surface of the layer correspond to the ones intervening between the polygonal chambers, and they are about 1 μ to 8 μ in width as measured on several preparations. In addition, we could recognize that the chambers are divided into following sub-chambers and micro-chambers by thinner conchiolin walls; sub-chambers are canie-shape and are 5~30 μ in width and composed of micro-chambers, 4~12 μ in width (Figs. 20 and 21). The width of these sub- and micro-chambers is in good agreement with the diameter of extinction blocks in a chamber. However, the micro-chambers show oblique extinction to the vertical walls of conchiolin which extincts always, as in figure 22. Thin organic matrix is deposited alternately with calcite crystals, and therefore, the layer shows a laminary structure, although the columnar structure is predominant. An elemental mineral lamina in the layer is approximatly 0.7 μ to 7.0 μ in thickness, while the conchiolin sheet running between them is about 0.04 μ to 0.5 μ in thickness. As seen in figure 21, an elemental mineral lamella is probably composed of the accumulated several thinner ones which are 0.2~0.4 μ in average thickness.

Very thick organic matrix lies at the boundary between the nacreous and prismatic layers with small round crystals very often scattered in it, in *Pinctada martensii* (Fig. 23). The thickness and feature of the organic layers vary in different portions or individual shells. This layer corresponds to the thick organic membrane deposited over the surfaces of the prismatic regions near the nacre.

ii) Nacreous layer

The nacreous layers show laminary structure, which is varied with the difference in size and mode of aggregation of crystals in the layer. Therefore, the size and mode of aggregation of crystals on the nacreous surface are governed directly

by variation of calcium carbonate concentration in the mother fluid transported throughout the mantle epithelium, as has been described in chapter I.

The nacre is usually divided into the marginal and central parts by an adductor and several pallial muscle scars, and the horizontal growth direction of the layer is recognized as the radial pattern running from the umbo toward the whole shell border. The shape and arrangement of the crystals in these two areas are very different from each other; the crystals, ranging 1 μ to 3 μ in size, are round and the parallel step pattern is observed in the ventral marginal regions during the period from summer to early autumn (Fig. 24). While in the central regions, as seen in figure 102 and table IX, the crystals in parallel growth exhibit well developed hexagonal tabular shape and they are approximately 3 μ to 8 μ in size, and are 2～3 times as large as those in marginal regions. And their aggregation shows a spiral pattern (Fig. 26). Aragonite crystals scattered on the nacreous surface increase in size, and come to contact with one another finally developing a thin crystal lamella. An organic membrane is, in general, sandwiched between them when one crystal joins with adjacent ones, and is found as groove on the inner nacreous surface (Figs. 25 and 122). Organic matrix on crystal surfaces often exhibits a reticular or finely granular membrane, as in figure 110 and 122, and corresponds to a membrane running between neighbouring crystal lamellae. The edges of the growing lamellae emerged on the inner surfaces show a step-like pattern similar to the geometrical patterns seen on crystal faces. In other words, the step remains in actively growing surfaces of the layer, and reveals various growth patterns by the changes of growth rate and mode of crystals.

As above mentioned, the superficial structure of the nacre in local areas is different from each other, and moreover, is varied widely with the difference of physiological conditions of animals and seasonal changes of their environments. Figures 27～31 present an example for successive variation of the nacreous surface in *Pinctada martensii*, under abnormal condition in summer. They show superficial structures entirely similar to those of animals in such unsuitable environments as sea water temperature falls below 13°C in winter, though the factors which have an effect on Ca metabolism seem to be different generally in these two cases. In both cases, the nacre lose its luster, or is covered by white veil of the shell salts and its superficial structures can be divided into following two types under electron microscope: (1) The surface shows the etching figure, and there no new crystals grow (Fig. 29). (2) Very fine crystals are deposited irregularly, and, in general, exhibits an irregular or imperfect form with etching figures (Figs. 30 and 129). Moreover, in winter, whole mineral surface is covered by thick organic matter indicating a homogeneous structure and of course, there is no new deposit of mineral substances (Fig. 110). Figures 32, 33, 35, 36, and 37 are vertical sections of shells in some species of Lamellibranch, and laminary structure in Gastropoda is illustrated in figures 34 and 38. Adjacent crystal lamellae are cemented with thin organic matrix which is found to be membraneous. The inner layer in these

shells is not fundamentally structurally different, although the thickness of the elemental mineral lamella and organic membrane is varied with different species; for example, the average thickness of crystal lamella being 0.3~0.6 μ in *Pinctada martensii*, 0.5~0.8 μ in *P. margaritifera*, 0.5~1.1 μ in *Unio margaritifera*, 0.6~1.2 μ in *Hyriopsis schlegeli*, 1.2~2.3 μ in *Quadrula undata*, 0.4~0.8 μ in *Haliotis discus*, and 0.4~0.6 μ in *Turbo cornutus*. Generally speaking, the mineral lamella is thicker in fresh water mussels than in marine mussels. The organic matrix sandwiched between each lamella is more thinner in thickness than the mineral lamella, and is less than 0.02 μ in these mussels except *Quadrula undata* that of which is about 0.04 μ in thickness. But the thick membrane, being about 0.1 μ, has rarely been found in *P. martensii* and is appeared to be formed immediately after hibernation (Watabe 1955, Wada 1957).

The organic membrane sandwiched between adjacent crystals in a lamella is never continuous to that of the other neighbouring lamellae since new crystal seeds are deposited at first on edges and corners of crystals in the underlying lamella and increase larger and larger. Consequently, the nacreous layer has not the columnar structure as usually seen in the prismatic layer. Under crossed nicols, horizontal thin slices show flamboyant or radial extinction running from shell center toward its margin, and under conoscopes they show a directions image of biaxial crystals (Fig.40). In longitudinal sections of the shell, the general nacre consists of several zonal extinction blocks which are 0.3~0.8 mm in width, as seen in figure 41. The width of these blocks is equal to the thickness of the layer produced in one year.

6 Crystalline structure of shell

i) Amphineura

The Chitonidae is in the lowest systematic position of molluscs. The soft part of *Liolophura japonia* is protected by the segmented shell which is built up of eight saddle-shaped plates overlapping as seen in text-figure 13. The mineral component of the shell is aragonite, and each plate consists of the ordinaly aggregation of crystallites. That is, *c*-axis orientation is nearly perpendicular to the inner surface of the plate, and their orthorhombic *b*-axes are oriented from posterior to anterior edge of each plate (Text-fig. 10). From the observations on the laminary structure and the external pattern of the shell, it appears that each plate enlarges toward anterior from posterior edge with the formation of new lamella on its inner surface.

The above results suggest that the crystalline structure of the shell plates depends upon the growth of the segmented shell.

ii) Pelecypoda (Prismatic and Nacreous layers)

Materials used in this work were right and left valves of 5 aged *Pinctada martensii* and *Pinna attenuata* obtained from Ago Bay in September 1957, and *P. mar-*

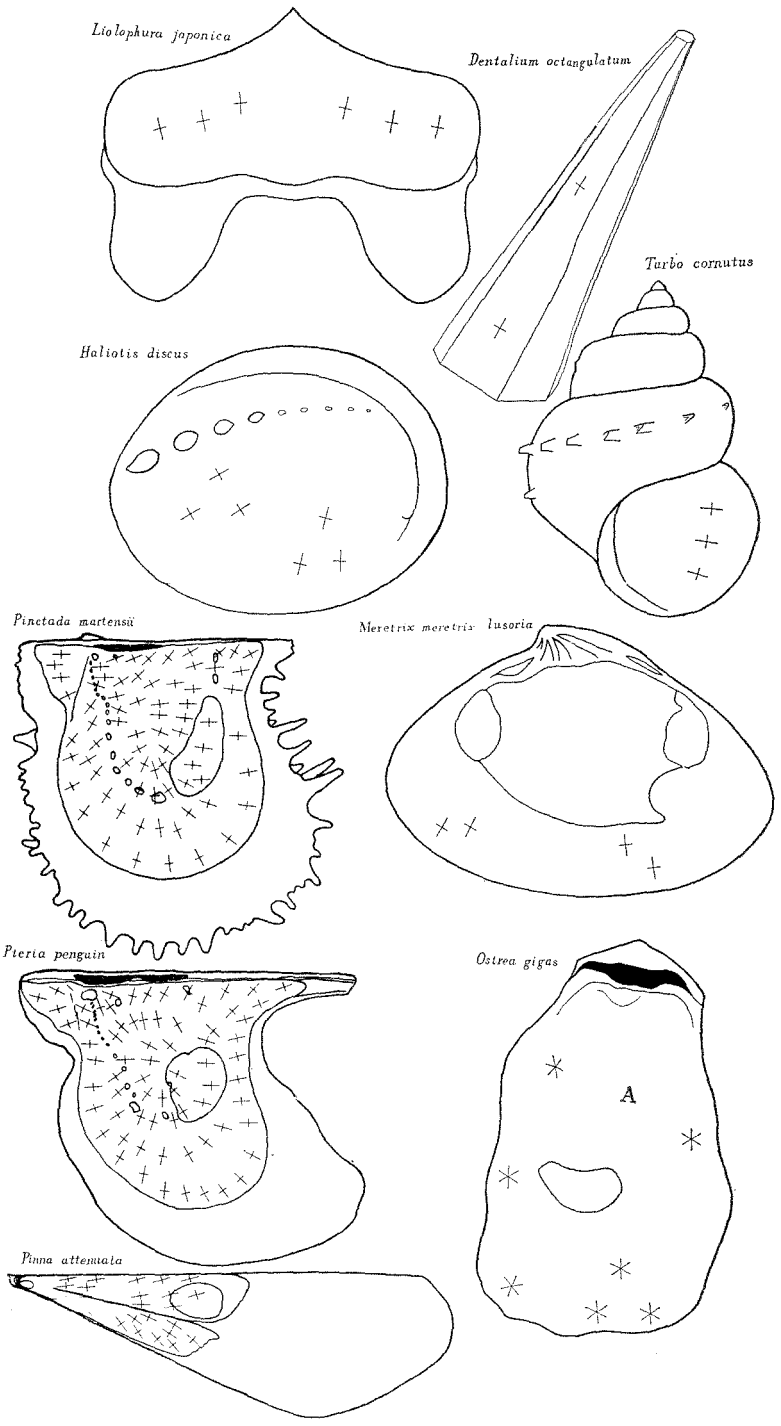
Liolophura japonica
Dentalium octangulatum
Turbo cornutus
Haliotis discus
Pinctada martensii
Meretrix meretrix lusoria
Pteria penguin
Ostrea gigas
A
Pinna attenuata

Text-fig. 10 Diagrams illustrating the crystalline structure of several molluscan shells. The longer straight line of each cross indicates the orthorhombic *b*-axis of micro-crystals in the aragonite shells, and the line indicates calcite *a*-axis in *Ostrea* shell.

garitifera and *P. maxima* from Kagoshima Bay and Arafura Sea, respectively. Besides, *Pteria prenguin* and *Meretrix meretrix lusoria* were used.

For X-ray diffraction analysis, vertical and parallel thin sections of known orientation in the shells were prepared in the following conditions. The shell fragments 10 × 5 mm were removed from various portions of valves, and were polished up to thin sections of about 0.2 mm in thickness for the investigation of two dimensional structure, and of such various thickness as 0.2 mm, 0.5 mm, and 1.0 mm for three dimensional structure. After Laue photographs were taken for all preparations, the relationships between the arrangement of crystallites and growth of the shell were examined by the rotating crystal method. The preparation was set perpendicular to a narrow monochromatic X-ray beam emitted from a copper target in Coolidge tube, and was rotated around a certain fiber axis being exposured to the incident X-ray beam. The reflexion pattern was recorded on a cylindrical film surrounding the preparation. The radius of the camera was 35.4 mm, and the diameter of the second slit used was 0.2 mm or 0.5 mm. The time of exposure was adjusted from 1.5 to 4 hours to different thickness of the preparation. Three directions chosen as rotation axes ran parallel, and at right angles, with the horizontal growth direction of the shell, and vertical to the inner shell surface, respectively.

Figure 42 is the diffraction pattern for a parallel section of the prismatic layer of *Pinna attenuata*, set perpendicular to the incident X-ray beam showing that the layer is built up of relatively coarse particle of micro-crystals which are oriented at random. From this fact and those obtained from polarizing and electron microscopical studies, it is assumed as follows : (1) The prismatic chambers develop independently from each other. (2) Since the layer consists of irregular aggregations of the chambers, $5 \sim 100\mu$ in diameter, it has a scattering effect for X-ray beam as coarse crystallites oriented at random. Although crystallites of calcite grow regularly in each chamber, Debye-Scherrer ring seems to occur in the general prismatic layer by the reason of the above mentioned crystalline structure. Accordingly, for the studies of crystalline structure of the prismatic layer, the diameter of the second slit must be smaller, or else the layer usually indicates Debye-Scherrer ring consisting of many fine grains, as in figure 42. The X-ray diagram shown in figure 43 is an example given by the parallel thin sections of the nacre of *Pinctada martensii* under the same experimental conditions. The position and the intensity of Laue spots occur symmetrically around the axis which runs parallel, or at right angles, with a horizontal growth direction of the layer, and they are diffused to the crescent-shape. It is possible to say from these results that some crystallographic axis of the crystallites of aragonite is roughly parallel with the horizontal growth direction of the nacre in the second dimension of space. X-ray diffraction photographs produced by rotating the different fiber axes in thin sections which are set perpendicular to the

incident X-ray beam are shown in figures 44, 45 and 46. In these photographs, figures 44 and 45 are given by the different fiber axes in a horizontal thin slice, the former being obtained with the direction parallel to the growth direction of a shell and the latter with the direction at right angles to the rotation axis of the former. The diffraction spots occur symmetrically on a series of straight horizontal lines above and below the equator, which is the horizontal line passing through the central spot. Here, the direction chosen as rotation axis can easily be determined by reading off the $\mathcal{L}$ values for all the layer line on Bernal's chart for the reason of that the spacing of the layer lines indicates directly the length of the edge of unit cell parallel to the rotation axis. Then, the spacing measured for figure 44 is about 7.9 Å and agrees well with the length of the orthorhombic *b*-axis of aragonite, that for figure 45 is about 4.9 Å and coincides with the length of the orthorhombic *a*-axis, while that for figure 46 equals to the orthorhombic *c*-axis, being 5.7 Å in length. In these diagrams, each diffraction spot having the form of a short arc must mean that microcrystals in the layer incline each other in a small angle to the certain fiber axis which is in good agreement with the growth direction of shells. Furthermore the fragments from various portions of the layer are more or less different in the reflexion spot, as seen in figures 45 and 50, and the degree of its diffusion becomes larger and larger as the preparation increases in width (Figs. 47 and 48). The symmetry in the position of reflexion spots will suggest that as a whole, their orthorhombic *c*- and *b*- axes are arranged parallel or nearly parallel along the directions of vertical and horizontal growth of the nacre, respectively.

The arrangement of crystallographic axes of aragonite in the inner layer of the nacre is investigated for *Pinctada martensii*, *Pteria penguin* and *Pinna attenuata* by the techniques of X-ray diffraction and conoscope, and is shown schematically in text-figure 10. It is obvious from this diagram that in the marginal regions, the arrangement of the orthorhombic *b*-axis of crystallites correspondes with the horizontal growth direction of the layer, in the central region but its arrangement is complicated. For the understanding of the relationships between crystal arrangement and shell growth, the author has attempted to represent the horizontal growth of the

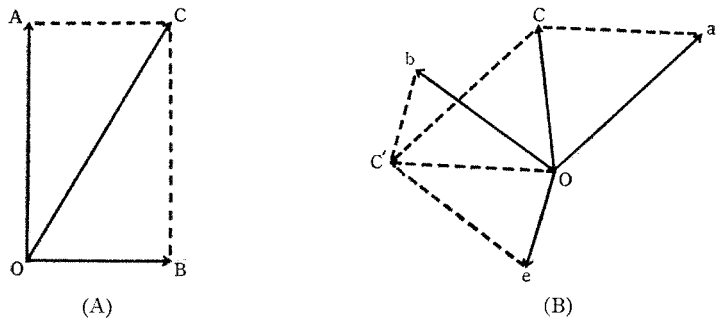

Text-fig. 11 Repersentation by the vectors for the horizontal growth of the nacre.
(A) : marginal regions of the layer, (B) : central regions of the layer.

layer in vectors. The horizontal growth seems to be able to represent the vector $\overline{OC}$ which is the sum of the vectors $\overline{OA}$ and $\overline{OB}$ in the marginal regions, as in text-figure 11 (A). In other words, the horizontal growth of shell is shown as a composition of the two vectors $\overline{OA}$ and $\overline{OB}$ which are represented by magnitude and direction of lines normal and parallel to hinge line, respectively.

$$\overline{OC} = \overline{OA} + \overline{OB}$$

The composited vector $\overline{OC}$ varies in magnitude and direction with portion to portion of the layer, since the magnitude of the lines OA and OB will vary relatively between different portions, and the line OB in anterior and posterior areas of the shell has opposite sign in its direction. That is, the magnitude of the vector $\overline{OB}$ is larger and larger than that of the vector $\overline{OA}$ as we approach from ventral part to anterior and posterior parts. But, in the central region (Text-fig. 11(B)), the horizontal growth may be represented by the vector $\overline{OC}$ which is the composition of the vectors $\overline{Oa}$ and $\overline{OC'}$, and can be expressed by the following equations.

$$\overline{OC'} = \overline{Ob} + \overline{Oc} \qquad \overline{OC} = \overline{Oa} + \overline{OC'}$$

where, the vectors $\overline{Oa}$, $\overline{Ob}$ and $\overline{Oc}$ are magnitude and direction of lines which are parallel to the direction of the translocation of adductor and pallial muscle scars and normal to the dorsal margin, respectively. The direction of the line $\overline{OC}$ is governed strongly by a vector which is the most predominant of them. The vectors $\overline{Oa}$ is more dominant than the other near an adductor muscle scars. And the vector $\overline{OC}$ appears to be the sum of only two vectors of them in such definite areas as that any one of these vectors can be neglected in comparison with others. The horizontal growth direction of the layer is in good agreement with the orthorhombic *b*-axis of crystallites, although that direction is complicated in the central region, as shown in text-figure 10.

Figures 49 and 50 are interesting reflexion photographs for the nacre of *Pinctada martensii*, which are taken in different thickness of the same part of a preparation, figure 49 being obtained with 1～0.5 mm thickness and figure 50 with about 0.2 mm thickness. There are found double spots in figure 49, and the position and intensity of these spots are rather asymmetrical in comparison with those in figure 50. This fact suggests that a particular plane is sandwiched in between 0.8 mm and 0.5 mm distance from the boundary of the nacreous and prismatic layers, and that the part is composed of the accumulation of two different layers which develop in more or less different direcctions. The thickness of these layers coincides with that of the zonal extinction blocks seen under crossed nicols, the latter being about 0.3 ～ 0.8 mm.

An example of the crystalline structure in the order Eulamellibranchia is carried out with the shell of *Meretrix meretrix lusoria* and is illustrated schematically in text-figure 10, showing that the orthorhombic *c*- and *b*-axes of aragonite in its inner layer are elongated in the directions vertical and horizontal to the inner shell surface, respectively. The idea of the author's vector representation, developed in *Pinctada martensii* and the other species of Anisomyaria, can be applied to the orientation of aragonite *b*-axes in the inner layer of *Meretrix* shell, and perhaps to

that of more members of Pelecypoda.

iii) Pelecypoda (Calcitostracum)

The calcitostracum build up the inner layer of *Ostrea*, *Notovola*, and *Chlamys* shells is calcite, the *c*-axis of which is perpendicular to the inner shell surface when the crystals are deposited on that surface. In *Ostrea gigas*, calcite *c*-axis in the chalky deposits runs also nearly vertical to the inner surface. While the orientation of calcite *a*-axis or $[10\bar{1}0]$ in the prismatic layer and the calcitostracum of various species is different considerably from each other. By incident X-ray paralleled to the calcite *c*-axis, the calcitostracum of *Ostrea gigas* generally produces the diffraction pattern as in figure 51. Similarly, that of *Notovola laqueatus* indicates the Laue spot in every portions. The symmetrical pattern in figure 52 is obtained for that layer of *O. gigas* by rotating around a definite direction in the horizontal section, and the rotating axis is the principal axis of calcite. The interlattice spacing calculated from this photodiagram is approximately 6.6 Å, which is equal to the length of *a*-axis in the unit cell of calcite. The *a*-axis orientation thus obtained on several portions of the same material is illustrated in text-figure 10. That *a*-axis orientation is comparatively regular, and appears to be endorsed by the electron microscopic observations in chapter V. The diffusion of the diffraction spots seen in the figure may be due to small inclination of *a*-axis among crystals themselves, to the curvature of the shell, and to the characteristics of the slices. The point A, the central part of the shell, shows the diffraction pattern consisting of some arc-like spots in X-ray analysis, as seen in figure 53, suggesting that the *a*-axis arrangement in that potion is distorted. As mentioned above, the calcite shells also consist of regularly aggregated crystallites. That is, the orientation of calcite *a*-axis in the calcitostracum and the prismatic layer is dependent of the growth of each layer.

While, the *c*-axis orientation of calcium carbonate crystals in the ligament of *Patinopecten yessoensis* is illustrated in text-figure 13, which indicates that the arrangement of crystallites is controlled through biological factors.

iv) Scaphopoda

Dentalium octangulatum has an octagonal horn-like shell, which completely envelops its soft part. Scaphopod shells do not indicate the spiral twist as seen in Gastropod ones, and elongate bending in one plane just like an ivory. Shell substances are attached to the base of the cone with the growth of the animal, and thus the shell grows. As the other groups of mollusca, the shells consist of the mosaic aggregation of aragonite crystals, the *b*-axis of which arranges nearly parallel to a definite direction of the shell. The direction correspondes with the shell length; namely, the growth direction horizontal to the inner shell surface (Text-fig. 10). While, *c*-axis orientation is nearly perpendicular to the inner surface of the shell. In the single crystal methods of X-ray analysis, the parallel sections of Scaphopod shell, in general, reveal the Laue spots diffused arc-like. The thin slices show characteristic directions image of optically biaxial crystal under conoscope.

v) Gastropoda

The apparent results of X-ray analysis on the nacres of *Turbo* and *Haliotis* shells do not always agree with the optical characters of the layer. The mineral component of the layer is aragonite which belongs to optically biaxial crystal, but under conoscope the aragonite of those shells is characteristic of optically uniaxial crystal as that of calcite in the greater part of the layer. The directions image at the certain parts of the microscope stage is distorted in a definite orientation. In several portions of the same preparation, the image exhibits the characteristic of aragonite, though the apparent optical angle is very small as compared with that of aragonite.

Figure 54 is X-ray diffraction diagram given by the thin slice of *Haliotis* shell cut almost perpendicular to aragonite *c*-axis of the layer, suggesting that aragonite crystals in the layer arrange in regular manner. But, the degree of perfection of the arrangement differs considerably from portion to portion of the nacre, and aragonite *b*-axis arrangement dose not see in some portions. Moreover, X-ray reflection pattern is varied with the difference in the thickness of the section. Therefore, it may be considered that the slip of mineral lamellae, in which aragonite *b*-axis runs nearly parallel with a definite direction, occurs in the process of the accumulation of the lamellae. The vector of the slip is controlled by the elongation and the movement of the mantle. The greater the curvature and the twist of shells, the larger the direction of the vector inclines. This conclusion is verified from the result that the slip of the lamellae in *Haliotis* shell is less than that in *Turbo* shell.

The above mentioned abnormality of directions image of the layer may be induced in the following five cases:

1) Disorder of crystal arrangement in one lamella.
2) Slip of the mineral lamellae in the third dimension of space.
3) Sections are cut obliquely to aragonite *c*-axis.
4) Twinning of aragonite crystals in the lamella.
5) Isomorphous minerals of aragonite type.

The first three are very often found in Gastropoda and the other groups of mollusca. Such disorder and slip appear to regularly occur through the biological factors. And in oblique sections the apparent optical angle is always larger. The last one depends chiefly upon the chemical components and crystal structure, however, it may be impossible from the results of X-ray and chemical analysis.

The crystalline structure of the nacres in *Haliotis discus* and *Turbo cornutus* is shown in text-figure 10, which indicates that the nacres consist of the mosaic arrangement of micro-crystals all having their orthorhombic *c*- and *b*-axes parallel or nearly parallel to the vertical and horizontal growth directions of the layer as that of Pelecypod shells. Generally speaking, Gastropoda has a spirally coiled shell emitting from an umbo through the general equation $r = f(\psi)\, e^{\frac{\theta}{\tan \lambda_0}}$ (Fukutomi 1953). The size of the shells increases by the growth at the margin of their apertures; namely, their elongation in the direction of the coiling may be induced by the

horizontal growth of the nacres in Gastropod shells. Therefore, the orientation of aragonite *b*-axis in the layer coincides well with the horizontal growth of the shell, and will also possibly be determined by the vector analysis which is attempted in Pelecipoda. The *c*-axis orientation in Gastropod shells is somewhat complex as compared with that in Pelecypod shells because the degree of the curvature of the former is larger than that in the latter. Calcium deposition in *Turbo* shell may not be carried out in whole inner surface of the shell but only in the limited area near its aperture. In *Haliotis* shell, the orthorhombic *c*-axis of aragonite in the inner layer elongates inclining a little to the inner surface (Fig.55). Moreover, *c*-axis orientation in more sharply curved areas of the shell changes more or less between upper and lower layers in the same portion, as seen in text-figure 14, B. To understand *c*-axis orientation in molluscan shells, we need to observe the condition of contact between the mantle and shell, and to investigate the effect of changes in the curvature of the inner shell surface during the increase in thickness of the shell. The condition of contact is different among various species, and the changes of the curvature of the inner shell surface is due to the twist of the visceral mass and to local variation of calcium deposition in the development of animals. That is, *c*-axis orientation is correlated with the changes in the curvature of shell, which are under the control of the biological and physicochemical factors, as explained in text-figure 13. The results may suggest that *c*-axis orientation is almost perpendicular to the boundary face of the mantle and shell.

vi) Cephalopoda

Cephalopoda is the most highly developed animals in invertebrates, and the several members in this group have a calcareous shell, but the others have only a horny vestige or no shell. *Argonauta argo* belonging to the order Nautiloidea has a large external spiral shell protecting its soft part. While *Sepia kobiensis* has a vessel-shaped shell embeded in the mantle. The mineral component of the former is calcite, and that of the latter aragonite. The comparative studies on the crystalline structure between external and internal calcalious shells will give us an excellent proof to elucidate the factor playing a directing role on crystal arrangement in the mineralized tissue.

In *Argonauta* shell, it is found by X-ray analysis that calcite *c*-axis is nearly perpendicular to inner surface. The *a*-axis or other crystallographic element of calcite in the shell appears to depond upon the growth of the shell in each lamella of every portions. The shell shows the optical characteristic of aragonite but not of calcite. That optical abnormality may probably be caused by the slip of mineral lamellae through the twist of the shell, as seen in Gastropod shell. That is, the slip of lamellae in the spiral coiling shells is not essentially different from the slip occurring in discontinuous layers of Pelecypod shells. The spiral coiling shell is considered to consist of the accumulation of each lamella slightly slipping in a definite direction through the twist of the shell. Such slip seems to occur, of course, in more sharply curved portions of Pelecypod shells. The longitudinal section of *Sepia* shell

is shown in figure 13. The shell consists of many chambers which are appended on the ventral side being surrounded by the anterior and posterior walls of siphuncle. Two elements are found in the formation of the chamber; the one is so-called "septa" which is thin mineral lamella. The other is "trabecula", which is thin mineral wall joinning adjacent septa, and is almost perpendicular to the septa. Now, if we make the thin slice cut vertically to the septa and take the trabecula as rotation axis, X-ray diffraction pattern is produced by the preparation as in figure 57. But, by incident X-ray which is vertical to the septa, the shell reveals the Debye-Scherrer ring in reflection pattern (Fig.56). The interlattice spacing calculated from the pattern in figure 57 completely accords with the length of *c*-axis in the unit cell of aragonite. That is, aragonite *c*-axis in the shell is nearly perpendicular to the septa; in other word, *c*-axis orientation is parallel to the trabeculae intersecting obliquely the posterior wall of the siphuncle since the septa slop downwards to that wall. While the orthorhombic *b*-axis of aragonite in the septa does not indicate such a parallel occurrence as seen in the other groups of mollusca with aragonite shell, and reveals rather irregular aggregation in X-ray analysis. The *c*-axis orientation in the posterior wall was not determined in the present investigation.

7 The relationships between crystal arrangement and mantle tissue

For the investigation of the factor which influences the arrangement of crystallites in the nacre, mantle transplantation was carried out with *Pinctada martensii* by the modified method of operation in pearl culture industry during the period from June to August in 1959. Namely, a piece of the mantle tissue, about 1 × 2 mm in dimension, was placed between two pieces of cover glass about 2 × 3 mm in size, and then was inserted into adductor muscle of another pearl oyster. For 10 days after operation, the cover glass was taken out from the adductor muscle at the interval of 2 days, and the living epithelium of the grafted mantle tissue was observed directly under the optical microscope. On the other hand, after cultivation for 1 or 2 months, the fragments of the inserted glass were collected, and the nacreous alyer formed was removed from the glass surface. Then the nacre was polished up to thin slices parallel to its surface, and these preparations were investigated for the arrangement of the crystallographic axis under the conoscope. The epithelial cells of the grafted mantle tissue were rearranged entirely in a few days after transplantation in summer as follows: The epithelial cells, at first, were elongated out from the definite cut surfaces of grafts, moved actively away from grafts, and then separated from one another. Secretion was introduced successively throughout the regenerated epithelium. Meanwhile the epithelial cells themselves were rearranged over the foreign substance and no longer wandered about. Therefore, it appears that the elongation and the movement of the epithelium during multiplication are never at random. Figures 58 and 59 show the transformed mantle piece investigated 4 days after the operation. The fibrous cells elongate out considerably from the definite cut surface of grafts, which crosses the major axis of the longitudinal muscular

bundle in the introduced mantle tissue. The direction of the elongation of the fibrous cells is very often in good agreement with the major axis of the longitudinal muscular fibres, and it appears that the epithelial cells of the transplanted mantle tissue have the tendency to largely elongate parallel to certain direction. Such phenomenon is thought to be due to the original polarity of these cells. But the elongation of the epithelium is considered to be varied slightly with the condition of cut surfaces of the grafted mantle piece and with the condition of the contact between grafts and foreign matters in the observation of several transplanted mantle.

The crystalline structure is investigated on the nacre formed by the secretive activity of the rearranged epithelium which is originated from the grafted mantle, and an example of it is illustrated schematically in figure 60. In the figure, it is assumed that the point O is the adhered part of the graft, since the prismatic substances are deposited in the dotted area, and, as have already been described in the author's separate paper, the size of the prismatic substances is smaller at the point nearer O, and the remarkable adhesion of organic matters is recognized in that point O. Aragonite crystals in the nacre develop by parallel growth, and their orthorhombic *b*-axes run nearly parallel from the point O toward the opposite side. And, in most case, they do not exhibit the radial arrangement emitting from the point O.

From the above mentioned experiments, it will be possible to be clear the relationships between crystal arrangement and the elongation of mantle as follows: The orthorhombic *b*-axis of crystallites of aragonite in the nacre is alike in parallel to the horizontal growth direction of the layer, in which, in general, the epithelial cells of the transplanted mantle piece are elongated powerfully through cell division. The elongation and the state of the mantle tissue may therefore be thought to be a main element which governs the arrangement of crystallites, and this theoritical idea is not contradictory to the crystalline structures resulted in the life of these shell-fishes. What is the determing factor on *c*-axis orientation? In the Japanese pearl culture, if a foreign substance is laid between the valve and the mantle, *c*-axis orientation of the mineral lamellae formed on the surface of the

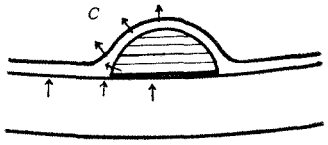

Text-fig. 12 Aragonite *c*-axis orientation in the nacreous layer formed on the surface of a foreign substance which is laid between the valve and the mantle.

foreign substance is nearly perpendicular to the growing surface at that time when the lamellae are mineralized, as shown in text-figure 12. The *c*-axis orientation, in other words, elongats perpendicularlly to the boundary face of the mineral lamella and the shell-forming tissue.

8 Discussion

It may be interesting to geologists and biologists that the shells crystallized out from the mother fluid which is produced by Ca metabolism in a life are characterized in mineral components and crystalline structure, as have been observed in this chapter. In particular, special attentions will be paid undoubtedly to (a) polymorphism of calcium carbonate, (b) the mosaic aggregations of crystallites and (c) structural difference between the nacreous and prismatic layers. The most important characteristic is that biological and biochemical factors affect usually all processes of shell mineralization.

Aragonite is a common mineral of inanimate objects irrespective of that mineral is metastable under ordinary conditions, and is optically biaxial negative in the orthorhombic system. Calcite belonging to the hexagonal system is a stable form of $CaCO_3$ and shows optically uniaxial negative. They show a typical example of polymorphism. In inanimate occurrences, the anhydrous carbonates are crystallized out either aragonite type or calcite type under the definite conditions of the mother fluid. That is, Magnesite, $MgCO_3$, Siderite, $FeCO_3$, Rhodochrosite, $MnCO_3$, etc. belong to calcite group, and Bromlite, $(Ca,Ba)CO_3$, Strontianite, $SrCO_3$, Cerussite, $PbCO_3$, belong to aragonite group. These minerals in each group exhibit isomorphism. Untill now, a large number of literatures about the polymorphism of calcium carbonate of inanimate objects or experimental preparations was made by Oesterr (1915), Saylor (1928), Bragg (1937), Takubo (1952), and Togari *et al.* (1955). They have reported that the formation of aragonite is promoted rather than calcite when carbon dioxide, alkali carbonate, or urea is included excessively in their mother fluid, and that the development of metastable forms is fosterred as temperature increases under the presence of divalent cations. The formation of aragonite is found in a high pH region of hot springs. It was pointed out by Saylor that organic anions in shell-fishes have a same effect as urea and alkali carbonate, and inhibit the development of crystal nucleus of calcite. According to his report, organic anions are adsorbed on calcite and prevent its growth, favoring the development of aragonite. Bragg (1937) stated that the divalent cations which are smaller in the ionic radii than calcium build carbonate of the calcite type, while those which are larger than calcium build carbonates of the aragonite type, suggesting that the ionic size of the divalent cations is the limiting factor on the structure of the carbonates. It was elucidated by Takubo *et al.* (1952) that the variation of the dielectric constants of such polymorphus minerals as aragonite and calcite depends chiefly on the chemical components and is in close relation with crystal structures. We shall pay a great attention to that the carbonic anhydrase is found in the shell-fishes with aragonite valve, whereas it is absent from the ones with calcite (Stolkowski 1951). Aragonite in molluscan shells is considerably different from that of inorganic occurrence by the presence of organic substances and the mother fluid prepared through the complex biochemical reactions. However, the high pH value and the high temperature can never hap-

pen in living organisms under normal physiological conditions, and some artificially added factors in the laboratory experiment are lacking in the shell mineralization under natural conditions. After all we must lead to the conclusion that the organic substance introduced through the mantle epithelium, carbonic anhydrase itself or HCO_3^- occurred in the reaction $CO_2 + H_2O \rightleftarrows H_2CO_3$, $H_2CO_3 \rightleftarrows HCO_3^- + H^+$, and such divalent cations as Mg, Mn, Pb, or Sr, closely relate with the production of polymorph of shell calcium carbonate. But the amount of the divalent cations contained in the shells is more different among various species and different habitats rather than the difference between calcite and aragonite shells. For instance, the amount of magnesium in the Cephalopod shell is the largest of all molluscan shells, and the inorganic constituents in the aragonite shells are very different according to various species, physiological characteristics, and ecological factors. If the relative ratio of the divalent cations in shell lime salts is in proportion to that of the divalent cations in the mother fluid and specializes among various species, anyone will not be able to affirm that in molluscs, the divalent cations of the mother fluid are the determining factor on the structure of carbonate.

Even if carbonic anhydrase which catalizes the above chemical reaction is thought to be related to the polymorphism of shells, the enzyme itself may not directly determine the structure of calcium carbonate, but associates with the supply of HCO_3^- and HCO^-, excess of which favors the formation of aragonite. This consideration comes from the following reasons. (1) The presence of carbonic anhydrase does not always coincided with the aragonite formation. (2) The enzyme is absent in the ground of shell mineralization, in the mother fluid, even though it exists in the mantle tissue (Kawai 1959. Personal communication). (3) Therefore, if the enzyme has a directing influence on shell mineralization, calcium carbonate must already be crystallized in a form of either aragonite or calcite within the mantle tissue.

As mentioned above, "enzyme theory" has some unsuitable facts. The author has described that a quality of some organic substances, in particular of conchiolin, is the most important determining factor on that polymorphism since the ratio of organic substance to mineral substance is not related to the formation of aragonite or calcite in calcification. The author will notice to the connection between atom or molecure in the organic material and calcium in the lattice of aragonite or calcite to clear up the mechanism of deposition and structure of calcium carbonate in the shell mineralization. According to Grégoire's (1955, 1958) and Tanaka's (1960) aspects on conchiolin, it is evident that the protein is somewhat different in structure and in amino acid components between aragonite and calcite shell materials. Harada *et al.* (1957) have reported that the dielectric constants of the mother fluid may be closely related to the crystal structure of calcium carbonate. In all cases, the investigations on the polymorphism of calcium carbonate in living organisms meet with various difficulties.

Shells are complex systems of organic matter and lime salt, and are crystalline substance separated from the mother fluid prepared through the mantle epithelium.

The prismatic layer is mostly composed of a honeycomb-like aggregations of polygonal prismatic chambers about 5～100μ in diameter, in which calcite crysals are piled up alternately with organic matter. The crystals exhibit, in general, spindle or tabular shape, and are less than 2μ in size. However, since organic matter sandwiched between adjacent chambers elongates as thick perpendicular wall from the outer side of the layer toward the inner side, the layer is predominant in columnar structure rather than laminary structure. Various stages of calcification are found in different parts of the same prismatic layer and crystalline material is also revealed in organic substance. In contrast with the prismatic layer, the nacreous layer shows the laminary structure and has no thick wall of organic matter, though thin organic membrane exists between individual crystals. The crystals are generally a hexagonal tabular, and the amount of the organic substance between crystals or lamellae is less than that in the prismatic layer. That is, structural characteristics of the prismatic and nacreous layers are caused by the difference of the spatial relationships between crystallites and organic matrix, and seem to result from the proper mode of crystal growth in each layer. It is therefore considered that the organic matter in shells is concerned directly with crystal growth and mineralization of the layers, and that the kind and structure of the organic matter play important roles in the process of calcification. The prismatic layer is not a single crystal as not the nacre, and consists of irregular aggregations of polygonal prismatic chambers. The development of the chamber is independent of each other and has no connection with the elongation of the mantle tissue. But crystallites of calcite grow independently by certain rules in each chamber, which very often shows the extinction as a single crystal or spherulite under crossed nicols. While calcite *a*-axis or $[10\bar{1}0]$ of *Ostrea* shell may run parallel with the horizontal growth of a lamella. Calcite in the calcitostracum seems to grow in close relation to the elongation of the mantle and the organic matrix. The nacres are somewhat different in crystalline structure from the prismatic layers, and consist of the mosaic arrangement of minute aragonite crystals all having the orthorhombic *b*- and *c*-axis parallel to the fiber axes, which run along the growth direction horizontal and vertical to the inner shell surface, respectively. Therefore, the *b*-axis arrangement of growing crystals on the nacreous surface is considered to be affected directly or indirectly by the elongation and the tension of the shell-forming tissue, which are in good agreement with the horizontal growth. But the orientation of aragonite *b*-axis in *Sepia* shell is at random having no relation to the shell growth, and differes from that of other groups. This shell is characteristically embedded in the mantle. Is that at random arrangement of the *b*-axis derived from such special mode of the shell formation? In the spherical pearl formation, a pearl is similarly completely enveloped by the epithelial tissue of the pearl-sac, which means that pearls are internal production in the epithelium derived from the grafted mantle piece. Nevertheless, aragonite *b*-axis of the nacre of the pearls is regularly oriented in close connection with the growth of the layer. This fact seems to suggest that the

difference in crystallographic axis arrangement is not due to the property of mineralization between internal and external shells but rather to the tension of the shell-forming tissue.

Crystals in inanimate objects very often grow with their *c*-axes parallel to a definite orientation. The property of *c*-axis orientation of crystals in the organisms will be described below. The relationships between the shell-forming tissue and *c*-axis orientation of shells are schematically shown in text-figure 13, which indicates

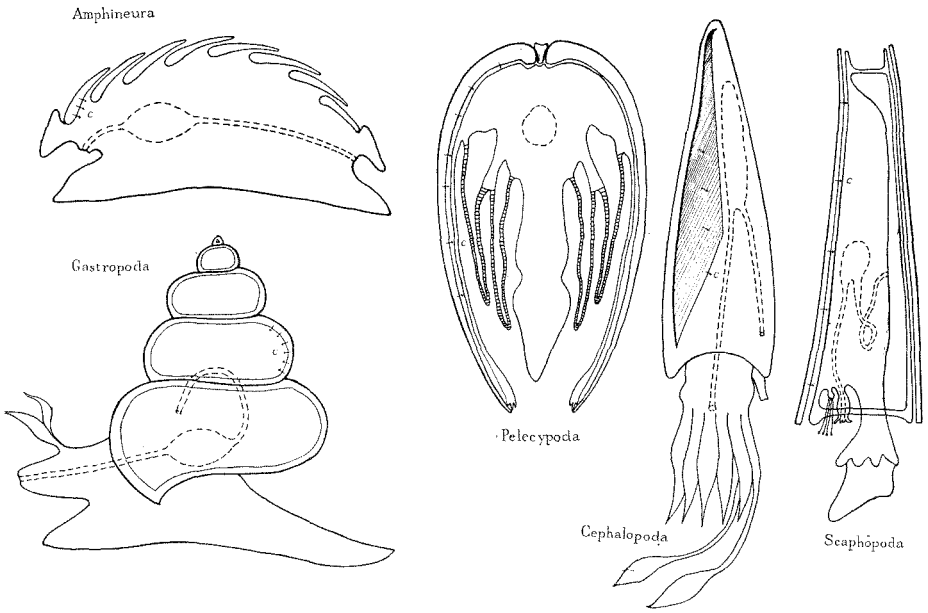

Text-fig. 13 The relationships between *c*-axis orientation in shells and the surrounding tissue indicate diagramatically in various groups.

that *c*-axis orientation is nearly perpendicular to the boundary face of the mantle and the shell in all groups. For instance, *c*-axis orientation is perpendicular to or inclines at small angles to the growing surface in the segmented shell of Chiton, in the coiling shells of Gastropoda and Cephalopoda, in the prismatic and nacreous layers of Pelecypoda, in the internal shell of *Sepia*, etc.. These results seem to mean that the vector of the growth of the mineralized tissue plays the role as the controlling factor on *c*-axis orientation in the organisms. If the vector of the shell growth is different in every species and various stages of the development of animals, *c*-axis orientation may be somewhat different in each shell and in each layer formed in various ages. Hynd (1954) and Ōta (1956) have suggested with the genus *Pinctada* that the growth ratio in the weight or the size of the shells is varied clearly with age and environment. They stated that the obliquity of the shells decreases with age. And we have already known that a resting zone or plane is formed when the growth of shell lime salts stops perfectly under abnormal conditions and unsuitable environment; for

instance, in winter when sea water temperature falls below 13° C. It has also been pointed out by the author that the layers above and below a resting zone are different in laminary structure, and that in most case, the horizontal growth direction of the upper layer is inclined at small angle to that of the lower layer. Hence, the orientation of orthorhombic *b*-axis of the crystallites is more or less different between two discontinuous layers accumulated successively. The three dimensional relationships between the arrangement of crystallites and the development of the nacre in the increasing age can be understood readily in text-figure 14, and can also be explained by the representation of the vector. The characteristic reflexion pattern of the nacres is due to the difference of the superficial and internal structures as mentioned above, and the position, shape, and intensity of the reflexion spots appear to be characterized by how crystallites arrange on the growing surface and in the internal part of the layer. Similarly, the optical abnormality of aragonite building up the shells, must be caused by the slip of mineral lamellae in third dimension of space, and by the disorder of crystal arrangement in second dimension of space during the growth of the shells.

As mentioned above, the shell structure is somewhat different in every species, but the crystalline structure is not different essentially among various species and is dependent on the dynamic forces in the mantle and the elongation of the organic matrix. The shell structure indicates the most profound varieties by the difference of spatial relationships between organic and inorganic components rather than by the structure of calcium carbonate. If the author must take notice of the structure of crystal, he shall point out variant crystalline structures seen among prismatic layer and calcite shells.

Although the present study on the crystalline structure of molluscan shells is limited only to the accumulation of the experimental data, the author should be propose the following idea from these data.

"Crystallographic axis arrangement of the mineralized tissues in organisms is controlled directly or indirectly by the elongation and the tension of the shell-forming tissue during the growth of animals. In the mineralization processes of the shells, a definite current is seen to be produced in the mother fluid by that dynamic forces in the mantle and then the current affects the crystal growth. As the most important role, those such forces must have the influence on the directing formation of organic matrix which is first formed in the shell mineralization. Then, the fibrous structure seen in the shells is assumed to be the result of epitaxial growth of the organic matrix and calcium carbonate crystals. However, since the elongation and the tension in the shell-forming tissue may be changed with such biological properties as ontogenical, ecological, and biochemical differences in every species, *c*-axis orientation of micro-crystals within a layer is not always perpendicular to the inner surface. And aragonite *c*- and *b*-axes show the disorder in one plane, there occurs slip of mineral lamellae in the accumulation of layers through the biological rules." This idea would be developed not only in all molluscan shells, but also in mineralized tissues of other organisms. Moreover, the general relation must be

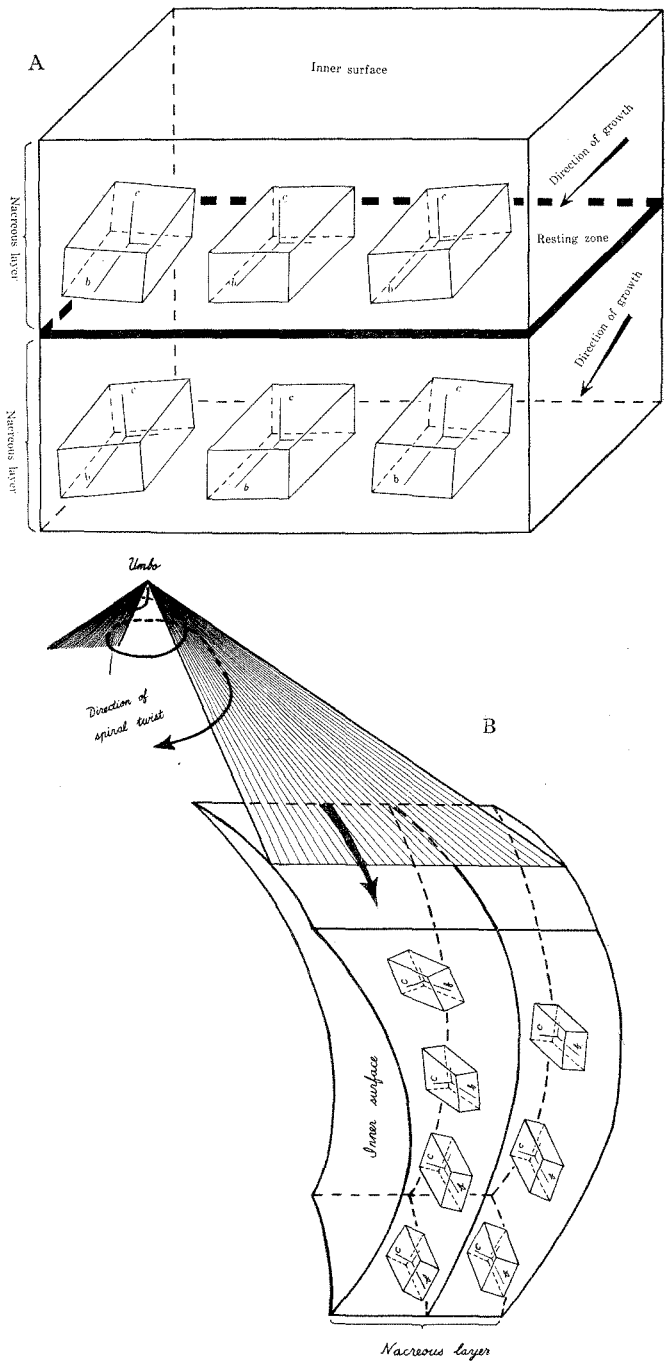

Text-fig. 14 Three dimensional representation of the relationships between the arrangement of aragonite crystal and the accumulation of the nacreous layer during shell growth. A : Pelecypod shell, B : Gastropod shell.

found between the mineralization mode and the crystalline structure of the calcarious tissues (Bourne 1956, Raup 1959, 1960).

9 Summary

1) Mineral component and structure of mollusean shells were examined by differential thermal analysis, X-ray diffraction, and electron microscope, and the results were discussed from the viewpoint of biocrystallography.
2) The nacres exhibited the laminary structure regularly accumulated with organic membrane and aragonite crystal, and consisted of the double fiber structure which was mosaic arrangements of crystallites, the ortherhombic *b*- and *c*-axes of which all ran in parallel or nearly parallel with the horizontal and vertical growth directions of the layer. It appeared that growing crystals on the inner surface were governed directly or indirectly by the elongation and the tension of the shell-forming tissue.
3) The prismatic layer in *Pinctada martensii* consisted of irregular aggregations of polygonal prismatic chambers, 5～100 μ in diameter, each of which is composed of canine-shaped sub-chambers, 5～30 μ in diameter, which were divided into micro-chambers, 2～15 μ in diameter, and showed predominantly columnar structure. The crystallites of calcite in each polygonal prismatic chamber were arranged by definite formulae, and these chambers themselves appeared to have no connection with the elongation of the mantle.
4) It seems that the organic matter secreted by the mantle expithelium plays important roles when shell salts are separated from the mother fluid.
5) Crystalline structure of shell was investigated on all groupes of molluscs.
6) Polymorphism of calcium carbonate crystal in molluscan shells was discussed.

Chapter III

The Organic Matrix of Shell

1 Introduction

Organic substance in molluscan shells has been known commonly as conchiolin and is considered to be a kind of albuminoid. Many workers have examined on the amino acid constituents of this protein by the techniques of paper chromatography. According to Grégoire *et al.* (1955), conchiolin consists of three fractions; water-soluble protein, scleroprotein, and polypeptide, which are somewhat different from each other in the amino acid constituent and morphorogical feature. Recently, mucopolysaccharide are observed histochemically in the organic matrix of the shells (Tsujii 1955 etc.).

The distribution of organic component in the nacre is studied by the electron microscope, and it has reported that the intercrystallinic and interlamellar organic matters exhibit reticular structure (Grégoire 1958). Organic substances in the mother fluid are considered to be secreted from mucous cells between the epithelial cells of the outer surface of the mantle and to play important roles on calcium transportation and on polymorphism of calcium carbonate in the shell. Organic component itself is transformed into conchiolin in shell mineralization. However, organic matrix is formed before the deposition of mineral matters and appears to be in close relation to the arrangement and the growth of mineral component during the process of shell formation. The author will investigate morphological and crystallographical structures of conchiolin to elucidate spatial relationships between mineral and organic components.

2 Materials and Methods

The specimens used in this work consist of *Pinctada martensii*, *P. margaritifera* and *P. maxima*. Small fragments removed from each material were decalcified with 10% aqueous solution of ethylenediaminetetra-acetic acid disodium salt at pH 7.5~8.0. For electron microscope, ultra thin sections were prepared in the following process. Fragments of decalcified shells were fixed with 0.5% osmic acid. The specimens embeded in the plastic were cut with a glass knife.

To be used for low-angle and high-angle X-ray diffraction, an organic matter, a decalcified shell, was washed sufficiently in distilled water and was dried at room temperature. X-ray powder diffraction was carried out by the same experimental conditions described in chapter II. And X-ray reflexion diagram for fragments of the organic matters was recorded on a cylindrical film. The exposed time was about 4 hours. On the other hand, organic matter was pulverized by using an agate mortar for differential thermal analysis. This analysis was done under the experimental conditions as described in chapter II and further was also performed in vacuum.

3 X-ray diffraction analysis of decalcified shell materials

Text-figure 15 is X-ray powder data of the organic matters in *P. martensii*. S-4 and S- are obtained by the dry specimens of decalcified prismatic and nacreous substances, respectively. In both case, two broad reflexion peaks are seen between 8° and 14°, and 16° and 25° in 2 θ. The interlattice spacings calculated from this

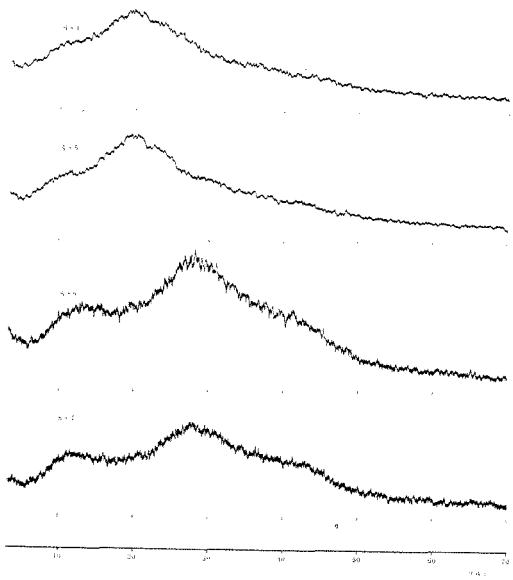

Text-fig. 15 X-ray diffraction data for conchiolin of the pearl oyster.
S—4 dry conchiolin of the prismatic layer
S—5 dry conchiolin of the nacreous layer
S—6 wet conchiolin of the prismatic layer
S—7 wet conchiolin of the nacreous layer

pattern are 7.89 Å and 4.35 Å on the average, and vary with conditions of specimens. The lattice spacings comparatively agree with those given by the powder specimens of *P. maxima* and keratin of wool. S-6 and S-7 are X-ray reflexion for the wet specimens corresponding to S-4 and S-5, respectively. Two broad reflexions mentioned above remove to between 9° and 16°, and 24° and 32° in 2 θ, and each spacing is about 6.41 Å and 3.15 Å.

X-ray photograph for the organic matters is shown in figure 61, and is given by incident X-ray beam parallel to the axis which stands vertically to the inner shell surface. The reflexion pattern shows Debye-Scherrer ring with halos and coincides in spacing with that of X-ray diffractometer. But, such fiber diagrams as found in keratin and collargen fibers can not be found in this pattern. At present, low-angle and high-angle X-ray diffractions are under investigation for the organic matters of shells by the devised techniques.

4 Differential thermal analysis for decalcified shell materials

The organic matters in the shell and several kind of amino acid are examined by differential thermal analysis, and its results are plotted in text-figure 16. The first three curves N-16, N-17 and N-18 are given respectively by phenylalanine, alanine and

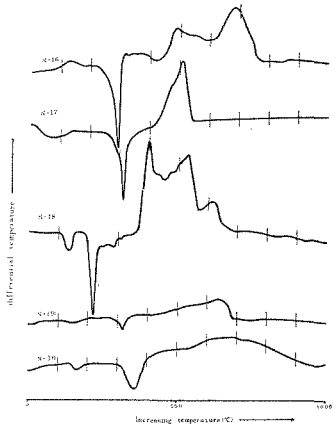

Text-fig. 16 Differential thermal anaIysis curves of conchiolin in the pearl oyster shell and several amino acids.
N—16 phenylalanine
N—17 alanine
N—18 glutamic acid
N—19 conchiolin of the prismatic layer
N—20 conchiolin of the nacreous layer

glutamic acid, which are amino acid contained greatly in the organic matters of mollusean shells. From these curves, generally speaking, amino acid has a sharp endothermic break in the range of 150°C to 380°C and one or more exothermic peaks between 350°C and 800°C. Besides, the curve of glutamic acid has a distinct endothermic break at about 130°C. These endothermic reactions seem to be due to the meltimg or the dissolution of amino acid and are somewhat different by the kind of amino acid. In differential thermal analysis curves for the organic matters in the prismatic and nacreous layers of *P. martensii*, small endothermic break is seen near 150°C, and larger broad endothermic break occurs between 300°C and 400°C (curves N-10 and N-11). The second endothermic break is considered to be due to the sum of the melting or the dissolution of contained amino acides in the organic matters. Thereafter, since the specimens begin to burn near 450°C, the exothermic peak takes place with increasing temperature.

On the other hand, in vacuum condition, all these specimens prove new characteristic curves instead of the exothermic peak, and also similar endothermic break, at 300~400°C (Text-fig.17). The techniques of differential thermal analysis may be applied for organic matters since thermal reaction depend upon the kind of amino acid.

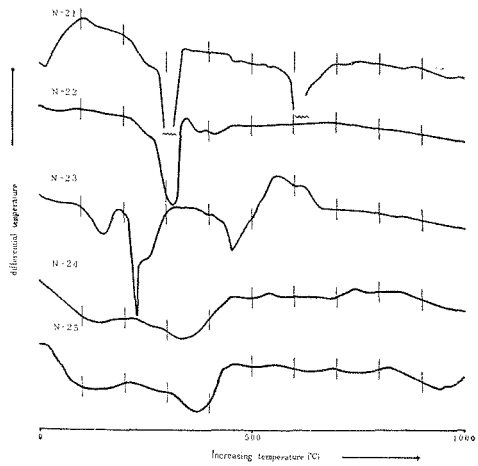

Text-fig. 17 Differential thermal analysis curves for the same specimens in text-fig. 16 in vacuum.
N—21 phenylalanine
N—22 alanine
N—23 glutamic acid
N—24 conchiolin of the prismatic layer
N—25 conchiolin of the nacreous layer

5 Electron microscopic observation on shell organic matters.

Unstained ultra thin sections of the decalcified specimens were first observed by the phase contrast microscope. Topography of organic matters in the prismatic layer is shown in figure 62. The darker parts are the organic matter cementing mineral salts which are compacted in the lighter parts. The organic interprismatic wall also indicates a laminary pattern, and the organic interlamellar membrane appears to be formed as continuous formations passing through each chamber (Fig. 62). Figures 64, 65 and 66 are electron micrographs showing the micro-structure of the conchiolin walls. This wall appears to consist of bead-like coards, which elongate in parallel with the long axis of the wall and are 700～1000 mμ in width. The interval of the cross-bands is 300～400 mμ at the center of figure 64. In figure 65 the coards are about 270 mμ in width and the interval of cross-bands is measured to be about 180 mμ. At high magnification, fibrous structure is observed in the organic interprismatic wall, but this structure is thought to be artifacts (Fig. 66). Microincineration of the horizontal section of decalcified prismatic layer is shown in figure 63. It is confirmed from this figure that inorganic matters are present in the organic matrix, though the mode of the combination of these inorganic matters and organic matrix is not yet clear.

On the other hand, the organic matter of the nacre exhibits membraneous or fibrous appearance in vertical section under optical microscopes (Fig. 67). The surface of the organic matter reveals reticular or fibrous structure showing the

lace-like appearance, as seen in figure 90. The organic interlamellar substance running between neighbouring crystal lamellae may consist of one or more fibres or membranes, which reveal bead-like structure, and many holes are observed in that substance (Fig. 68). The interval of cross-bands in the bead-like fibre is about 100~200 mμ. The adjacent interlamellar membranes are connected by the intercrystallinic membrane, and in general, unit crystal is surrounded perfectly by these membranes (Fig. 68). Horizontal sections of the decalcified nacreous layer always extinct independently of the direction of the incident light under crossed nicols. While its longitudinal sections show double reflection in one given direction, and conchiolin membrane of the nacre shows straight extinction in horizontal growth direction of the layer. These results may suggest that z-axis is vertical to the inner shell surface, and that, as a whole, the nacreous conchiolin elongates alike in the fibre axis which run parallel with the horizontal growth of the layer.

6 Discussion

Conchiolin, organic matter in molluscan shells, has been assumed to be analogus to keratin. Recently, the organic matter in mother-of-pearl of molluscan shells was divided into three elements of water soluble protein, scleroprotein, and polypeptide from the bases of structure and amino acid constituents. And in comparison with the structural elements of chitin of insects, they were called "nacrine", "nacrosclerotine", and "nacroïne", respectively (Grégoire, Duchâtean and Florkin 1955). Grégoire (1957) reported that in the pattern of structure, the reticulated membranes of conchiolin were assorted into three classes such as the Nautiloid pattern, the Gastropod pattern, and Pelecypod pattern, which were characterized by the shape, the size, and the dens of hole, or by the shape and the size of the trabeculae. The reticulated membrane of the nacreous conchiolin of *Pinctada martensii* has the characteristics of the just described Pelecypod pattern. In ultra thin section of the nacreous conchiolin, the holes also is observed here and there in the membrane (Fig. 68). The organic matter in shells appears to be composed of conchiolin fibres or coards with linearly aligned fine granulars. The orientation of the fibres or the coards is comparatively regular, and coincides with the horizontal growth direction in the nacre, and with the vertical growth direction in the prismatic layer. But some micro-structures, the artifacts, occur in the preparation (decalcification, fixation, cutting), and intermineral matrix and the elements of conchiolin must be variously altered in size and thickness.

The interlattice spacings of the organic matrix in the prismatic and nacreous layers are similar between each other and change under different experimental conditions of specimens such as wet or dryness. Conchiolin is considered to consist of two elements which show Deby-Scherrer ring and halos in X-ray diffraction analysis. In the present experiments, the smallest periodicity of conchiolin (i.e., unit cell) could not be determined. The above mentioned results seem to be due

to that the techniques of X-ray analysis are unsuitable for the studies of the organic matters in shell, to that its structure is broken in the process of decalcification, or to that it consists of noncrystalline material or is amorphous. Although microstructure of the organic matter could not be determined by X-ray diffraction methods, the results obtained from polarizing and electron microscopic observations suggested that conchiolin elongated towards a definite orientation, which was assumed to agree with the growth directions of the layers. It is considered that in shell formation, the organic matrix formed at first is governed by the tension and the elongation of the mantle and affects the deposition of mineral matters. Moreover, a little amounts of calcium may be to the organic ones.

7 Summary

1) The organic matter of molluscan shells was investigated by means of electron microscope and X-ray diffraction.
2) Conchiolin membrane and wall appeared to consist of many fibres or coards, in which cross-bands and holes were found.
3) X-ray diagrams for the organic matter were composed of Debye-Sherrer ring and halos.
4) Membraneous conchiolin may elongate in parallel with a definite direction.
5) It seems that some inorganic components bound to organic ones exist in molluscan shells.

Chapter IV

Electron Diffration and Electron Microscopic Investigations on the Calcification of Shell

1 Introduction

It is of interest to investigate how inorganic crystallites are grown in or on organic matrix during the shell formation since the nature of the organic matrix is considered to be closely related to the growth and the lattice of inorganic crystals. As described in chapter III, the growth and the structure of the organic matrix appeared to affect the deposition of mineral matters in several electron micrographs, though this idea could not be confirmed by the techniques of X-ray diffraction in the present work. So there is the problem whether the possibility of this idea is supported by the observation of the deposition of mineral matters.

The variation of shell lime salts in the early developmental stages of the pearl oysters has been reported by Watabe (1956) as follow: The mineral component of the prodissochonch I and II was dahllite and calcite, respectively. Few study on crystal structure of shell salts in the process of calcification has yet been found except his report, although mineral components of recent and fossil shells are examined chemically and physically by many workers. Our knowledge about calcification is insufficient for understanding the mechanism of mineralization in shell. So it is an important subject to investigate the growth and the crystal structure of inorganic matters which are crystallized in the early stages of calcification. The author will attempt in this chapter to answer to the above mentioned questions.

2 Materials and Methods

The larvae of *Pinctada martensii* used in this study were collected with a plankton net at the water of the pearl farm in Ago Bay, Mie Prefecture in Japan, and were also obtained by artificial fertilization. The young shells less than 2 mm in length in the sedentary state were picked up from the collector hanging over 0.5 to 2 meters deep in the sea. On the other hand, a glass coverslip was inserted between the mantle and the valve, and the experimental animals were placed in the sea water for few days in summer and for one month in early winter. Immediately after taken out from the pearl oyster, the one of the coverslip was fixed in 98% ethanol, and the another was washed carefully in fresh water and then was dried at room temperature.

The deposits on the inserted glass were observed at first by the optical and polarzing microscopes, and thereafter two-step replica of acethylcellulose-carbon was prepared for electron microscopic works (refer chapter V). The mineral components and the crystal structures of these deposits and larval and young shells were investigated by the selected area electron diffraction method. That is, these shell substances pulverized by grinding in an agate mortor were mounted on speci-

men holders with collodion and were observed under the three stage electron microscope (HU-10). X-ray analysis was applied for the specimen sufficiently obtained to complete the results given by electron diffraction.

3 Crystal structure of the shell substance in its various developmental stages

The offspring of Pelecypoda is maintained by external fertilization. In *P. martensii*, the spawning season covers the period from June to August. The fertilized eggs develop rapidly during several days of the free living stage, and thereafter change into the sedentary state. The prodissochonch I occurs when the embryo develops into D-shaped larva about 20 hours after the fertilization (Kobayashi and Yuki 1952). The larval shell in the umbo stage, about 13 days after fertilization, consists of both prodissochonch I and II, which are different from each other in structure.

The shell substance from D-shaped larva of *P. martensii* gives electron microscopic image as figure 69 and shows the rosette and granular forms with homogeneous membrane. The electron diffraction pattern of these matters is composed of reflexion spots and Debye-Scherrer ring as shown in figure 70, and the interlattice spacings of the crystal calculated from this pattern are shown in table V. The spacing is in agreement with that of dahllite as in the case of the result obtained by Watabe (1956) except the 5.37 Å and 4.41 Å reflexions, but those reflexions do not coincide with that of aragonite or calcite. Figures 71 and 72 are electron micrograph and diffractogram produced by a fragment of the larval shell in the umbo stage. N-pattern in the diffractogram is considered to be given by the incident electron beam normal to the (0001) plane of the single crystal of calcite in the shell of the umbo larva. In this experiment, aragonite can not be found in the shell substance of the umbo larva. The young shell in the sedentary state exhibits network structure of polygon under optical microscopes, and it is difficult to observe morphologically the formation of the nacreous matter in the specimen which is less than 1 mm in shell length. Whereas, it is possible to observe the deposits of the prismatic and nacreous matters in the young shell which is more than 1 mm in length. Figure 74 is electron diffraction pattern corresponding to the electron micrograph shown in figure 73, and suggests that the one fragment of the yuong shell less than 1 mm in size consists of irregular aggregates of fine crystals of calcite and aragonite (Table VI). And the another fragment of the same specimen shows electron micrograph and diffractogram in figures 75 and 76 and is proved to be of aragonite. Of course, the young shell more than 1 mm in length has both mineral components of aragonite and calcite, as shown in figures 78 and 80 respectively, though shell substances exhibit same fine granular structure in figures 77 and 79.

The results which are measured from electron diffraction pattern without X-ray diffraction analysis may sometimes come to erroneous conclusions. In the present experiment, two minerals entirely different from each other in crystal

Table VI Electron and X-ray deffraction data of shell substances in various developmental stages and shell formation.

apatite *1		dahllite *2		aragonite *3		calcite *3		D-shaped shell *4		young shell *4		deposite on the glass	
d (Å)	I	d (Å)	I	d (Å)	I	d (Å)	I	d (Å)	I	d (Å)	I	d (Å)	I
								5.37	s				
								4.41	s				
						3.88	10					3.88	4.5
		3.75	2										
				3.40	40					3.42	s	3.40	4
3.38	ms	3.34	1.5			3.37	4	3.34	s				
				3.27	18							3.29	8
3.08	ms	3.02	1.5			3.04	96			3.05	s	3.04	34.5
				2.87	5	2.85	5					2.86	2.5
2.81	s												
2.73	s	2.72	10	2.70	23			2.75	m	2.70	s	2.70	3
2.60	w	2.60	1										
2.49	ww			2.48	30	2.50	14			2.50	m	2.50	5
				2.41	6								
				2.37	23								
				2.34	11								
						2.29	16					2.29	4.5
2.25	mw	2.24	2										
				2.19	7								
2.13	w	2.11	0.5	2.11	17	2.09	14					2.09	4.2
				1.98	24					1.98	s	1.98	2.5
1.93	m	1.93	2.5			1.91	18	1.96	s			1.91	5.5
1.88	mw	1.87	1.5	1.88	15	1.88	16					1.88	5
1.82	ms	1.83	2.5	1.81	9			1.81	m				
1.78	ww												
1.75	w			1.74	18							1.75	2
				1.73	7							1.73	1.2
1.70	w	1.71	0.5					1.70	w				
1.64	ww	1.62	0.5			1.63	4						
						1.60	17			1.60	w	1.60	2
1.58	w					1.59	3						
				1.56	4								
		1.51	0.2	1.50	3.5	1.52	5			1.51	w	1.52	2
1.47	w	1.49	0.2	1.47	3	14.7	3						
1.43	m	1.44	1.0	1.43	3	1.44	5						
				1.41	4	1.42	4						
				1.36	4.5								
1.34	ww	1.33	0.2			1.35	2						

*1 Kubo's data. *2 Rosebery's data. *3 The interllatice spacings obtained form S-1 and S-2 in text-fig. 6. *4 Electron diffraction.

system and axial ratio seem to be discussible only from electron diffractograms, though the discussion is imperfect.

4 Mineralization in early stages of the shell formation

One of the first deposits grown on the inserted glass exhibits rounded and irregular shapes which are positive in the test of metachromasia reaction, as seen in figures 81 and 85. Contrarily, another is a membrane with homogeneous structure under optical microspcoes, and is faintly stained in the test. The former is stained deeply by von Kossa's silver method, but the latter is lightly stained. The deposits become unstained when they are placed in acids and the aqueous solution of ethylenediaminetetra-acetic acid disodium salt for several hours. And both of them are dissolved perfectly by sodium hypochlorous acid, and are extinct usually through crossed nicols. The deposits increase gradually in size and, in general, have the concentric pattern just like "Liesegang rings" during growth (Fig. 84). From these experiments, the deposits are considered to be organic matters with inorganic components, which can not be found by optical and polarizing microscopes. Practically, by electron microscopes fine crystals of mineral matter are observable in or on the organic matter, which shows usually extinction under crossed nicols (Figs. 90 and 91). The diffraction pattern is given by the matters which can not be decided to belong to either organic or mineral component from the morphological viewpoint (Figs. 92 and 93).

The homogeneous organic membrane shows the reticular structure in a definite orientation under electron microscopes as in figure 90, and is similar to that of the nacres (Grégoire 1958). In figure 90, the new membrane develops covering the underlying one, in or on which large and small crystals are deposited. Two small crystals seen at the middle part of this figure appear to suggest that the deposition of mineral matters is in close relation to the network of the organic membrane. On the other hand, the round organic matters which are positive in the metachromasia reaction, are deeply stained at its central area and narrow circular zone, as are shown by black parts in figure 81. In this case, it seems that mineral matters first occur near the strongly stained parts as in figure 82. Crystallites of the mineral matter are located radially towards the center of the organic matter, and concentric pattern can also be found there. Under crossed nicols, mineral area is extinct at the same time or shows partial irregular extinction (Fig. 86). The deposits which are extinct usually at their center are very often revealed as seen in figure 83. Seventh column in table VI is X-ray diffraction data obtained by these deposits. It is obvious that the formation of other minerals except aragonite and calcite does not take place throughout the calcification of the adult specimen of *P. martensii* in this experiment. From electron diffraction patterns of these crystals, it is verified that the *c*-axes of crystallites stand vertically to the surface of the inserted glass. Crystals grown freely from each other exhibit rhombic, irregular or circular shape (Figs. 86, 87 and 88). The ground substance which is

laid under them is of the organic matter with many small mineral crystals, as seen in figures 91 and 94. Figures 95 and 96 show shell salts formed on the glass. These crystals are calcite and are extinct at the same time under crossed nicols. The surface of the crystals is uneven markedly, and there are sometimes found growth steps in figure 96. In any case, micro-crystals develop in dendritic growth in figures 95 and 97.

As shown in figures 87 and 97, the branchings extended from a common center of a crystal are very often seen to spread out just like the ribs of a fan at its periphery. Such growth appears to be a crystal in dendritic growth take place during the branching formation, and may be so-called "corner growth" (Papapetrou 1935). There is often revealed the very similar growth to the spherulite of high molecular substances during the formation of shell substances on the glass (Fig. 88). The circular deposits in figure 88 show the windmill-like extinction through crossed nicols, as seen in figure 89. Figure 98 is an electron micrograph showing the superficial structure of the deposits which may be called "spherulites" or "hedgehog dendrite" of the shell lime salt, and there is found the radial pattern as the spherulite of nilon (Kobayashi and Masuzawa 1960). The crystallites which branch off from a center or limbs are spindle or needle in shape (Fig. 100), and electron beams reflected from the thin atomic layer of the crystal give N-pattern which consists of only the index (*hk*0) of calcite (Fig. 101). This result shows that the incident electron beam is nearly parallel with the *c*-axis of the calcite. Although the mechanism of formation of the spherulite in the shell salt has not yet been resolved, the successive processes of the spherulite formation seem to be demonstrated in figure 99. The next crystal with spindle or needle form meets near the center of the first one having a little inclination to the latter, and both may be grown in contact with each other at a definite plane. When such crystal formations are repeated, the limbs will be formed radially around a common center. These crystals in replicas are of indefinite forms, as shown by the positive images in figure 99, and their growth appears to correspond essentially with those of inorganic matters in figures 7 and 91.

5 Discussion

Crystalline structure of molluscan shells during its development has not yet been investigated except Watabe's work on D-shaped larva of *P. martensii*. He stated on the bases of refractive indices and electron diffraction data that prodissochonch I was dahllite, while prodissochonch II was calcite. The 5.37 Å reflexion in figure 69 is the strongest, and can not be found in the diffraction patterns given by Watabe and in the data for dahllite shown by Robertson *et al.*. Although this reflexion was considered to be due to the existance of sodium chloride, 5.37 Å and 4.41 Å were unable to be seen in the interlattice spacings of halocit. Other several reflexions agree comparatively with Watabe's result. However, the inorganic part of D-shaped larva of *P. martensii* is evidently different from that of umbo larva,

young and adult shells, and is thought to be composed of a kind of appatite, though electron diffraction data are not verified by X-ray analysis. The 5.37 Å and 4.41 Å reflexions will be confirmed by means of X-ray diffraction in the future. In *P. martensii*, mineralization of shell substances during its development and on the inserted glasses seems to begin with the deposition of calcite rather than aragonite. This fact must not be applied to mineralization of all molluscan shells, since shell substances are characterized by the nature of the mother fluid secreted through the mantle epithelium but are not characterized by the various stages of mineralization. Accordingly, the change of mineral components is considered to be due to the nature of the mother fluid which is accompanied with the change in the secretive faculty or the differentiation of the mantle tissue.

Crystallites of shell lime salt, calcite, must be fundamentally developed in dendritic growth. Therefore, when a number of crystallites grows following definite formulae in characteristic aggregates and orientations, their aggregates show rhombic form, corner growth and spherulite, as seen in figures 86, 87 and 88. The first two are extinct at the same time under crossed nicols. But corner growth and spherulite of shell salt are not a single crystal, and unit particle of crystallites exhibits spindle forms. The *c*-axes of crystallites usually stand normal to the inner shell surface. In calcification of molluscan shells, organic matters are first formed and have a directing influence on the deposition of mineral ones. This idea may also be possibly supposed from the pareobiological viewpoint on the relationships between the metabolism of shell substances and evolution of molluscs.

It can be expected that the crystalline and morphological structures of organic matters are in connection with the arrangement of crystallites of mineral matters, and that its nature affects the polymorphism of shell calcium carbonate. Besides, it can be assumed that in shell mineralization, the molecule of the organic matters also plays a role as crystal seeds.

6 Summary

1) Mineralization of molluscan shells was investigated from the mineralogical and biological points of view.

2) The inorganic part of D-shaped larva of *Pinctada martensii* differs from that of umbo larva, young and adult shells. The metabolism of inorganic substances must be changed remarkably while D-shaped larva develops into umbo one.

3) In *Pinctada martensii*, change of shell mineral constituents was found during its development. Calcite was deposited more fast rather than aragonite. This fact seems to suggest that the differentiation of the mantle tissue may occur as the development of that animal progresses, since characteristic shell substances are separated from each mother fluid produced by the definite mantle tissues which are different from each other in histology and cytology.

4) Corner growth and spherulite of shell salt are not a single crystal but consist of definite aggregates of many crystallites of calcite, which exhibits spindle shape.

Chapter V

Crystal Growth of Shell

1 Introduction

For these several years, crystal growth of molluscan shells has been studied by means of electron microscopes and was discussed only on the viewpoint of crystallography. However, more recent works have taken into account the biological and biochemical factors for that study. In the Watabe's work on *Ostrea*, it has reported that a mantle plays an important role for making the flat inner surface of a shell. It has been pointed out by the author's report regarding aragonite crystals on the nacreous surface of *Pinctada martensii* that the velocity and the mode of growth are varied with the seasonal changes of environments and the difference in the physiological conditions, ageing of animals, and locality in the same shell. The characteristic of the shell structure and the mother fluid around growing crystals has been written mainly on the Japanese pearl oyster, *Pinctada martensii* (Dunker), in chapter I. Molluscan shells are the crystalline substances from the solution transported through a shell-forming tissue, whose secretive activity is governed by the physiological conditions of each animal during its development and seasonal changes of its environments. Of course, the conditions of the mother fluid are different among the various species. Crystal growth of shells may be related closely to the natures of the liquid and the solid phases in the grounds of mineralization. The purpose of this chapter is to make clear the characteristic of crystal growth in the shell formation.

2 Materials and Methods

The materials used in this study were *Pinctada martensii*, *Pinna attenuata*, *Anomia lischki*, *Ostrea gigas*, and *Chalmys nobilis*, which were collected in Ago Bay, Mie Prefecture in Japan, during the period from August 1958 to Septemner 1959. After the specimens were killed, soft bodies were removed from shells, and inner surfaces of which were washed carefully by hands with distilled water as these newly growing crystals were easily exfoliated with a small external force. The inner shell surface was directly observed by using the vertical illuminator of Leitz Panphot, and several portions were selected for electron microscopic observations. Two-step replicas of acethylcellulose-carbon were made according to the method of Fukami using the sheet of acethylcellulose instead of plastics. Carbon films were vaporized on the sheet, which was dissolved away in methyl acetate.

3 Aragonite crystals grown on the surface of the nacres

In *Pinctada martensii*, the basal plane (001) of aragonite crystal is parallel to the inner surface of nacres; namely, as mentioned in chapter II, their orthorhombic *b*-axes are arranged each other in parallel to the horizontal growth direction of the

Table VII Frequency of angles appearing on basal plane of aragonite crystals in the nacre of *Pinctada martensii* (indicated angle A and B in Fig. 102).

Angle A		Angle B	
degree	frequency	degree	frequency
111	1	116	1
112	5	117	1
113	5	118	3
114	10	119	5
115	19	120	11
116	64	121	17
117	18	122	18
118	11	123	53
119	8	124	16
120	4	125	11
121	3	126	5
122	2	127	3
		128	1
		129	1

layer. Measuring the angles appeared in the basal planes from several electron micrographs, they are shown in table VII, and 116° and 123° are found to be dominant. In aragonite crystal, 116° is the angle between 110 and $1\bar{1}0$, and 123° the angle between 010 and 110. Aragonite crystals in the shell, in general, exhibit hexagonal tabular shape, in which (110) is predominant, (010) comparatively small, and (100) usually absent, as seen in figure 110, but (010) sometimes disappears completely. If, in the initial stage of the growth, crystals are small hexagon with good (110) and (010) facets in a solution uniformly supersaturated, the individual faces extend outward at right angles to each surface, and there is no change during the growth except their sizes growing bigger. If crystals grow as small circular shape bounded with the curved faces of (110) and (010), or with faces of high indices in the initial stage, (110) and (010) develop gradually, and then crystal form will exhibit larger hexagon bounded by plane faces. However, when a small crystal grows up larger, in some cases, every point on one growing surface advances at the same speed, though the rate of growth velocity of each face seems to be different, and crystal edges show clear plane, as seen in figure 102. In another case, small crystals come to join together, or be included by larger one, and growing surfaces are irregular (Fig. 103). The (001) face exhibits a stepped, rugged or smooth appearance during the growth. Such, a stepped surface occurs by layer growth (Fig. 104), and the rugged membrane covering crystals may probably be organic matrix (Figs. 110 and 122).

One of the most important factors determining crystal size is assumed to be the various degrees of calcium carbonate concentration in the mother fluid which is produced by the secretive activity of a mantle tissue. That concentration of the mother fluid surrounding crystals is not only governed by that secretive activity varied with the seasonal changes of environments, in particular, of water temperature and with physiological conditions of each animal, but also by that in different areas of the same mantle. The variation of crystal size throughout a year is summar-

ized in comparison with the amount of calcium carbonate deposition on pearl surface in table VIII. Table VIII and text-figure 4 show that when the lime deposition is the maximum, a large number of small crystals takes place on all the nacreous

Table VIII Variation of particle size of aragonite crystals in the central region of the nacre, in *Pinctada martensii*, throughout the year.

Size (μ) / Month	~0.5	~2.0	~4.0	~6.0	6.1~	The amount of $CaCO_3$ deposition (mg/10 days)
I	133	48			2	—
II ~ III	79	78				—
IV ~ VI	12	68	23	22	4	3
VI ~ VII		12	26	11	2	4
VIII ~ IX		63	109	46		9
X ~ XI		45	64	38	5	4
XII	152	71	35	57	37	2

surfaces, and bigger crystals occur as the deposition decreases, but when the deposition is minimum, crystal size again diminishes. If the calcium carbonate concentration in the mother fluid is varied in proportion to the amount of lime salt deposition on the inner shell surface, the above mentioned fact may show that the bigger crystals will grow slowly at the certain value of supersaturation of the calcium carbonate solution, as indicated by B_1 and B_2 in text-figure 4. In the season when the concentration of the mother fluid is assumed to be greater, though its measured concentration is minimum, crystal grains will grow rapidly (A in Text-fig. 4). And moreover, we shall notice in the parts C_1 and C_2 under the state of slight supersaturation, extremely small crystals lie on the edges and the corners of larger one exhibiting complex appearances with dissolution of crystal faces. The inverse relationships between particle size of crystals and the amount of calcium carbonate deposition can also be confirmed in table IX. The table shows an example of the

Table IX Comparison of the particle size of crystals scattered in local areas of the nacre in September (*P. martensii*).

Region / Size (μ)	Margin	Center
	frequency	frequency
~ 1	41	3
~ 2	19	14
~ 3	4	60
~ 4		13
~ 5		5

comparison of the size of crystals scattered on marginal and central parts of the same nacre, and suggests that the particle size in the rapidly growing portion (i.e., marginal region) is smaller than that in the slowly growing one (i.e., central region). Now,

the relationships between the particle size of aragonite crystallites and the amount

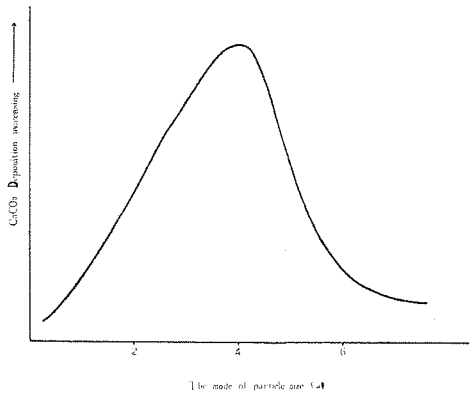

Text-fig. 18 The change of particle size with the amount of $CaCO_3$ deposition.

of calcium carbonate deposition in the central region are illustrated in text-figure 18, in which it can be seen that the mode of particle size exhibits about 4μ under the largest amount, the increase with the decreasing amount, and below 0.5μ under the smallest amount.

On the other hand, crystal form will also be characterized by the chemical conditions and concentration of the mother fluid which varies with the difference in the secretive function of a mantle. It is evident from text-figures 1 and 4 that the velocity of the general growth in weight of a shell runs roughly parallel with the seasonal change curve of sea water temperature, but the former never coincides with the latter. Here, if the relationships between crystal form and rate of $CaCO_3$ deposition are investigated, we shall notice as follows: 1) When animals are in normal physiological conditions, the maximum value of the velocity of growth will be, in general, brought during summer to autumn, sea water temperature in these seasons ranging from about 22°C to 28°C (i.e., shown by A in the curve of lime salt deposition), and growing crystals indicate round, or hexagonal tabular form with somewhat round corners as seen in figures 105 and 106. 2) If the growth velocity decreases to such value as marked by B_1 ans B_2 in text-figure 4, they will develop into hexagon bounded by plane faces (Fig. 102). But crystals grown in B_1 often take place the complex forms with serrated edges, as shown in figure 107, and the dissolution of crystal faces is recognized from time to time (Fig. 108), whereas not so complex forms as that of the former is yet found in B_2. 3) As shown in figure 109, the complexity of the crystal growth increases with the lessening degree of $CaCO_3$ deposition since crystal surface must be repeated alternately growth and dissolution. 4) If the sea water temperature falls below 13°C for so long times (i.e., indicated by broken line), crystal growth ceases completely, and at least the edges and corners of crystals become round under the dissolution phenomena (Fig. 111). 5) Immediately

after hibernation, the organic substance comes to be deposited remarkably over all nacreous surface of some shells (Fig. 110). 6) In spring when the water temperature raises up more than 13°C, the growth of new crystals begins (Figs. 112 and 113). 7) In summer, if shells continue to live under abnormal physiological conditions, the growth of the nacre is interrupted, and it can be seen that nacreous surfaces are sometimes partially dissoluted and there are often found to be dissolving with definite etching orientations on the (001) faces (Fig. 30). As the vitality of animals recovers to normal condition, large numbers of small crystal are deposited here and there on the dissolved surface, though new growing crystals show etch figures in most case, as in figure 30.

In any case mentioned above, the size and the shape of growing ones in shells seem to be dependent on the pH value and calcium concentration of the mother fluid which is charactarized by different physiological conditions of animals. And organic and other inorganic ions, impurities in crystal growth, introduced into the grounds of mineralization through the mantle tissue will also have influence upon crystal growth.

Aragonite crystals are deposited in parallel or almost parallel to the fiber axis which is in good agreement with the growth direction horizontal to the inner surface of the nacre, in which such parallel arrangement of crystals must be usually produced by the biological factors influencing the process of shell growth. Figure 114 indicates the overgrowth of aragonite crystals only seen in the limited areas near posterior muscle scare of *Pinna attenuata*. Concentric polygonal pattern on the (001) face of crystals consists of a number of parallel growths which will extend and cover the surface of another underlay. The same index faces lie down in parallel with each other, such as revealed by $(h_1\ k_1\ l_1)_A$, $(h_1\ k_1\ l_1)_B$, $(h_1\ k_1\ l_1)_C$... and $(h_2\ k_2\ l_2)_A$, $(h_2\ k_2\ l_2)_A$, $(h_2\ k_2\ l_2)_C$ ... and etc. as in figure 115. In figure 116, aragonite crystals in the nacre of *Pinctada martensii*, probably in nearly all species of Pelecypoda, grow parallel one another as described above except several ones. Practically the author's experiment for the regeneration of the grafted mantle epithelium concerning the cultured pearl and shell formation has been verified that such biological factors as the elongation and the movement of a shell-forming tissue influence directly or indirectly the arrangements of crystals. But it can be not explained by these investigations why aragonite belonging to optically biaxial crystal makes its orthorhombic *b*-axis arrange parallel to the horizontal growth direction of the shell. Therefore, the present author has already paid the particular attention to X-ray diffraction analysis for conchiolin of the shells, though the reflection pattern does not show the fiber diagram. The reflection pattern for conchiolin consists of two or three broad bands of Debye-Scherrer ring with halos and shows the characteristic of such substance as amorphous or noncrystalline, as described in chapter III. Nevertheless, electron microscopic images have shown that the major fiber axis very often correspondes to the orthorhombic *b*-axis or the (110) plane of aragonite crystal. Since crystallites of lime salts in the nacres grow in parallel to a definite orientation on conchiolin

membrane, a basic substance which is first formed in calcification, parallel growth of aragonite in the layer would be explained by such idea as oriented overgrowth or epitaxial growth of the minerals in nature. Namely, when the growth of the clystals of one substance on another takes place in parallel orientation, such growth phenomenon is commonly termed "epitaxy", and both substances have the similar crystallographic structure. In the nacres, the structure of conchiolin is considered to be related closely with the length of the orthorhombic *b*-axis of the unit cell of aragonite. Therefore, it can be expected that crystals of shell develop by epitaxial growth. In the view of these experiments and idea mentioned above, it may probably be considered that parallel deposition between aragonite crystal grains in the nacres is very closely related with the lattice dimension and the periodicity of conchiolin, the orientation of which is affected strongly by the tension and the movement of a mantle tissue. Furthermore, the superficial structure of the matrix will be one of the limiting factors upon oriented growth. In general, small crystals on the edges and the corners of larger ones develop by parallel growth in winter, and exhibit complex features bounded by imperfect faces (Fig. 117). If no isolated crystals exist on the nacreous surface which is relatively smooth, small crystals will occur first on the boundary of ones in underlying lamella, or in correlation with crystallographic structures of the underlying substances, as in figure 118. During summer to autumn, crystals grow larger and larger, whereas in winter, they are unable to grow larger and show imperfect forms, as seen in figure 117, being deposited. However, nearly most ones are deposited parallel to one another. Crystal grains joining together on their (110) planes, develop into the tree-like aggregations, as shown in figure 119, which are seen usually under rapid growth. The extension of branchings consisting of large numbers of crystal grains, occurs in a direction at a certain angle to a main stem, and it runs roughly parallel to each other, and must be followed by the rules of crystallography. The group of crystals grown in such fashion may be considered as so-called dendritic growth. Watabe's observations for crystal growth of aragonite on the cultured pearl surface have also recognized branchings inclined at small angle to each other in the process of dendritic growth. Furthermore, when we observe crystal growth of aragonite in the pearl oyster shell, we can see rarely the parallel growth as in figure 120, in which crystal particles join together on their (010) faces and form a branching extending from the ledge of a lamella. Such the succession of crystal grains joining one another in parallel orientation is probably seen to be a kind of dendritic growth. Twin of aragonite exhibits regular hexagonal form which consists of three grains joining together on its twinning face (110), as seen in figure 112, exhibiting every twinning types of aragonite at all times during growth of the nacre.

Very often we can see growth spirals created by screw dislocation emerging on the (001) face of aragonite crystal grains in the nacre of *Pinctada martensii* during April to December. The ledge starting from a dislocation rotates spirally toward a crystal edge clockwise or counter-clockwise, as shown in figures 121 and 122. In

the most case, the shape of the spiral exhibits hexagonal, as seen in figure 121, depending upon the growth rate on crystallographic directions, but a circular spiral seems to occur when an individual crystal is round (Fig. 122). The step heights of the growth spirals will be divided into two types as follows; the one is unequal from one portion to another, and the other equal in every portion of the ledge. The results obtained by metal shadow-casting show that the step heights of these polygonal spirals are less than 50 Å in the center of the growth spiral, though they are measured about 1000~5000 Å at near part of the crystal edges. But it is not possible with electron microscopes to measure accurately the step heights, because organic substance, which is about 200 Å in thickness, grows on crystal surface (Fig. 122).

There is often found concave dissolution on the (001) face of crystals, as seen at the upper left in figure 118, and convex growth will be seen occasionally under abnormal physiological conditions of the animal (Fig. 129). Both of them show the appearance with dissolution and etch pits, and come to occur under similar physiological conditions of the animals. A large number of etch pits is revealed on the (001) face of crystals at an early stage of crystal dissolution, as seen in figure 123, and in more advanced stage of dissolution, crystal shape is round and finally is undistinguishable by a general retreat of the faces, edges, and corners (Figs. 125 and 126). In the process of etching, etch pits may occur along such weak points involved in crystalline solid as surface cracks, dislocation and the boundary between micro-crystals. Sometimes mosaic structure consisting of micro-crystal aggregation is visible on the (001) face of a large crystal as the succession of very small oriented etch pits under electron microscopes (Fig. 124), though crystals are protected from dissolution by the presence of the organic substance. On the other hand, in a certain time after hibernation, new growing crystals show indefinite shapes bounded by imperfect faces as in figure 112. There occurs a cliff, probably consisting of the (110) and (010) faces, on the inner surface of the nacres, because growth of the certain faces of crystals is inhibited by some factors. And we can see the layers extending from portions inside the face boundaries, or from the corners and edges of crystals (Figs. 127 and 128). Besides, in winter to spring, growth hillocks of round form often take place on the surface of a cliff and basal plane under low supersatulated solution, and growth and dissolution of crystal are repeated on the inner surface (Figs. 109 and 127). It is conceivable from these electron micrographs and text-figure 4 that in the process of shell mineralization, ionic exchange and recrystallization occur on the exposed surface of mineral cryatal and in lamella which are in contact with the mother fluid.

In such variety of crystal growth of shells, it is considered that impurities are introduced into the mother fluid around growing crystals through the mantle tissue in a definite time of a year. In every case, the presence of impurities seems, therefore, to be one of the most important factors determining the size and shape of crystals as same as the degrees of supersaturation. The form and size of aragonite are different among various species of Lamellibranchs, suggesting that the mother fluid

in the ground of crystallization is more or less different in each species.

4 Calcite crystals grown on the surfaces of the prismatic layer and calcitostracum

Calcite crystal of shells has occurred as individual particle, or as aggregation in prismatic layers, and is in needle, spindle, or hexagonal tabular form. As mentioned in chapter II, the prismatic layer of *Pinctada martensii* shows a bee-hive structure consisting of many prismatic chambers. On the inner surface, a large number of minute crystals of these chambers comparatively regularly aggregates, elongating radially from the center of each chamber to the boundary, or parallel to a definite direction of the chamber. Accordingly, almost all prismatic chambers show similar extinction of the single crystal or spherulite under crossed nicols of the polarizing microscope (see chapter IV). The form and size of calcite crystal particles are not distinct in the prismatic layer of *Pinctada martensii*, though they are fundamentally seen to be in extremely small tabular or spindle form, as shown in figures 130 and 131. In the growth process of a prismatic chamber, the organic substance is formed before the mineralization of the layer, and seems to affect the deposition of micro-crystals of mineral substance as in the case of nacreous layers. It may probably be impossible to explain the spatial relationships between crystallites and organic substance in the prismatic chamber without the above mentioned idea. Figure 100 is an electron micrograph of hedgehog-like dendrite of calcite crystals grown on the surface of a fragment of glass coverslip placed between the mantle and shell, indicating that they are not single crystals, but consist of the orderly aggregations of micro-crystals related closely with the organic matrix. Micro-crystals in a large mosaic crystal exhibit tree-like formation, as seen in figure 131. However, in the formation of the prismatic layer, a large number of the needles of calcite with organic matters develops as the prism and large crystal in dendritic or parallel growth under crystallographic and biological rules. And neighbouring prisms come to combine together, and thus a polygonal prismatic chamber is formed. New layers supplied on central portion of the crystal surfaces spread toward the corners and edges, and there are so often found concentric patterns like "Liesegang rings" on the growing surface of prismatic chambers; their surfaces being the (0001) face of calcite, as seen in figures 8 and 96. The form and size of calcite crystal seem to be remarkably varied by the difference of calcification in local areas of the prismatic layer rather than by the variety of the mother fluid with the seasonal changes of its environments. Though, of course, chemical and physical conditions in the grounds of crystal growth are assumed to be important factors determining crystal form and size. For instance, in the periphery of the growth process of the prismatic layer, the thick membrane of organic matrix is formed first, and so the new micro-crystals of mineral salt appear to precipitate dependently on underlying sunstances (Figs. 6 and 7). There are found oriented deposition and dendrites of calcite crystals in or on the organic matrix in the early stage of mineralization. In any case, the growth and the arrangement

of micro-crystals of individual chamber seem to be independent of each other during the growth.

On the other hand, calcite crystal grains in *Chlamys nobilis* and *Ostrea gigas* are deposited nearly parallel to one another, though the orientation of elongation is more or less different from one portion to another. The form and size of crystals are different makedly among various species: for example, in *Ostrea* and *Anomia*, crystal particle exhibits tabular form, while in *Chlamys*, that is needle-shaped (Figs. 132, 134 and 135). These facts appear to suggest that the mother fluid around growing crystal is specific in each species. As seen in the case of aragonite crystals in the nacre, very small crystals are scattered here and there on the growing faces of a larger crystal of calcite (Fig. 133), and there sometimes dendritic growth is seen clearly. The growth and dissolution of crystal faces are sensitive to the change of chemical and physical condition in the mother fluid throughout the development and seasonal changes in the secretive activity of a mantle. The corner growth and spherulite of shell lime salt have been detailed in chapter IV.

5 Discussion

Since old times, for the investigation of crystal growth and dissolution phenomena, various particular apparatus have been devided by different workers, who have attempted interesting experiments in the laboratory. Thus such particular phenomena as dendritic, corner and parallel growth have been explained by their theoretical ideas, and a special attention has been paid to the influence of impurity added to the ground of crystal growth on the separation of a solid phase from a solution or melt, and on the crystal habit. These ideas have been utilized for the explanation of the crystal growth of minerals in the inanimate objects. On the other hand, in the deposition of shell lime salts Schmidt (1923) found recrystallization, dissolution, twinning, overgrowth and parallel growth. The dendritic growth of lime salts was observed by Watabe (1955). However, several workers have discussed on the crystal growth of shells only on the crystallographic viewpoint, and have not taken into account very important other factors influencing shell formation. The author (1957) has pointed out that the mode and the velocity of crystal growth in the shell are varied by physiological conditions and age of animals, different regions of the shell and the seasonal changes of its environments. And the author thought that the chemical and physical variations occurred in the solution around growing crystals by the difference in the secretive function of the mantle correlated with the above mentioned factors. Later, the author (1960) has also confirmed that, such mechanical force as the elongation and movement of the mantle has a direct effect on the arrangement and growth of lime salts of the shells.

The above observations show that crystal growth of shells is not different from that of inanimate objects except biological characteristics; such as the biochemical reactions by which calcium is supplied throughout the mantle tissue from outside of a body to the inner surface of a shell, a direct effect of organic matrix on the separat-

ion of the solid phase from the liquid phase, and the role of a mantle. The mode and velocity of crystal growth will be governed by divergent degrees of supersaturation of calcium carbonate in the mother fluid. However, the form and size of crystals are different clearly between B_1 and B_2 under nearly same value of the observed concentration of calcium ions, as shown in text-figure 4. This seems to mean that the other elements in the fluid, for instance, the true concentration, pH value, viscosity and etc., are also varied with the difference in the biological conditions in each period. Furthermore, it can be expected that impurity which is introduced in the grounds of mineralization through the mantle tissue in definite times, interferes on the crystallization of lime salts and on the crystal habit. The presence of impurity previously described appears to be suggested by the growth of imperfect crystals, and also by the interesting experiments of Sawada (1959) for color change of the shell exposed to γ-ray. Chemical conditions and calcium carbonate concentration of the mother fluid are controlled by the variation of physiological condition of an animal throughout its life and by seasonal changes of its environments, and, in addition, by the variation of its vitality. Under a normal condition, crystals grown on the inner shell surface develop in twinning, overgrowth, parallel and dendritic growths as seen in inanimate objects. Dissolution of crystals occurs under low concentration of carbonate or under very low value of pH of the fluid. Frequently, we can see screw dislocation emerged on the (001) face of aragonite, and etch pits arranged along the weak points involved in crystals under an electron microscope. The author therefore considers that nearly all crystals in the nacres will contain dislocations by the reason of that they grow at low supersaturation, and this hypothesis will be proved by X-ray analysis, and by the investigation of etch figure under electron microscopes in the future studies.

Parallel growth of calcium carbonate crystals in the mineralized tissue of molluscs would be explained by the following theoretical idea. At the first step of mineralization, the tension and the movement of the shell-forming tissue influence directly the orientation of growth of so-called conchiolin, the structure of which is assumed to affect the deposition of mineral matters. Two substances consisting of different constituents as organic matrix and mineral salts are separated from a same mother fluid, and show orderly alternate deposition. In this case, crystallites of mineral salts relate closely to the molecular structure of conchiolin and grow in parallel orientation with the matrix; i.e., shell salts are considered to develop by epitaxial growth. Practically, aragonite crystals in the nacres seem to have their orthorhombic *b*-axis related closely with the fiber axis of conchiolin, and calcite crystals in the prismatic layer have their c-axis coincided with that fiber axis. Moreover, it seems to be possible that colloidal organic matter in the mother fluid has already revealed definite orientation by the movement and the tension of the mantle. In the shell formation, the organic substance, however, is formed first and has a direct influence on the deposition of the mineral salts. Another role of organic matrix appears to be the protection of lime salts against general dissolution phenomena, though the

matrix may have sometimes interfered on crystal growth as if it is impurity. In the case of the prismatic layer, the form and size of crystals seem to vary at different stage of calcification. Of course, they differ among various species.

Generally speaking, the growth of individual crystal in shells appears to be essentially similar to that of minerals in inanimate objects, but the biological and biochemical factors influence directly on the crystal growth until the liquid phase changes to the solid phase. Here, the author should propose an idea that the mineral and organic matters in molluscan shells develop by epitaxial growth. In the epitaxy of the shell substances, the author wishes to resolve the problem on the connection between organic and mineral materials.

6 Summary

1) Crystal growth of shells was observed under the electron microscopes, and the results were discussed taking into account the biological factors.
2) There were found twin, screw dislocation, overgrowth, recrystallization, dendritic and parallel growth on the inner shell surface. And shell salts were dissolved under low concentration of calcium carbonate and acidification of the mother fluid. But the form and size of crystals appeared to be almost constant under similar conditions of calcium metabolism. Moreover, in the investigation of the crystal growth of shells, it is necessary to take into account the effect of impurity introduced through the mantle.
3) In the process of calcification, the organic matrix was formed first and seemd to have great effect upon the deposition of mineral salts. Here, special attention was paid on such dynamic force as the tension and movement of the mantle.
4) The mother fluid around growing crystals may be characterized by the seasonal changes of calcium metabolism, and of course, by the difference of species.
5) Parallel growth of shell salts would be explained by the theory of epitaxial growth.

Chapter VI

The Mechanism of Formation of the Spiral Growth Steps

1 Introduction

In the processes of formation of the nacres in molluscan shells, spiral pattern can very often be found on its inner surface, but it has been known that the pattern is different among various species or even in local areas of the same shell. Generally, the central part of the spiral is the highest, and the ledge of a spiral will descend outward from the central to the marginal part of it by one step in each complete turn. Therefore, the spiral growth is very similar to the geometrical patterns observed on the crystal surface grown by the screw dislocation. The nacre is a complex system consisting of both organic and inorganic substances, which are separated from the particular solution produced by the secretive activity of a mantle tissue. Crystallites of mineral matter in the layer are arranged regularly in the third dimension of space, as mentioned in chapter II. The mechanism of growth of crystals in the nacre may be explained by the theory of growth of single crystal. Of course, the ground of crystal growth is produced by the particular function of a living thing. Accordingly, the development of spiral steps is effected by the variation of its function following seasonal changes of the environment surrounded the pearl oyster. Generally speaking, the parallel pattern is seen in the marginal region of a nacre, and spiral or circular pattern is found in the central region. Since crystal growth of shells takes place only in a life, it is very difficult to resolve the mechanism of the spiral growth. It will be described in this chapter that the spiral growth of the nacre is very similar to the one by the screw dislocation under low supersaturation. The possibility of the extention of the screw dislocation theory to the present case will be discussed below.

2 Materials and Methods

Almost all experiments in this chapter were carried out on *Pinctada martensii*, which was collected at Ago Bay, Mie Prefecture in Japan.

The works described in this chapter were done by the techniques shown in chapter V. Celluloid replicas were prepared according to the Suzuki's method. The growth pattern of the nacre was observed easily under the optical microscope by the help of the above replica.

3 Observations

In general, length and weight growth of shell are recognized throughout the development of animals, and growth steps are formed certainly on the inner surface for the growth of shell. As described in chapter II, the step is provided by the emergence of the growth fronts of crystal lamellae on the inner shell surface, and the step patterns have various appearances due to the different modes of growth and arrangement of lime salts. Table X shows the relation between the spiral growth and the

Table X Variation of the growth pattern in different species.

Pattern	Species
irregular and parallel	*Meretrix meretrix lusoria, Tapes variegata, Corbicula japonica, Notovola albicans, Chlamys nobilis, Ostrea gigas, Anomia lischki*
parallel and spiral	*Pinctada martensii, P. margaritifera, P. maxima, Haliotis discus, Mytilus edulis, Pinna attenuata, Hyriopsis schlegeli, Unio margaritifera, Cristaria plicata spatiosa*

kind of the molluscs and indicates that spiral growth is absent from the inner surface of shells consisting of calcite (i.e., *Ostrea gigas, Notovola albicans, Chlamys nobilis, Anomia lischki*), and in the aragonite shells without any pearl luster (i.e., *Meretrix meretrix lusoria, Corbicula japonica, Tapes variegata*). In the bivalves with the spiral steps, the spiral can not be seen in the prismatic layers and occurs in the limited areas of the nacres, as shown in chapter II. It has already been known that the spiral growth can not be observed in the rapid growing portions. It seems that in animal kingdom general concentration of the solute in the mother fluid is usually lower than the critical point of supersaturation. From the fact that the growth steps ascend gradually by one step toward the central part of shell, it is supposed that the parallel pattern observed in the marginal part of nacres is resulted from the border of the growth spirals. However, the steps can be made not only by the spiral growth, but also easily by the cliff as seen at a dislocation.

The spiral pattern of the nacres is greatly different from the patterns observed on the surface of single crystal. The surface made by the dislocation mechanism and non-close-packed surface of perfect crystals exhibits a step pattern. Molecules absorbed on the crystal surface and the steps can diffuse along the edge of the steps toward kink positions, and thus the steps can advance. On the other hand, the growth spirals of the nacres may not be advanced by adsorption and diffusion of the molecules but can be developed by deposition and addition of crystallites of lime salts. Since the nacres are considered to be a mosaic crystal, the spiral growth of the nacre would be explained by the mechanism of the growth of single crystal. A number of spiral pyramids is found on the inner nacreous surface of *Pinctada martensii*, and the rotating of spirals is assorted into the clockwise type and the counter-clockwise type, as seen in figures 26, 136 and 137. The shape and density of growth spirals vary, depending upon the mother fluid which is characterized under various physiological conditions and upon the locality in the nacre. In addition, either clockwise or counter-clockwise type is largely predominant when they occur densely, though the frequency of these both, as a whole, is almost equal. Individual spirals consist of a number of growth steps spreading from the respective sources, and their sphere of influence is bounded clearly by the hyperbolic curves of intersection between each spiral (Fig. 136). If one spiral grows in the nearest distance from another, the sources of the adjacent spirals will be involved in a growth pyramid and

they show the similar behavior seen in the interaction of two or more screw dislocations of the same sign or of the opposite sign, as shown in figures 26 and 136. Thus, when one spiral in a growth pyramid consisting of several sources is more predominant than the others, all spirals except the well-developed one diminish and at last will disappear.

Crystallites of aragonite in the growth spiral grow parallel to one another except several crystals, as seen in figure 138, and it is proved by comparison with the results shown in chapter II that their orthorhombic *b*-axes are alike in the direction parallel to the horizontal growth of the shells (Text-fig. 19). The crystal arrangement in the growth spiral is met with nearly parallel to or at small angle to that in neighbouring spirals (Figs. 139 and 140). In addition, the crystal arrangement of their orthorhombic *b*-axes in the whole areas of the nacre relates closely to the growth vector of the shell.

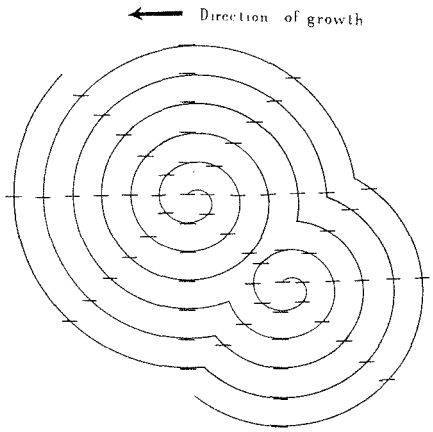

Text-fig. 19 Schema showing the relationships among the crystalline structure, the growth spiral, and the horizontal growth direction of the nacre. Straight lines indicate the orthorhombic *b*-axis of aragonite.

The source of the growth spiral is assorted into two types; in one case, one or more crystals adsorbed on the central part of growth pyramids develop by screw dislocation and the step starting from the dislocation which emerges on the (001) plane rotates around the source outwards. In another case, any crystal with a screw dislocation can not be found at the center. The growth fronts emitted from the center of one spiral may interfere by those of other spiral, and so, if the step height is unequal among each spiral, a number of cliffs takes place on the surface of ledges near the intersection, irrespective of somewhat different orientation of crystal elongation in neighbouring spirals. If the step height and the crystal arrangement show similar states to each other, the growth fronts originating from various sources come to combine perfectly at the boundary of the growth pyramids.

By the application of metal shadow-casting techniques, the step heights of some

spirals are examined on the nacre of *Pinctada martensii* under electron microscopes, and are measured to be about 1000 ~ 5000 Å which is equal to the thickness of a lamella. By the same manner, the step heights are determined to be different among various species from such values as 5000~8000 Å for *P. maxima*, 5000~8000 Å for *P. margaritifera*, 4000~6000 Å for *Turbo cornutus*, 4000~8000 Å for *Haliotis discus*, to such value as 18000 Å for *Quadrula undata*. In any case, the step height is equal to the thickness of a lamella in the nacres.

The shape of the growth spiral will depend upon the properties of growth fronts and such biological factors as the growth of animals. The most spiral patterns originated from screw dislocations, exhibit polygonal shapes which are attributed to the growth ratio of the ledge upon crystallographic orientations. On the other hand, the ratio of advance of growth fronts in the spiral growth of the nacres appears to be independent of the crystalline structure of the layer. Hence, circular spirals will result without exception. However, the shape of growth spirals does not vary with the crystallographic orientation in the nacreous surface, but is effected strongly by the vector of the tension and movement of a mantle tissue. This suggests that a small external force during the movement of a mantle has directing influence on the adsorption and arrangement of crystals. In addition, the concentration of calcium carbonate in the mother fluid will become locally unhomogeneous in the ground of crystal growth by the external force. Thus the advance of the growth fronts is succeeded at a different ratio in various orientations, and spirals will be distorted along a certain direction. In practice, the growth pyramids are merely distorted along the horizontal growth direction of the layer, and exhibit a simple ellipse, as seen in figure 141. The ratio of the distortion seems to be increased in proportion to a increasimg magnitude of its elongation.

Since molluscs is a poikilothermal animal, its Ca metabolism varies largely with the seasonal changes of the temperature of sea water. If we wish to examine successive stages of the development of the growth spiral on the nacres, it may be fully established by the observation for seasonal change of the spiral growth. Crystal growth of shells begins rapidly as Ca metabolism normalizes after hibernation (see chapter V). A new crystal of lime salts is formed first on the portions consisting of appropriate surfaces for adhesion of them, so a number of crystals will be deposited continually around a first adsorbed crystal. For instance, filaments of algae which encroaches the shells may perform the role as a crystal seed. As seen in figure 143, it is very often recognized that if the growth point of *Conchocelis*-filaments emerges on the inner shell surface, new crystals grow first near that point, from which growth pattern spreads radially. Figures 142~149 are the typical profiles showing successive stages of the development of the growh spiral at all seasons, although the growth pattern is quite different under various conditions of the mother fluid. In an early stage of formation of the layer, individual crystals are scattered here and there, and the growth pattern is indistinct, or irregular. Soon after, the end of the growth steps rotates as clockwise or counter-clockwise, and small growth spirals occur at the

Table XI The relationships among the concentration of Ca ions in the mother fluid, the amount of $CaCO_3$ deposition and spiral growth in central region of the shell in *Pinctada martensii* during the year (1958～1959).

Month	No. of the step in a spiral	Density of spiral per 5 mm^2	The distance between steps (μ)	Growth pattern	The shape of spiral	The amount of $CaCO_3$ deposition (mg/10days)	Concentration of Ca^{++} in the mother fluid (γ/cc)	pH of the mother fluid
VIII ～ IX	25 ～ 50	16 ～ 20	16 ～ 50	spiral. circular	symmetry	7	340～360	8.0～8.2
X ～ XI	15 ～ 25	5 ～ 15	20 ～ 50	spiral, circular	symmetry	4	370～420	8.2～7.9
XI ～ XII	5 ～ 15	3 ～ 13	30 ～ 70	irregular, spiral, circular	twofold axes of symmetry	2	420～450	7.9～7.7
I	5 ～ 8	2 ～ 10	20 ～ 70	irregular	asymmetry		450	7.8～7.5
II ～ III	—	—	—	disappear	indistinct	0	450～480	7.5～7.7
III ～ V	2 ～ 10	1 ～ 10	30 ～100	irregular	asymmetry		480～400	7.6～7.8
V ～ VI	5 ～ 15	1 ～ 12	30 ～100	irregular, spiral, circular	twofold axes of symmetry	3	400～390	7.6～8.0
VI ～ VII	10 ～ 20	20 ～	16 ～ 50	spiral, circular	symmetry	4	400～390	7.6～8.1

large density in unit area as in figure 145. The greater the concentration of calcium carbonate, the larger the rate of rotation of the spiral must be increased, and the ledges turn and turn about the source of spirals. Thus well-developed growth spirals will result (Fig. 147). The growth spiral diminishes under decreasing concentration of calcium carbonate (refer Fig. 148).

Development and emaciation of the spiral growth are controlled directly by the variation of physicochemical and biochemical factors which interfere with the process of calcification. The relationships between the spiral growth and physicochemical elements in the mother fluid are summarized in table XI. After hibernation, the observed concentration of Ca ions decreases successively, and will reach the minimum value in the period between August and October, in which the deposits of calcium carbonate show the maximum value. At the beginning of calcium carbonate deposition, in the portion B_1 in text-figure 4, the spiral exhibits various forms having twofold axes of symmetry, as seen in figure 143. The spacing between the steps is varied widely in different direction from the source and, in general, is very large. The density of the growth spiral is the larger during the short time of crystal growth with the increase of the deposition and soon several ones of these growth spirals develop more predominantly than the others, and the spacing between the steps becomes narrow gradually. The spiral pyramid consists of a large number of the ledge spreading from the center outward with nearly equal spacing in the part A of text-figure 4, and the most of them shows regular round shape. Although the observed concentration of Ca ions in the mother fluid is at maximum in the period from winter to spring at the parts C_1 and C_2 in text-figure 4, the growth of crystals stops perfectly or takes place slightly. As has been described in chapter V, because crystals grow imperfectly and dissolve partially, it is, in general, difficult to recognize the development of the growth spiral. While the observed concentration of Ca ions in the mother fluid increases step-by-step as decreasing rate of the deposits, at the part B_2 in text-figure 4, the development of the spiral may progress in the inverse direction in the process of successive variation of the spiral growth. This was observed during the period from April to September. That is, the spirals are not well-developed, but they will be replaced gradually by the spirals with wide spacing of the step, as seen in figure 148. As mentioned above, irrespective of the increasing or the decreasing process of $CaCO_3$ deposition, the resultant figures of the growth spiral are similar to each other under the same conditions of the mother fluid. However, the shape of the growth spiral depends upon the velocity and the mode of growth of crystals adsorbed on the growth fronts.

The constant relations may be kept among the development of the growth spiral, the velocity of $CaCO_3$ depositions, and the observed concentration of Ca ions in the mother fluid which is produced through the mantle tissue. In addition, it can be inferred from table X that those factors themselves keep up the definite relationships with the pH values of the mother fluid and the body fluid. The curve of $CaCO_3$ deposition runs relating to the pH curve of the mother fluid as has been shown in

chapter I. The variation of pH is assumed to give direct influence not only upon the solubility of calcium carbonate, but also upon the nature of the mother fluid itself, and thus the crystal arrangement will be effected.

4 Discussion

A large number of the steps is needed for the growth of shells, and the step is provided by the spiral growth of micro-crystals in the genus *Pinctada* and the others. The steps originating from the source of the spirals can advance by rotating from the center of the spiral to the edges as clockwise or counter-clockwise. The development of the spiral growth of the nacres seems to be quite similar to the resultant patterns observed at successive stages of the development of the growth spiral which is created by the screw dislocations. The development of the growth spiral is governed by the concentration of calcium carbonate in the mother fluid. It is obviously impossible that the concentration of the solute in the ground of crystal growth produced by a life reaches such a high supersaturation as produced artificially in a laboratory. And that concentration is considered to be always below the critical point of supersaturation. The larger the concentration of calcium carbonate, the greater the rate of growth of spirals increases under such supersaturation. The shape of the growth spiral appears to be analogous to that by the screw dislocations.

In *Pinctada martensii* and all exemined materials, the nacre is not a single crystal but is considered to be a mosaic crystal, as described in chapter II. Hence, the growth of shells is thought to be explained by the mechanism of the growth of single crystals. If the crystal growth of shell salt is attempted to be elucidated only the fact that individual crystal particles are surrounded by the organic material, we may draw the conclusion that the growth of crystals has no relation to each other. However, a large number of very fine hole is recognized on the organic membrane, as has been pointed out by Grégoire *et al.* (1955), and some calcium in mineral matter is assumed to combine in an ionic bond with the suitable parts of the organic matrix, or the crystallites of lime salt on the organix matrix seem to be developed regularly by epitaxial growth (see chapter V). If these we make such the assumption, it is thought that the crystallites of shell salt grow in close relation to one another. Text-figure 20 is

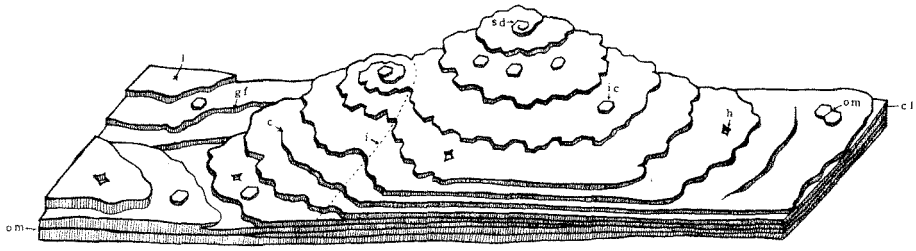

Text-fig. 20 Three dimensional representation of the growth spiral of the nacre. c cliff. cl crystal lamella. gf growth front. h hollow. i intersection of adjacent growth spiral. ic isolated crystal. l ledge. om organic matrix. sd screw dislocation of unit crystal.

the schematic drawing of the relationships between the growth spiral and the crystallites of aragonate in the third dimension of space. The rate of advance of the growth ledges emitted from the center of the growth spiral is independent of the crystallographic orientations in the nacre, and a circular spiral will result. But, since the arrangement of the orthorhombic *b*-axis of the crystallites is affected greatly by the magnitude and the elongation of a mantle tissue, the shape of a growth spiral may extend merely along the elongation of a mantle, and an oval spiral will result.

Besides, we shall take note of that the spiral growth can be seen only in aragonite shells but is never observable in calcite ones. The spiral growth is, however, not revealed in aragonite shells of some species, the structure of which is widely different from the aragonite shells with the spiral growth. Therefore, the spiral growth of shell salts also appears to depend upon the differences of the mineral constituents and the mode of crystal growth. Dawson and Vand (1951) observed on a single screw dislocation emerging on the (001) plane of long-chain paraffin, C_{36} H_{74}, by using the electron microscopes, and pointed out that the step height is 43 ± 5 Å which is equal to the X-ray units cell. Amelinchx (1951) with silicon carbide crystals has shown that the step heights of some spirals are up to 35 Å. On the other hand, Forty (1952) showed that the step height of the growth spirals emerged on (0001) planes of CdI_2 crystals often is several hundred Å. Moreover, in metal crystals, growth of Cd crystals from vapour were observed by Pollock and Mehl (1955), who have pointed out that the step height of the growth spirals on the (0001) plane is in the range of 1000 Å to 1500 Å. The step heights of the growth spirals seen on the nacreous surface (i.e., the (001) planes of aragonite crystals in the layer) are about $1000 \sim 5000$ Å which are not of monomolecular thickness. However, since the step height on the crystal faces grown by screw dislocations is not only an unit cell and monomolecule, the spiral growth of the nacres is also considered to be compatible with the theory of screw dislocations for single crystal.

When two or more growth spirals of same sign or opposite sign come into contact with each other, the respective spiral is intersected with the adjacent one. Then the interactions between the neighbouring spirals are very similar to those of the adjacent screw dislocations. The concentric pattern of the growth pyramids seen on the nacres can be explained by the effect of counter balance of two dislocations.

Sears (1959) has shown that the cylindrical growth of tobacco mosaic virus molecule would be elucidated by the dislocation mechanism. He has pointed out that the pH of its circumstance will relate closely to cylindrical growth. The spiral growth of the nacre, in *Pinctada martensii*, is never found when the pH of the mother fluid is less than 7.5, but developes largely near the pH of 8.0. However, it is clear from the above data that in the process of Ca metabolism, the pH of the mother fluid directly affect the growth of crystals in calcification, and its value is somewhat different between various animals.

As discussed above, the mechanism of the spiral growth of the nacres is explained reasonably accurately by developing the theory of the dislocation mechanism of crys-

tal growth.

5 Summary

1) The growth spiral of the nacres was investigated in connection with physical and chemical conditions of the mother fluid for resolving the mechanism of the spiral growth of Pelecypoda.
2) The general concentration of the mother fluid transported through a mantle tissue seems to vary usually below the critical point of its supersaturation, and to be characterized by different physiological conditions of animal. Accordingly, the shell salt may be crystallized from low supersaturation of the solution. Under such supersaturation, the greater the concentration, the more rapid the development of the growth spiral progresses.
3) The surface of the nacre corresponds to the (001) plane of aragonite crystals, and the orthorhombic *b*-axis of which is arranged regularly in the third dimension of space. Hence, the nacre is considered to be a mosaic crystal.
4) Generally speaking, it appears that the growth spiral of shells exhibits the circular shapes and the rate of advance of the growth fronts is independent in different crystallographic orientation of the nacre. Since the distortion of the spiral elongates along the vector of the horizontal growth direction of the layer, the elongation of the distortion agrees roughly with the orthorhombic *b*-axis of crystallites in the nacres.
5) The development and the counter balance of the growth spiral with same sign or opposite sign are quite similar to those obsereved as the screw dislocations.
6) The step heights of the growth spiral, in *Pinctada martensii*, are about 1000～5000 Å and are not monomolecular thickness. The step height is different widely between various species.
7) The growth spiral can not be observed in calcite shells.
8) The growth spiral detected in animal kingdom is assumed to be controlled more or less by the value of pH in the ground of crystal growth.
9) It is proposed that the mechanism of the spiral growth of shells can be probably explained by developing the theory of dislocations.

References

Amerlinchx, S. 1951. Spiral growth on carborundum crystal faces. Nature 167, 939.

Ashikaga, C. 1951. Biochemical studies on the pearl oyster (*Pinctada martensii*) IV. On the chemical composition of the various tissues and also of the meat of the different ages. J. Agr. Chem. Soc. Japan 24, 432.

Bear, R. S. and Rugo, H. J. 1951. The results of X-ray diffraction studies on keratin fibers. Ann. N. Y. Acad. Sci. 53, 627.

Beck, C.W. 1950. Differential thermal analysis curves of carbonate minerals. Am. Mineral. 35,207.

Beedham, G.E. 1954. Properties of the non-calcarious materials in the shell of *Anodonta cygnea*. Nature 174,750.

———1958. Observation on the mantle of the Lamellibrancnhia. Quart. J. micro. Sci. 99,181.

Bevelander, G. and Benzer, P. 1948. Calcification in marine molluscs. Biol. Bull. 94,176.

Bevelander, G. 1951. A study of calcification in molluscs with special refference to the use of P^{32} and Ca^{45}. New York J. Dentist. 21,305.

———1952. Calcification in molluscs. III. Intake and deposition of Ca^{45} and P^{32} in relation to shell formation. Biol. Bull. 102, 9.

Bourne, G.H. 1956. The biochemistry and physiology of bone. New York.

Bragg, W.L. 1937. Atomic structure of minerals. New York.

Buckley, H.E. 1951. Crystal growth. New York.

Bunn, C.W. 1945. The chemical crystallography. Oxford.

Chore, K.E. 1954. Aspect of the biochemistry of magnesium. 1. Calcareous marine organisms. J. Geol. 62,266.

Dana, J.D. 1951. System of mineralogy II. New York.

Dawson, I.M. and Vand, V. 1951. Observation of spiral growth-steps in *n*-paraffin single crystals in the electron microscope. Nature 167, 476.

Faust, G. T. 1950. Thermal analysis studies on carbonates. I. Argaonite and calcite. Am. Mineral. 35, 207.

Forty, A.J. 1952. Phil. Mag. 43, 72. (cited by Verma, 1953)

Frankenheim, L. 1860. Pogy. Ann. Phys. 33,1. (cited by Buckley, 1951)

Freeman, J.A. and Wilbur, K.M. 1948. Carbonic anhydrase in molluscs. Biol. Bull. 94,55.

Frey-Wyssling, A. 1953. Submicroscopic morphology of protoplasm. Amsterdam.

Fukami, A. 1958. On a high resolution pre-shadowed carbon replica method and its direct stripping technique. J. Electronmicroscopy 6,18.

Fukutomi, T. 1953. A general equation indicating the regular forms of molluscan shells, and its application in geology, especially in paleontology I. J. Fac. Sci. Hokkaido Univ. 3.

Grégoire, C., Duchâteau, G. and Florkin, M. 1955. La trame protidique des nacres et des perles. Ann. inst. Océanog. 31,1.

Grégoire, C. 1957. Topography of the organic components in mother-of-pearl. J. Biophys. Biochem. Cytol. 3,797.

———1958. Sur la structure, étudiée au microscope électronique, des constituants organiques du calcitostracum. Arch. internat. Physiol. Bioch. 66,658.

———1958. Structure et topographie, étudiées au microscope électroniques, des constituants organiques de la nacre chez 24 èspeces (10 familles) des Gastéropodes et de Pélécypodes. ibid. 66,667.

———1960. Further studies on structure of the organic components in mother-of-pearl, especially in Pelecypods 1. Bull. Inst. royal. Sci. natur. Belg. 36,1.

Harada, Z. and Goto, M. 1957. On an experimental condition favourable for the formation of aragonite. J. Mineral. Japan 3,137.

Hirata, A.A. 1953. Studies on shell formation. II. A mantle-shell preparation for in *vitro* studies. Biol. Bull. 104,394.

Holtz, A.H. and Seekles, L. 1952. Direct titration of calcium in blood serum. Nature 169.

Horiguchi, T. 1956. Biochemical studies on *Pteria* (*Pinctada*)*martensii* ((Dunker) and *Hyriopsis schlege-*

li (v. Martens). IV. Absorption and transference of Ca^{45} in *Hyriopsis schlegelli*. Bull. Japan. Soc. Sci. Fish. 23, 710.

———1959. Biochemical studies on *Pteria* (*Pinctada*) *martensii* and *Hyriopsis schlegeli*. VIII. Trace components in the shells of shellfish, part 1, 2. ibid. 25, 392, 397.

———1960. Biochemical studies on *Pteria* (*Pinctada*) *martensii* and *Hyriopsis schlegeli*. XII. On the apparent ion products of $[Ca^{++}] \times [CO_3^{=}]$, $[Ca^{++}] \times [HPO_4^{=}]$ and $[Ca^{++}]^3 \times [PO_4^{\equiv}]^2$ in blood and tissue fluids of shell-fish. ibid. 26, 701. XIII. Effects of the organic acids upon the concentration of Ca ion in shell-fish. ibid. 26, 708.

Hynd, J.S. 1954. A revision of the australian pearl-shells, genus *Pinctada* (Lamellibranchia). Aust. J. Mar. Freshw. Res. 6, 98.

Jodrey, L.H. 1953. Studies on shell formation. III. Measurements of calcium deposition in shell and calcium turnover in mantle tissue using the mantle-shell preparation and Ca^{45}. Biol. Bull. 104, 398.

Kado, Y. 1953. On the scheme of the shell structure of Lamellibranchs. J. Sci. Hiroshima Univ. Ser. B, 14, 243.

———1954. The distribution of alkaline phosphatase in mantle tissue of bivalves. ibid. Ser. B, 15, 183.

———1960. Studies on shell formation in molluscs. ibid. Ser. B, 19, 163.

Kawai, D.K. 1954. Carbonic anhydrase in pearl oyster. I. Distribution and some properties of the enzyme. Mem. Coll. Sci., Univ. Kyoto Ser. B, 19, 39.

———1955. Carbonic anhydrase in pearl oyster. II. Changes of the enzyme activity in relation to growth and seasons. Publ. Seto Mar. Biol. Lab. 5, 89.

Kawakami, I.K. 1952. Studies on pearl-sac formation. I. On the regeneration and transplantation of the mantle pieces in the pearl oyster. Mem. Fac. Sci. Kyushu Univ. Ser, E, 1,83.

Kikuchi, . 1928. Diffraction of cathode rays by mica. Jap. J. Phys. 5, 81.

Kobayashi, K. and Masuzawa, K. 1960. The world through the electron microscope. Japan electron optics Lab. Co., Ltd.

Kobayashi, S. and Tobata, M. 1949. Studies on culture of pearl. II. Activity of pearl-oyster in winter. Bull. Japan Soc. Sci. Fish. 14, 196.

Kobayashi, S. 1950. Daily rhythmic activities of pearl oyster. A preliminary note, presuming the presence of "pearl-enzyme" in the shell-fishes which secret beautiful nacreous substances. J. Fuji Pearl Inst. 1, 17.

Kobayashi, S. and Yuki, R. 1952. Artificial breeding of pearl oyster, *Pinctada martensii* in tanks. Bull. Japan Soc. Sci. Fish. 17, 65.

Kokubo, S. 1929. Studies on the pH and the CO_2-content of the blood. Pericardial fluid, and of the body fluid of the oyster with special reference to their response to the altered condition of sea water. Sci. Rep. Tohoku Imp. Univ. 4,207.

Kōzu, S. and Kani, K. 1934. Thermal expansion of aragonite and its atomic displacements by transformation into calcite between 450°C and 490°C in air. Imp. Acad. Japan Proc. 10, part I, 222. part II, 271.

Lang, A. 1896. Text-book of comparative anatomy II. New York.

Maroney, S.P., Barber, A.A. and Wilbur, K.M. 1957. Studies on shell formation. VI. The effects of dinitrophenol on mantle respiration and shell deposition. Biol. Bull. 112,92.

Mayer, F.K. 1931. Rontgenographiche Untersuchungen an Gastropodenschalen. Jena. Zeitschr. Naturw. 65, 487.

Mayer, F.K. and Weineck, E. 1932. Die Verbreitung des Kalzium karbonates in Tierreich unter besonderer Berucksichtigung der Wirbellosen. Jena. Zeitschr. Naturw. 66,199.

Mori, S. 1948. Daily rhythmic activities of "Martens" pearl-oysters (*Pinctada martensii* (Dunker)). Venus 15, 46.

Nakahara, H. 1957. Some morphological features of pearl-sac tissues in relation to the normal and abnormal pearl production in the pearl-oyster (*Pinctada martensii*). J. Fac. Sci. Hokkaido Univ. Ser. 6, 13, 268.

———1961. Determination of growth rates of nacreous layer by the adoministration of tetracycline.

Bull. Natl. Pearl Res. Lab. 6, 607.

Oesterr, C.Z. 1915. Berg. and Huttenw. 45. (cited by Saylor, 1928)

Ojima, Y. 1952. Histological studies on the mantle of pearl oyster (*Pinctada martensii* Dunker). Int. J. Cytol. 17, 134.

Ôta, S. 1956. Observations on the growth and external character of pearl-oyster in Ômura bay. Bull. Natl. Pearl Res. Lab. 1, 25.

Papapetrou, A. 1935. Z. Krist. A93, 89. (cited by Buckley, 1951)

Pollock, W. I. and Mehl, R. F. 1955. Spiral growth of cadmium crystals from the vapor phase. Acta Met. 3, 213.

Raup, D.M. 1959. Crystallography of echinoid calcite. J. Geol. 67, 661.

———1960. Ontogenetic variation in the crystallography of echinoid calcite. J. Paleontol. 34, 1041.

Robertson, J.D. 1941. The function and metabolism of calcium in the invertebrata. Biol. Rev. 16, 106.

Sawada, Y. 1959. Studies on the change of color of the pearl and the pearl oyster shell by the radiation of γ-ray. Bull. Natl. Pearl Res. Lab. 5, 395.

Saylor, C.H. 1928. Calcite and aragonite. J. Phys. Chem. 32, 1441.

Schmidt, W.J. 1921. Über den kristallographischen Charakter der Prismen in den Muschelschalen. Ztschr. allgen. Physiol. 19, 191.

———1924. Bau und Bildung der Perlmuttermasse. Zool. Jahrb. 45, 1.

Sears, G.W. 1959. Growth of tabacco mosaic virus particles. Science 130, 1477.

Stolkowski, J. 1951. Essai sur le determinisme des formes minéralogique du calcaire chez les êtres vivants (calcaires coquilliers). Ann. Inst. Océanogr. 26, 1.

———1957. Le calcium et la vie. Paris.

Sudo, T. 1958. Chemical mineralogy II. Japan.

Suito, E., Takiyama, K. and Takahashi, M. 1957. Electron microscopic studies on alkaline earth carbonates. (I) Formation by carbonic acid gas method. (II) Electoron microscopic and diffraction studies on precipitated. Bull. Chem. Soc. Japan 78, 1732.

Suzuki,K. 1957. Biochemical studies on the pearl oyster (*Pinctada martensii*) and its growing environments. I. The seasonal changes in the chemical components of the pearl oyster, plankton and marine mud. Bull. Natl. Pearl Res. Lab. 2,57.

Takubo, J. and Ukai, Y. 1952. On the relations between the dielectric constants and chemical constitutions, crystal structures of carbonate and sulphate minerals. Mem. Coll. Sci., Univ. Kyoto Ser. B, 20,121.

Tanaka, S. and Hatano, H. 1952. Studies on the seasonal changes in the chemical constituents of the pearl oyster. Publ. Seto Mar. Biol. Lab. 2,341.

Tanaka, S., Hatano, H. and Itasaka, O. 1960. Biochemical studies on pearl. VIII. Occurrence of calcite, aragonite and dolomite in pearl and shell. Bull. Chem. Soc. Japan 33,182. IX. Amino acid composition of conchiolin in pearl and shell. ibid. 33,543.

Thiele, J. 1934. Handbuch der systematischen Weiohfierkunde. Jena. Gastav. Fischer 3, 826.

Togari, K. and Togari, S. 1955. Conditions controlling crystal form of calcium carbonate minerals. I. The influence of the temperature and the presence of magnesium ion. J. Fac. Sci., Hokkaido Univ. Ser. 6, 9,55.

Tohustone, Merwin, and Williamson. 1916. The several forms of calcium carbonate. J. Geol. 24, 729.

Tsujii, T. 1955. Histochemical studies of nucleic acids on shell- and culture pearl formation. Bull. Biogeograph. Soc. Japan 16-19,88.

Tsujii, T., Sharp, D.G. and Wilbur, K.M. 1958. Studies on shell formation. VII. The submicroscopic structure of the shell of the oyster *Crassostrea virginica*. J. Biophys. Biochem. Cytol. 4,275.

Tsujii, T. 1960. Studies on the mechanism of shell- and pearl-formation in mollusca. J. Fac. Fish. Pref. Univ. Mie 5,1.

Tsutsumi, J. 1928. An examination of micro-crystals of calcium carbonate in molluscan shells by

means of X-rays. Mem. Coll. Sci. Univ. Kyoto Ser. A, 11, part I, 217. part II, 401.
Verma, A.R. 1953. Crystal growth and dislocation. London.
Wada, K. 1956-1957. Electron-microscopic observations on the shell structures of pearl oyster (*Pinctada martensii*). I. Observations of the calcite crystals in prismatic layers. Bull. Natl. Pearl Res. Lab. 1,1. II. Observations of the aragonite crystals on the surface of nacreous layers. ibid. 2,74. III. On the laminary structure of shell. ibid. 2, 86.
———1958. The crystalline structure on the nacre of pearl oyster shell. Bull. Jap. Soc. Sci. Fish. 24, 422.
———1959. On the arrangement of aragonite crystals in the inner layer of the nacre. ibid. 25, 342.
———1959. Microscopic observations of cultured pearls at their early formation III. Bull. Natl. Pearl. Res. Lab. 5, 357.
———1960. The relation between the crystalline structure of the cultured pearls and the elongation of the transplanted mantle tissue in the process of pearl-sac formation. Bull. Jap. Soc. Sci. Fish. 26, 549.
———1960. Crystal growth on the inner surface of *Pinctada martensii* (Dunker) I. J. Electronmicroscopy 9, 21.
———1961. On the relationship between shell growth and crystal arrangement of the nacre in some Pelecypoda. Venus 21, 204.
Watabe, N. 1952. Relation between water temperature and nacre-secreting activity of pearl-oyster *Pinctada martensii*. J. Fuji Pearl Inst. 2,21.
———1954. Electron-microscopic observations of the aragonite crystals on the surface of the cultured pearls 1. Rep. Fac. Fish., Pref. Univ. Mie 1, 449.
———1956. Dahllite identified as a constituent of Prodissoconch I of *Pinctada martensii* (Dunker). Science 124, 630.
Watabe, N., Yoshii, G. and Okada, Y. 1957. Studies of shell formation in young pearl oyster, *Pinctada martensii* (Dunker), using Ca^{45}. Bull. Jap. Soc. Sci. Fish. 23, 139.
Watabe, N., Sharp, D.G. and Wilbur, K.M. 1958. Studies on shell formation. VIII. Electron microscopy of crystal growth of the nacreous layer of the oyster *Crassostrea virginica*. J. Biophys. Biochem. Cytol. 4,281.
Winchell, A.N. 1942. Elements of optical mineralogy. New York.
Wilbur, K.M. and Jodrey, L.H. 1952. Studies on shell formation. I. Measurement of the rate of shell formation using Ca^{45}. Biol. Bull. 103, 269.
———1955. Studies on shell formation. V. The inhibition of shell formation by carbonic anhydrase inhibitors. ibid. 108, 359.

Explanation of Figures

Abbreviations used in Figures

a: anterior, as: adductor muscle scare, cnl: central region of the nacreous layer, d: dorsal, g: gill gc: the ground of crystal growth, hl: hinge line, hy: hypostracum, icm: intercrystallinic membrane, ie: inner epithelium, if: inner fold, ilm: interlamellar membrane, ipw: interprismatic wall, li: ligament, lm: longitudinal muscle, ma: peripheral area of the mantle, mb: pallial area of the mantle, mf: middle fold, mnl: marginal region of the nacreous layer, nl: nacreous layer, o: organic membrane, oe: outer epithelium, p: posterior, pl: prismatic layer, ps: pallial muscle scare, sf: shell fold, tm: transverse muscle, v: ventral.

Fig.1. A micrograph showing the ground of crystal growth in the shell of Lamellibranch. Transverse section of the decalcified shell of *Mytilus edulis*. × 48
Fig.2. Transverse section of the mantle of *Pinctada martensii*. × 18
Figs. 3 and 4. Microincinerated mantle of *P. martensii* showing distribution of inorganic granules. × 18, × 54
Fig.5. The outline of the inner side of the valve in *P. martensii*. × 3/5
Fig.6. Large and small round crystals in definite orientation on the growth front of the prismatic

lamina. Prismatic chambers are laid down under thick conchiolin membrane having the oriented fibrous structure, and the boundary of the underlying chambers is observed as a groove on the membrane. × 3300

Fig.7. Dendritic growth of mineral substance deposited along the boundary of underlying polygonal chambers. × 3000

Fig.8. The edge of a growth process showing round mineral matters in oolitic aggregation on thick organic membrane. × 150

Fig.9. Oolitic aggregation of mineral matters on the prismatic layer near the nacreous layer. × 140

Fig.10. Rosette shape of prismatic substance. × 170

Fig.11. Prismatic chambers themselves in the upper layer dividing into several smaller chambers during the layer formation. × 150

Fig.12. Pattern near the boundary of prismatic and nacreous layers. The prismatic layer shows honycomb zone. × 90

Fig.13. Prismatic lamina of *Pinna attenuata* stained by von Kossa's method. × 150

Figs.14 and 15. Chambers with round shape in prismatic region near the nacre. Organic substance sandwiched between chambers climbs up mineral part, and in the end, covers perfectly on mineral substance. × 4000

Fig.16. Polygonal chambers in the middle part of the prismatic layer. Conchiolin walls running as grooves between mineral portions. × 3000

Figs.17 and 18. Polygonal chambers of the prismatic layer under crossed nicols. × 350

Fig.19. Directions image of the chambers of the prismatic layer in *P. martensii* and *Pinna attenuata*.

Fig.20. Vertical section of the prismatic layer etched with 0.1% HCl, showing thick conchiolin walls and thinner ones running perpendicular to the inner shell surface. Mineral substance is densely compacted in the polygonal prismatic chambers bounded by conchiolin walls. × 6000

Fig.21. Positive replica obtained from fracture surface of the prismatic layer showing laminary structure and distribution of organic matrix. × 3000

Fig.22. Vertical thin slice under crossed nicols. × 350

Fig.23. Round crystals scattered in thick organic layer between the prismatic and nacreous layers. The nacre can be found in upper part. × 3000

Fig.24. Parallel growth pattern of the nacre. × 37

Fig.25. A highly magnified portion in Fig.24. × 2000

Fig.26. Spiral growth of the nacre. × 37

Figs.27 and 28. General change of growth pattern under abnormal condition of *P. martensii* in summer. × 190, × 440

Fig.29. Dissolution phenomena of the shell salt in the same condition and species as above. × 2000

Fig.30. New crystal grown on the etching surface of the shells of animal recovering health. × 2000

Fig.31. Ridge-like aggregation of lime salt in the shells of animal recovering health. × 2000

Fig.32. Laminary structure of the nacre in *P. martensii*, showing spatial relationships between organic and mineral matters. Organic matter is seen as reticulated membrane between individual crystals and between mineral lamellae. × 15000

Figs.33 and 38. Laminary structure of the nacres in *Hyriopsis schlegeli* × 8800, *Turbo colnutus* ×4400, *Quadrula undata* × 4400, *Unio margaritifera* × 4400, *Pinctada margaritifera* × 4400, and *Haliotis discus* × 8800, respectively.

Fig.39. Nacreous surface fractured obliquely. × 3000

Fig.40. Directions image given by the parallel thin slice of the nacre in *P. martensii*.

Fig.41. Thin slice of the nacre under crossed nicols, showing three zones which are different from each other in extinction. × 60

Figs.42 and 43. X-ray diffraction pattern given by parallel thin slices of the prismatic layer in *Pinna attenuata* (Fig.42) and the nacre in *P. martensii* (Fig.43).

Figs.44 and 46. Rotation photographs of the nacre in *P. martensii*. Fig.44 rotated around the axis parallel to the horizontal growth direction of the layer; in Fig.45 the direction of the rotation axis is at right angle to the axis in Fig.44; in Fig.46 the direction parallel to the vertical growth of the layer is selected as rotation axis.

Figs.47 and 48. Reflexion spots produced by the different width of the same preparation, with 5 mm in width in Fig.47 and with 0.5 mm in width in Fig.48.

Figs.49 and 50. Rotation photographs given by the different thickness of the same preparation; Fig.49 obtained with 1～0.5 mm in thickness and Fig.50 with about 0.2 mm in thickness.

Fig.58. A living mantle tissue of 4 days after operation. × 30

Fig.59. Showing the edge of the same graft in Fig.58. × 250

Fig.60. Schema showing relation between the initial elongation of the epithelium and the crystalline structure of the nacre secreted by the rearranged epithelium derived from a graft. The point O is considered to be the adhered part of the grafted mantle piece, and the dotted area indicates the deposition of prismatic substances.

Fig.61. X-ray pattern given by the organic matrix of the nacre.

Fig.62. Topography of organic matrix in the decalcified prismatic layer shown by the phase contrast microscope. × 900

Fig.63. The distribution of inorganic components in the organic matrix obtained from decalcified prismatic layer by the techniques of microincineration method (horizontal section). × 120.

Fig.64. Ultra thin section of the decalcified prismatic layer of *P. martensii* showing sub-micro structure of the organic matrix. Mineral substances are compacted in positive parts before decalcification, and the negative part indicates the presence of organic substance. Striation is found in the cords. × 5200

Fig.65. Sub-micro structure of the interprismatic conchiolin wall in the prismatic layer of *P. martensii*. The conchiolin wall consists of many cords of conchiolin about 0.1～0.5 μ in width. × 6200

Fig. 66. Showing fibrous structure of the organic matrix in the prismatic layer. ×10000

Fig. 67. Vertical section of the decalcified nacreous layer under the phase contrast microscope showing topography of the organic matrix. ×2800

Fig. 68. Topography and structure of the organic matrix in the nacre. Striation of the cords of conchiolin. ×17000

Figs. 69～80. Electron micrographs and diffraction patterns for the shell substances during the development of *P.martensii*; D-shaped larva in Figs. 69 and 70, Umbo larva in Figs. 71 and 72, by young shell less than 1 mm in shell length in Figs. 73, 74, 75 and 76, and young shell between 1 mm and 2 mm in shell length in Figs. 77, 78, 79 and 80. ×9000

Fig. 81. Organic matters grown on the glass, inserted between mantle and valve. ×380

Fig. 82. Mineral substance deposited on the organic matters on the similarly inserted glass. ×380

Fig. 83. The same preparation as used in Fig. 90 under crossed nicols. ×520

Fig. 84. Deposition of organic and mineral components on the inserted glass in *Pinna attenuata*. ×390

Fig. 85. Rosette-shaped organic matter which is deeply stained in the test of metachromasia reaction. ×520

Fig. 86. Showing well-developed rhombic form of calcite deposited on the inserted glass coverslip. ×520

Fig. 87. Unit crystal of calcite which is considered to develop by corner growth. ×520

Fig. 88. Spherulite of the shell salt formed on the inserted glass. ×520

Fig. 89. The same part used in Fig.88 under crossed nicols. ×520

Fig. 90. Reticulated structure of organic membrane. It is worthy of notice that there are relationships between the networks of the organic matter and deposition of small crystals in the middle part of the figure. Arrows indicate these small crystals. ×10000

Fig. 91. Dendritic growth of mineral matters on the organic matrix. ×3000

Figs. 92 and 93. Electron micrograph and diffractogram for the first formed shell substance on the inserted glass. N-pattern is given by mineral matter. ×8000

Fig. 94. Crystals of mineral matter in or on the organic matrix. ×6600

Fig. 95. Superficial structure of unit crystal of calcite in Fig. 86. ×5000

Fig. 96. Growth pattern seen on the (0001) plane of calcite. ×3000

Fig. 97. Dendrites of micro-crystals grown on the surface of unit crystal of calcite. ×5000

Fig. 98. Radial pattern on the surface of the spherulite of shell salt. ×19000

Fig. 99. Successive processes of growth of shell lime salt in the spherulite formation. ×10000

Figs. 100 and 101. The crystalline structure and the shape of the spherulite by using extraction replica. The electron micrograph and diffraction pattern suggest that spherulite composed of calcite is analogus to hedgehog dendrite in structure. ×450

Fig. 102. Aragonite crystals of well-developed form on the inner surface of the nacre of the pearl oyster which was collected from Ago Bay in December, showing the tabular idiomorphic shape bounded by the (110), (010), and (001) planes. They develop by parallel growth. ×13000

Fig. 103. A large crystal consisting of mosaic aggregates of smaller crystals, about 1～0.7 μ in size ×13000

Fig. 104. Stepped surface of aragonite crystals during growth. ×6500

Figs. 105 and 106. Aragonite crystals deposited during the period from August to early October. Since they have rounded corners and coverd edges, their shapes exhibit circular. The boundary of crystals is found clearly in Fig. 105 (×6400), and new growing crystals are connected with the underlying crystal lamella by the bridges of shell substances in Fig. 106 (× 12000).

Fig. 107. Growth of aragonite crystals seen in the spawning season, showing complex forms with the serrated edges. ×9500

Fig. 108. Dissolution of shell salts in the spawning season ×6500

Fig. 109. Growth hillocks revealed on the (001) plane of aragonite in winter. ×6500

Fig. 110. Organic membrane formed on the surface of mineral substance as soon as after hibernation. ×16000

Fig. 111. Dissolution of aragonite crystals in hibernation. The edges and corner become round with dissolution. ×4500

Fig. 112. Triple twin of aragonite and indefinite shapes of small shell lime salts occurred in spring ×4500

Fig. 113. Growth and dissolution of new crystals deposited on the old lamella formed before hibernation. ×9500

Fig. 114. Photograph showing a typical example of overgrowth of aragonite crystals seen in the limitted area near the posterior adductor muscle scare of *Pinna attenuata*. ×210

Fig. 115. Schema illustrating the overgrowth in Fig. 122.

Fig. 116. Parallel growth of aragonite crystals in *Pinctada martensii*. ×2200

Fig. 117. Oriented growth of small crystals on the edges and the corners of larger ones in the period from January to early February. The crystals are dissolved slightly, and exhibit round shapes. ×17000

Fig. 118. Small crystal adsorbed along the boundary between crystals in the underlying lamella, and concurve dissolution of a crystal in the upper left. ×4500

Fig. 119. An example for dendritic growth of aragonite crystals in *P. martensii*. ×6700

Fig. 120. A branching consisting of a group of aragonite crystals which join with each other on the (010) plane. ×9500

Fig. 121. Screw dislocation with hexagonal shape of unit crystal of aragonite grown on the nacreous surface of *P. martensii*. ×9500

Fig. 122. Screw dislocation with circular shape emerged on the (001) plane of aragonite, and concentric growth pattern on the crystal in the lower left. The granular background is organic membrane, on which small crystals develop here and there. Organic matrix is sandwiched

between adjacent crystals, and the boundary of crystals can be found as the straight lines on the surface. ×13000

Figs. 123~126. Successive stages of general dissolution of shell salts, showing mosaic structure occurred by the development of etch pits in Fig. 124. ×6500, ×6200, ×3000, ×11000

Fig. 127. Round growth hillocks on the side faces of aragonite, and layers extending from certain positions of the (001) face. ×15000

Fig. 128. Steep cliff of crystal lamella. ×11000

Fig. 129. Curve surface of aragonite seen in weakening shells. ×2000

Fig. 130. Growth of micro-crystals of calcites in the prismatic layer. ×9000

Fig. 131. Dendritic growth of spindle crystallites of calcite in *P. martensii*. ×6000

Fig. 132. Parallel growth of calcite in *Anomia lischki*. ×450

Fig. 133. Calcite crystals with tabular forms, and micro-crystals growing on the (0001) plane of larger ones in *A. lischkei*. ×6400

Fig. 134. Tabular shapes of calcite crystals in the calcitostracum of *Ostrea gigas*. ×6400

Fig. 135. Needles of calcite seen in the calcitostracum of *Chlamys nobilis*. ×6500

Fig. 136. A typical feature for growth spirals of the nacre. The center of the spiral is the highest, and the ledge goes down gradually toward the perimeter of the spiral just like the contour-line in a map. ×85

Fig. 137. The opposite sign spirals in the upper part and the same sign ones in the lower part ×85

Fig. 138. Photograph showing the relationships between the crystal arrangement and the growth spiral in the center of a growth pyramid. ×300

Figs. 139 and 140. The relative arrangement of aragonite crystals near the boundary of two adjacent growth spirals of the same sign (Fig. 139), and those of the opposite sign (Fig. 140). ×300

Fig. 141. The distortion of the growth spirals in posterior of the shell. ×50

Figs. 142~149. Seasonal changes of the growth spiral of the nacre in *P. martensii* showing following patterns : The irregular growth pattern newly grown on the old one which is formed before hibernation as seen in Fig. 142; concentric pattern developing around *Conchocelis*-filaments in Fig. 143 ; the growth pattern in April in Fig. 144 ; that pattern in May in Fig. 145; that pattern in the period from June to August in Fig. 146 ; that pattern during the period from late August to early October in Fig. 147; that pattern in winter in Fig. 148, and the dissolution of growth pattern in hibernation in Fig. 149. ×60

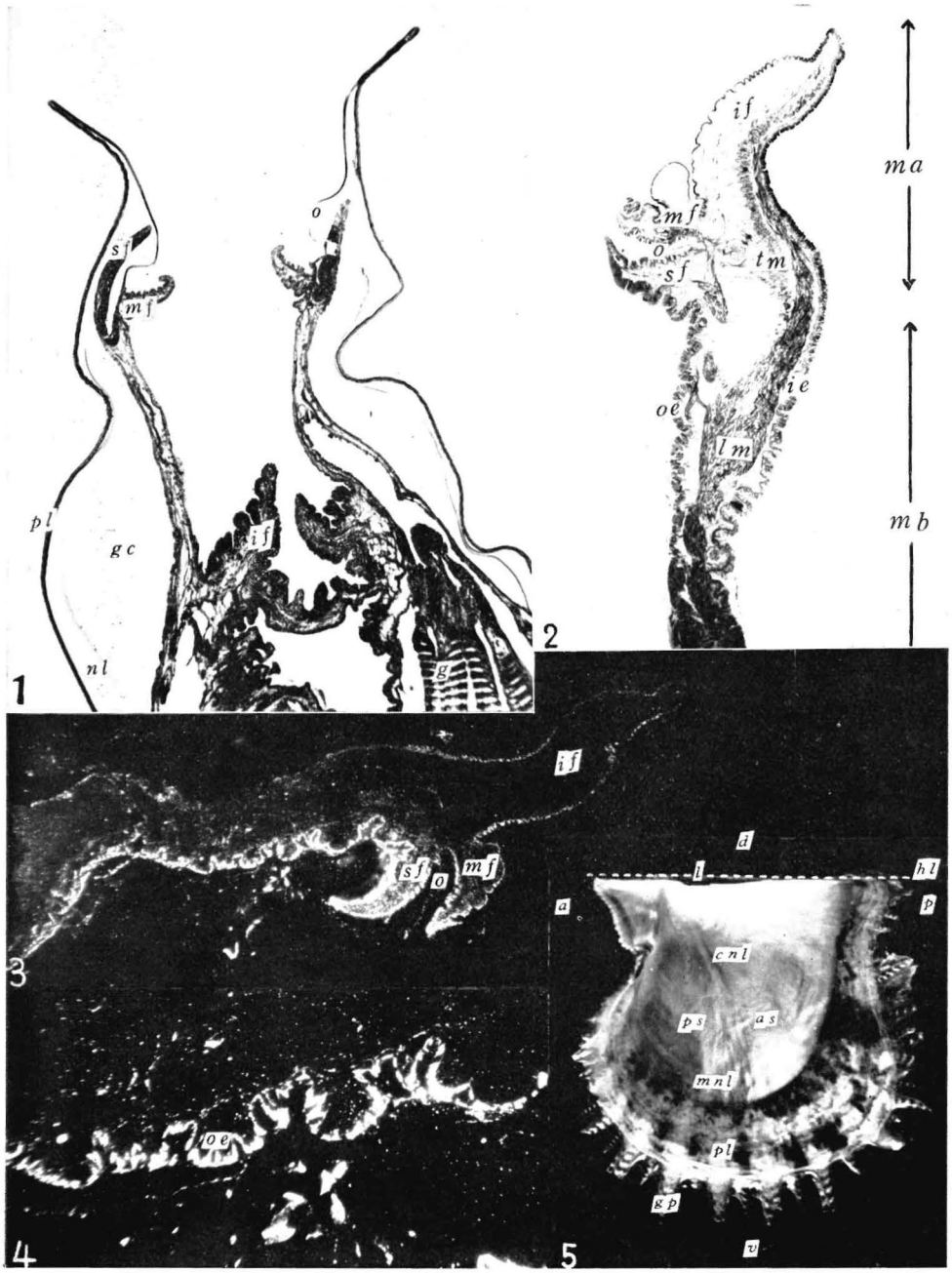
1
sf
mf
o
pl
gc
if
nl
g
2
if
mf
o
sf
tm
ie
oe
lm
ma
mb
3
if
sf
o
mf
4
oe
5
d
l
hl
a
p
cnl
ps
as
mnl
pl
gp
v

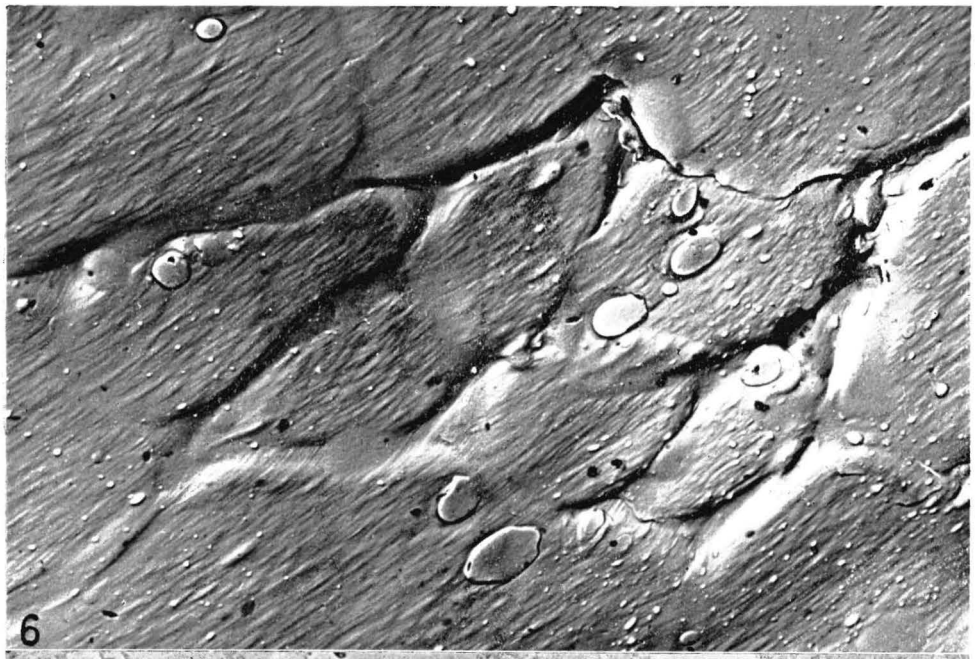

6

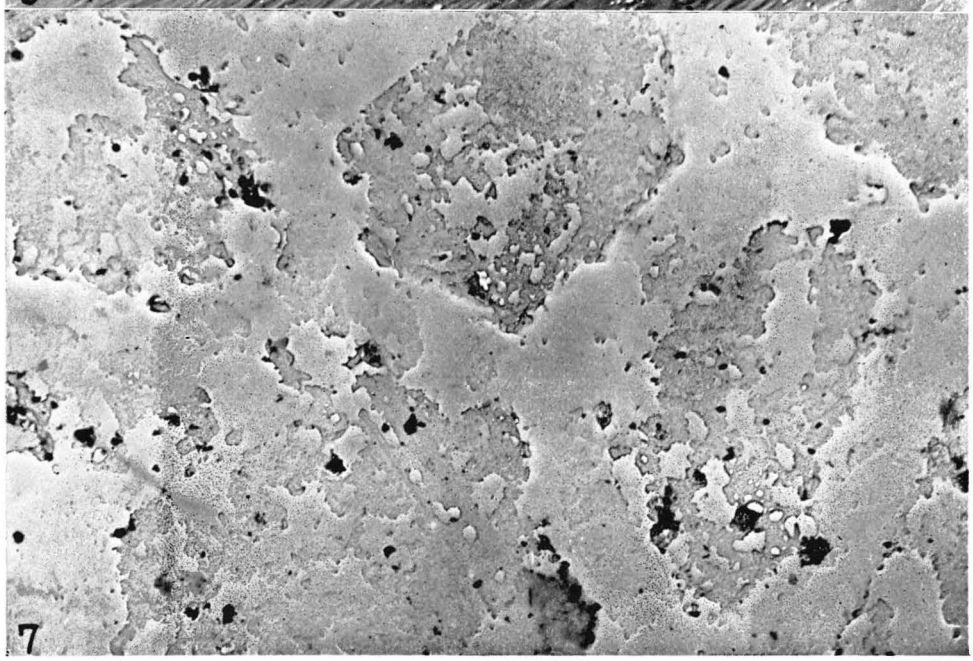

7

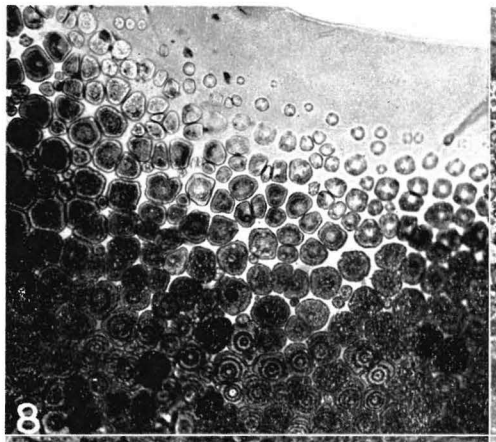
8

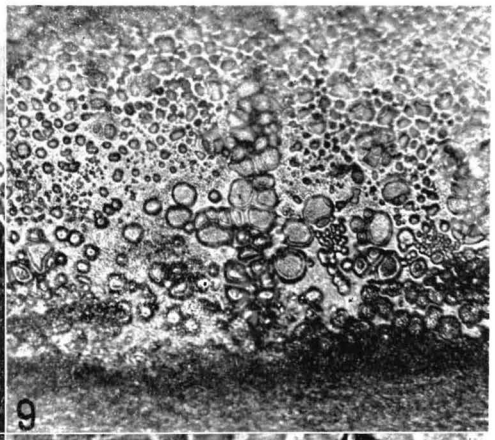
9


10

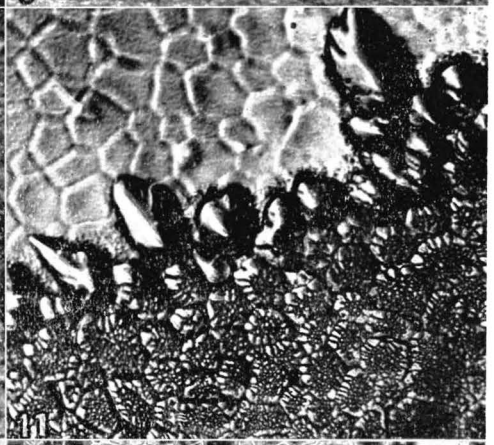
11

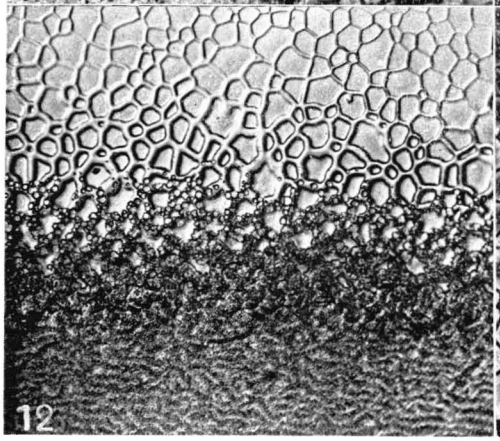
12

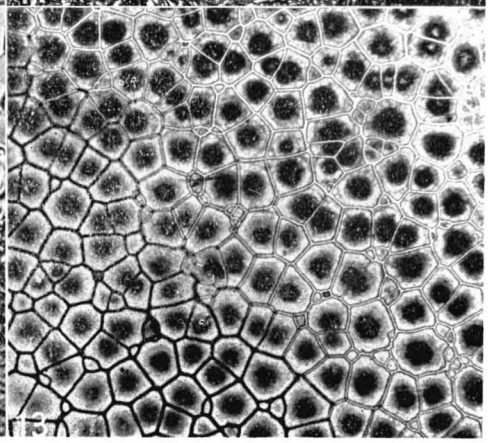
13

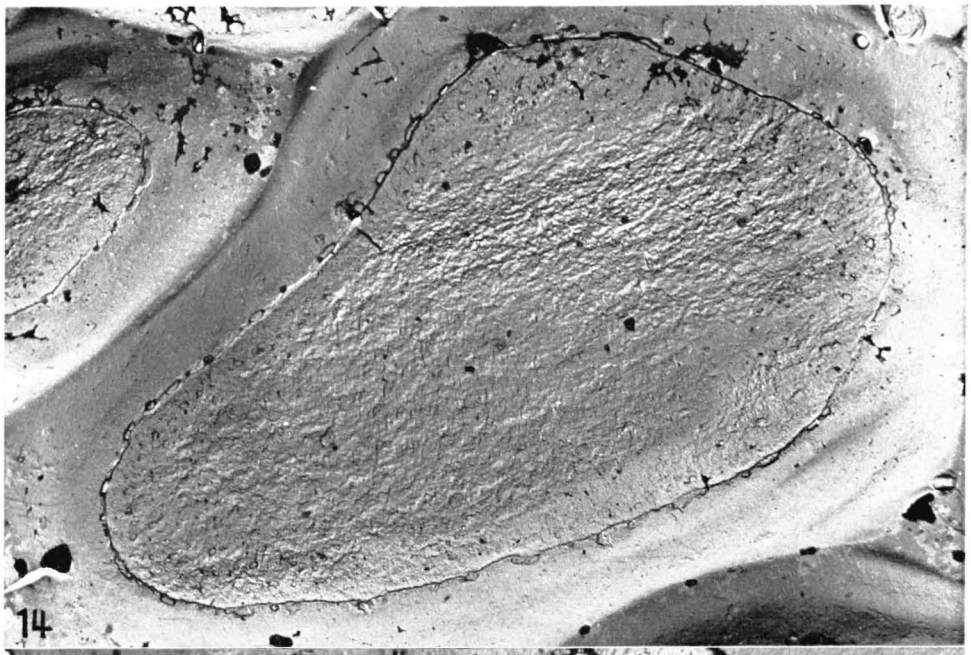
14

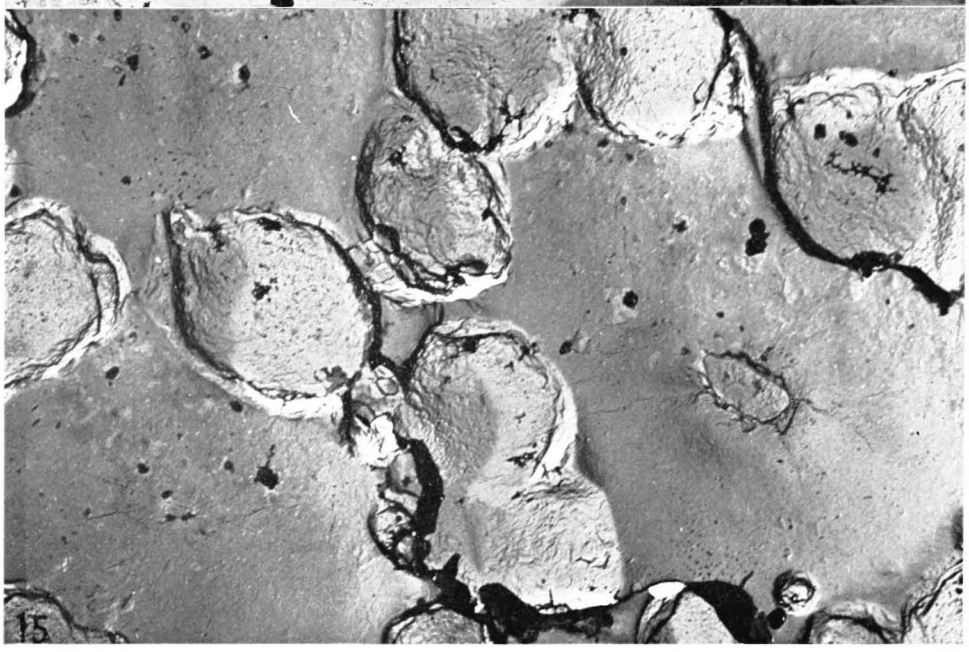
15

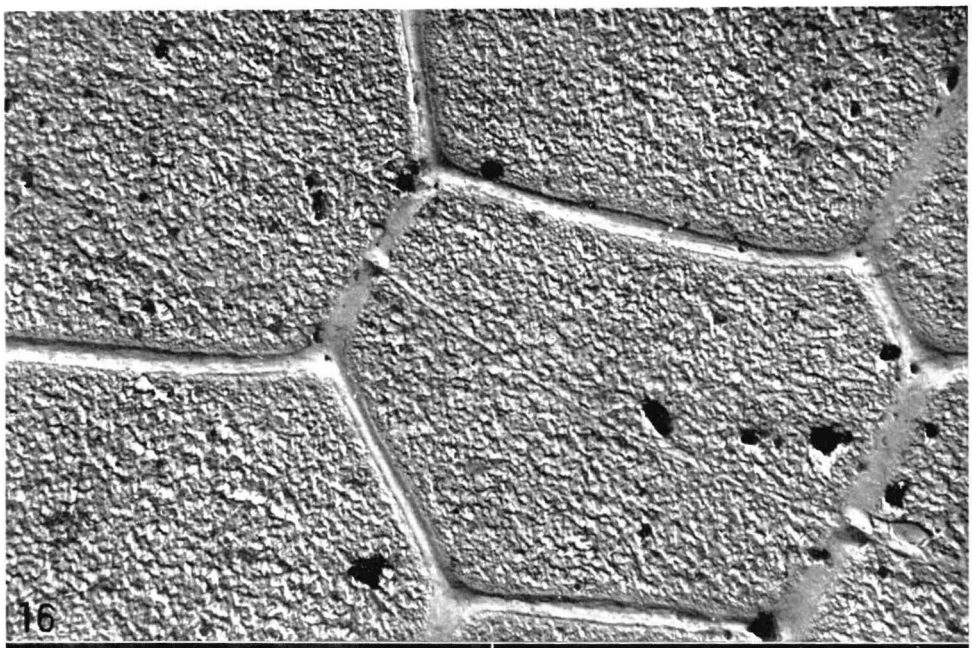
16

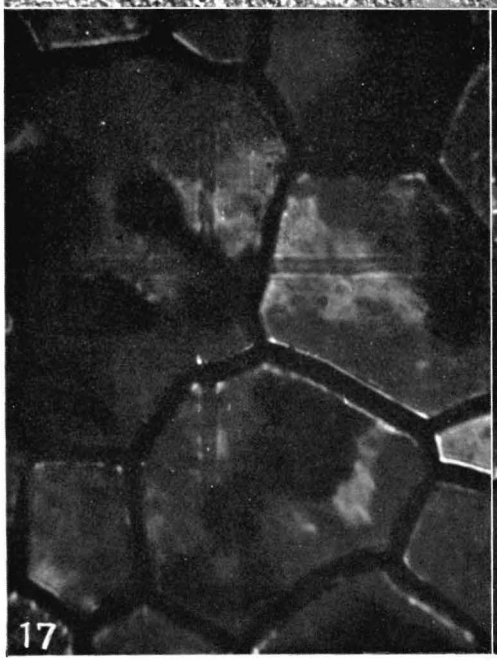
17

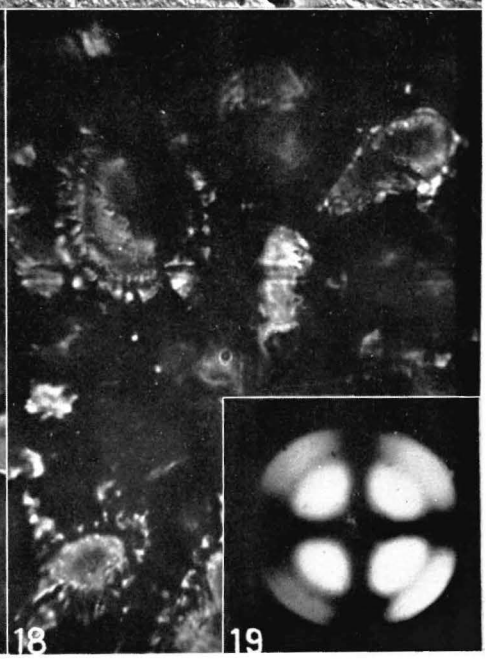
18
19

20

21

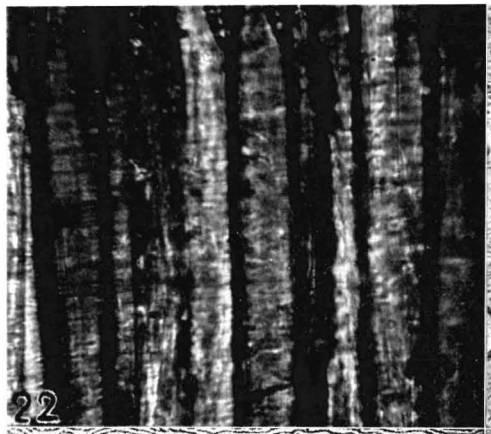
22


23

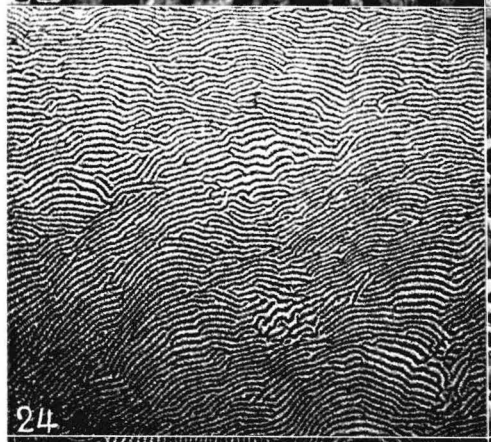
24

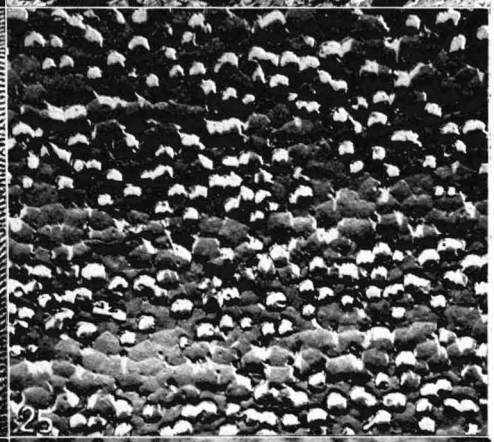
25

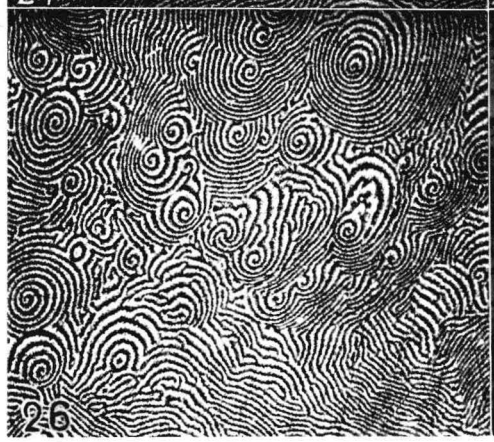
26

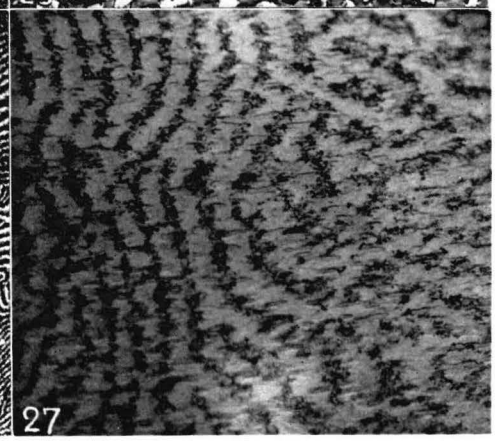
27

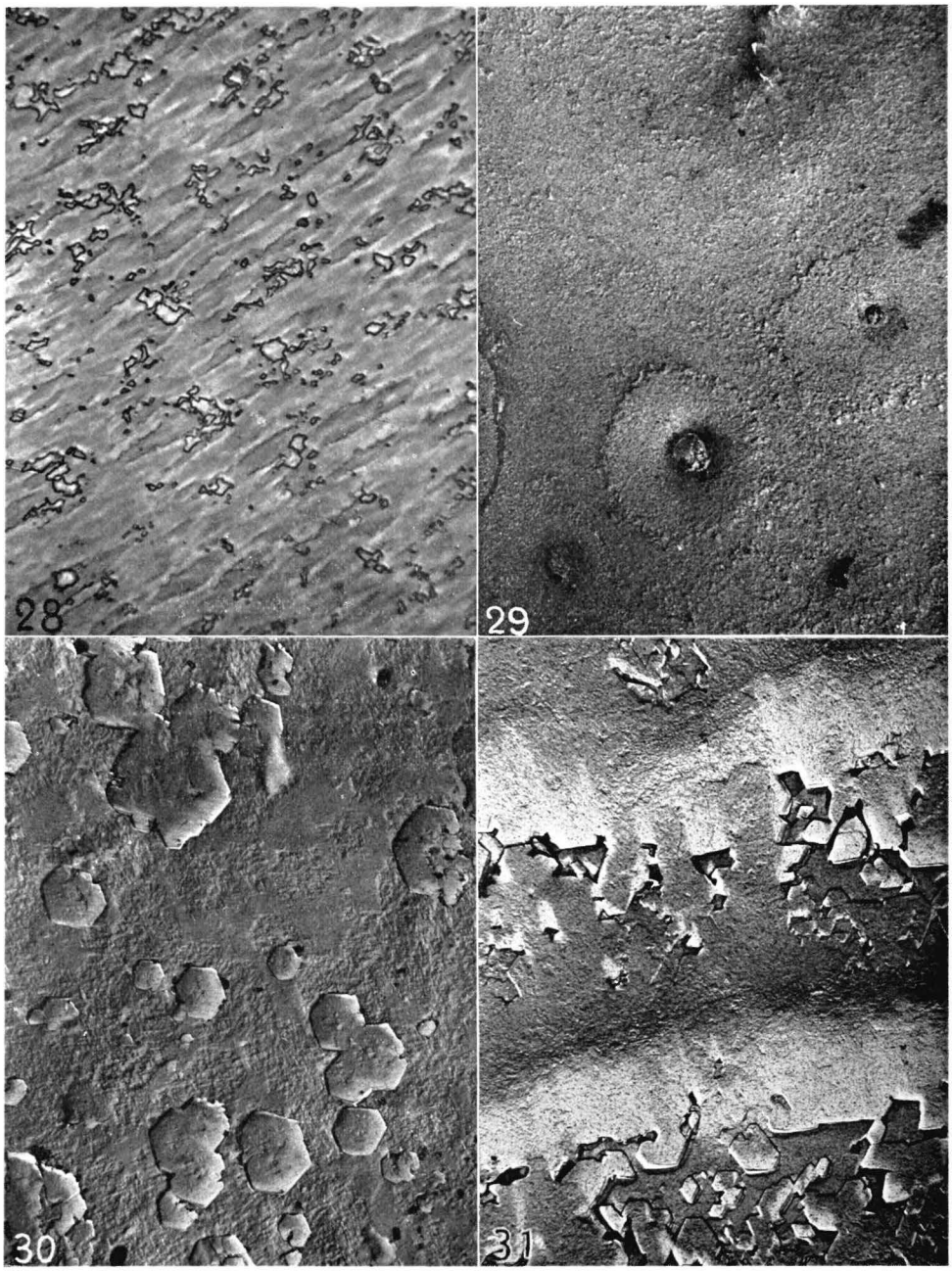
28
29
30
31

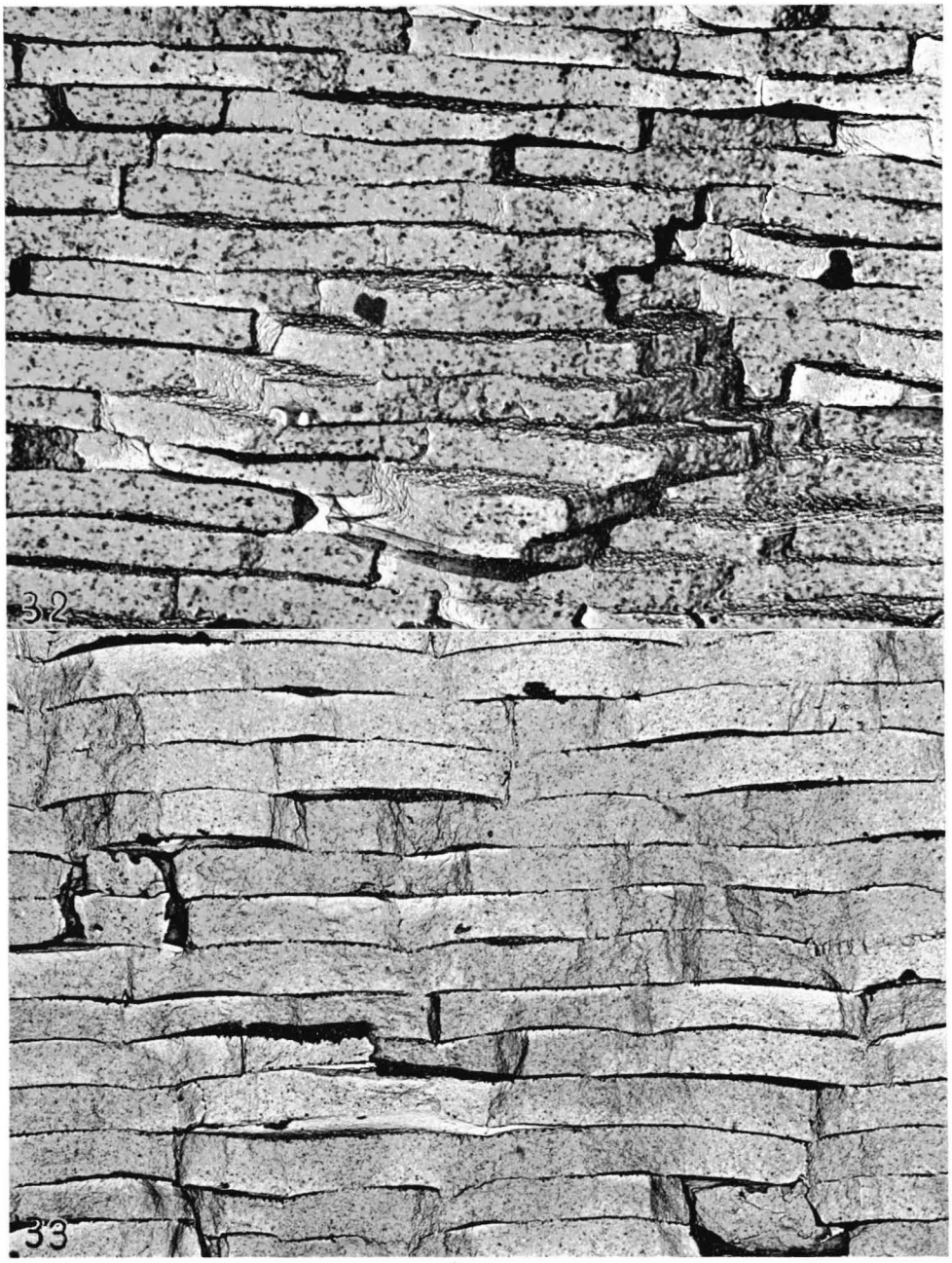
3.2
33


35
36
37


38


39

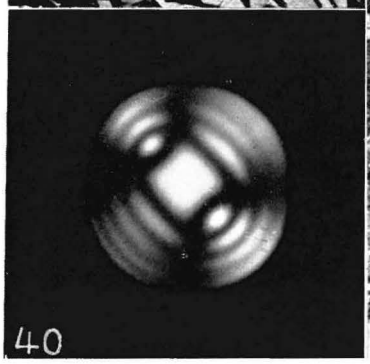
40

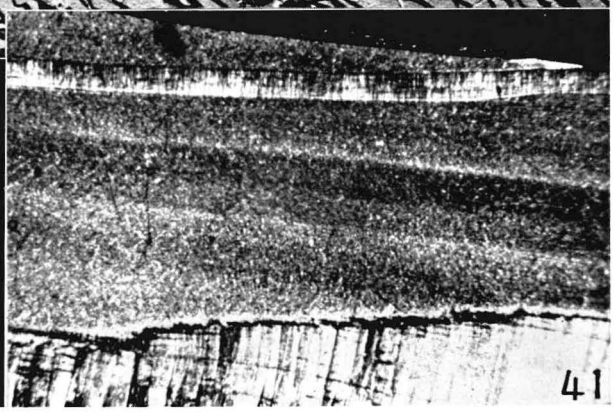
41

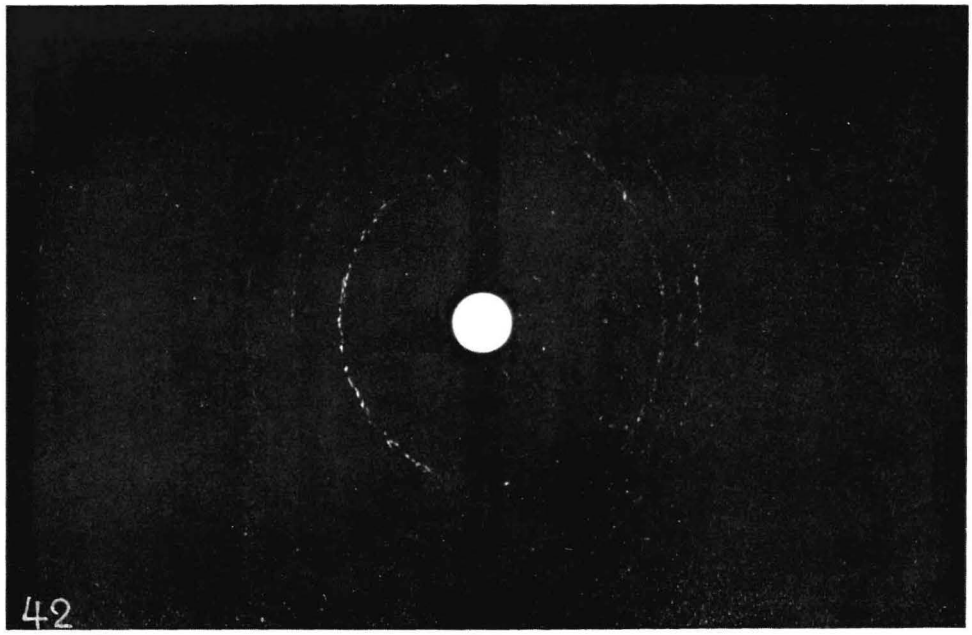
42

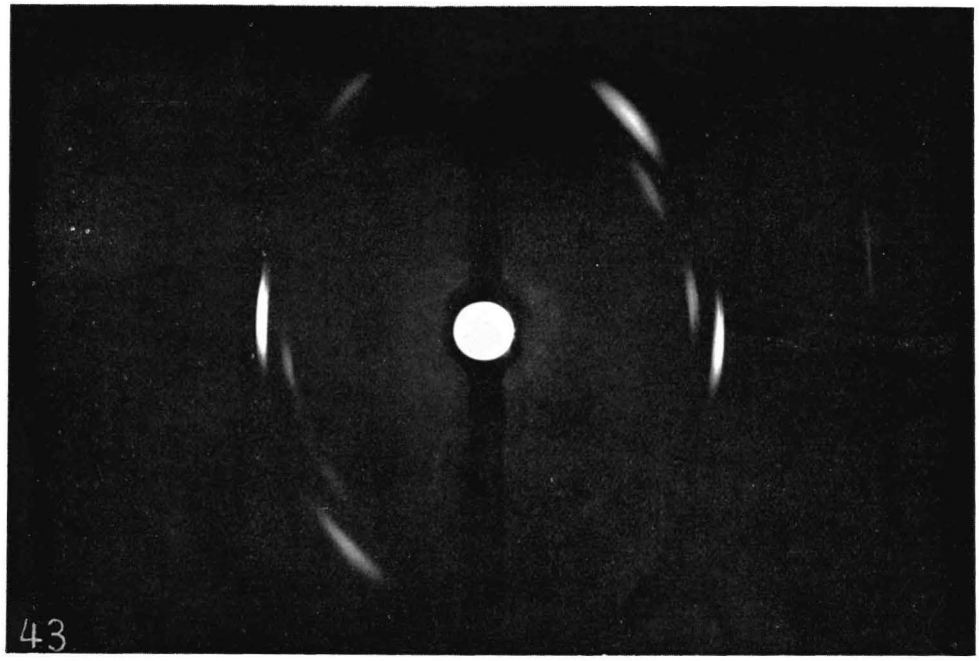
43

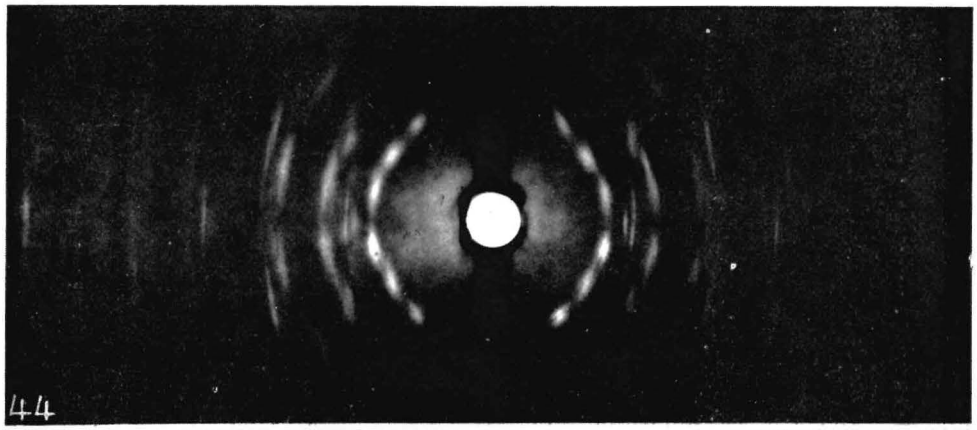
44

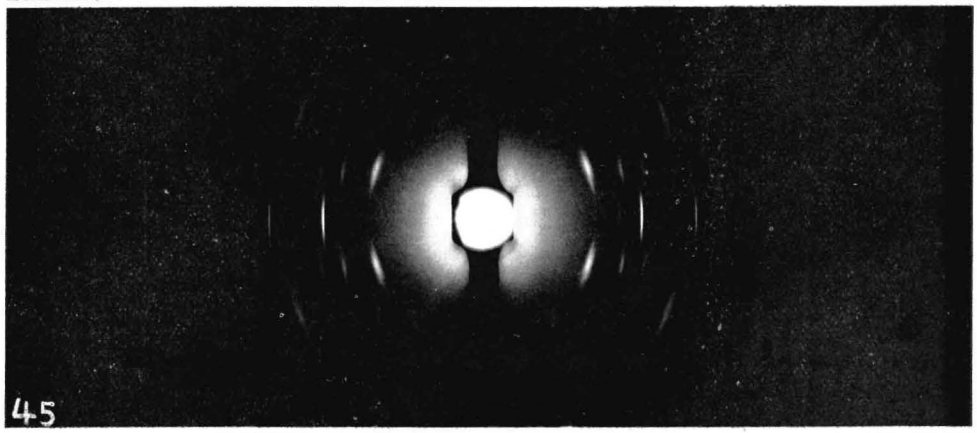
45

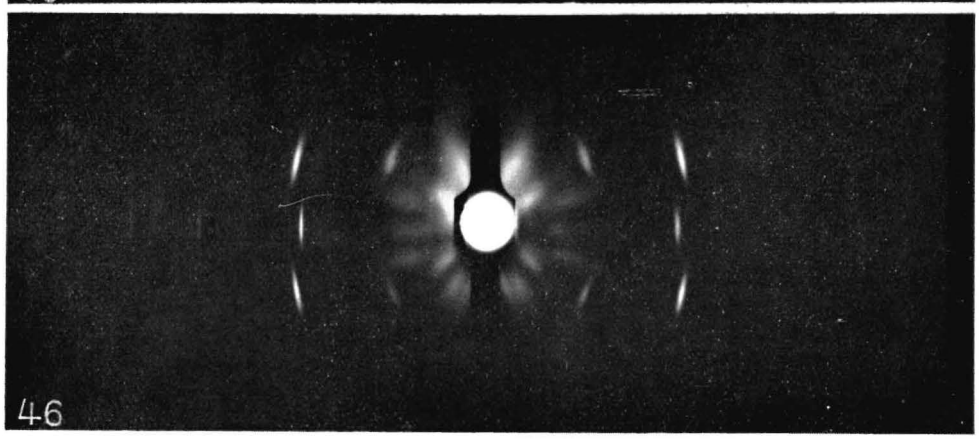
46

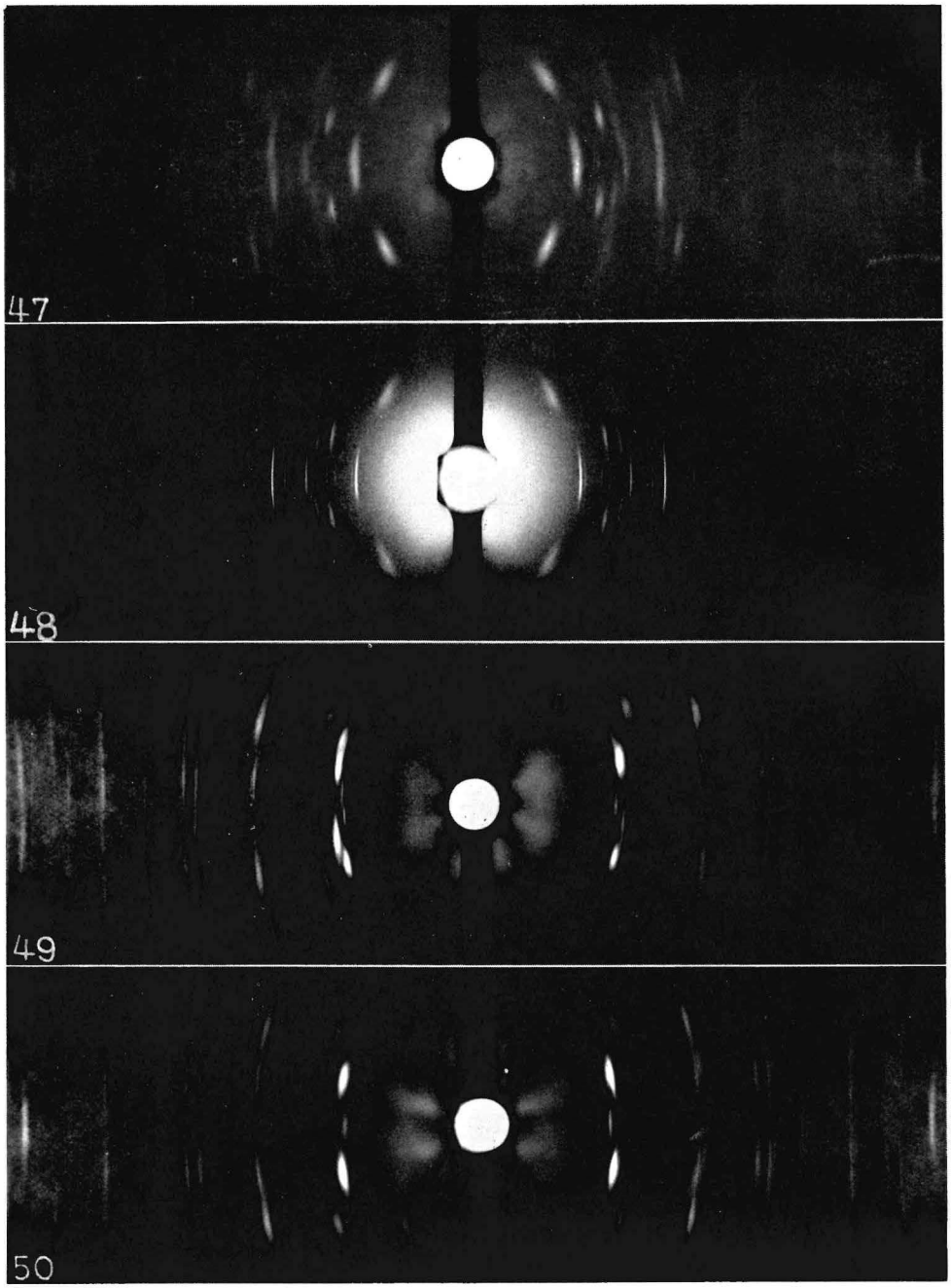
47
48
49
50

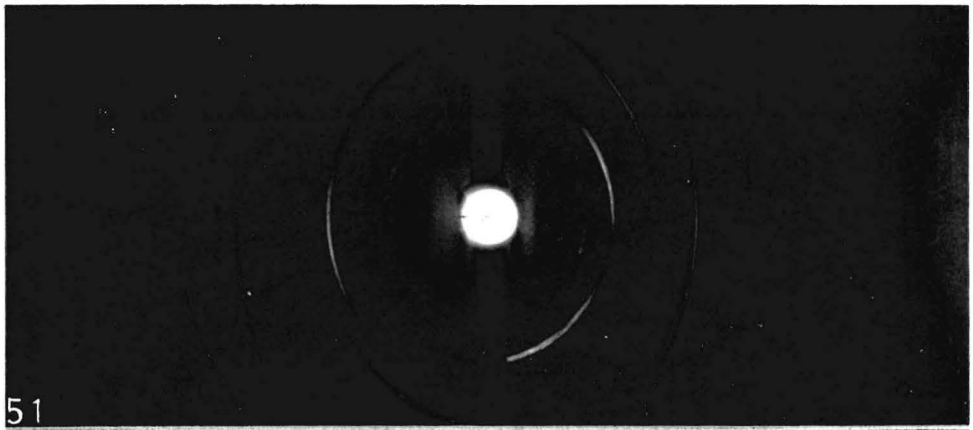

51

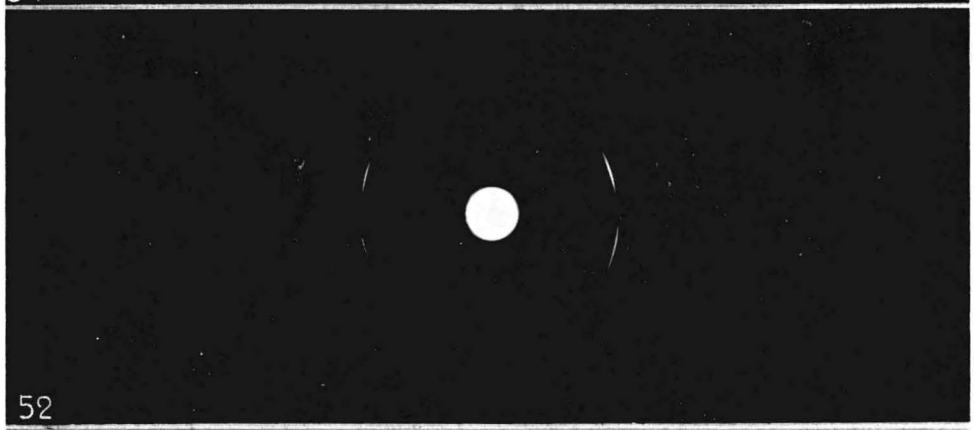

52

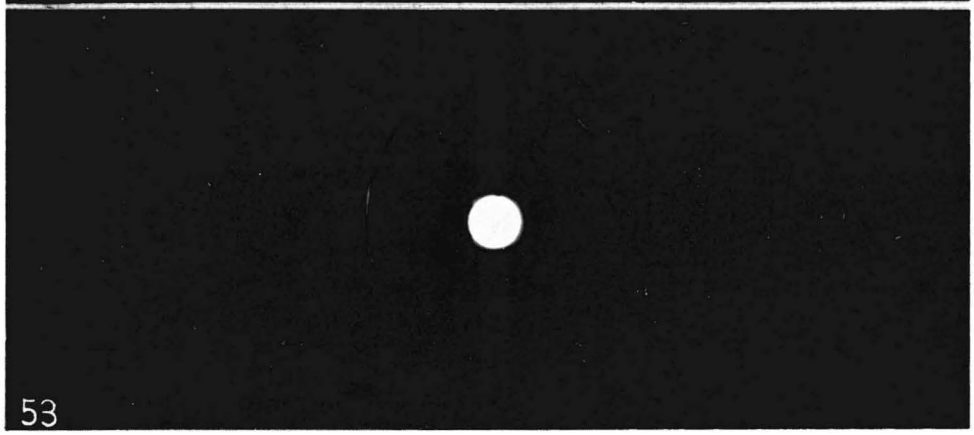

53

54
55
56
57

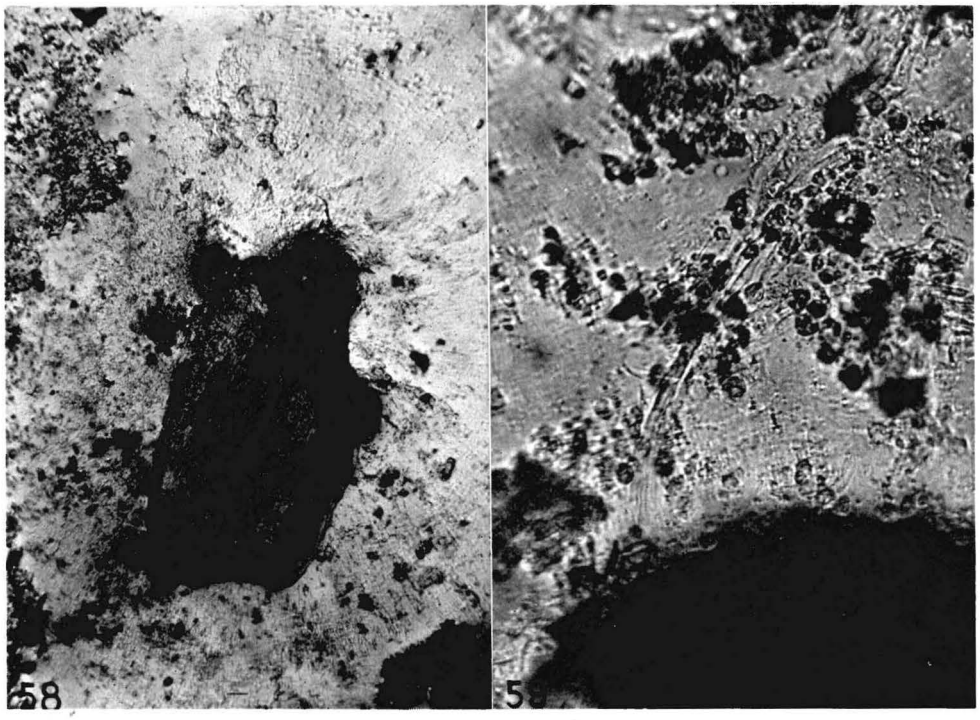
58
5

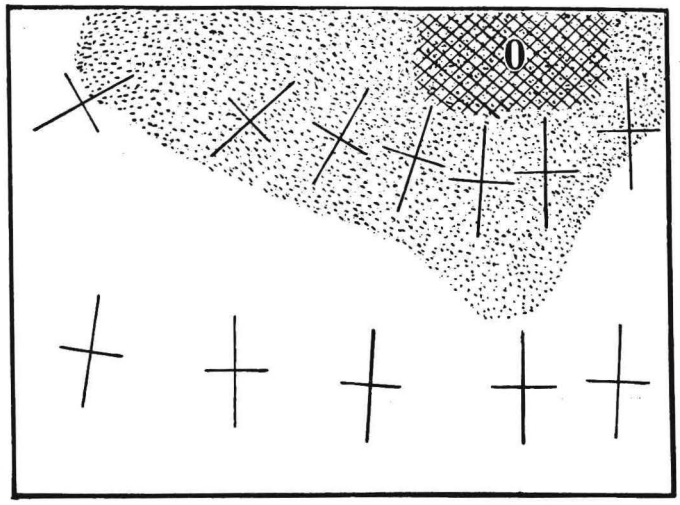
0
60

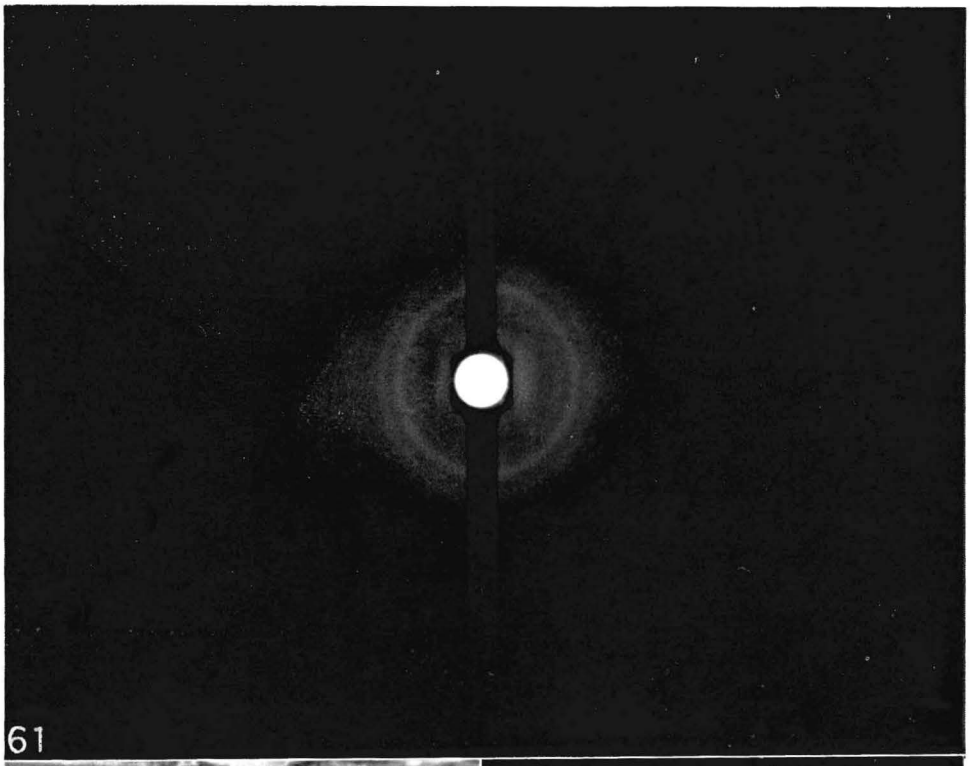

61

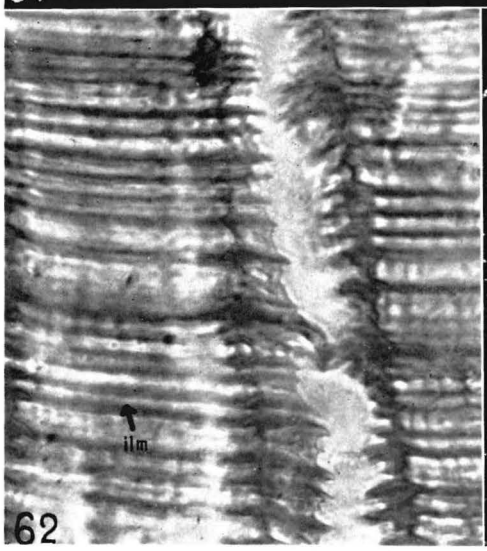

62

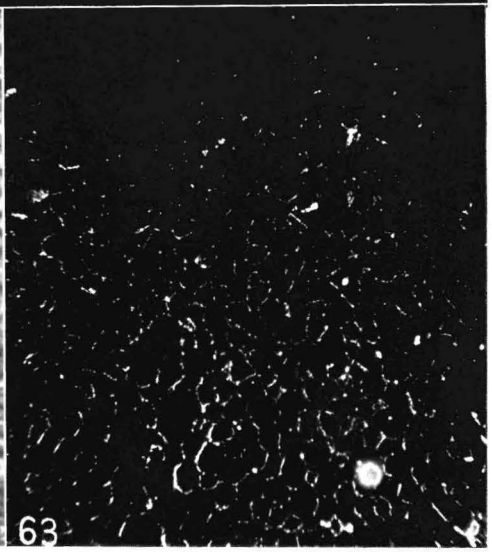

63


ipw
64

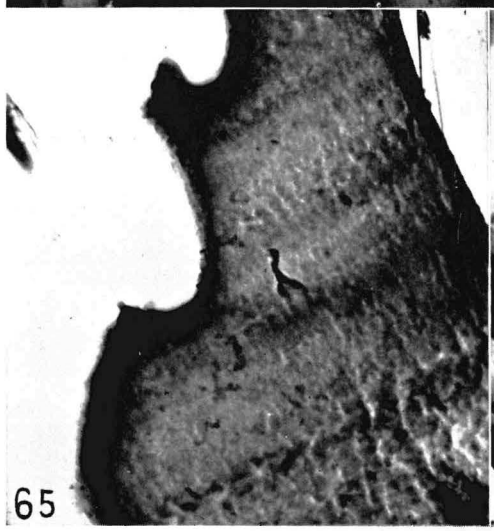
65

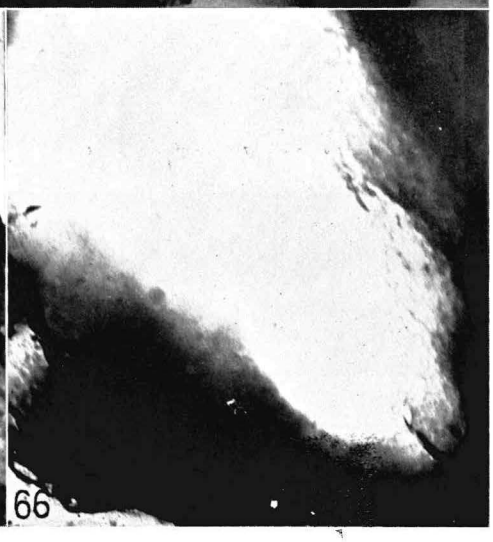
66

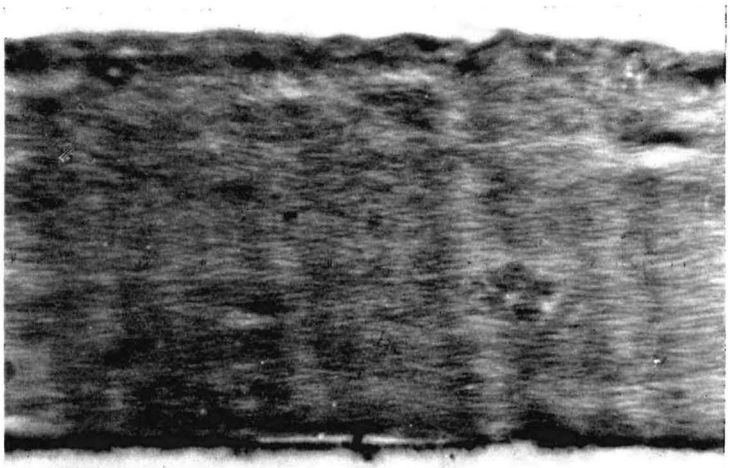

67

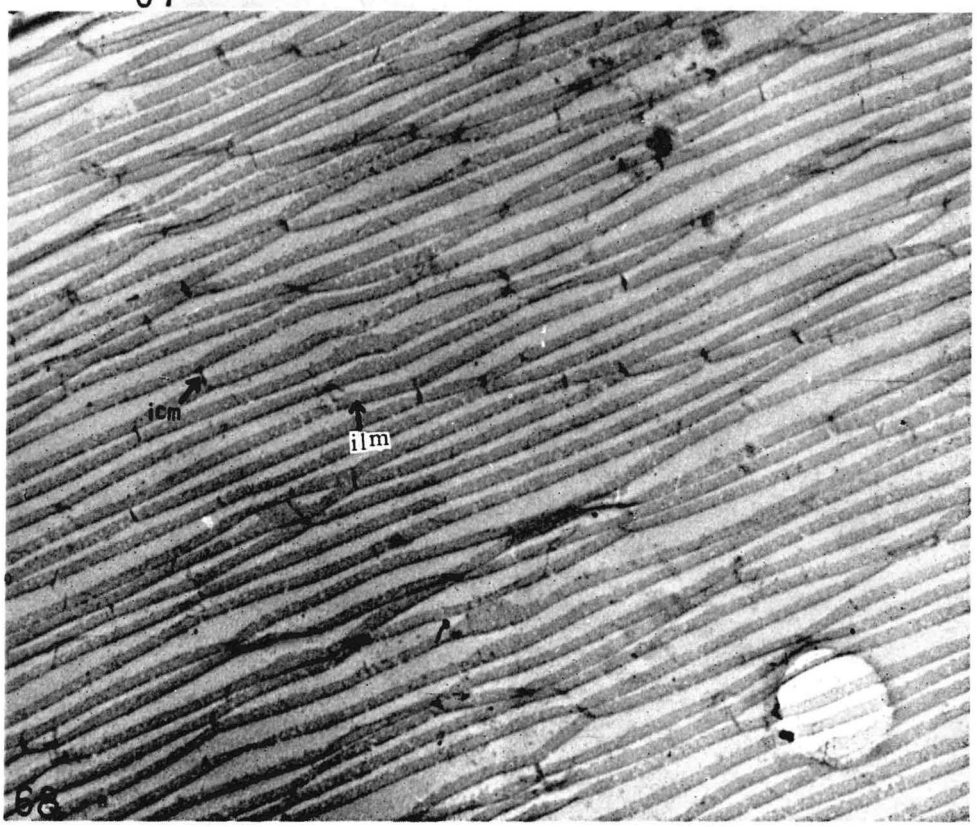

66

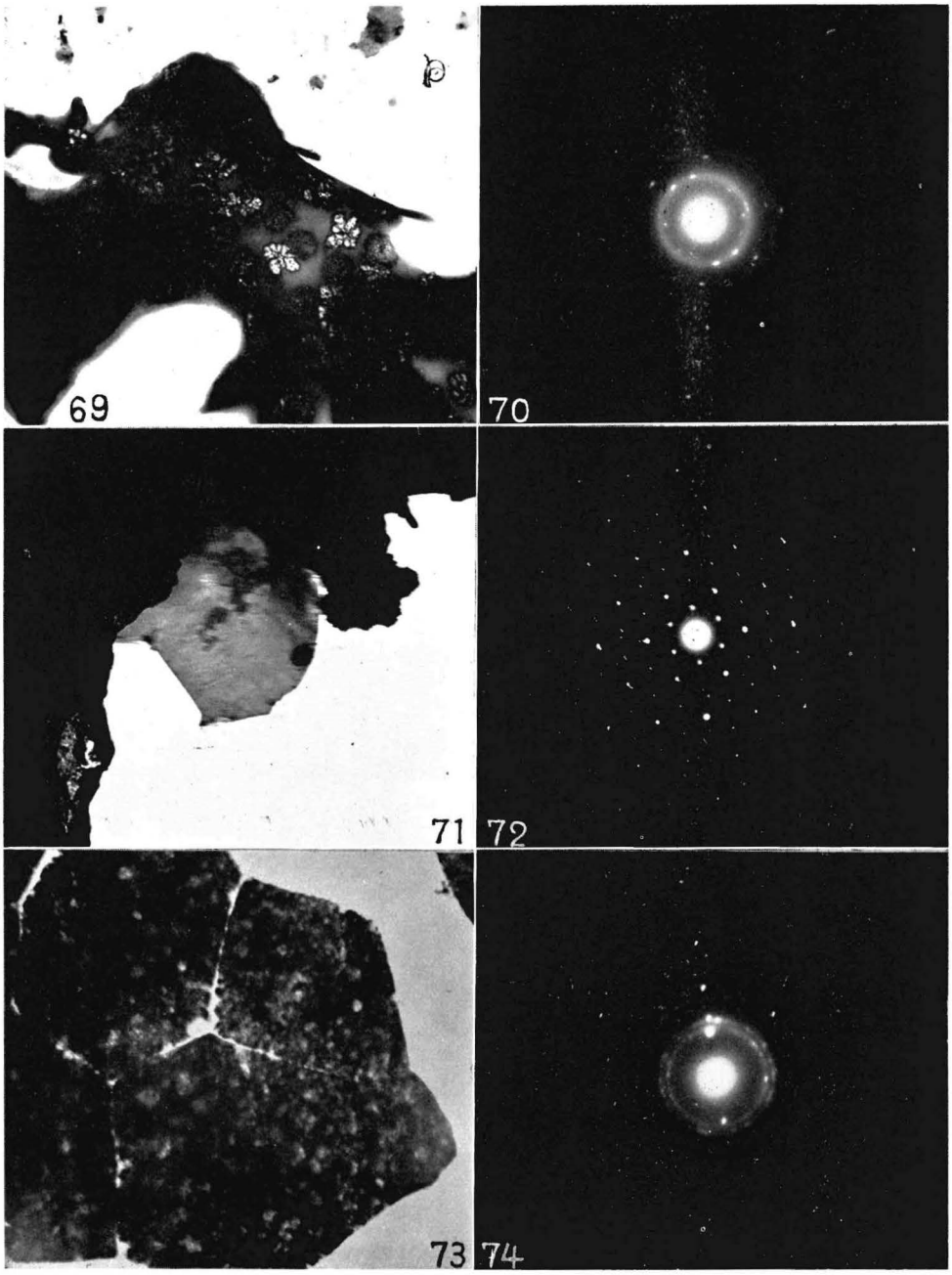
69
70
71
72
73
74


75

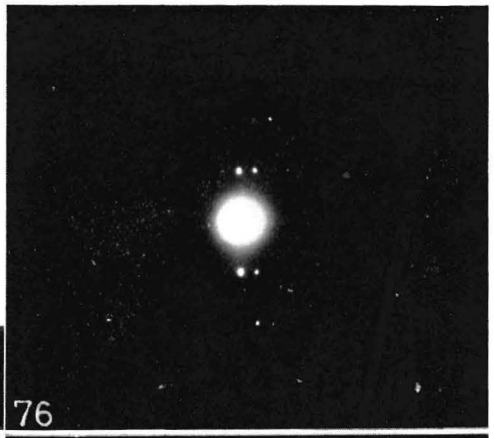
76

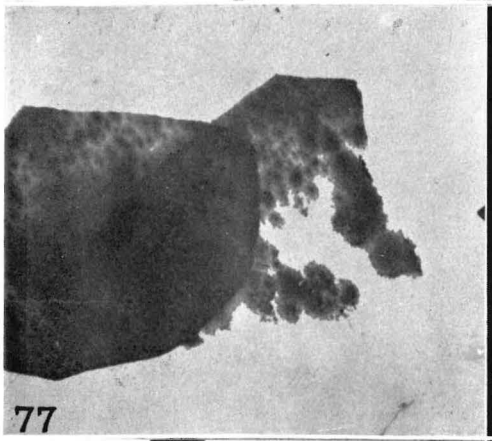
77


78

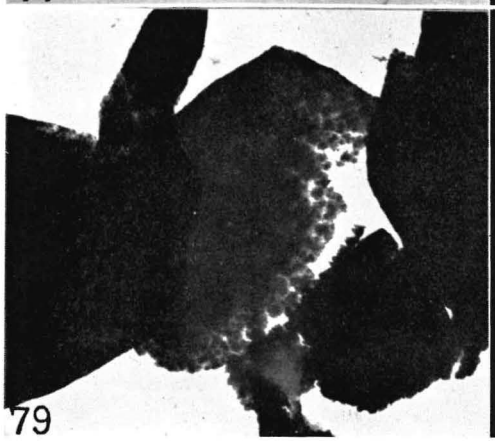
79

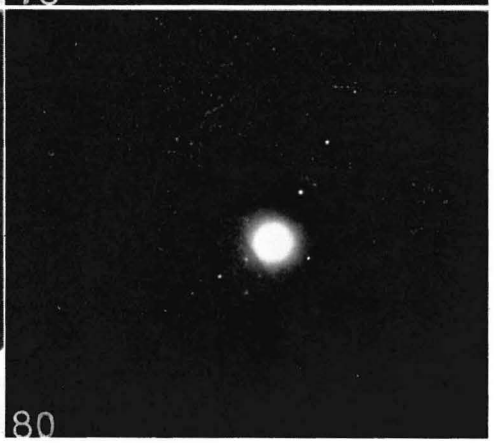
80

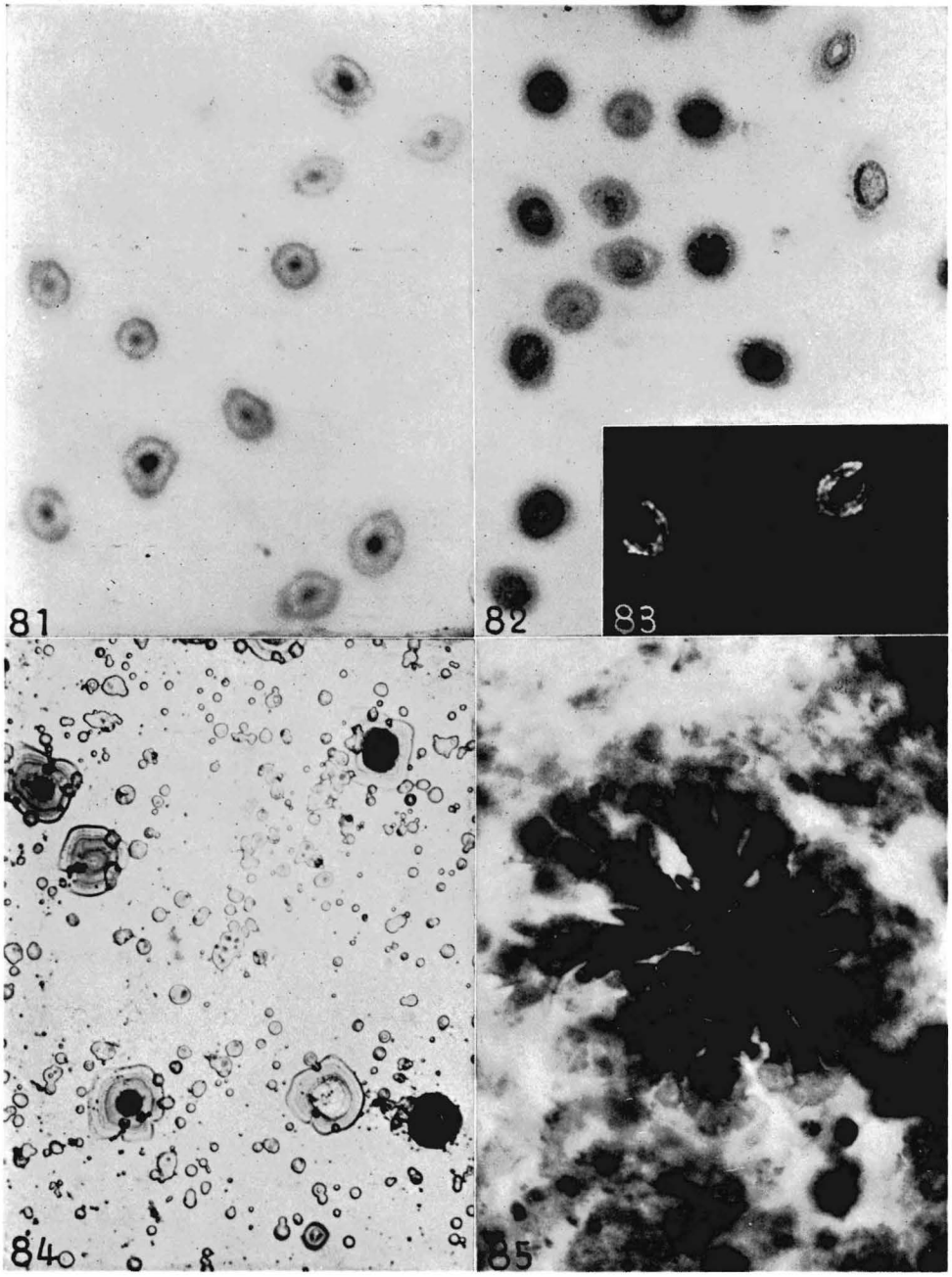
81
82
83
84
85

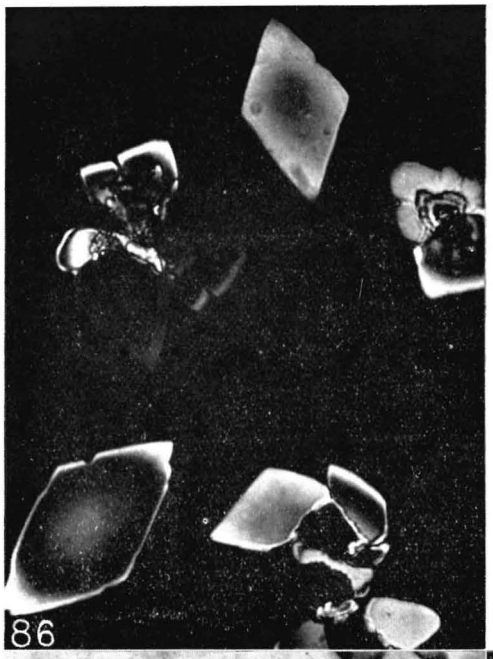
86

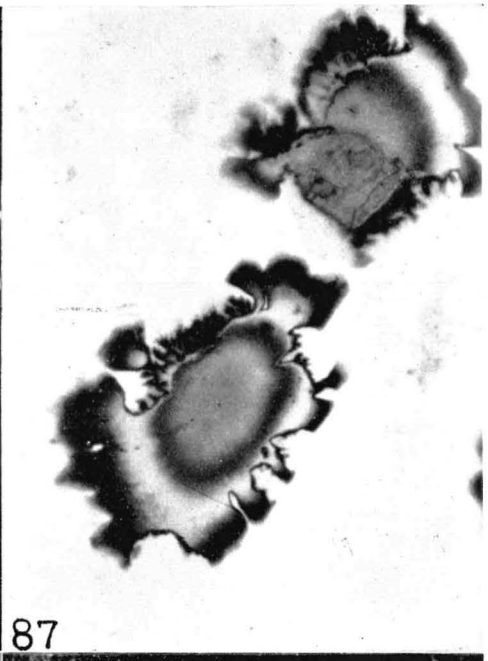
87


88

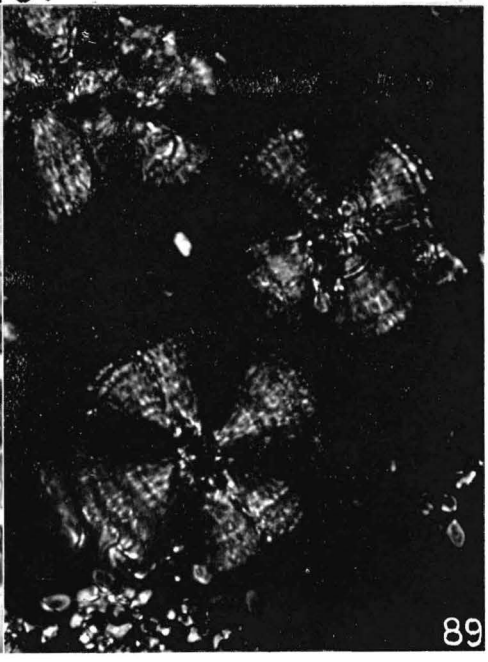
89

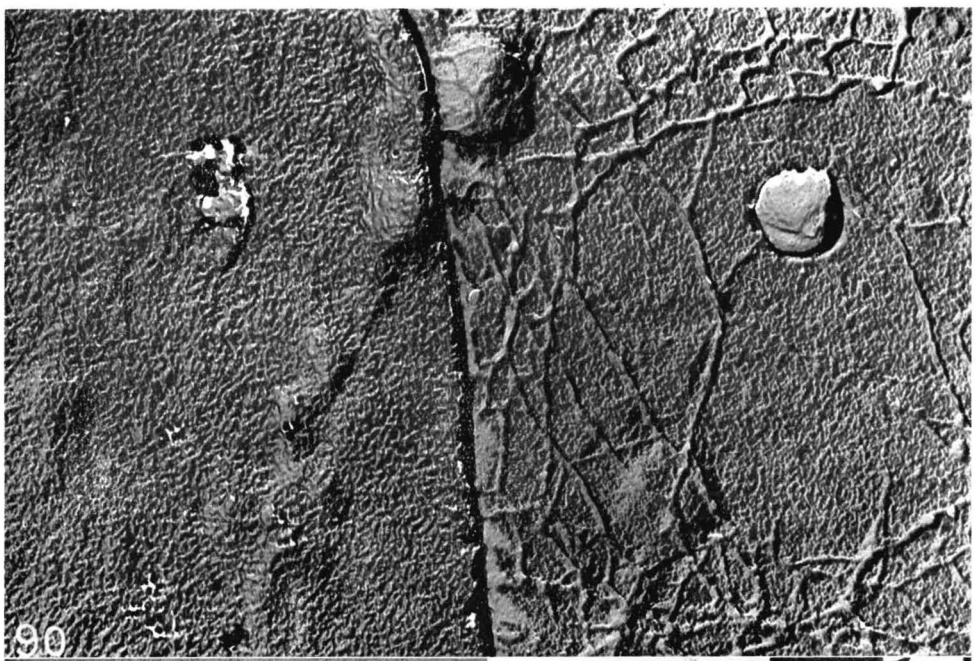
90

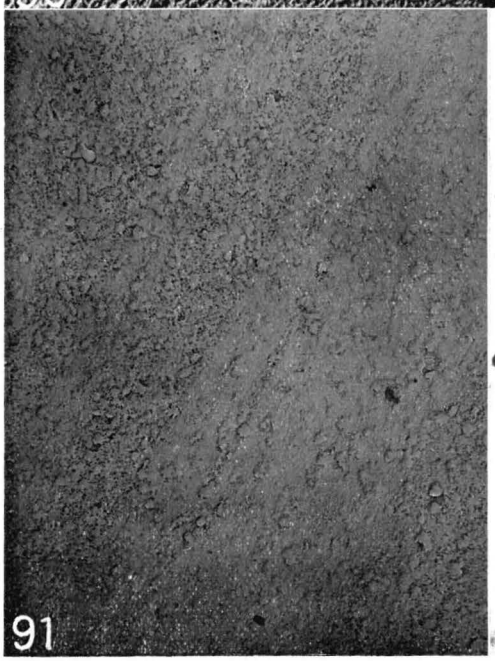
91

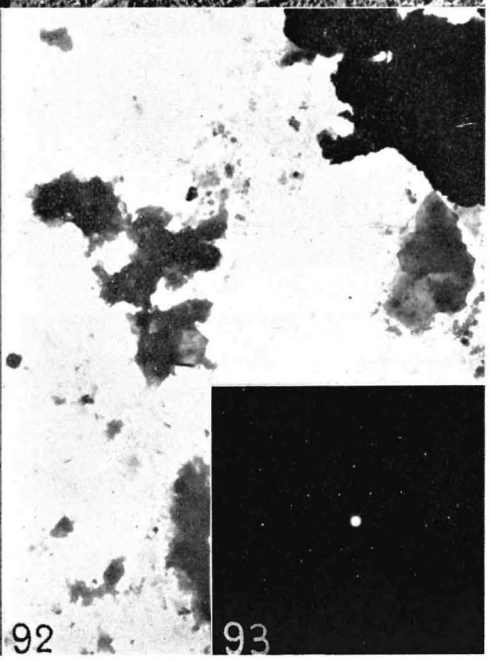
92
93

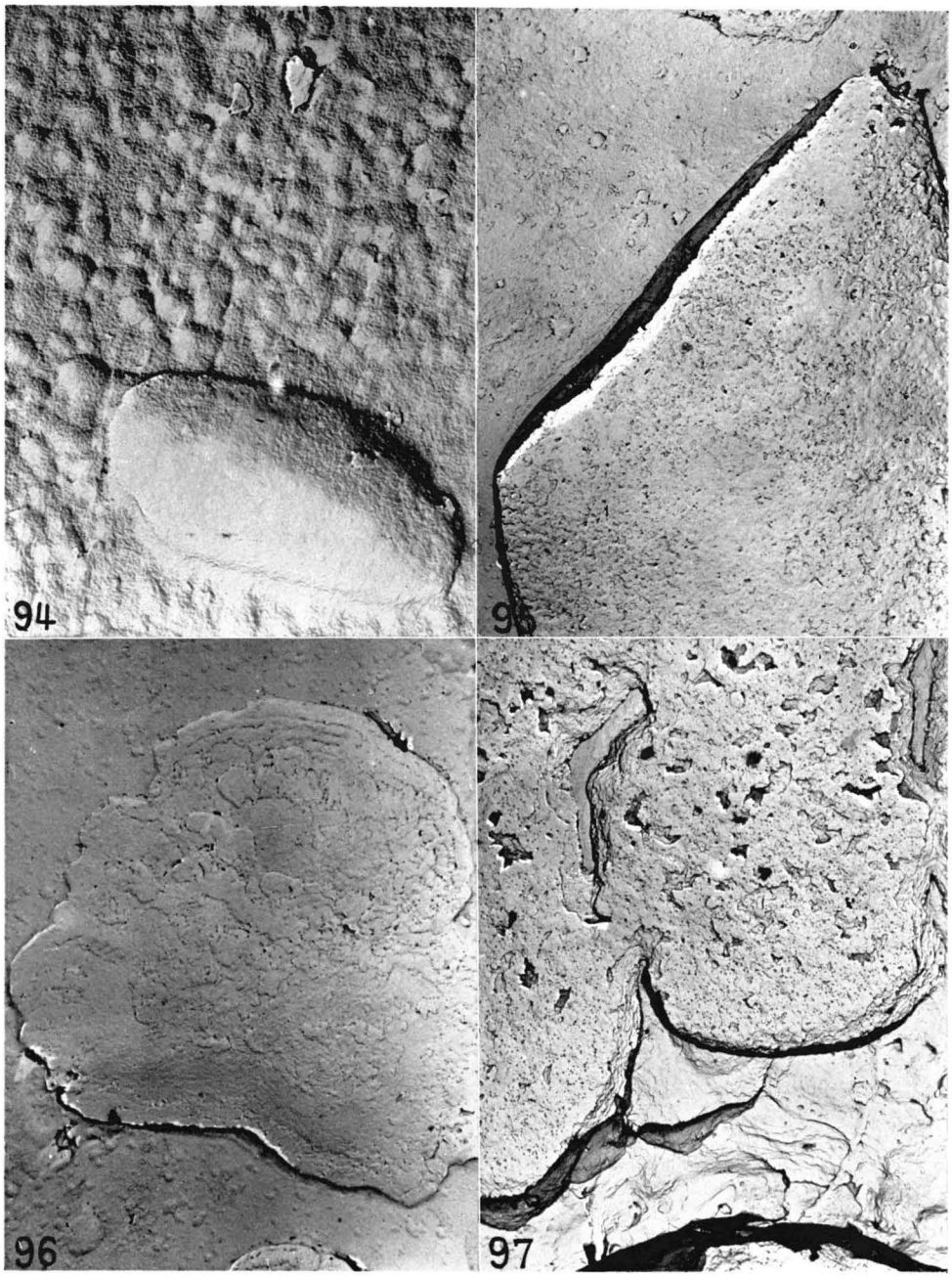
94
96
97


98

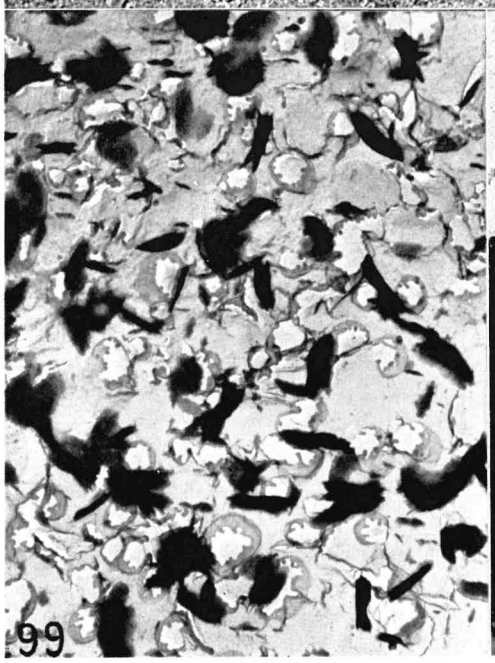
99

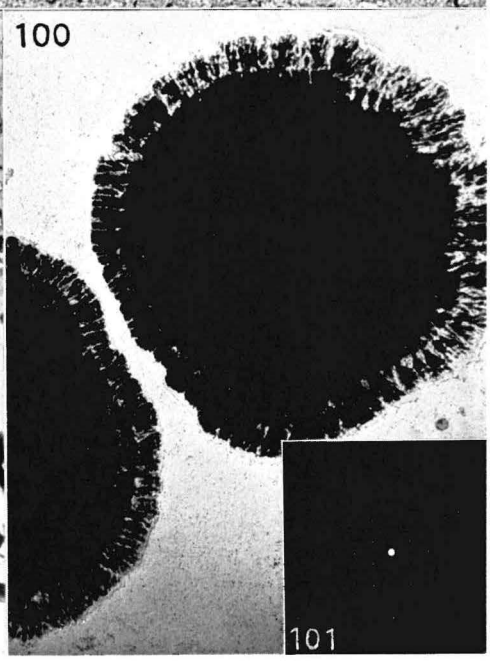
100
101

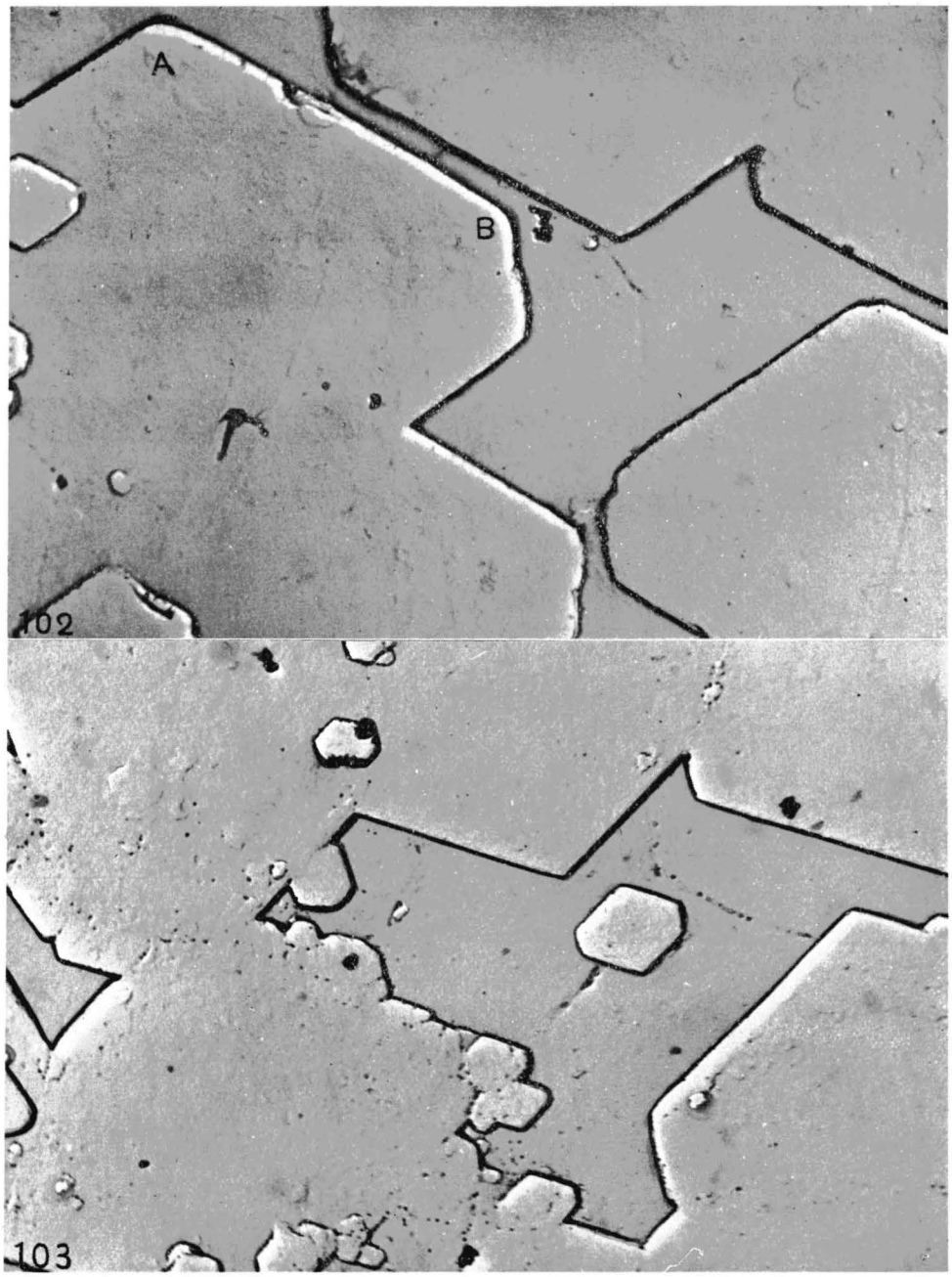
A
B
102
103

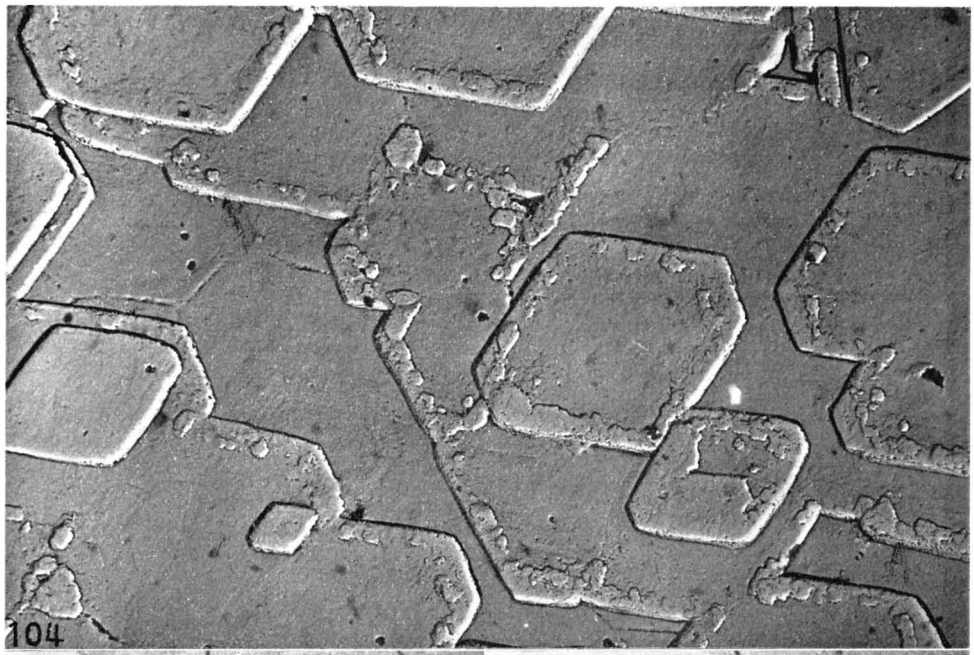
104

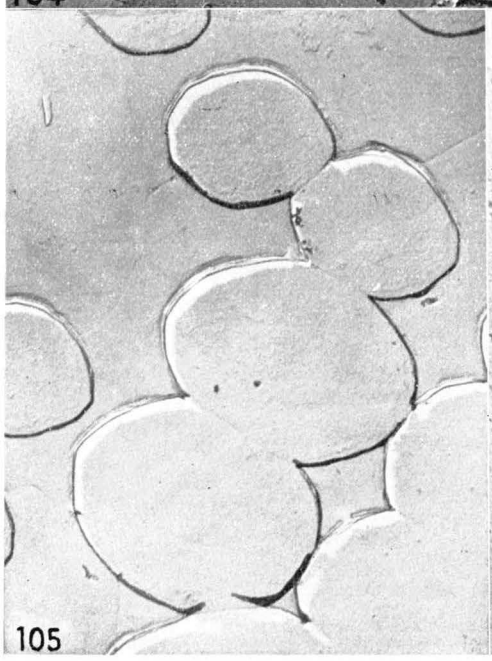
105

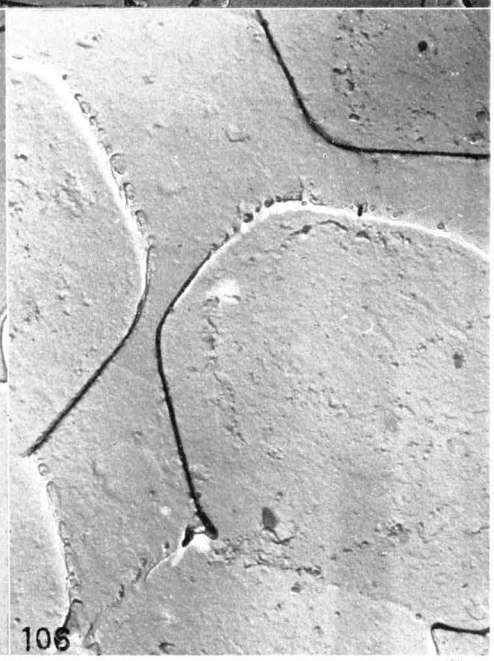
106

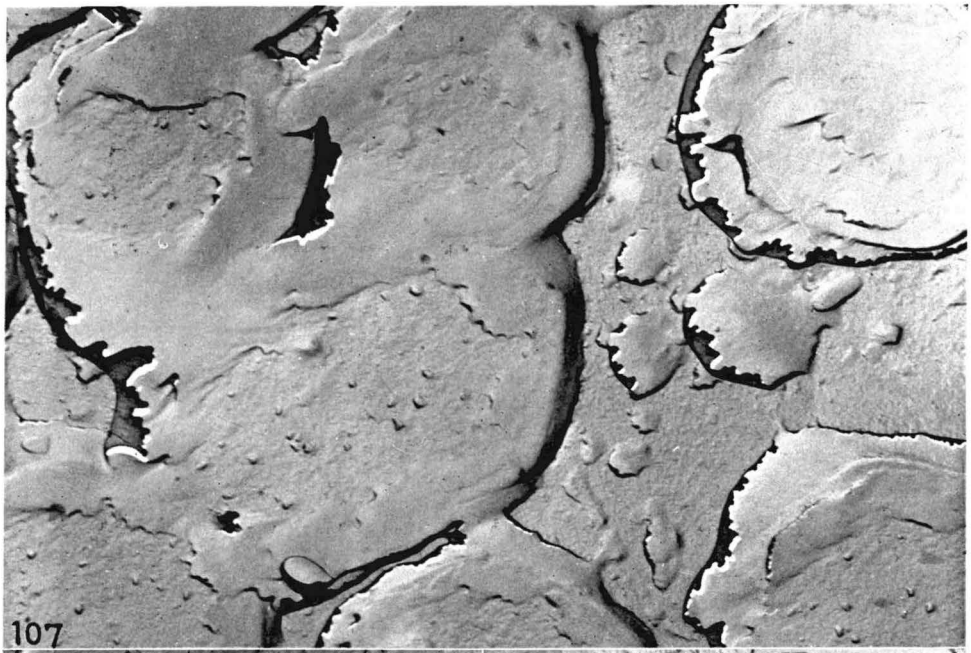
107

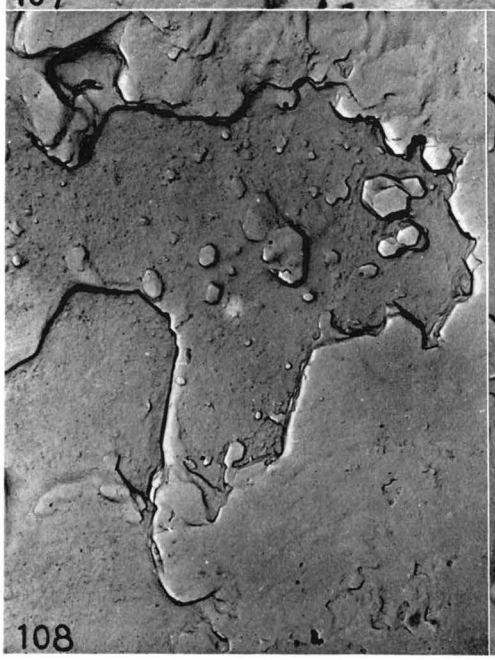
108

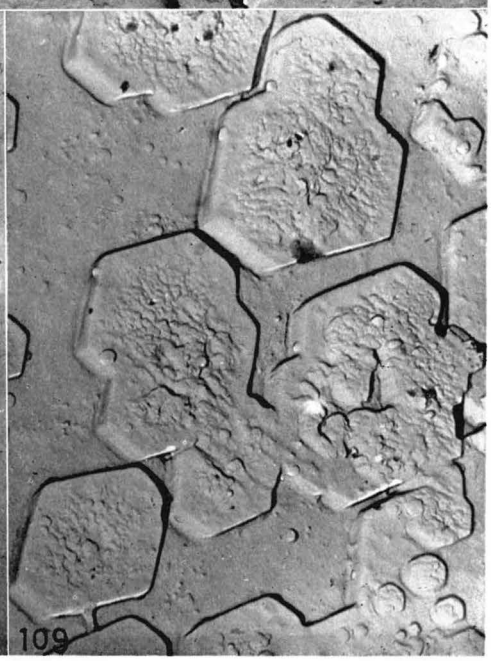
109


110
111

112

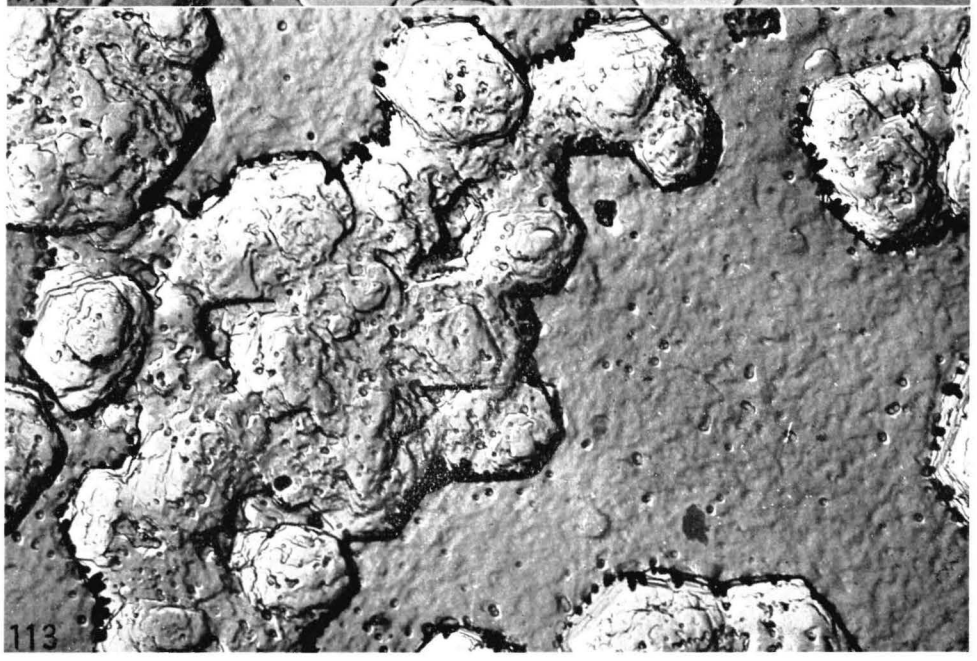

113

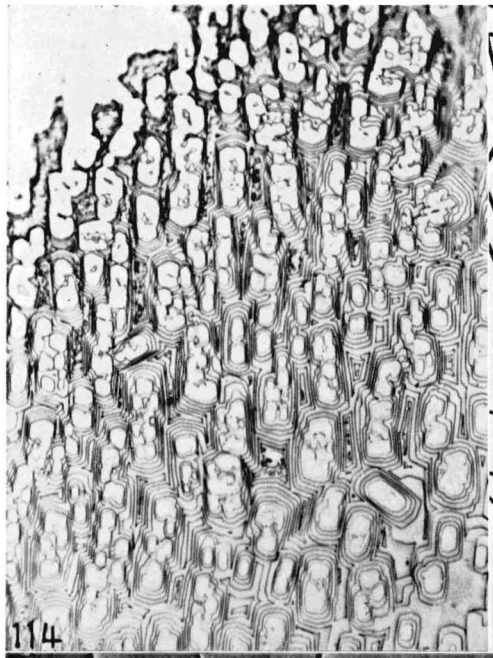

114

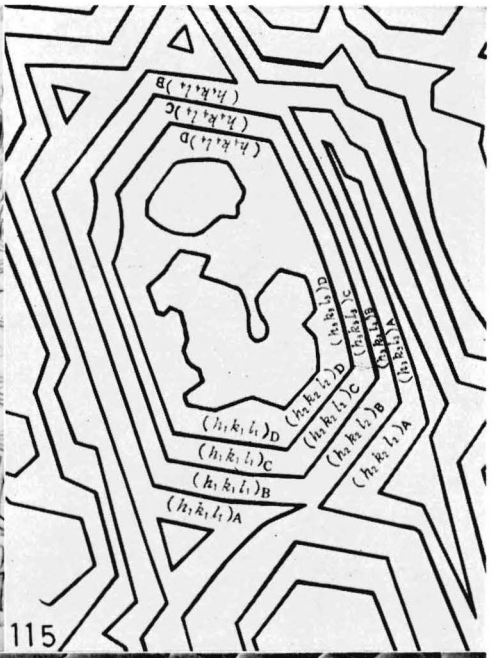
$(h_1k_1l_1)_D$
$(h_1k_1l_1)_C$
$(h_1k_1l_1)_B$
$(h_1k_1l_1)_A$
$(h_2k_2l_2)_D$
$(h_2k_2l_2)_C$
$(h_2k_2l_2)_B$
$(h_2k_2l_2)_A$

115

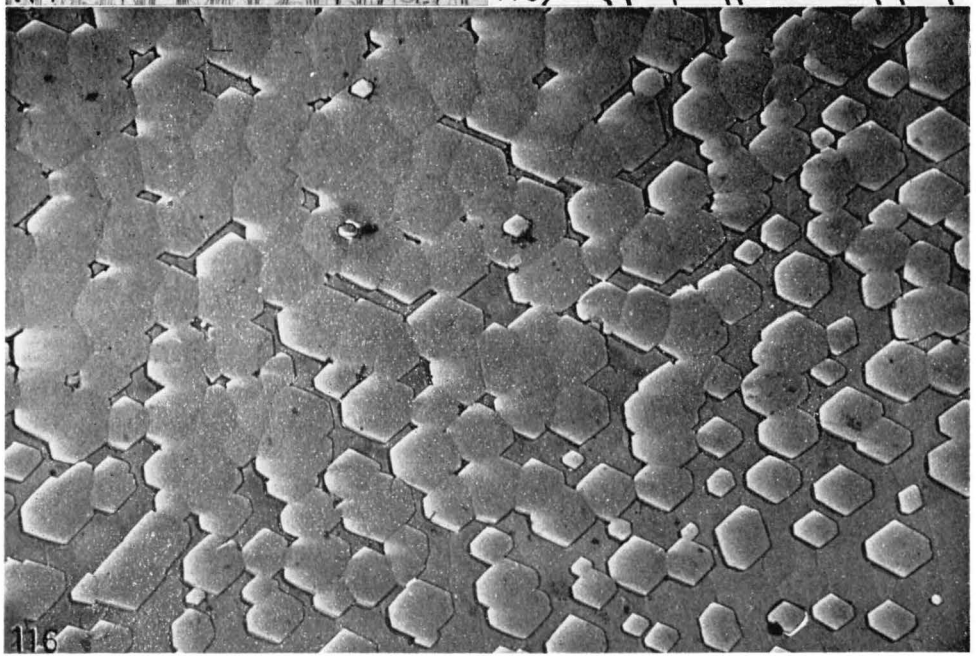

116

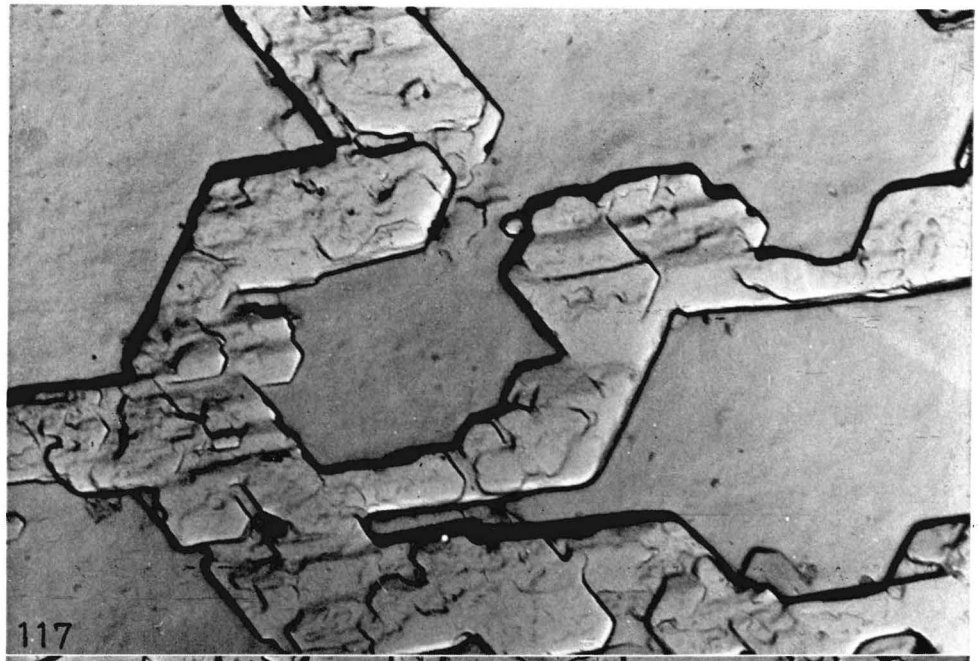
117

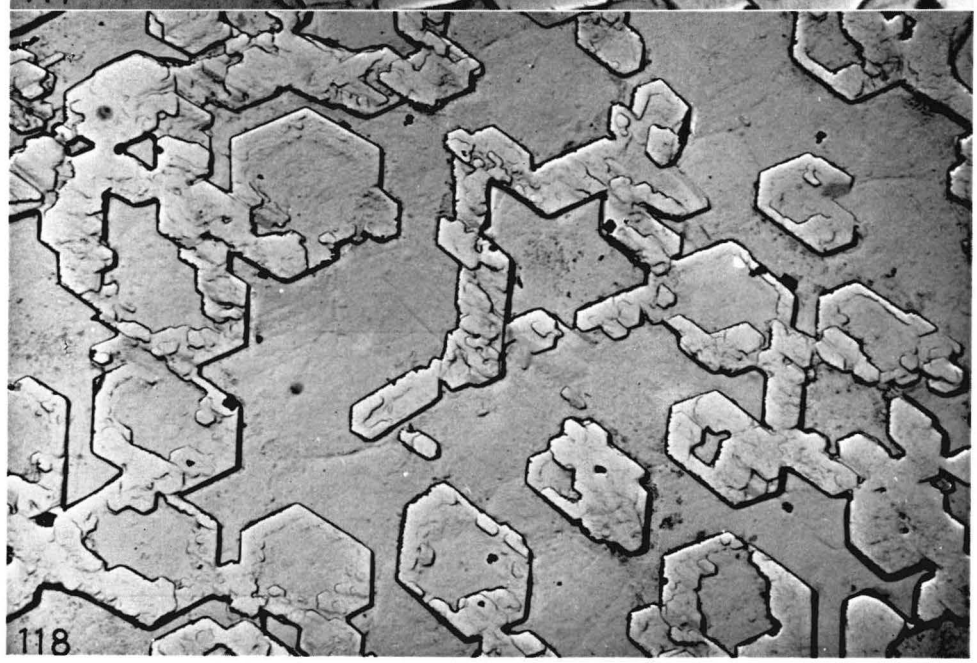
118

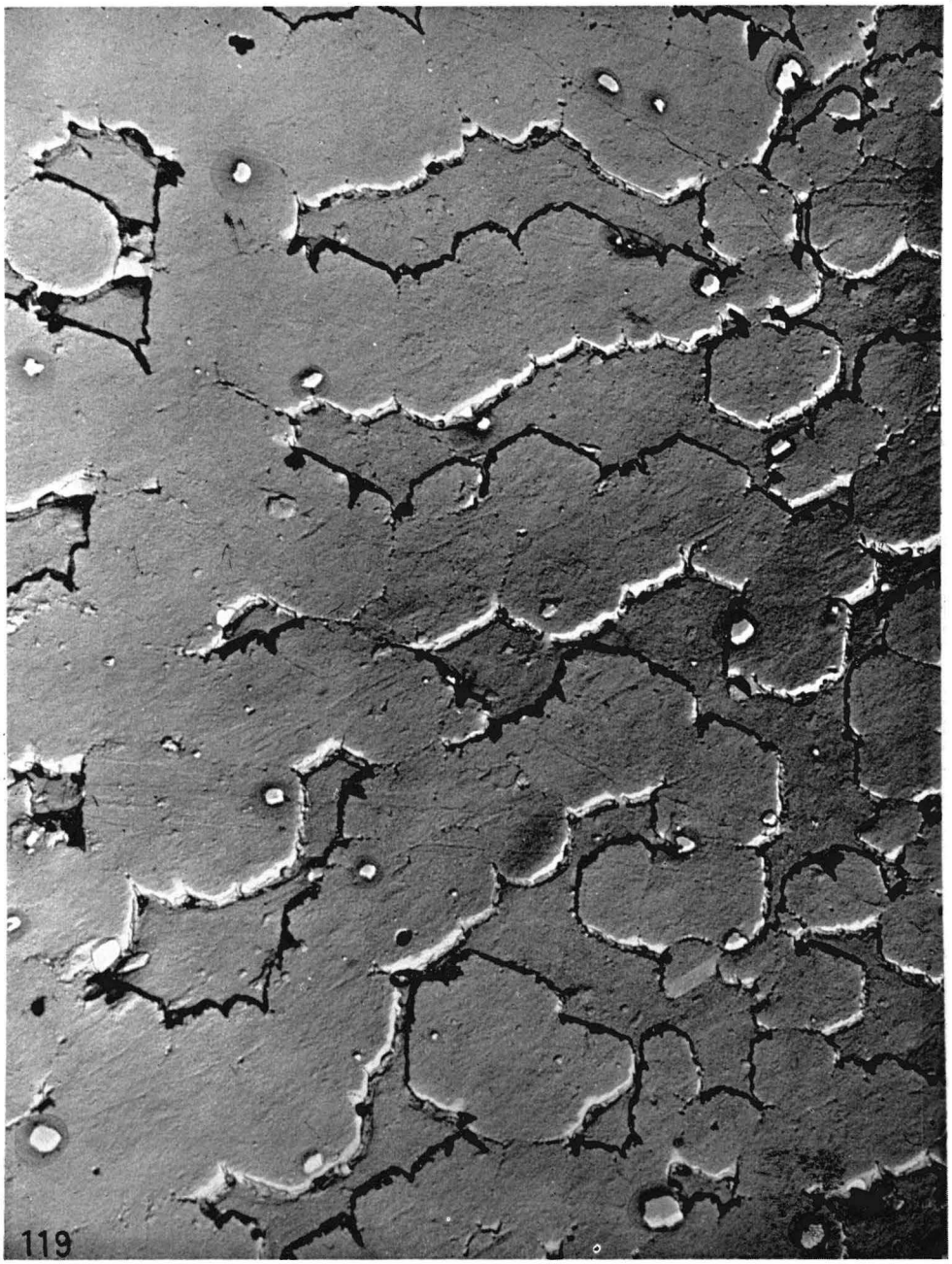
119

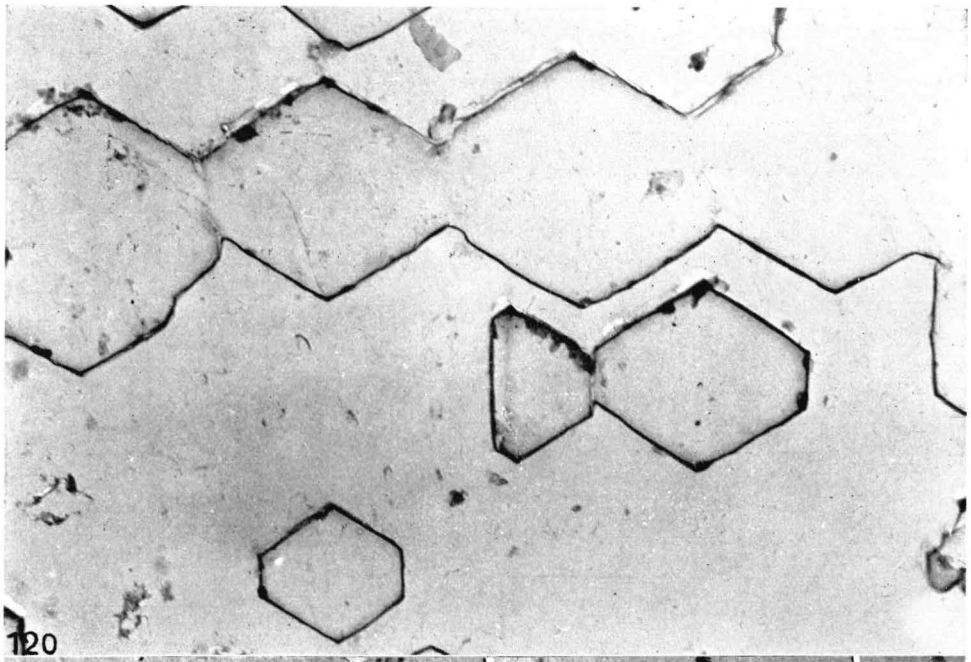

120

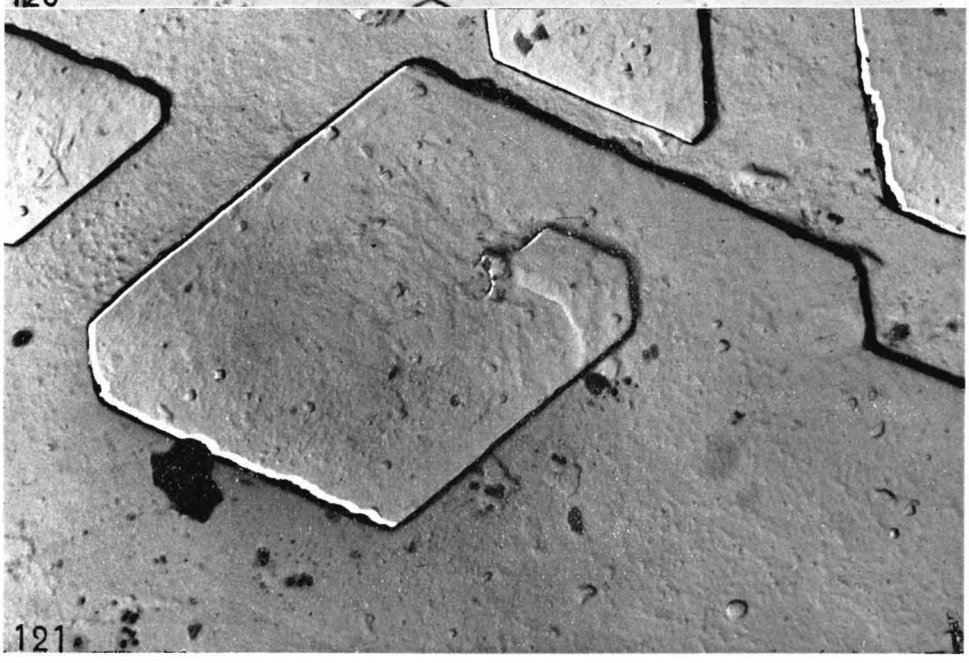

121


122

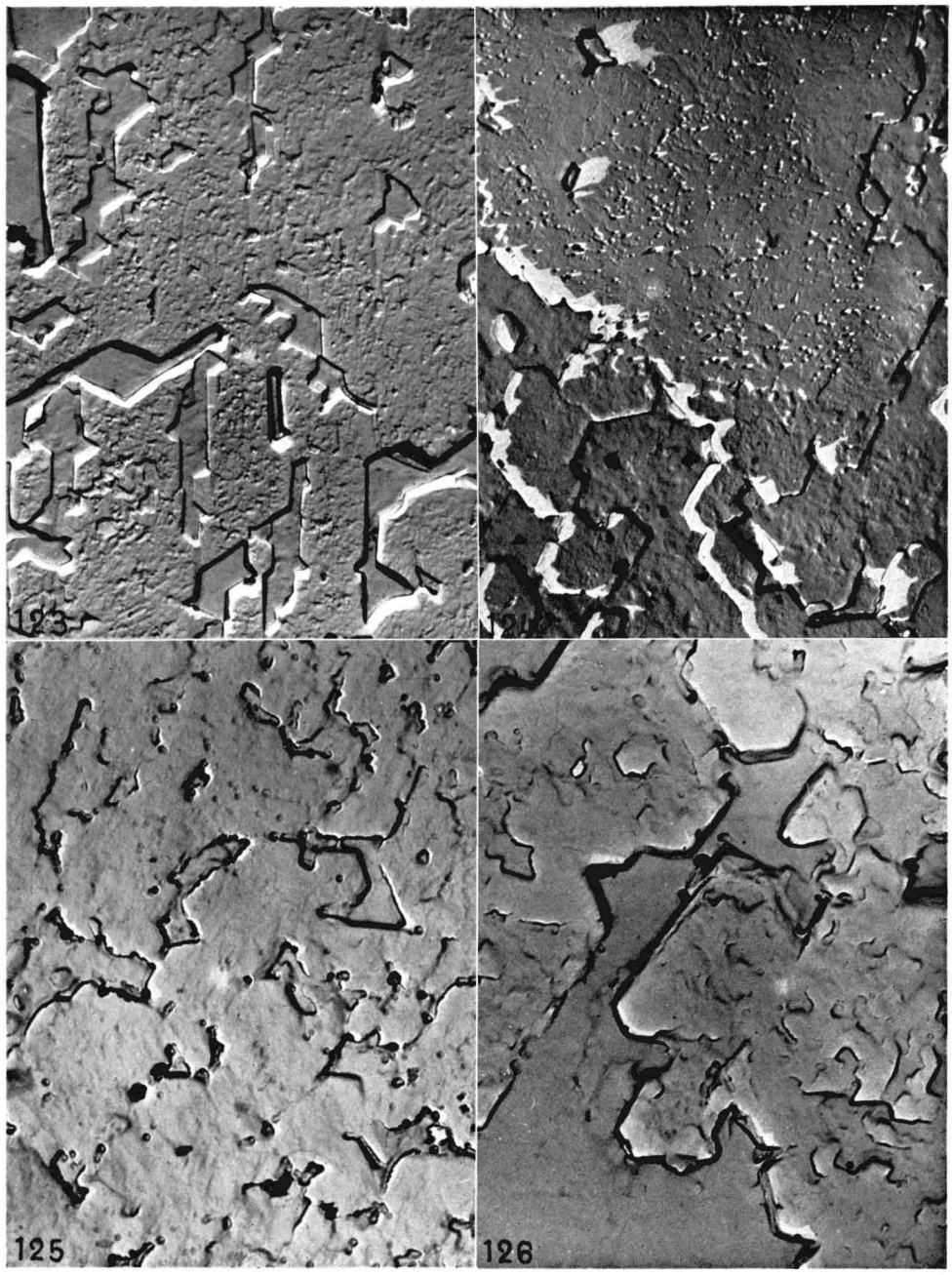
123
125
126

127

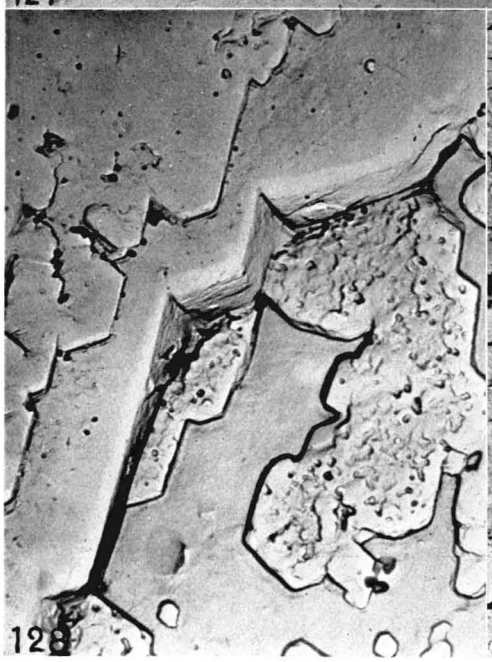

128

129

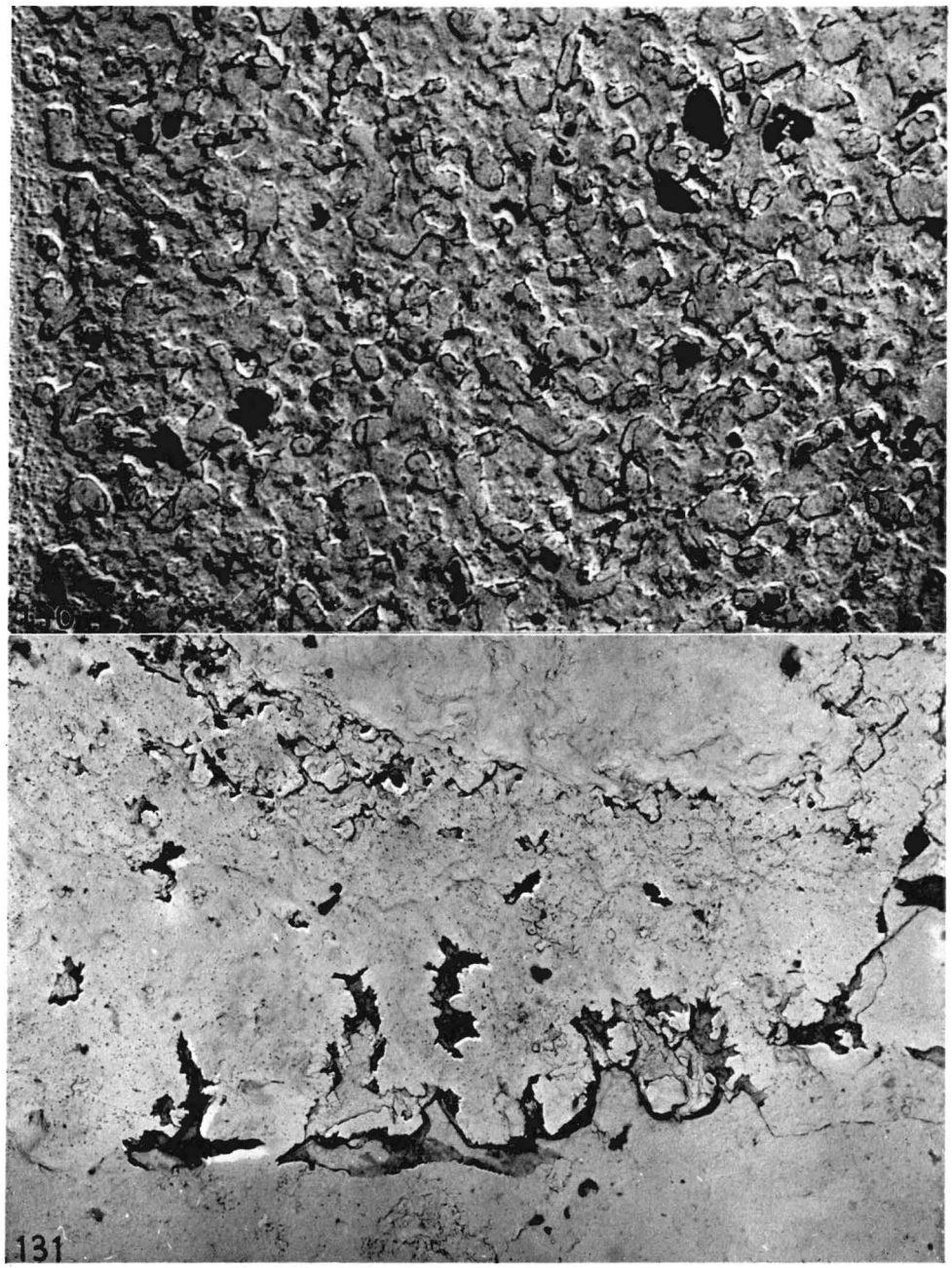
131

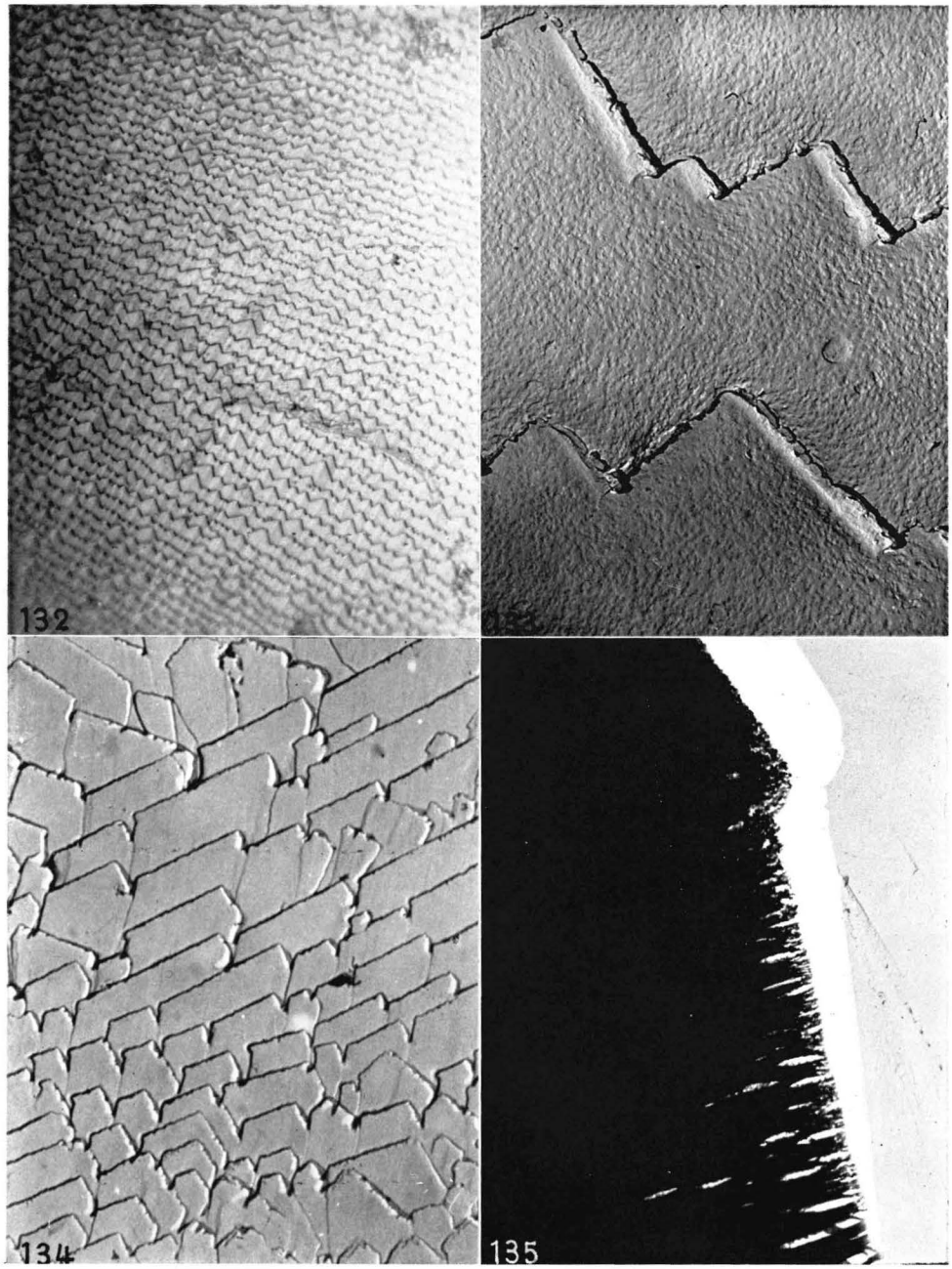
132
134
135

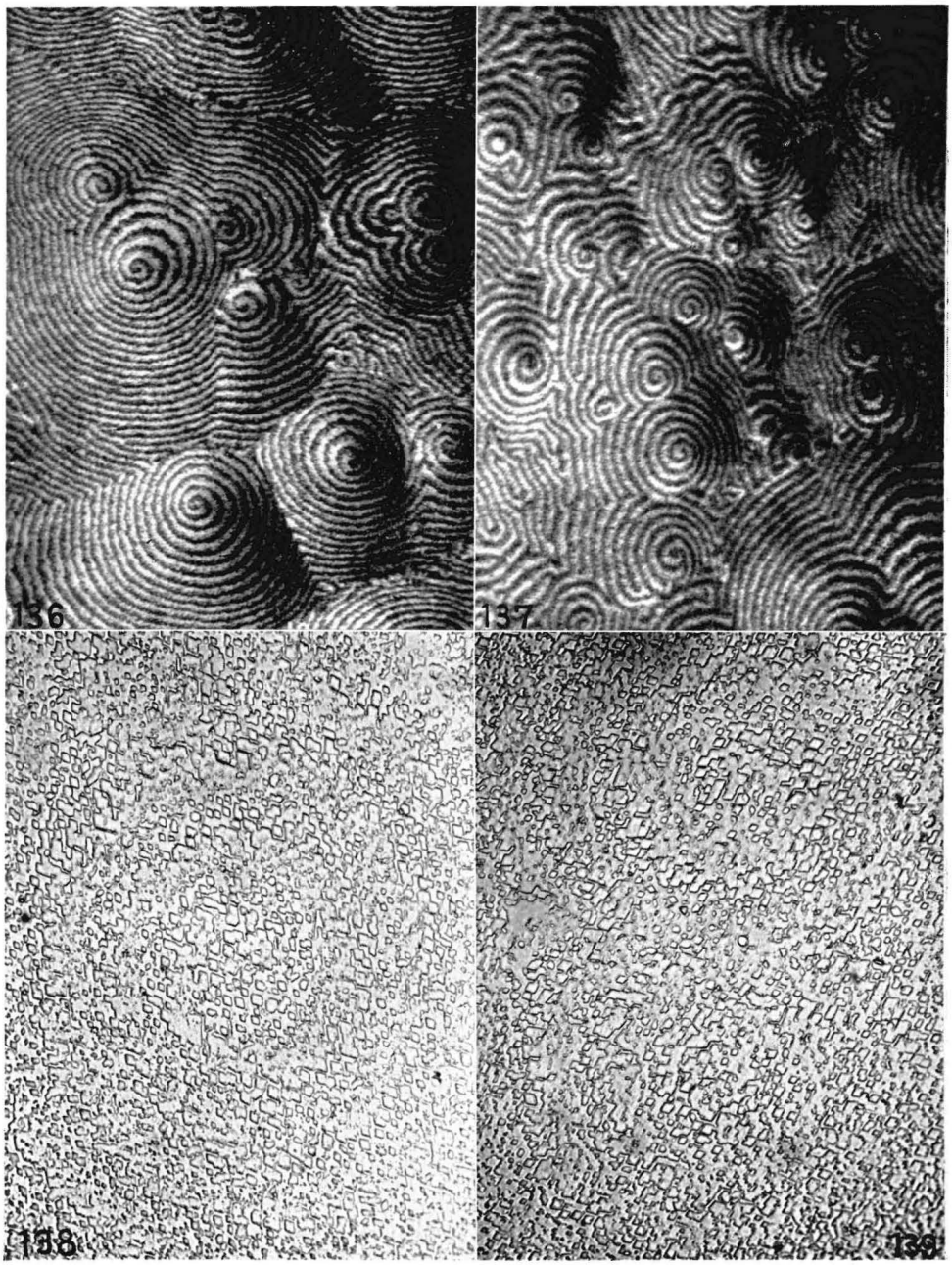
136
137
138
139

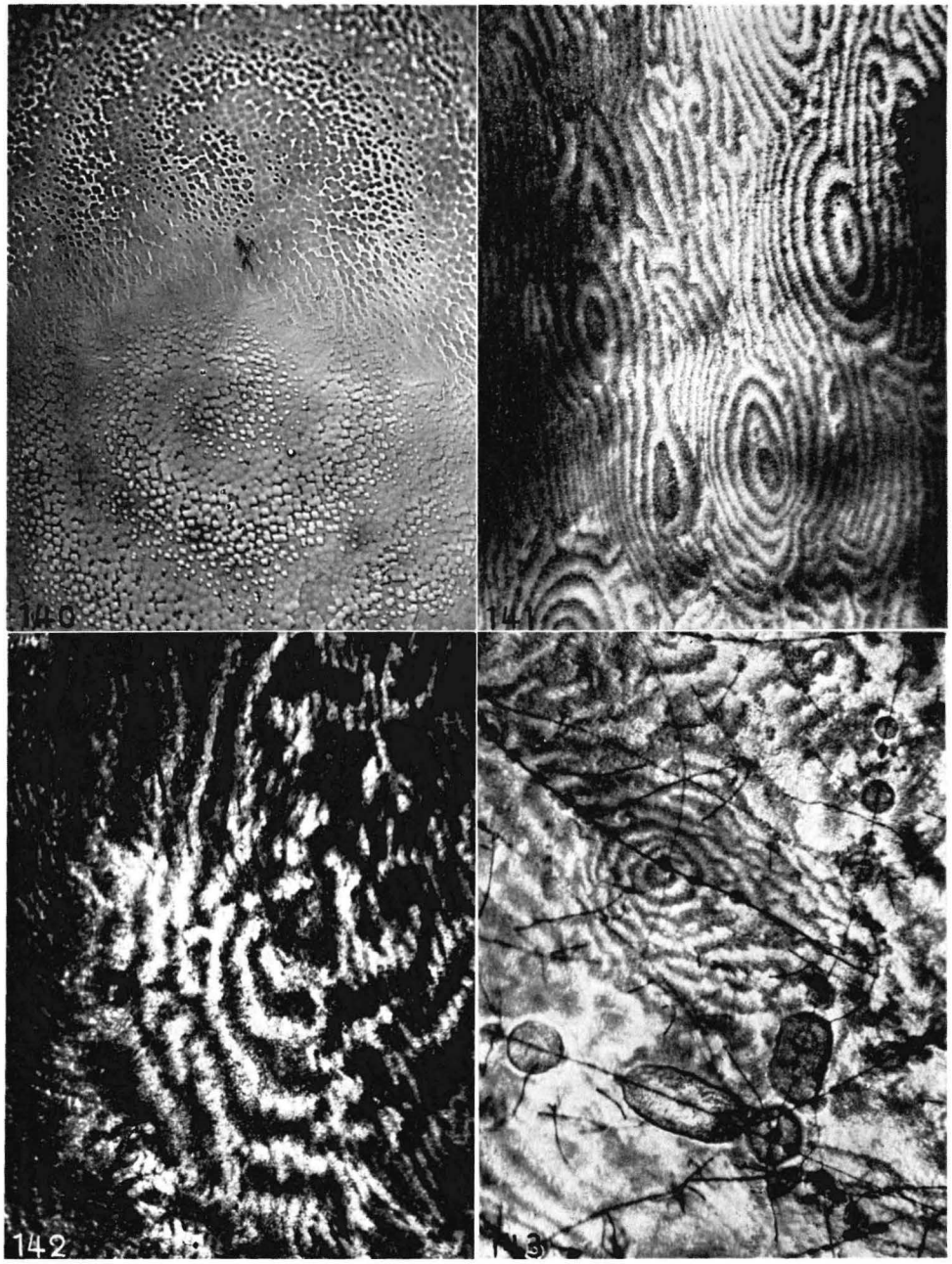
140
141
142
143

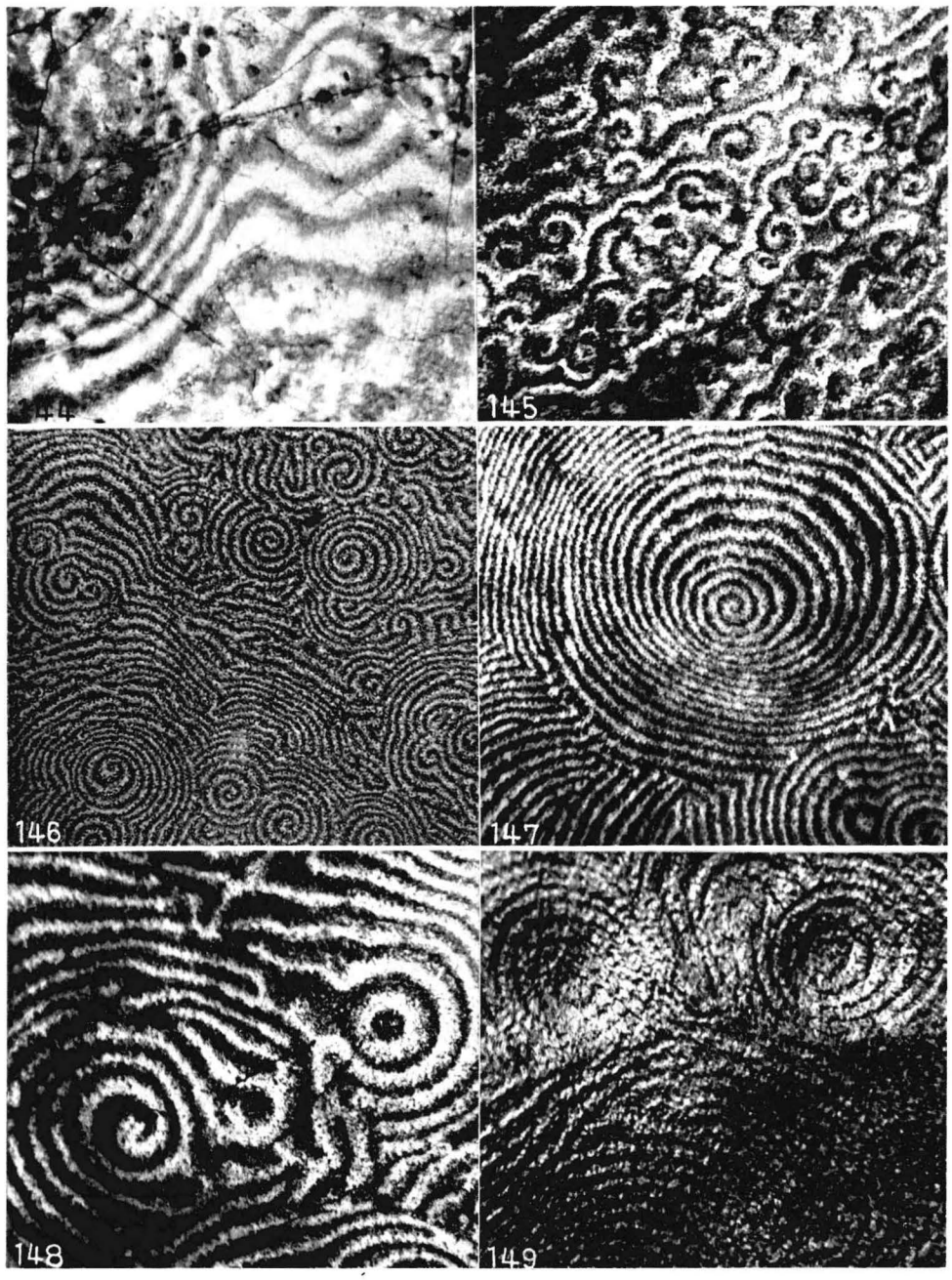
144
145
146
147
148
149

真珠漁場における餌料基礎生産と漁場の海洋構造について

I. 密殖と食物連鎖の関係*, 1), 2)

上野福三・井上啓晴3)

三重県立大学水産学部

緒　　言

養殖真珠の中心地である三重県英虞湾は，近年密殖とか，漁場の老化現象によつてアコヤガイ（*Pinctada martensii*）の異常大量斃死や真珠品質の低下などが見られる。しかるに真珠養殖漁場の環境解析は長期にわたつて組織的に行なわれた例が少なく，古川等（1958）によるもののほかはほとんど断片的観測にすぎなかつた。このためアコヤガイをめぐる環境，特にその餌量生産機構の解明は真珠養殖技術発展のために特に望まれていたことである。著者等はこの問題について解明の端緒を求める目的を以って，漁場の基礎生産力に及ぼすアコヤガイ養殖の影響について観測，解析したので報告する。

アコヤガイ，カキの餌料については内海区水産研究所，国立真珠研究所などの研究により微細有機懸濁物質であるとされている。しかしこの有機懸濁物質の由来について考えると，当然漁場の食物連鎖の一環になければならず，人工的に手が加えられたものではないのであるから，漁場の基礎生産力に負うべきものと考えられる。一方真珠養殖業は農業と比較するとすこぶる幼稚な段階にあり，餌料を人工的に制御することなく，天然の生産に依存している。すなわち草食性二枚貝であるアコヤガイの餌料は全くその漁場が持つている基礎生産力に支配されることになる。したがつて異常大量斃死，漁場の老化は寄生虫の異常増殖のごとき突発的事故以外は，まずアコヤガイを中心とする食物連鎖の回転に異常が生じたと考えられる。しかしながらこの解析には海水の物理化学的要素，植物プランクトン，アコヤガイのすべてにわたつて検討する必要があり，非常に大がかりとなる。この

---

* Fukuzo Uyeno and Hiroharu Inouye. Relationship between basic production of foods and oceanographical condition of sea waters in pearl farms, with special reference to relationship between overcrowding culture and food chain around pearl oyster. With English summary, p. 845. Bull. Natl. Pearl Res. Lab. 7: 829—864. 1961.

（国立真珠研究所報告　7:　829—864.　昭和36年7月）

1)　昭和34，35年度農林省漁業試験研究費補助金による研究（沿岸浅海資源の増殖を目的とする環境改善方法及びその生産効果見積りに関する研究）報告書

2)　昭和33年度財団法人東海学術奨励会奨学資金の補助も受けた

3)　現在井上物産株式会社勤務

ため著者等は1959年に主として一般海洋観測を実施し，夏季の停滞が食物連鎖の廻転に大きく影響していることを予察し，引続き1960年に基礎生産力，クロロフイル量，栄養塩量，アコヤガイ濾水量等を測定して密殖漁場における停滞と基礎生産力との関係をさらに深く解析した。

1. 測定漁場ならびに測定方法

測定対象漁場としては両年共真珠養殖の中心的漁場である英虞湾を主として選び，これも比較的良好な漁場と，密殖の影響があるとされている漁場の2点を観測した。1959年は

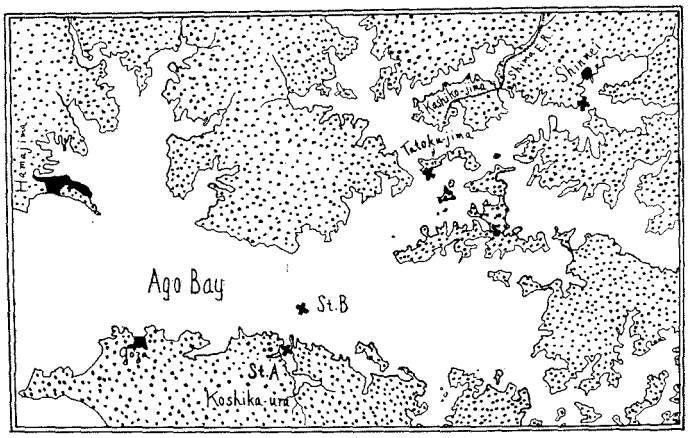

Fig. 1. Location of Stations in Ago Bay.

前者として多徳島を，後者として神明を，1960年には前者として越賀浦の湾口の北方約400mの英虞湾口に接する開水面内を（St. B），後者として枝湾である越賀浦の内部（St. A）を選定した（Fig. 1）。近年真珠養殖業が発展するにつれていかだが密集し，神明及び越賀浦では航路筋を残すのみとなつており，養殖貝の成長はあまり見られない様な状態である。一方多徳島及び St. B ではいかだの密集度も前述ほどではなく，比較的良質の真珠を生産する漁場である。

観測実施期間：当初は避寒漁場から養殖貝が帰り，湾内で多数の養殖の開始される5月から始め，避寒のためいかだの撤収の行なわれる11月までを計画したが，準備や整理が思うにまかせなかつた上に伊勢湾台風やチリ津波という大突発事故に見舞われ，観測回数は少なくなつてしまつた。1959年の多徳島は6月14日，28日，7月24日，8月16日，18日，9月13日，11月29日の7回，神明にて6月14日と8月17日の2回である。1960年は両地点とも6月19日，7月12日，28日，8月10～11日，9月1～2日，18～19日の6回である。以上の地点とは別に近年開拓され，現在では相当の生産額をあげている瀬戸内海漁場中より，1959年は愛媛県伯方島の2漁場（森，北浦）（Fig. 2）を，1960年は岡山県白石島の2漁場（高島，鳥の口）（Fig. 3）を選定，参考として盛夏中にそれぞれ一回あて（前者は8月25～26日，後者は8月17～18日）観測した。

観測項目：1959年は水温，塩素量，酸素量，硅藻量でこのほか酸素法による基礎生産量

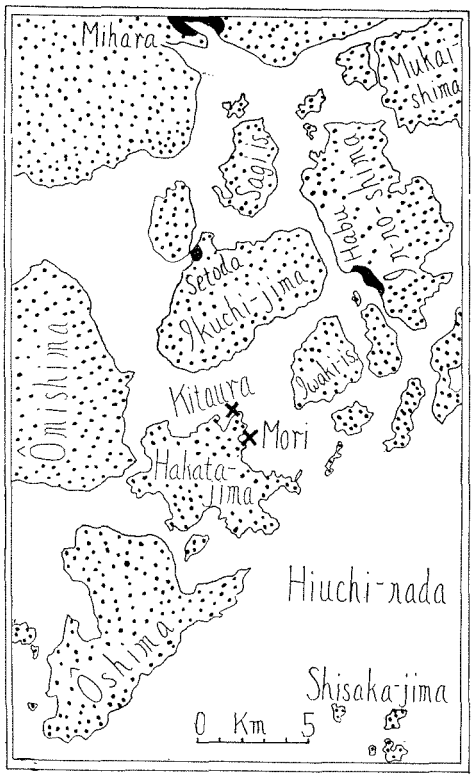

Fig. 2. Location of stations in Hakata-jima.

の測定を実施したが，植物プランクトンが非常に少なく，伯方島のほかは成果が得られなかつた。1960年は上記のほか，透明度，燐酸塩，アンモニア態窒素，亜硝酸態窒素，硝酸態窒素，全炭酸塩，クロロフイル量，

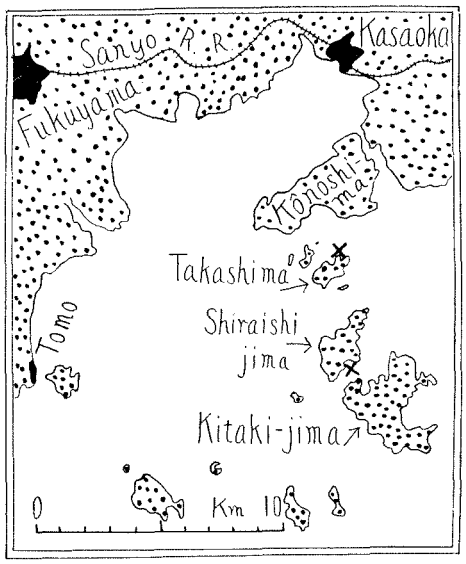

Fig. 3. Location of stations in Shiraishi-jima.

C^{14} による基礎生産量について測定した。また4年貝 100個を両漁場観測点に金網かごに入れ，全観測期間を通じてつるし，観測時に排泄物を集め，そのクロロフイル量を測定した。なお白石島漁場についてはクロロフイル定量操作に失敗したためその結果を得られなかつた。

処理の方法：水温，塩素量，透明度，酸素量，燐酸塩，亜硝酸塩については海洋観測指針（気象庁，1958）によつた。アンモニア態窒素については Witting-Buch 法（Barnes, 1959）に基づいたが沈澱を完全に避けることが困難となり，観測の後半には測定不能となつた。硝酸塩については北村（1958）によつた。クロロフイルの定量及び C^{14} による基礎生産量の測定は西条（1957）により，プランクトンの濾過は前者は東洋濾紙 No. 5C を，後者は東洋濾紙 No. 5C を用いたのち一部の試料についてさらにその濾液をメンブランフイルター No. 1 で濾過した。全炭酸の定量は猿橋（1955）による微量拡散分析法を菅原等（1960）により改良された方法に基づいた。植物プランクトンの採集は採水法により，100cc の試水中より濃縮，検鏡，算定した。アコヤガイ排泄物中のクロロフイル測定は前記海水の場合に準じた。アコヤガイ消化管内でクロロフイルが全く分解しないと仮定することにより，垂下層の海水中のクロロフイル量と排泄物中のクロロフイル量とからアコヤガイの濾水量を求めた。観測期間中の試験貝の成長による影響は4年貝のため既にほとんど成長が止まつており，ないものとした。

本研究の実施に当つては終始懇切な御助言，御鞭撻を頂いた上，両年の内海漁場の観測には観測船「かもめ」を提供された広島大学水畜産学部長松平康男教授，ならびに同学部小山治行助教授に深甚なる感謝の意を表する次第である。1959年の観測に当つては臨海実験場及び試験いかだ使用の便宜を供与された上，両年を通じ種々御助言を頂いた国立真珠研究所長高山活夫氏に対し心から謝意を表する。このほか，観測に協力された国立真珠研究所員各位，また伯方島漁場観測の便宜を供与された志摩真珠協同組合ならびに同社作業場員各位，1960年の観測実施に当つて作業場，作業船を提供されるなど種々の便宜を供与された井上物産株式会社社長井上太市氏並びに観測その他に御協力頂いた同社養殖場従業員諸氏，白石島漁場観測の便宜を与えられた笠岡真珠有限会社社長佐藤忠勇氏及び観測に御協力頂いた同社専務竹中喜久三氏他同社従業員各位に御礼申し上げる次第である。このほか観測や分析に当つては，広島大学水畜産学部遠藤拓郎氏，本学学生三谷勝次，森安良，白木弘一，萩田健二，高田征司の諸君の御協力を頂いたことに感謝する。

2. 観 測 結 果

a) 1959年

予備的観測であつたので概要のみを記す。各要素の鉛直分布は代表的な6月14日，8月16～18日の英虞湾と8月25日伯方島森のものについて Fig. 4～7 及び Table 1 に示した。硅藻の検鏡結果は省略した。

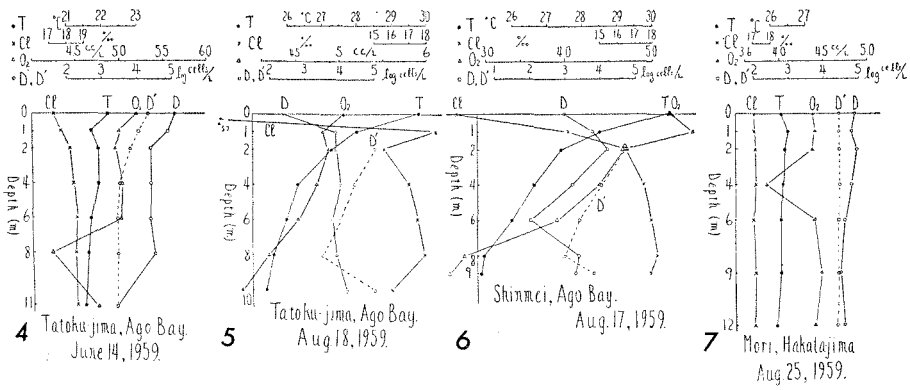

Fig. 4. Vertical distribution of temperature (T), chlorinity (Cl), dissolved oxygen (O_2), and total cell number of diatoms (D: actual observation, D′: mean value in the sea south off Honshu referred to Uyeno 1959) at Tatoku-jima, Ago Bay in June 14, 1959

Fig. 5. Vertical distribution of temperature (T), chlorinity (Cl), dissolved oxygen (O_2), and total cell number of diatoms (D: actual observation, D′: mean value in the sea south off Honshu referred to Uyeno 1959) at Tatoku-jima, Ago Bay in August 18, 1959.

Fig. 6. Vertical distribution of temperature (T), chlorinity (Cl), dissolved oxygen (O_2), and total cell number of diatoms (D: actual observation, D′: mean value in the sea south off Honshu referred to Uyeno 1959) at Shinmei, Ago Bay in August 17, 1959.

Fig. 7. Vertical distribution of temperature (T), chlorinity (Cl), dissolved oxygen (O_2), and total cell number of diatoms (D: actual observation, D′: mean value in the sea south off Honshu referred to Uyeno 1959) at Mori, Hakata-jima in August 25, 1959.

i)　水温

水温は6月14日には上下層ほとんど差が見られない。その後徐々に上下差を増し，8月16～18日にはその差が 5°C を示した。その後は急速に回復し，9月13日には約 1°C となり，11月29日には全く上下差がなくなつている。表面水温の最高は神明の8月17日に見られた 30.0～30.5°C である。底層も同日，同地点で 26.7°C であつた。伯方島は両地点共全層 26.2～26.4°C である。

ii)　塩素量

塩素量は内湾であるから多少の上下差が見られるのは当然であるが，8月16～18日の観測時には台風のため表層で 5.7～8.0 Cl‰ という低い値を記録している。この時には中層以下も 18 Cl‰ 以下となつているが，他の観測時はいずれも 18.5 Cl‰ 前後を示している。一方伯方島は全層 17.0～17.1 Cl‰ である。

iii)　酸素量

酸素量は多徳，神明両地点共7月24日までは 4.5cc/L 前後，80%以上の飽和量を示しているが，8月16日には 2,4m 層に低下が見られ，養殖貝の呼吸の影響と思われる。神明ではこの低下が底層まで及び，飽和度56%となつている。これは上述のほか排泄物の分解による消費が相当大きくなつていることを示すものである。9月13日には上下差は極めて少なくなり，上層より補給のあつたことを示している。伯方島では盛夏にもかかわらず上下層ほとんど差が見られない。

iv)　硅藻量

硅藻総細胞数は 1 *l* 当りの細胞数の対数値で示し，上野（1958）による本州南岸における種々の水温及び塩素量の組合せに対する平均硅藻量値と比較した。この平均硅藻量は表層の資料に基づくため，光合成の極大層ではこれより大きくなるべきであるし，深層では低くなるべきであるが，比較的深度の浅い地点のみを対象としたため，光の影響は無視した。当初6月14，28日には上層に多く，下層に少ないが，その差は比較的少なく，水温及び塩素量より求めた平均値より多いが，傾向は全く並行している。平均値より多いのは *Chaetoceros compressus* や *Leptocylindrus danicus* の様な小型種が多く，また *C. affinis* などもいちじるしく小型の細胞が多いためと思われる。その後 *Nitzschia seriata* や *Thalassiothrix frauenfeldii* の様な比較的高かん(鹹)性暖水種に主体が移行するが，量的傾向は表層から漸次平均値より少なくなる傾向が見えはじめ，8月16～18日には全層，全地点が平均値より少なくなる。また最も少なくなるのは 4m 層で，底層ほど平均値に近くなる。この時は全般に低かんとなつているため *C. affinis*, *Skeletonema costatum*, *C. laciniosus* などの低かん性種が主となつている。この観測時は表層が著しく低かんとなつていたが，淡水硅藻の *Cyclotella* sp.（*C. glomerata*?）が大増殖して海水が白濁した。細胞数は最大 10^9cells/L を越えた。9月13日には酸素量，水温が成層状態からやや回復を示しているのに対し，なお平均値より著しく少なくなつている。優占種は *Bacteriastrum varians*, *C. radicans* で高かんになつたことを示す。11月29日には *Asterionella japonica* が大増殖し，*Skeletonema costatum* など小型種が多くなつてふたたび平均値より高くなつた。伯方島では低かんのため，*Skeletonema costatum*, *Nitzschia paradoxa*, *A. japonica* が優勢で，細胞も大きいものが多い，量的にも全く本州南岸の平均値と同量である上，上下層間に量の差が全くない。

b) 1960年

各観測時の各要素の鉛直変化を Fig. 8～23 に，観測値を第2表に示した。

i) 水温

水温は前年同様6月19日には両点共上下層ほとんど差が見られなかつた。その後上下差は漸次増し，7月12日には St.A では 4.9°C, St.B では 4.5°C となつたが観測時の天

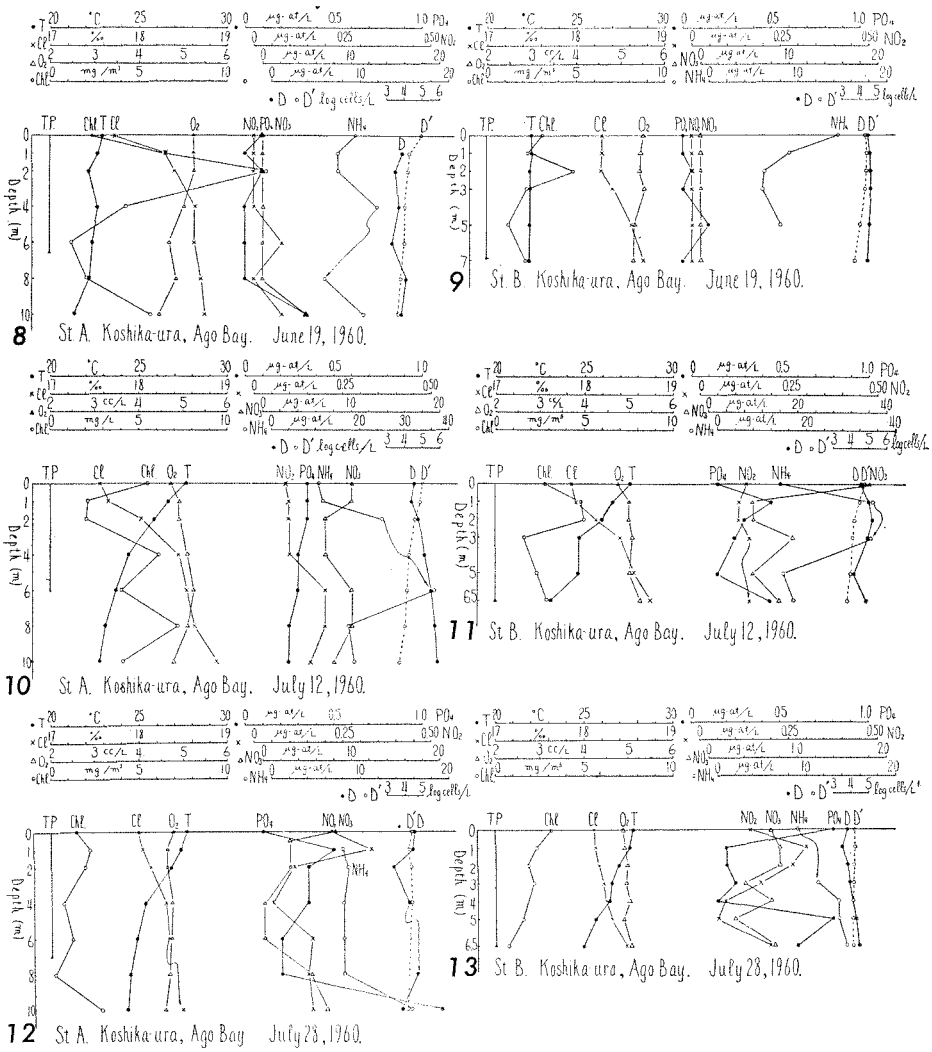

Fig. 8. Vertical distribution of temperature (T), chlorinity (Cl), transparency (T. P.), dissolved oxygen (O_2), phosphate-P (PO_4), ammonium-N (NH_4), nitrite-N (NO_2), nitrate-N (NO_3), chlorophyll content (Chl.) and total cell number of diatoms (D: actual observation, D′: mean value in the sea south off Honshu referred to Uyeno 1959) at St. A, in Ago Bay in June 19, 1960.

Fig. 9. Vertical distribution of temperature (T), chlorinity (Cl), transparency (T. P.), dissolved oxygen (O_2), phosphate-P (PO_4), ammonium-N (NH_4), nitrite-N (NO_2), nitrate-N

(NO_3), chlorophyll content (Chl.) and total cell number of diatoms (D: actual observation, D′: mean value in the sea south off Honshu referred to Uyeno 1959) at St. B, in Ago Bay in June 19, 1960.

Fig. 10. Vertical distribution of temperature (T), chlorinity (Cl), transparency (T. P.), dissolved oxygen (O_2), phosphate-P (PO_4), ammonium-N (NH_4), nitrite-N (NO_2), nitrate-N (NO_3), chlorophyll content (Chl.) and total cell number of diatoms (D: actual observation, D′: mean value in the sea south off Honshu referred to Uyeno 1959) at St. A, in Ago Bay in July 12, 1969.

Fig. 11. Vertical distribution of temperature (T), chlorinity (Cl), transparency (T. P.), dissolved oxygen (O_2), phosphate-P (PO_4), ammonium-N (NH_4), nitrite-N (NO_2), nitrate-N (NO_3), chlorophyll content (Chl.) and total cell number of diatoms (D: actual observation, D′: mean value in the sea south off Honshu referred to Uyeno 1959) at St. B, in Ago Bay in July 12, 1960.

Fig. 12. Vertical distribution of temperature (T), chlorinity (Cl), transparency (T. P.), dissolved oxygen (O_2), phosphate-P (PO_4), ammonium-N (NH_4), nitrite-N (NO_2), nitrate-N (NO_3), chlorophyll content (Chl.) and total cell number of diatoms (D: actual observation, D′: mean value in the sea south off Honshu referred to Uyeno 1959) at St. A, in Ago Bay in July 28, 1960.

Fig. 13. Vertical distribution of temperature (T), chlorinity (Cl), transparency (T. P.), dissolved oxygen (O_2), phosphate-P (PO_4), ammonium-N (NH_4), nitrite-N (NO_2), nitrate-N (NO_3), chlorophyll content (Chl.) and total cell number of diatoms (D: actual observation, D′: mean value in the sea south off Honshu referred to Uyeno 1959) at St. B, in Ago Bay in July 28, 1960.

候の影響もあつて以後上下層差はさして大きくはならないが，底層の水温は徐々に高くなり，9月18日まで 27°C 前後を示した。8月10～11日には St.A では上下層 2.9°C の差に対し，St.B では 0.2°C となつている。これは観測時に台風の影響を受けたためで，St.B の方が開水面のため攪拌が大きかつたことを示している。この観測時から9月1～2日まで両点共 0, 1, 2m の3層でアコヤガイの臨界水温とされている 28°C を越えている。この間前年の多徳や神明で見られた 30°C 以上の高温は観測されかつたが，St.A 附近で行なつている井上物産養殖場の観測によると，8月2日以降 2m 層 28°C 以上，表層で 30°C 以上を示し，8月8日まで続いたことがある。0.2m 層が 28°C を越えたのはその後8月24～27日がある。9月1～2日の観測時以降は下降するが，極めてわずかで St. A の中層以深は逆に上昇している。このため上下層差は極めてわずかとなつた。

白石島漁場は前年の伯方島と同様上下差が全く見られない。全層 27 ±0.4°C である。

ii) 塩素量

塩素量は英虞湾に大きな流入河川がないため，降水があつてもその影響はほとんど表層のみで，前年の台風後に見られた様な 2m 層以深の低下は全く見られない。むしろ外洋水の流入で中層以深がいちじるしく高かんとなることが多く，6月19日の観測時から8月10日まで 2m 層以深で 18 Cl ‰以下となることはなく，8月10日には 18.5 Cl ‰以上となつている。9月1～2日以降は台風，前線の停滞の影響を受けてやや低くなり，9月18日には 17.5 Cl ‰附近まで下降する。しかし St.A の底層附近は影響を受けず，18 Cl ‰以上を保つている。

一方白石島では内海のため比較的大きな上下層差が見られるが，全層低かんで，17 Cl ‰を越えるのは底層のみであること，上層から下層まで徐々に変化していることから考え，上下差1～2 Cl ‰ということは内海としては少ないと考えられる。

iii) 酸素量

6月19日 St.A の 6m 層以深が幾分低く，底層で 4.48cc/L，飽和度 85.0％を示したが，7月12，28日にはその様な傾向はなく，全層比較的平均している。しかしながら7月28日には St.A では全層にわたり飽和度が 100％以下となり，St.B との間に差が生じている。8月10日には St.A 1,2m 層に著しい低下が見られ前年同様アコヤガイの呼吸によ

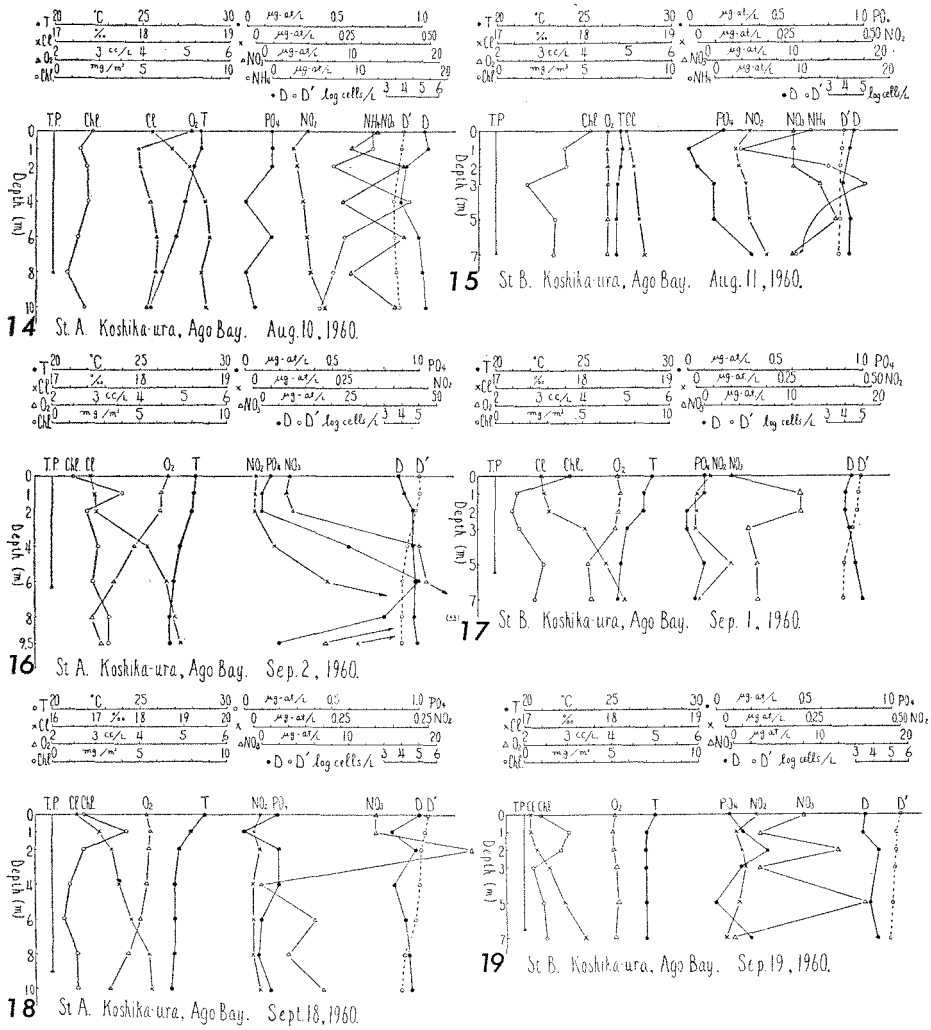

Fig. 14. Vertical distribution of temperature (T), chlorinity (Cl), transparency (T. P.), dissolved oxygen (O_2), phosphate-P (PO_4), ammonium-N (NH_4), nitrite-N (NO_2), nitrate-N (NO_3), chlorophyll content (Chl.) and total cell number of diatoms (D: actual observation, D′: mean value in the sea south off Honshu referred to Uyeno 1959) at St. A, in Ago Bay in August 10, 1960.

Fig. 15. Vertical distribution of temperature (T), chlorinity (Cl), transparency (T. P.), dissolved oxygen (O_2), phosphate-P (PO_4), ammonium-N (NH_4), nitrite-N (NO_2), nitrate-N

(NO_3), chlorophyll content (Chl.) and total cell number of diatoms (D: actual observation, D′: mean value in the sea south off Honshu referred to Uyeno 1959) at St. B, in Ago Bay in August 11, 1960.

Fig. 16. Vertical distribution of temperature (T), chlorinity (Cl), transparency (T. P.), dissolved oxygen (O_2), phosphate-P (PO_4), ammonium-N (NH_4), nitrite-N (NO_2), nitrate N (NO_3), chlorophyll content (Chl.) and total cell number of diatoms (D: actual observation, D′: mean value in the sea south off Honshu referred to Uyeno 1959) at St. A, in Ago Bay in September 2, 1960.

Fig. 17. Vertical distribution of temperature (T), chlorinity (Cl), transparency (T. P.), dissolved oxygen (O_2), phosphate-P (PO_4), ammonium-N (NH_4), nitrite-N (NO_2), nitrate-N (NO_3), chlorophyll content (Chl.) and total cell number of diatoms (D: actual observation, D′: mean value in the sea south off Honshu referred to Uyeno 1959) at St. B, in Ago Bay in September 1, 1960.

Fig. 18. Vertical distribution of temperature (T), chlorinity (Cl), transparency (T. P.), dissolved oxygen (O_2), phosphate-P (PO_4), nitrite-N (NO_2), nitrate-N (NO_3), chlorophyll content (Chl.) and total cell number of diatoms (D: actual observation, D′: mean value in the sea south off Hohshu referred to Uyeno 1959) at St. A, in Ago Bay in September 18, 1960.

Fig. 19. Vertical distribution of temperature (T), chlorinity (Cl), transparency (T. P), dissolved oxygen (O_2), phosphate-P (PO_4), nitrite-N (NO_2), nitrate-N (NO_3), chlorophyll content (Chl.) and total cell number of diatoms (D: actual observation, D′: mean value in the sea south off Honshu referred to Uyeno 1959) at St. B, in Ago Bay in September 19, 1960.

るものと思われる現象を示している。底層でも減少が見られ，排泄物などの有機物分解による消費と思われる。9月2日には異常が最も極端で，St.A では全層，St.B でも 5m 層以深で飽和量90%以下となつている。特に St.A 4m 層以深では減少が著るしく，8m 層では 2.91cc/L, 60.2 %を示している。この様な現象は前年の神明で見られた値よりやや高い。9月18～19日には両地点とも飽和量85%前後で低いが，前回の観測時 St.A の中層以深で見られた著しい低下はやや回復し，8, 10m 層の底層附近のみそれぞれ 3.74, 3.29 cc/L, 77.6, 68.6%となつている。

瀬戸内海，白石島漁場では両地点共底層が幾分減少しており，前年の伯方島漁場より上下差が見られる。しかしながら最低値といえども 3.94cc/L, 80.4 %である。

iv) 燐酸塩

燐酸塩は内湾では一般に夏季に減少し，浅層ではほとんど検出不能となることが多い。本観測でも6月19日には St.A の底層にわずか見出されているのみで，他はほとんど検出されなかつた。しかるに7月12日に St.A で全層，St.B で1～3mの垂下層附近と底層にわずかながら検出される様になり，8月10には St.B も下層にやや多くなつて来る。9月2日には St.A ではさらに増加し，4～8m 層には非常に多量となつているのに対し，St.B では微量となつている。9月18日にはふたたび7月の状況附近まで回復し，両地点とも垂下層附近に多少検出される程度となつた。

一方白石島では両地点とも少なく，高島では上下層ほとんど差がないが，鳥の口は多少底層が多くなつている。

v) アンモニア態窒素，亜硝酸態窒素，硝酸態窒素

観測の当初6月19日にはアンモニア態窒素が多少検出されるが，他の亜硝酸態窒素，硝酸態窒素はほとんど検出されない。その後7月12日には両点共全層亜硝酸態及び硝酸態窒素が検出される様になり，アンモニア態窒素も増加が見られる。7月28日には垂下層のア

ンモニア態窒素の増加が目立つほか8月10日まで各要素共徐々に増加している。しかるに9月2日には St.B がふたたび減少し，亜硝酸態窒素がほとんど検出されなくなつているのに対し，St.A では 4m 層以深にきわめて大量に検出されるに至り全層のアンモニア態窒素及び，亜硝酸，硝酸の極大層の絶対値は測定不能となつた。しかしながらアンモニア態窒素においては鉛直分布の傾向は検知され，亜硝酸，硝酸と全く同様と思われた。また

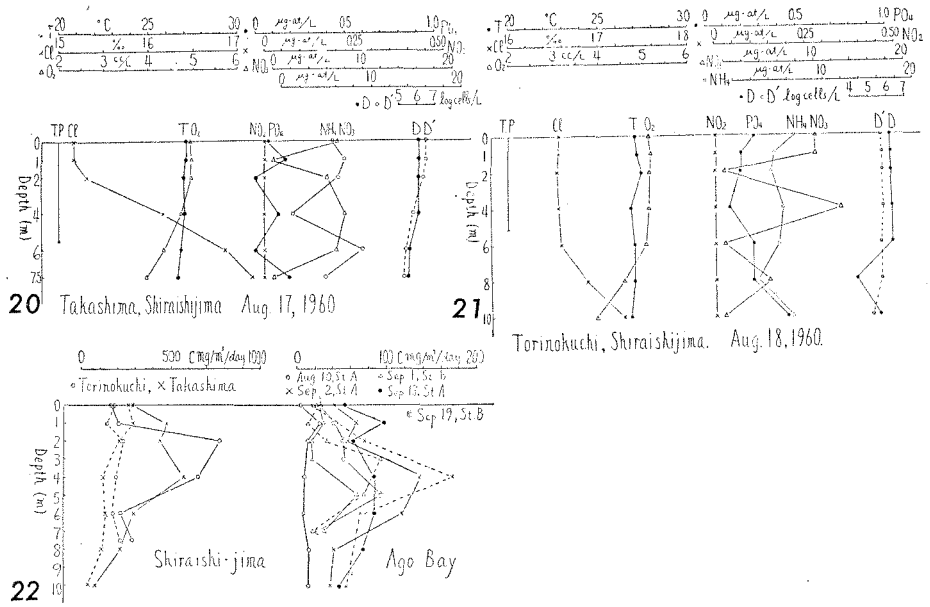

Fig. 20. Vertical distribution of temperature (T), chlorinity (Cl), transparency (T. P.), dissolved oxygen (O_2), phosphate-P (PO_4), ammonium-N (NH_4), nitrite-N (NO_2), nitrate-N (NO_3) and total cell number of diatoms (D: actual observation, D′: mean value in the sea south off Honshu referred to Uyeno 1959) at Taka-shima, Shiraishi-jima in August 17, 1960.

Fig. 21. Vertical distribution of temperature (T), chlorinity (Cl), transparency (T. P.), dissolved oxygen (O_2), phosphate-P (PO_4), ammonium-N (NH_4), nitrite-N (NO_2), nitrate-N (NO_3) and total cell number of diatoms (D: actual observation, D′: mean value in the sea south off Honshu referred to Uyeno 1959) at Torinokuchi, Shiraishi-jima in August 18, 1960.

Fig. 22. Vertical distribution of primary productivity. Thin lines show the distributions of microplankton (residues of filter paper Toyo No. 5 C) and nannoplankton (residue of membrane filter which is filterated the filtrate of filter paper).

アンモニア態窒素も他の二つと同様全観測を通じて最大値を示したと考えられる。最も多量に検出されたのは 8m 層であるが，4，6m 層にも多く，2～4m 層すなわち垂下層を境として大きな躍層が存在している。9月18日には St.A も回復し，St.A では前回の観測時とは逆に 4m 層以深ではほとんど検出されていないのに対し，2m 層以浅で検出されている。この浅層での検出は河川水よりの供給と考えられる。

白石島漁場では亜硝酸態窒素は全く検出されず，硝酸態窒素が浅層で幾分検出されたのは附近に大肥料工場があるためと考えられる。アンモニア態窒素は全層大差なく微量検出されている。

vi)　クロロフイル量

6月19日には両地点とも 2m 層に極大値が見られるが，7月12日には St.A の 1, 2m 層に減少が見られ，7月28日には両点とも減少し，St.A では上下層の差がわずかとなり，St.B では表層から底層まで徐々に減少する傾向を示す様になる。8月10～11日にもこの傾向は継続して現われているが，9月1～2日になると両点共浅層，特に養殖貝の垂下層附近の1～2m 層は減少し続けるのに対し，4m 層以深は増加の傾向を示す。9月18～19日には全般に絶対値はきわめて低いが，分布傾向はおおむね旧に復している。しかしながら St.A ではなお2～4m 層での減少が目立つている。

vii)　硅藻量

総細胞数（D）については前年の場合と同様上野（1958）による本州南岸表層の平均値（D′）と比較した（Fig. 7～22)。当初は時によつて多少平均値より増減はあるが，全観測時にわたつて平均値の変化とほとんど同傾向を示している。しかしながら前述のクロロフイル量と同様に時を経るにしたがつて下層では増加して平均値より常に多くなるのに対し，浅層は減少してこの逆となる傾向が見られる。特に9月1日は1, 2m 層の減少が明確となる。St.A ではこの傾向が7月28日には既に見られ，9月18日に最も顕著となる。白石島では前年の伯方島同様上下層ほとんど差がなく，かつ平均値とほとんど一致する。英虞湾との総細胞数の差は約10倍である。

出現種は当初6月19日には *Chaetoceros affinis*, *C. compressus* を主とするが量が比較的少なく，*Rhizosolenia stolterfothii*, *Bacteriastrum varians* などの比較的高かん性の内湾種が多く出現した。その後水温の上昇と塩素量の降下によつて7月12日には *C. affinis* が増加し，*Skeletonema costatum*, *Nitzschia seriata* などの純内湾性種が増加したが，7月末より高かんとなつたため，全般に減少してふたたび主体は *C. affinis* のみとなつて減少した。9月1～2日にはふたたび低かんとなつたので，*S. costatum* や *Thalassionema nitzschioides* が増加した。9月19日には組成的にはこの傾向が継続するが St.B では量がいちじるしく減少した。また鞭藻の *Ceratium furca* が中層で増加している。一般に St.A と St.B で組成的には大差ないが，St.B の方が多少外洋的傾向を示している。

白石島では前年の伯方島同様，出現種の細胞も英虞湾に比して大きく，色素量も多い様に見受けられた。低かんであるから *S. costatum* が圧倒的に多く，*T. nitzschioides*, *C. compressus*, *C. pseudocurvisetus*, *C. affinis*, *N. seriata* 等の純内湾種が多い。

viii)　C^{14} による基礎生産量

8月10日の観測時より実施した英虞湾両地点の生産量の鉛直変化を白石島両地点のものと一括して Fig.23 に示した。絶対値は観測時の天候に大きく左右されるので傾向の変化についてのみ述べる。8月10日には雨天のため絶対値が小さく，またメンブランフイルターによる nannoplankton 及び St.B の測定を欠いたが，その鉛直変化には明確に 1, 2m 層での突出が目立つている。しかるに9月1～2日と18～19日にはこの突出部が4～6m 層に認められる。これは nannoplankton でも同様である。一方白石島では濾紙の場合は1～4m 層に明確な突出部が見られるが，メンブランフイルターでは上下層にほとんど差が認められない。結局クロロフイル量の場合ほど顕著ではないが，ほぼ同様で盛夏になるにしたがつて上層の生産量が減少し，下層特に垂下層の直下が大きくなる傾向を示してい

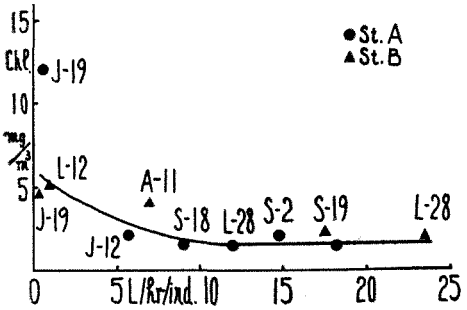

Fig. 23. Relation between filtering rate of pearl oyster (abscissa) and chlorophyll content in culturing layer (2m) (ordinate). J: June, L: July, A: August, S: September.

る。なお英虞湾と白石島の生産量を比較すると，東洋濾紙 No.5C では3～4倍，メンブランフイルターでは 1.5～2倍といずれも白石島が大きい。しかしてメンブランフイルターの方が濾紙 No.5C より差が小さい原因は判明しないが今後の餌量問題解析上興味あることである。

iX) アコヤガイの濾水量

前述の様な方法で排泄物中のクロロフイル量より濾水量を求め，垂下層のクロロフイル量及び水温との関係を検討した（Fig.24, 25)。この結果環境水中のクロロフイル量が 5mg/m³ 以下，水温 26°C 以上になると濾水量が急速に増大することがわかつた。小林・松井（1953）によれば鰓の繊毛運動及び心臓の搏動からアコヤガイの最適水温は12～23°C であるという。しかし両氏の測定値では繊毛運動の最高は水温 28～30°C に見られている。これは水温と濾水量に関する上記の事実を裏書するものと考えられる。しかしながら植物プランクトン量との関係については従来の研究例を見ないので，水温と植物プランクトン量のいずれが大きく影響するかについて推論し得ない。また濾水量が最高 23L/nr/ind. を示しており，辻井等（1957）の結果に比し著しく大きくなつている。これは海水中のクロ

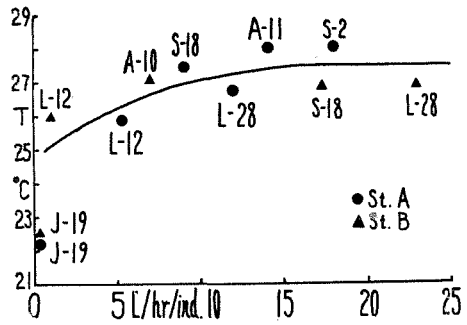

Fig. 24. Relation between filtering rate of pearl oyster (abscissa) and water temperature in culturing layer (2m) (ordinate). J: June, L: July, A: August, S: September.

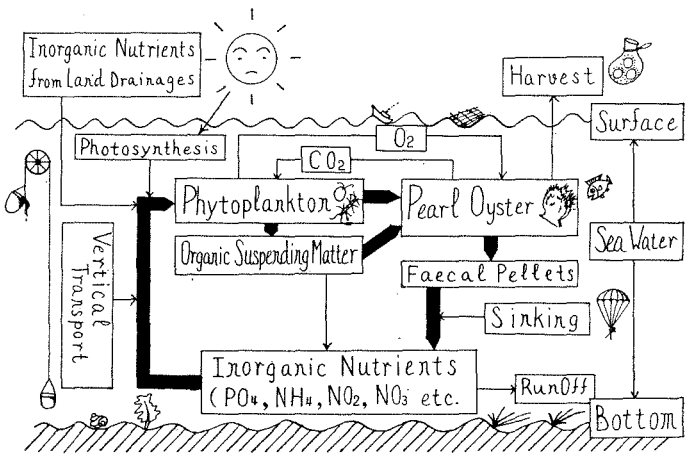

Fig. 25. Schematic representation of food chain around pearl oyster in the sea.

ロフイル量の測定に濾紙（東洋 No. 5C）を用いたために微細なプランクトンが脱落したことによると思われる。前述の様に 5C を通過する nannoplankton の光合成量が，英虞湾では 5C に残る microplankton とほぼ同量あることから考えると，排泄物は粘液に包まれているためにほとんど完全に 5C で集められるから，濾水量は上述の約½であると考えられる。瀬戸内海漁場では分析の手違いから測定出来なかつた。

3. 考　　察

以上を綜合して考察すると，英虞湾では夏季表層の水温上昇と共に表層では栄養塩，植物プランクトンが減少するのに対し，下層では栄養塩の著しい増加，植物プランクトン量ならびにその光合成量の増加，酸素量の減少が見られる。この変化は 8 月中旬までは徐々に行なわれるが，以後急速に悪化し，枝湾，湾奥では栄養塩の増加は極度に達し，はなはだしいところは酸素量が極度に減少する。しかるに開水面ではこの様な極度化の起る前に回復している。一方瀬戸内海漁場では盛夏といえども上下層に各要素ともきわめて変化に乏しく均一となつている。この上下両層の極端な差は 2 ～ 4m 層に見られ躍層としてきわめて急激な変化を示している。これはアコヤガイの垂下層と一致している。したがつて浅層に植物プランクトンが少ないということは餌料が不足していることを示すわけで，Fig. 24 に現われている様に急激な濾水量増加を示した部分では明らかに餌料不足になつているのではないかと考えられる。

いま真珠漁場における食物連鎖について考えてみると，一般的には Fig. 26 に示すごとく，アコヤガイの排泄物は栄養塩として植物プランクトンに供給される。しかしながら燐酸塩のように溶出の早いものは比較的容易に供給されるが，バクテリアによる分解を必要とするため溶出の遅い窒素源は固形物として沈降し，底層に堆積する。底層は植物プランクトンの光合成に有効な光に乏しいため，植物プランクトンの利用に供するためにはこれを表層附近まで運び上げる必要がある。かくして表層の植物プランクトンは有効に光合成

を行ない増殖する。この植物プランクトンは直接アコヤガイの餌料となり，一部は死滅後分解してふたたび栄養塩に帰する。またこの分解過程において有機懸濁物質となりアコヤガイの餌料にもなる。したがつてアコヤガイ飼育量を一定とした場合，その餌料が充分であるためには，排泄物の栄養塩化及びその表層への運搬ならびに植物プランクトンの増殖が充分でなければならない。もしこの一部分でも欠ければ循環は停止し，停止部分で物質の蓄積がおこり，その先では欠乏がおこることは当然である。

いま上述の1960年9月2日の英虞湾 St.A の状態を考えてみると，栄養塩が下層に蓄積しており，不足しているのは餌料たる植物プランクトンであるということになる。この両者の間に介在するのは鉛直混合による栄養塩の上層への運搬であるから，結局停止しているのは鉛直混合ということになる。この場合栄養塩はこの部分で停止すると完全に循環している状態と幾分様相を異にして来る。すなわち英虞湾の観測当初や瀬戸内海漁場ではアンモニア態窒素以外ほとんど検出されていない。これは燐酸塩の場合は溶出が早く，また吸収も早いため検出されないのである。また窒素化合物の場合は有機物からの溶出がまずアンモニア態窒素でなされ，植物プランクトンに吸収されなかつた余剰分がバクテリアの作用により亜硝酸，硝酸と変化する。したがつて循環がすみやかに行なわれている間は亜硝酸，硝酸は検出されないことになる。もし鉛直混合による運搬が停止した場合には，アンモニア態窒素は底層附近に停滞し，亜硝酸，硝酸と変化する。また燐酸塩も分解が早いといつても吸収されずに蓄積するものが見られることになる。これが9月2日のA点の状況と考えられ，1959年8月17日の神明は更に進行した状態と思われる。この場合もちろん底層附近といえども水深が 10m 前後であるから，透明度が8～9m あることから考えて補償深度以浅であり，植物プランクトンの光合成は行ない得る。しかして栄養塩が豊富であるから増殖し得るので，本州南岸表層の平均値と比較してもなお多い値は示しているが，光度の減少は対数的であるから光度不足の影響は大きく，これが制限要因となるため蓄積された栄養塩を底層附近だけでは利用し尽くせない。その結果栄養塩は増加の一方をたどつたことになる。

この場合アコヤガイ及び附着生物の成長に使われた物質量及び海潮流で外部に持ち去られた物質量は循環せず，不足することが考えられる。アコヤガイによる消費には2種あり，その1は実際に増肉として使用されたもので，他は新陳代謝に必要なエネルギーとして消費されたものである。これら損失の補償については現在まで論ぜられたものを見ないが，上述の循環系に外部より来る物質補給も当然考えられる。そのうち大きなものとしては河川水よりの栄養塩補給および光合成に供される太陽のエネルギーがある。これらの補給が損失と見合つているかどうかは今論ずるには資料が全くない。しかしながら河川水からの補給は低かんとなつて現われ，表層に補給されるのであるから英虞湾の様に流入河川がなく，盛夏の観測時にはむしろ高かんであつたことから考えるとこの補給は英虞湾の場合さして意味があるとは思えない。しかるに同一湾内の非常に近接した2点で一方は底層附近でおびただしい栄養塩の蓄積が見られ，他方はその傾向は見られたが極度化以前に回復していること，かつ一方は枝湾内にあり，他方は開水面にあることから考えて，両点ともほとんど物質循環が閉鎖しており，外部との損失ならびに補給はさして問題にならないのではないかと考えられる。もちろん白石島の場合は栄養塩，植物プランクトン量には上下差がないが，塩素量値に上下差が見られ，河川水の補給が大きいのではないかということが

考えられ，必ずしも循環系のみを考えるわけにはゆかないと思われる。また伯方島の場合は強潮汐流のため塩素量値すらも上下差がなく，白石島も潮汐流が相当大きいことから考え，これらの瀬戸内海漁場ではアコヤガイの大量飼育で物質循環量が増しているというより，むしろ漁場自体の肥沃度が高いためにアコヤガイ飼育の影響がないと考えて然るべきと思われる。

次にこの様な鉛直混合停止による水質悪化の程度について考えると，枝湾内のA点の9月2日の場合，飼育しているアコヤガイ自体に対し蓄積された排泄物，これの分解によつて生じた酸素欠乏が影響を与えているかどうかという問題がある。今回のA点は作業場附近にあり，この附近のいかだに全期間を通じて垂下されていたアコヤガイは試験貝しかなく，養殖貝は常時B点附近に置かれ，手術その他の作業上一時置かれるものが多い地点であつた。この試験貝は観測終了時までに死滅したのは100個体中3個体のみで，死亡率が高いとはいえない。このことから考えて9月2日の状態がその前後何日間継続したか分らないから断定的結論は下せないが，アコヤガイにはこの程度ではさして影響を与えなかつたのではないかと考えられる。しかしながらさらに極度化した場合には無酸素状態，ひいては硫化水素の発生が考えられ，過去に湾奥部でその様な事例も見られたのであるから，この鉛直混合の停止が悪影響を及ぼす可能性は充分考えられる。また植物プランクトン増殖にとつてアコヤガイの排泄物蓄積は栄養塩の補給になるのであるから好条件といえるのであるが，光度不足のためこれを利用し尽くせない状態にあつた場合，かえつて抑制的な働きをしないかという問題が考えられる。これはクロロフイル量，硅藻細胞数，光合成量が一般的な形態より底層附近で増加していたり，表層の平均値と比較して多かつたりする事実から考え，好条件下にあると考えられる。しかしながらこれとて無酸素状態や，硫化水素発生の場合には悪影響が予想される。

また下層での過度の栄養塩蓄積に到る時間的経過についても問題がある。前述の様に栄養塩の増加の経過をみると，当初はA, B両点ともほぼ同程度に徐々に進行している。しかるに8月10日～9月2日の間にA点は極度に悪化したのにB点はさした変化なく，むしろ回復している。この事実は変化が当初徐々に進行し，後に急速化することを意味する。これは前述のアコヤガイの濾水量と水温および垂下層のクロロフイル量との関係をみると双方ともある限度を越すと急速に濾水量が増していることから考え，この限度に達すると，植物プランクトンの捕食による減少，排泄物量の増大，すなわち栄養塩の下層での蓄積が急激化することが考えられる。しかしてこの急激化に見合うために物質循環の速度を急速化せねばならず，そのためには栄養塩の上層への補給の急速化が要求される。一方日射による表面水温の上昇は鉛直安定度を高め，鉛直混合を妨げ，むしろ逆効果を示す。すなわち餌料の減少は停滞によつておこり，その停滞は表面水温の上昇によつておこる。しかるに表面水温の上昇と餌料の減少はアコヤガイの濾水量を増大せしめますます餌料を減少させるという結果を生じ，停滞がある限度に達すると悪化が急速化するのは消費と補給の双方を活発化させるため当然といえる。この濾水量の急増のおこる限度は一応クロロフイル量 5mg/m^3 以下，水温 26°C 以上と見られるが，相乗的効果のあらわれるものである上，資料数が少ないので今後さらに実験によつて確かめる必要があると考える。またSt.Aは極度化したのにSt.Bはその様なことがなかつたので，著しい悪化は枝湾内のみの現象と考えられる。このことは英虞湾でも開水面は盛夏といえども比較的枝湾部より上下層の水

の混合が行なわれやすいといえる。

次に回復についてであるが，9月18日の観測時を回復した状態と考えるかどうかについては多少疑問がある。というのは9月1～2日の状態より水温の上下差はなくなつて多少鉛直混合が行なわれたであろうことは想像される。しかしながら全要素が正常に復したとは断定出来ない。栄養塩は表層では両点とも増加しているが，B点では下層においても前回より増加している。硅藻量は両点共，本州南岸の平均値よりいちじるしく少ない。C^{14}による基礎生産量は1～2m層に増加の傾向は見られるが，4～6m層になお大きな突出部がある。これらの事実は下層に蓄積された栄養塩が上層へ運ばれたか外部へ流出したか，とにかく散逸したことを示している。またクロロフイル量が表層附近で増加の傾向を示していること，表層の栄養塩が増加していることから，表層附近の状況がよくなつたことも示される。しかしこの栄養塩は鉛直混合の結果のみとは考えられず，当時見られた降水に起因する陸水の流入によるとも考えられる。しかしながら9月1～2日のSt.Aの状況がSt.Bには見られなかつたのであるから前述の様に枝湾内の極地現象と考えられ，もし水平か鉛直かいずれにせよ混合が行なわれれば容易に解消するであろうということは想像される。この混合は恐らく今回は低気圧の通過による攪拌と想像されるが，この季節には大なり小なり台風の影響を受けることがあるほか，比較的降水量の多い季節であるから9月に入ると比較的急速に回復が行なわれるであろうと思われる。この回復の速度は全く攪拌の行なわれ方によると思われるから，いつから回復するとは一概にはいえないが，恐らく9月中には回復するものと思われる。しかしながら悪化の程度がさらに極端となつた場合は底質に多くの有機物を含む結果，その上部の海水が混合で平常状態に近くなつても，底質の浄化が進まず翌年まで持ち越すこともおこりかねない。この様な場合は漁場の老化現象ということになる。

4. 結論ならびに要約

以上を綜合すると，英虞湾では盛夏に支湾内及び湾奥で鉛直混合の停止と密殖のため物質循環に阻害がおこり，下層に栄養塩の蓄積がおこつて水質が悪化し，上層では餌料源たる植物プランクトンに欠乏を来すことが考えられる。湾口附近の開水面ではこの様な現象のおこる以前に回復している。また変化は当初は徐々に，後には急速に現われ，期間は8月中旬より9月初旬までと思われる。急速悪化の原因はアコヤガイの濾水量増大が水温と餌料不足の双方によつて増大するためと考えられる。

これらのことから盛夏期以外は枝湾内といえどもおおむね現在の養殖量でも食物連鎖上をほぼ物質循環が完全に行なわれていると考えられる。しかしながら盛夏には少なくも枝湾内は完全に物質循環に阻害がおこり，極度化した場合には大量斃死や漁場の老化を起すだけの素地は充分にあるといえる。また開水面の場合も極度化はしていないが同一傾向の変化は微弱ながら現われている。一方瀬戸内海漁場の場合は資料が少ないが，強い潮汐流による上下攪拌，多量の陸水混入による大きな肥沃度によつてアコヤガイ飼育による影響とおぼしき変化が環境要因中に見られない。

上述の様に物質循環の阻害による水質悪化はその期間が短いこと，現象が極地的で英虞湾内ですら場所によつて著しく違うことから，以上の問題のみに限ればその対策は技術的

に解決すべきこととも考えられる。本質的には盛夏期に上下層の海水を人工的に攪拌して下層の栄養塩を上層へ補給してやればよいのであるが，枝湾といえども水深 10m 前後もあるのであるから問題は大きい。したがつて現在一部で行なわれている様に余力の充分ある瀬戸内海漁場などの他の肥沃な漁場へ盛夏のみ養殖貝を移動さすことを考えるのも一解決方法ではないかと考えられる。しかして極地性があるということは，対策も漁場個々の特性に基づいて立てられるべきものと考えられる。

Summary

Many of the pearl culturists have their farms in Ago Bay. Sometimes the unexpected death of many pearl oysters and senile decay of farms at the innermost parts of the bay occur. The authors confirmed that these phenomena result from inharmonious rotation of nutrient substances in the food chain around the pearl oyster. The supply of nutrient salts for phytoplankton is abnormal in shallow waters. The supply stops in late summer and phytoplankton reduces in shallow water, while nutrient salts innumerably increase in deep water. These phenomena are exceedingly prominent in the innermost parts and in small branch bays.

Various elements of sea water are distributed almost uniformly in June from surface to bottom, even in the innermost parts of the bay. However, the abnormal phenomena becomes evident according to the increase of the difference of temperature between surface and bottom, because the supply is stopped by vertical stagnation. The change is gradual in the early stage but after mid-August it increase rapidly. This rapid change is result of the increase of the filtering rate of pearl oysters which is accelerated by the rise of temperature over 26°C and the reduction of chlorophyll content to less than 5 mg/m^3 in the culturing layer. At the farms in the Inland Sea the above mentioned phenomena are not observed. It may be due to the large fertility and the perfect vertical mixing by strong tidal currents.

The fundamental countermeasure is the artificial mixing of sea water, but it is very difficult because it involves much labour and expense. Therefore, it may be best to move many of the pearl oysters in Ago Bay to Inland Sea in mid-summer. Some culturists have already put this plan into operation.

参　考　文　献

1) Barnes, H. 1959. Apparatus and methods of oceanography—Chemical. London.
2) 古川　厚・野上和彦・久岡　実・篠岡久夫・木村三郎・村主昭也・山口　昇・関　政夫・柴原規計・沢田保夫・丹下　孚　1958. 三重県下主要真珠養殖場予備調査結果について. 三重水試研究報告　6: 1—46.
3) 北村　弘行　1958. 黒潮における Nitrate-Nitrogen. 海と空　34: 11—19.
4) 気象庁　1958. 海洋観測指針. 東京.
5) 小林　博・松井淳平　1953. アコヤガイの環境変化に対する抵抗性の研究. (1)　鰓の繊毛運動に

就いて. 農水講研報 3 (2) 123—131.
6) 猿橋 勝子 1955. 微量拡散分析法. Japan Analyst 4: 337—339.
7) 西条 八束 1957. 湖沼調査法. 東京.
8) 菅原 健・田中元治・金森 悟・大森貞之 1960. 微量拡散法による天然水中の全炭酸の定量装置の改良. 日本海洋学会大会講演.
9) 辻井 禎・大西候彦 1957. アコヤガイの濾過水量及び捕食の実験的研究 I. 濾過水量について. 国立真珠研報 3: 194—201.
10) 上野 福三 1958. 本州南岸附近の硅藻量と海況との関係, 主として重要種の水温および塩素量に対する一般的特性について. 海と空 34: 92—112.

Table I. Results of oceanographical observations in Ago Bay and Hakata-jima in 1959.

Tatoku-jima, Ago Bay. June 14, 1959

Depth	T°C	C1‰	O_2cc	%
0 m	22.2	17.23	5.19	98.1
1	21.7	17.67	4.99	94.0
2	21.9	18.17	4.95	94.3
4	21.9	18.37	5.03	95.9
6	21.7	18.53	5.02	95.7
8	21.6	18.46	4.22	80.3
11	21.5	18.50	4.74	90.0

Shinmei, Ago Bay. June, 14, 1959

Depth	T°C	C1‰	O_2cc	%
0 m	23.0	16.33	5.45	103.5
1	22.5	18.87	5.55	107.2
2	22.4	17.79	5.17	98.7
4	21.9	18.36	5.10	97.2
6	22.0	18.32	5.10	97.4
8	21.4	18.46	4.66	89.5
10	21.4	18.49	4.52	75.9
12	21.2	18.46	4.14	78.3

Tatoku-jima, Ago Bay. Aug. 18, 1959

Depth	T°C	C1‰	O_2cc	%	KIcc	%
0 m	29.7	5.7	5.03	95.4	6.76	100.0
1	28.0	—	4.80	—	6.47	95.5
2	27.3	15.59	4.87	98.6	5.95	88.0
4	26.3	16.98	4.73	97.9	4.73	69.9
6	26.0	17.50	4.52	91.9	4.45	65.8
8	25.6	17.89	4.19	84.7	2.16	31.9
10	25.4	16.00	3.89	76.5	2.45	36.2

Shinmei, Ago Bay. Aug. 17, 1959

Depth	T°C	C1‰	O_2cc	%
0 m	30.1	6.1	5.54	106.0
1	29.1	12.9	5.23	106.1
2	28.3	11.4	5.37	105.4
4	26.5	17.01	4.38	89.2
6	26.1	16.78	4.49	90.4
8	26.0	—	—	—
10	25.3	18.01	2.78	56.0

Mori, Hakata-jima. Aug. 25, 1959

Depth	T°C	C1‰	O_2cc	%
0 m	26.3	17.02	4.38	88.7
1	26.5	17.03	4.40	89.5
2	26.4	17.11	4.37	88.6
4	26.4	17.13	3.84	80.2
6	26.3	17.05	4.40	89.2
9	26.3	17.14	4.48	90.7
12	26.2	17.08	4.41	89.0

Table II. Results of oceanographical observations in Ago Bay and Shiraishi-jima in 1960.

St. A, Koshika-ura, Ago Bay Date: June 19, 1960. Transparency: 6.5m

Depth	Temp.	Cl	O_2		PO_4-P	NO_2-N	NO_3-N	NH_3-N	Chloro-phyll	Diatoms log cells/L	
m	°C	‰	cc/L	%	μg/L	μg/L	μg/L	μg/L	μg/m3	D	D′
0	23.0	17.73	5.22	101.2	0.10	0	0	9.5	2.4	—	5.0
1	22.7	18.29	5.25	101.4	0	0	0	7.5	6.5	3.9	4.3
2	22.2	18.41	5.31	101.5	0.10	0	0	7.5	12.2	3.5	4.2
4	22.7	18.64	5.02	97.3	+	0	0	12.0	4.3	3.7	4.0
6	22.4	18.62	4.69	90.4	+	0.08	+	—	1.2	3.3	4.0
8	22.2	18.70	4.84	93.1	0	0	0	6.0	2.2	4.1	3.8
10	21.4	18.75	4.48	85.0	0.35	0.08	5	10.5	5.7	3.8	3.8

St. B, Koshika-ura Ago Bay Date: June 19, 1960. Transparency: 6.8m

0	22.5	18.29	5.51	106.0	+	0	0	14.5	3.1	4.4	4.4
1	22.5	18.29	5.43	104.4	0	0	0	9.0	2.3	4.5	4.4
2	22.4	18.28	5.42	104.2	0.05	0	0	6.2	4.9	4.6	4.4
3	22.4	18.41	5.54	106.3	0	0	0	6.0	2.3	4.6	4.3
5	22.4	18.62	5.26	101.2	0.15	0	0	8.3	1.2	4.5	4.0
7	22.4	18.75	5.28	101.9	0	0	0	—	2.2	4.4	3.7

St. A, Koshika-ura, Ago Bay Date: July 12, 1960. Transparency: 6m

Depth	Temp.	Cl	O_2		PO_4-P	NO_2-N	NO_3-N	NH_3-N	Chloro-phyll	Diatoms log cells/L	
m	°C	‰	cc/L	%	μg/L	μg/L	μg/L	μg/L	μg/m3	D	D′
0	27.7	17.57	4.76	101.3	0.35	0.09	10	10.5	5.5	4.5	5.0
1	26.7	17.66	4.92	101.0	0.35	0.10	10	11.5	2.1	4.4	4.9
2	25.9	18.03	4.92	100.0	0.35	0.10	7	25.0	2.0	4.8	4.6
4	24.4	18.44	5.08	101.2	0.30	0.10	7	—	6.1	5.1	4.2
6	23.7	18.53	5.22	102.6	0.30	0.20	10	36.4	4.0	5.5	4.1
8	23.1	18.62	5.11	99.6	0.25	0.20	10	17.5	7.2	5.7	4.0
10	22.8	18.88	4.77	93.2	0.35	0.16	8	18.5	4.1	5.8	3.7

St. B, Koshika-ura, Ago Bay Date: July 12, 1960. Transparency: 6.5m

0	27.6	17.86	4.77	99.8	0.15	0.13	36	14.2	2.8	4.6	4.8
1	26.6	17.91	5.01	103.1	0.45	0.11	10	35.0	4.8	5.0	4.5
2	26.0	18.13	5.00	102.0	0.30	0.11	10	—	5.0	5.2	4.2
3	24.7	18.40	5.08	101.6	0.25	0.14	19	34.2	1.6	5.0	4.1
5	24.7	18.54	5.07	101.4	0.15	—	10	15.0	2.3	4.1	4.0
6.5	23.1	18.75	5.28	103.1	0.45	0.14	16	17.4	2.9	4.9	3.8

St. A, Koshika-ura, Ago Bay Date: July 28, 1960. Transparency: 6.0m

Depth	Temp.	Cl	O_2		PO_4-P	NO_2-N	NO_3-N	NH_3-N	Chloro-phyll	Diatoms log cells/L	
m	°C	‰	cc/L	%	μg/L	μg/L	μg/L	μg/L	μg/m3	D	D′
0	27.7	17.99	4.76	99.8	0.10	0.22	8	—	1.4	4.5	4.5
1	27.3	18.03	4.62	96.3	0.50	0.33	3	8.0	2.2	4.4	4.2
2	26.7	18.12	4.62	95.5	0.35	0.11	3	9.0	1.9	3.3	4.3
4	25.3	18.29	4.72	95.4	0.35	0.05	+	8.0	0.7	4.2	4.2
6	24.8	18.32	4.68	93.6	0.20	0.16	0	8.0	1.2	—	4.2
8	24.4	—	4.65	—	0.20	0.15	5	8.0	0.2	4.6	—
10	24.2	18.46	4.55	90.3	1.10	0.16	7	15.7	2.8	3.8	4.1

St. B, Koshika-ura, Ago Bay Date: July 28, 1960. Transparency: 6.5m (bottom)

0	27.7	18.11	4.87	102.3	0.80	0.14	7	9.0	3.1	3.8	4.2
1	27.5	18.12	4.91	102.7	0.20	0.30	8	—	2.3	3.5	4.2
2	26.9	18.16	4.96	102.5	0.20	0.26	8	—	1.8	3.8	4.1
3	26.5	18.20	4.93	101.4	0.25	0.17	4	11.3	2.1	3.9	4.1
4	26.3	18.25	5.00	102.7	0.15	0.07	7	13.6	—	—	4.1
5	25.6	18.30	4.87	99.0	0.80	0.05	3	13.6	1.5	4.2	4.1
7	24.9	18.47	5.03	101.0	0.60	0.20	7	14.5	0.7	4.4	4.1

St. A, Koshika-ura, Ago Bay. Date: August 10, 1960. Transparency: 8m

Depth	Temp.	Cl	O_2		PO_4-P	NO_2-N	NO_3-N	NH_3-N	Tot. CO_3	Ass.C*	Chloro-phyll	Diatoms log cells/L	
m	°C	‰	cc/L	%	μg/L	μg/L	μg/L	μg/L	mg/L	mg/m3/day	μg/m3	D	D′
0	28.4	18.12	5.15	109.6	0.15	0.15	13	11.5	82.5	4.6	2.2	5.2	4.0
1	28.4	18.35	3.93	83.8	0.15	0.11	10	11.5	69.3	25.5	1.5	5.4	3.9
2	28.0	18.54	3.98	84.3	0.15	0.12	16	7.0	79.2	12.4	1.9	4.1	3.7
4	27.5	18.74	4.22	89.0	0	0.14	9	15.7	71.2	9.0	2.0	3.9	3.5
6	27.0	18.79	4.38	91.6	0.15	0.15	16	8.3	106.7	7.4	1.4	4.9	3.5
8	26.2	18.69	4.33	90.2	0	0.16	10	7.0	77.0	13.0	0.8	5.1	3.4
10	25.5	18.74	4.19	85.3	0.05	0.20	15	5.5	83.6	12.2	1.8	5.3	3.8

* Filter Paper (Toyo No. 5C)

St. B, Koshika-ura, Ago Bay. Date: August 11, 1960. Transparency: 7m

0	27.1	18.49	4.55	95.2	0.20	0.32	10	11.0			5.4	4.4	3.9
1	27.2	18.53	4.54	95.0	0	0.27	10	3.0			3.9	4.2	3.8
2	27.1	18.57	4.52	94.6	0.05	0.34	10	13.0			4.0	—	3.7
3	27.0	—	4.54	—	0.15	0.10	13	17.2			1.8	3.8	—
5	26.9	18.64	4.53	94.8	0.15	0.06	15	—			3.4	4.3	3.7
7	26.9	18.70	4.51	93.6	0.36	0.20	10	9.0			3.3	4.2	3.6

St. A, Koshika-ura, Ago Bay　Date: September 2, 1960.　Transparency: 6.3m

Depth	Temp.	Cl	O_2		PO_4-P	NO_2-N	NO_3-N	Tot. CO_3	Ass.C*	Ass.C★	Chloro-phyil	Diatoms log cells/L	
m	°C	‰	cc/L	%	μg/L	μg/L	μg/L	mg/L	mg/m3/day	mg/m3/day	μg/m3	D	D′
0	28.2	17.44	4.65	97.7	0.15	0.09	8	63.8	41.6	19.8	1.8	3.8	5.0
1	28.1	17.48	4.51	94.5	0.10	0.03	7	70.9	66.0	—	4.2	4.1	5.0
2	28.0	17.50	4.50	94.3	0.10	0.05	9	72.6	55.8	75.2	1.8	4.6	4.8
4	27.3	18.10	3.89	81.0	0.60	0.62	45	75.9	137.4	166.6	1.0	4.6	4.3
6	26.9	18.31	3.41	70.7	1.00	2.10	47	70.4	116.6	70.4	0.7	4.8	4.0
8	26.7	18.39	2.91	60.2	0.80	>	>	66.0	41.0	—	1.4	4.7	4.0
9.5	26.7	18.47	3.14	65.1	0.20	3.00	18	72.6	36.4	54.8	1.4	4.9	4.0

St. B, Koshika-ura, Ago Bay　Date: September 1, 1960.　Transparency: 5.5m

0	29.0	17.52	4.80	102.6	0.10	0.04	3	66.0	25.0	21.8	0.9	4.4	4.9
1	28.5	17.55	4.85	102.8	0.10	+	11	67.1	26.4	13.2	2.6	4.0	4.8
2	28.5	17.62	4.81	101.9	+	0	11	60.5	17.2	31.8	2.1	4.0	4.7
3	27.6	18.03	4.77	99.8	+	0	5	64.9	18.8	91.2	0.5	4.3	4.4
5	27.2	18.27	4.12	85.8	0.10	0.10	6	72.6	66.0	71.6	1.1	4.6	4.0
7	27.0	18.47	4.20	87.5	0.05	0	6	60.5	30.0	18.4	2.3	5.0	3.9

* Filter Paper (Toyo No. 5C)
★ membrane filter

St. A, Koshika-ura, Ago Bay　Date: September 18, 1960.　Transparency: 9m

Depth	Temp.	Cl	O_2		PO_4-P	NO_2-N	NO_3-N	Tot. CO_3	Ass.C*	Chloro-phyll	Diatoms log cells/L	
m	°C	‰	cc/L	%	μg/L	μg/L	μg/L	mg/L	mg/m3/day	μg/m3	D	D′
0	28.7	10.56	4.16	87.4	0.20	0.05	13	66.0	51.0	1.1	5.0	5.5
1	27.9	17.07	4.24	88.3	0	0	13	82.5	97.0	0.9	3.4	5.3
2	27.3	17.38	4.20	86.8	0.20	0.02	24	90.2	61.8	2.4	4.8	5.1
4	27.0	17.53	4.16	85.6	0.20	+	+	92.4	85.0	3.4	3.6	5.0
6	27.0	17.80	4.00	82.6	0.10	+	6	93.5	86.0	1.4	4.2	4.8
8	27.0	18.20	3.74	77.6	0.08	+	3	90.2	55.6	1.6	4.4	4.2
10	26.8	18.27	3.29	68.6	0.15	0.02	7	130.9	41.0	1.3	4.6	4.0

St. B, Koshika-ura, Ago Bay　Date: September 19, 1960.　Transparency: 6.5m

0	27.5	17.07	4.05	83.7	0.08	0.09	8	77.0	24.4	1.6	3.5	5.5
1	27.0	17.07	4.01	82.2	0.15	0.03	3	75.9	40.7	0.9	3.4	5.3
2	27.0	17.15	4.06	83.2	0.30	0.05	12	74.8	51.4	3.7	4.3	5.3
3	27.0	17.39	4.12	83.	0.15	0.05	3	80.3	53.1	1.8	—	5.2
5	27.0	17.46	4.15	85.4	+	0.04	15	90.2	91.2	1.0	4.8	5.1
6.5	27.0	17.70	4.08	84.3	0.20	0	0	50.6	23.6	0.7	4.2	4.9

* Filter Paper (Toyo No. 5C)

Torinokuchi, Shiraishi-jima Date: August 18, 1960. Transparency: 5.1m

Depth	Temp.	Cl	O_3		PO_4-P	NO_3-N	NO_3-N	NH_3-N	Tot. CO_3	Ass.C *	Ass.C ★	Chloro-phyll	Diatoms log cells/L	
m	°C	‰	cc/L	%	μg/L	μg/L	μg/L	μg/L	mg/L	mg/m3/day	mg/m3/day	μg/m3	D	D′
0	27.0	16.56	5.10	104.1	0.26	+	10	6.8	132.2	261.4	262.2	1.1	6.2	5.7
1	27.1	16.55	5.15	103.1	0.19	0	10	4.5	94.6	470.6	304.8	0.9	6.2	5.7
2	27.4	16.54	5.13	103.7	0.19	0	0	4.2	123.2	435.2	229.8	2.4	6.2	6.7
4	26.8	16.55	5.11	103.7	0.13	0	13	5.5	125.4	558.4	119.8	3.4	6.3	5.8
6	27.0	16.58	5.04	102.6	0.26	0	0	5.0	107.8	299.2	131.6	1.4	6.3	5.7
8	27.0	16.87	4.57	93.8	0.26	0	5	2.7	114.4	203.8	110.4	1.6	4.3	5.7
10	26.8	17.27	3.94	80.4	0.45	0	+	6.5	63.8	60.0	30.2	1.3	5.6	5.2

Takashima, Shiraishi-jima Date: August 17, 1960. Transparency: 5.5m

0	27.1	15.16	4.92	98.8	0.07	0	7	5.8	42.9	167.6	188.8	1.6	6.1	6.5
1	27.1	15.17	4.96	99.6	0.17	0	+	7.0	31.9	206.8	142.0	0.9	6.1	6.5
2	27.0	15.31	4.97	99.8	0	0	5	6.3	89.1	772.2	226.8	3.7	6.1	6.4
4	27.0	16.16	4.77	96.8	0.13	0	8	2.2	122.1	645.3	197.2	1.8	6.1	5.8
6	26.8	16.86	4.35	88.4	0	0	7	9.0	46.2	213.6	173.4	1.0	5.5	5.5
7.5	26.6	17.16	3.97	80.9	0.19	0	+	4.8	74.8	280.4	212.8	0.7	5.7	5.7

* Filter Paper (Toyo No. 5C)

★ membrane filter

Table III. Plankton diatoms in Ago Bay and Shiraishi-jima, Koshika-ura, Ago Bay. June 19, 1960 cells/100cc

Station	A							B					
Depth (m)	0	1	2	4	6	8	10	0	1	2	3	5	7
Diatomae Total		905	305	506.5	207	1386	604	2685	2805	4025	3904	3561	2360
Asterionella japonica		—	—	—	—	—	—	—	15	40	48	—	—
Bacteriastrum elongatum		—	—	—	—	—	—	—	—	—	—	25	—
B. comosum		—	—	10	—	—	—	—	35	—	—	15	—
B. varians		45	—	12.5	27	24	24	205	65	85	8	120	75
Cerataulina bergonii		10	—	—	—	6	4	15	—	15	—	15	5
Chaetoceros atlanticus v. *neapolitana*		—	—	2.5	—	—	—	—	5	—	—	—	—
C. coarctatus		—	—	—	—	—	—	—	—	—	—	—	10
C. danicus		—	—	—	—	26	60	—	25	45	88	50	35
C. eibenii		40	12.5	10	6	—	12	15	35	30	88	30	90
C. denticulatum		45	7.5	—	—	—	—	5	—	—	8	30	10
C. pendulus		—	—	—	—	—	4	—	5	—	—	—	—
C. peruvianus		—	—	—	3	—	4	—	—	—	8	5	—
C. affinis		175	70	14	39	90	136	900	965	1185	1384	960	645
C. brevis		35	7.5	25	9	14	—	—	—	—	—	—	—
C. compressus		130	35	122.5	21	4	96	285	470	450	432	645	280
C. constrictus		—	—	—	—	—	—	—	—	30	48	25	50
C. costatus		—	—	—	—	24	—	25	160	90	—	—	—
C. curvisetus		25	—	—	—	82	—	205	120	75	352	325	250
C. didymus		—	—	—	—	—	8	15	25	80	24	10	70
C. diversus		—	—	—	—	4	—	—	—	15	—	—	—
C. laciniosus		10	17.5	17.5	9	580	24	—	60	30	40	10	65
C. lorenzianus		35	—	10	21	20	—	65	125	160	200	60	80
C. pseudocurvisetus		—	—	55	—	260	—	110	50	305	80	150	25
C. radicans		15	—	—	—	—	—	—	—	—	—	—	—
C. tortissimus		—	—	—	—	22	—	—	85	—	—	115	—
C. spp.		—	—	—	—	—	—	—	—	15	—	30	—
Clymacodium biconcavum		—	—	—	—	22	—	30	—	—	—	—	—
Corethron hystrix		—	—	2.5	—	—	4	—	—	5	—	—	—
Coscinodiscus marginatus		—	—	5	—	2	—	—	—	—	—	—	—
C. radiatus		—	—	2.5	—	4	—	—	—	—	8	—	5
Dactyliosolen mediterraneus		—	—	—	—	—	—	—	—	5	—	15	—
Eucampia cornuta		—	—	—	—	—	—	—	—	25	—	—	—
E. zoodiacus		—	—	—	—	—	—	—	—	—	40	—	—

Guinardia flaccida	—	2.5	—	—	—	—	—	30	10	—	—	—
Hemiaulus hauckii	—	—	5	—	42	—	—	5	55	24	5	—
Lauderia borealis	15	7.5	—	—	—	8	—	10	10	176	75	15
Leptocylindrus danicus	170	—	—	—	42	12	15	105	55	120	90	45
Nitzschia closterium	5	—	—	—	—	12	—	—	—	—	—	—
N. delicatissima	—	—	—	15	2	12	—	—	—	—	—	—
N. longissima	10	—	—	6	4	—	—	—	—	—	—	—
N. paradoxa	—	—	—	—	—	—	—	—	—	—	—	35
N. seriata	—	—	—	—	—	8	10	—	50	—	—	—
Rhizosolenia alata f. *gracillima*	—	—	—	—	—	—	5	5	—	—	5	—
R. calcar avis	—	—	—	—	—	—	5	—	—	—	—	—
R. setigera	—	—	—	—	—	—	5	5	5	—	—	—
R. stolterfothii	140	145	152.5	15	78	168	750	380	1135	720	725	405
R. styliformis	—	—	—	3	—	—	—	—	—	—	15	—
Skeletonema costatum	—	—	50	15	14	—	20	20	20	—	—	125
Thalassionema nitzschioides	—	—	10	18	16	4	—	—	—	8	5	40
Thalassiothrix frauenfeldii	—	—	—	—	4	4	—	—	—	—	—	—
Dionflagellata and Zooplankton Total	10	5	25	30	54	48	25	50	60	40	0	25
Salpingella ricta	—	—	—	—	—	—	—	—	—	—	—	5
Steenstrupiella steenstrupii	—	—	—	—	2	—	—	—	—	—	—	—
Tintinnopsis cylindrica	—	—	—	—	—	8	—	—	—	—	—	—
T. mortensenii	—	—	—	—	6	—	—	—	—	—	—	—
T. lobiancoi	—	—	5	3	—	—	—	—	—	—	—	—
Tintinnus lusus undae	—	—	—	—	—	—	—	5	—	—	—	—
Dictiocha fibula	—	—	—	9	2	8	—	—	5	—	—	—
Mesocyna corymorpha	—	—	—	—	2	—	—	—	—	—	—	—
Ceratium furca	—	—	—	—	—	4	—	5	—	8	—	—
C. fusus	—	—	—	—	—	—	5	10	—	—	—	—
C. tripos	—	—	—	—	—	—	—	5	—	—	—	—
Gonyaulux sp.	5	—	—	—	—	—	—	—	—	—	—	—
Peridinium roseum	—	—	—	—	—	—	5	—	—	—	—	—
P. inflatum	—	—	—	—	—	—	—	5	—	—	—	—
Noctiluca scintillans	—	—	—	—	—	—	—	5	5	—	—	—
Paracalanus parvus	—	—	—	—	—	—	—	—	10	8	—	—
Oithona nana	—	—	—	3	—	—	5	—	—	—	—	—
Cirripedia Nauplius	—	2.5	—	—	—	—	—	—	—	—	—	—
Copepoda Nauplius	5	2.5	20	15	42	28	10	15	40	24	—	10

Koshika-ura, Ago Bay. July 12, 1960. cells/100cc

Station Depth (m)	A 0	1	2	4	6	8	10	B 0	1	2	3	5	6.5
Diatomae Total	3160	2555	6330	12850	33410	49640	60400	4060	11020	17340	10560	12570	7290
Asterionella japonica	—	—	—	—	—	240	—	—	—	—	—	—	—
Bacteriastrum elongatum	—	—	—	—	—	200	—	—	—	—	—	—	—
B. comosum	—	—	—	—	—	200	—	—	—	—	90	90	—
B. varians	—	25	230	390	1290	800	1300	200	40	300	570	120	150
Cerataulina bergonii	40	30	40	120	60	40	—	—	180	60	180	—	60
Chaetoceros danicus	—	5	—	—	—	120	300	20	—	—	—	—	30
C. denticulatum	30	30	110	360	690	800	—	40	120	300	210	300	150
C. eibenii	5	—	—	—	—	200	—	—	—	90	120	—	60
C. pendulus	—	—	—	—	30	—	—	20	—	30	—	—	—
C. peruvianus	—	—	—	—	—	—	—	—	20	30	—	—	—
C. affinis	1305	970	2950	6420	13500	27080	5800	2300	6640	12420	10	8310	4380
C. brevis	10	—	50	120	330	—	—	—	—	—	60	—	150
C. compressus	550	320	20	1320	2700	880	—	—	140	—	90	90	—
C. constrictus	—	—	—	—	—	—	—	—	80	—	—	—	—
C. costatus	—	—	—	—	1290	400	—	60	—	210	—	—	—
C. curvisetus	50	65	160	900	990	960	2900	—	200	720	900	930	360
C. didymus	25	110	80	270	1200	840	5000	100	200	270	360	270	—
C. diversus	—	15	—	—	—	—	—	—	40	90	—	—	—
C. laciniosus	200	515	1200	1260	4020	4040	3000	600	2020	1380	840	1020	240
C. lorenzianus	85	65	180	240	570	400	800	—	300	540	330	60	150
C. messanensis	—	—	—	—	—	—	—	—	—	—	—	—	90
C. pseudocurvisetus	—	50	30	—	—	120	1300	—	300	—	90	300	—
C. tortissimus	—	—	—	—	900	—	—	—	—	—	—	—	—
C. spp.	85	—	50	—	—	—	—	—	—	—	360	—	—
Coscinodiscus marginatus	—	—	—	—	—	—	100	—	—	—	—	—	—
Dactyliosolen mediterraneus	5	—	10	—	—	—	—	—	20	—	—	—	—
Eucampia cornuta	—	—	—	—	60	40	200	—	—	—	—	—	—

E. zoodiacus	—	—	—	—	—	—	—	—	—	—	—	330	—
Guinardia flaccida	—	—	—	—	—	40	—	—	—	—	—	—	—
Hemiaulus hauckii	5	35	10	210	180	600	1000	60	60	120	90	510	60
Lauderia borealis	—	—	20	—	—	—	100	—	—	60	60	—	30
Leptocylindrus danicus	—	75	—	60	270	560	800	60	180	180	300	—	60
Nitzschia closterium	—	10	10	30	—	40	200	—	—	—	—	—	—
N. delicatissima	145	—	—	60	120	40	—	—	—	—	—	—	—
N. longissima	5	—	—	—	—	—	—	20	—	—	—	—	—
N. paradoxa	—	—	—	—	420	480	—	—	—	—	—	—	—
N. seriata	15	45	330	630	1670	3760	18500	160	120	120	240	—	—
Rhizosolenia alata f. gracillima	5	—	—	—	—	—	—	—	—	—	—	—	—
R. bergonii	—	—	—	—	60	40	100	—	—	—	—	30	—
R. calcar avis	—	—	—	—	30	40	—	—	—	—	—	—	30
R. setigera	—	—	10	60	—	80	300	—	—	30	—	30	60
R. stolterfothii	440	5	—	—	—	160	800	—	—	150	—	—	60
R. styliformis	—	—	—	—	120	—	—	—	—	—	30	—	—
Skeletonema costatum	140	185	840	340	1260	5600	14300	300	260	150	—	—	150
Thalassionema nitzschioides	10	—	—	60	1530	720	3600	120	80	240	30	180	1020
Thalassiothrix frauenfeldii	5	—	—	—	120	—	—	—	20	—	—	—	—
Dinoflagellata and Zooplankton Total	5	20	20	0	30	0	0	40	20	0	0	0	0
Ceratium furca	5	—	—	—	—	—	—	—	—	—	—	—	—
C. fusus	—	5	10	—	—	—	—	—	—	—	—	—	—
Amphorella amphora	—	—	—	—	—	—	—	20	—	—	—	—	—
Steenstrupiella steenstrupii	—	—	—	—	30	—	—	—	—	—	—	—	—
Tintinnopsis cylindrica	—	5	—	—	—	—	—	—	—	—	—	—	—
Dictiocha fibula	—	—	—	—	—	—	—	20	—	—	—	—	—
Oithona nana	—	5	—	—	—	—	—	—	—	—	—	—	—
O. similis	—	—	—	—	—	—	—	—	20	—	—	—	—
Copepoda Nauplius	—	5	10	—	—	—	—	—	—	—	—	—	—

Koshika-ura, Ago Bay. July 28, 1960. cells/100cc

Station Depth (m)	A 0	1	2	4	6	8	10	B 0	1	2	3	5	6
Diatomae Total	2830	2600	210	1525		440	680	600	344	660	890	1575	2375
Bacteriastrum comosum	—	—	—	—		—	15	—	—	—	—	—	—
B. varians	—	—	—	—		15	30	—	2	50	15	—	30
Chaetoceros danicus	—	—	—	—		—	—	—	—	—	—	—	7.5
C. denticulatum	—	—	—	—		20	80	7.5	4	—	—	—	72.5
C. eibenii	—	—	—	32.5		30	75	—	2	—	—	—	—
C. pendulus	—	—	—	—		2.5	—	—	—	—	—	—	—
C. affinis	2300	2415	177.5	47.5		165	120	25	292	555	745	30	50
C. brevis	5	—	10	—		—	—	—	—	—	—	—	—
C. compressus	20	35	—	—		37.5	50	—	—	—	—	—	—
C. curvisetus	55	30	—	—		—	25	—	—	—	—	—	—
C. didymus	55	10	12.5	15		—	5	—	6	—	—	15	—
C. laciniosus	235	110	7.5	—		22.5	105	7.5	34	—	55	25	—
C. lorenzianus	—	—	—	—		7.5	—	—	—	—	—	—	5
C. pseudocurvisetus	—	—	—	—		—	65	—	—	—	—	—	—
C. spp.	25	—	—	—		—	—	—	—	—	—	—	20
Coscinodiscus radiatus	—	—	—	—		—	—	—	—	—	—	25	—
Leptocylindrus danicus	75	—	—	—		—	—	5	2	35	—	—	—
Nitzschia closterium	—	—	—	—		—	—	—	2	—	—	2.5	—
N. delicatissima	—	—	2.5	5		17.5	30	2.5	—	5	10	2.5	12.5
N. longissima	5	—	—	17.5		—	10	—	—	—	—	—	—
N. seriata	15	—	—	—		20	30	—	—	10	40	5	32.5
Rhizosolenia alata f. gracillima	—	—	—	10		32.5	—	—	—	—	—	—	—
R. alata f. indica	—	—	—	—		5	—	—	—	—	15	—	—
R. bergonii	—	—	—	—		—	—	—	—	—	—	—	2.5
R. calcar avis	—	—	—	2.5		—	—	—	—	—	—	5	—
R. setigera	—	—	—	5		—	—	—	—	—	—	—	2.5

R. stolterfothii	—	—	—	—	—	—	—	—	—	—	62.5	—
R. styliformis	—	—	—	—	—	—	—	—	—	—	7.5	—
Skeletonema costatum	40	—	—	15	65	40	7.5	—	—	—	—	—
Thalassionema nitzschioides	—	—	—	—	—	—	5	—	5	10	—	—
Thalassiothrix frauenfeldii	—	—	—	2.5	—	—	—	—	—	—	—	2.5
Dinoflagellata and Zooplankton Total	10	20	0	15	10	5	2.5	6	5	25	0	2.5
Ceratium furca	5	—	—	—	—	—	—	4	—	—	—	—
C. fusus	—	—	—	—	2.5	—	—	—	—	—	—	2.5
Amphorella amphora	—	—	—	—	2.5	—	—	—	—	—	—	—
Dadayiella ganymedes	—	—	—	7.5	—	—	—	—	—	5	—	—
Salpingella ricta	—	—	—	—	—	—	—	—	—	10	—	—
Noctiluca scintillans	—	—	—	—	2.5	5	—	—	—	—	—	—
Oithona similis	5	—	—	2.5	—	—	—	—	—	—	—	—
Copepoda Nauplius	—	20	—	5	2.5	—	2.5	2	5	10	—	—

Koshika-ura, Ago Bay. July 10-11, 1960. cells/100cc.

Station / Depth (m)	A 0	1	2	4	6	8	10	B 0	1	2	3	5	7
Diatomae Total	16000	26670	1270	840	2890	11970	19620	2340	1420		670	1845	1675
Asterionella japonica	—	—	—	—	—	—	300	—	—		—	10	15
Bacteriastrum elongatum	—	—	—	—	120	300	—	—	—		—	—	—
B. comosum	—	—	—	—	—	—	—	60	—		—	—	—
B. varians	—	—	—	40	150	810	810	—	—		—	65	40
Cerataulina bergonii	—	—	—	—	—	—	60	—	—		—	—	30
Chaetoceros danicus	—	—	—	—	5	—	—	45	20		—	—	10
C. denticulatum	—	—	—	—	—	—	—	—	10		—	5	—
C. eibenii	—	—	—	—	10	—	—	—	—		—	10	—
C. pendulus	—	—	—	—	—	—	—	—	—		—	—	5
C. affinis	15450	25440	685	160	475	840	1830	285	180		165	100	160
C. brevis	—	—	—	—	—	—	—	—	60		—	—	—
C. compressus	—	240	100	95	50	4470	4770	810	270		45	575	115
C. curvisetus	—	—	—	—	50	—	300	45	—		—	390	550
C. didymus	150	210	40	40	90	480	600	45	170		65	135	75
C. diversus	—	—	—	—	20	—	90	—	—		30	—	—
C. laciniosus	350	780	270	260	260	960	3210	705	190		100	110	80
C. lorenzianus	—	—	—	—	—	60	—	—	50		—	35	—
C. pseudocurvisetus	—	—	—	—	—	—	—	—	—		—	50	75
C. tortissimus	—	—	—	—	—	180	—	—	—		—	—	—
C. spp.	—	—	—	—	75	—	—	—	—		—	—	—
Corethron hystrix	—	—	—	—	—	—	—	—	—		5	—	—
Dactyliosollen mediterraneus	—	—	—	5	45	210	150	—	—		—	—	10
Guinardia flaccida	—	—	—	—	—	—	—	—	—		10	—	15
Leptocylindrus danicus	—	—	5	35	125	1230	1140	15	90		30	20	10
Nitzschia closterium	—	—	—	5	—	—	—	—	—		—	—	5
N. delicatissima	—	—	—	10	15	30	60	15	10		—	5	—

N. longissima	—	—	5	—	5	—	—	—	—	—	—	—
N. paradoxa	—	—	150	—	—	—	—	—	—	—	—	—
N. seriata	—	—	10	80	325	1140	1170	180	160	90	65	150
Rhizosolenia alata f. *gracillima*	—	—	—	—	—	—	30	—	—	—	5	—
R. bergonii	—	—	—	—	—	—	—	—	—	10	—	5
R. calcar avis	—	—	5	—	5	—	—	30	10	5	20	5
R. setigera	—	—	—	—	15	30	30	—	—	5	20	20
R. stolterfothii	—	—	—	—	—	—	—	—	—	25	85	25
Skeletonema costatum	—	—	—	90	295	1230	5010	240	120	75	95	220
Stephanopyxis palmeriana	—	—	—	—	—	—	—	—	—	—	5	20
Thalassionema nitzschioides	50	—	—	20	20	—	60	—	80	10	4 0	35
Dinoflagellata and Zooplankton Total	0	60	10	10	10	0	0	195	60	20	5	25
Ceratium furca	—	—	—	—	—	—	—	—	—	—	—	5
C. fusus	—	—	—	—	—	—	—	15	—	5	—	—
Dadayiella ganymedes	—	—	—	—	5	—	—	—	—	—	—	5
Epiplocylis sp.	—	—	5	—	—	—	—	—	—	—	—	—
Favella azorica	—	—	—	—	—	—	—	15	—	5	—	—
Metacylis anurifera	—	—	—	5	—	—	—	—	—	—	—	5
Rhabdonella spiralis	—	—	—	—	—	—	—	—	10	—	—	—
Tintinnus lusus undae	—	—	—	—	—	—	—	—	10	—	5	5
Calocalanus pavo	—	—	—	—	—	—	—	15	—	—	—	—
Oithona similis	—	—	—	—	—	—	—	—	10	—	—	—
Oikopleura spp.	—	—	—	—	—	—	—	15	—	—	—	—
Copepoda Nauplius	—	60	5	5	—	—	—	120	30	10	—	5

Koshika-ura, Ago Bay. September 1-2, 1960. cells/100cc

Station Depth (m)	A 0	1	2	4	6	8	10	B 0	1	2	3	5	7
Diatomae Total	615	1135	4130	3800	6352	5280	8314	2470	910	1026	2296	3904	9980
Asterionella japonica	—	—	—	—	104	—	184	—	—	—	32	—	650
Bacteriastrum comosum	—	—	—	—	—	—	40	—	—	—	16	—	100
B. varians	—	25	—	65	128	100	16	75	—	42	24	48	120
Biddulphia longicrulis	—	—	—	15	40	—	8	—	—	—	—	8	20
B. sinensis	—	—	—	5	24	20	8	—	—	—	—	—	20
Cerataulina bergonii	20	—	5	25	16	—	8	—	—	—	—	16	10
Chaetoceros denticulatum	—	30	—	—	—	—	—	—	—	—	—	—	—
C. eibenii	—	—	—	—	—	20	—	—	—	—	—	—	—
C. peruvianus	—	—	—	15	—	—	—	—	—	—	—	—	—
C. affinis	—	120	—	45	88	—	136	40	25	24	104	56	60
C. brevis	—	—	—	10	32	160	16	—	—	8	32	24	40
C. compressus	—	—	—	—	—	—	—	—	—	4	—	—	—
C. constrictus	—	—	—	—	—	—	—	—	—	8	—	—	—
C. curvisetus	—	10	—	110	104	160	96	10	—	4	104	56	—
C. didymus	—	—	—	235	200	100	24	40	—	2	24	160	20
C. diversus	—	—	—	—	24	—	24	25	—	—	—	16	—
C. laciniosus	35	50	—	230	144	280	152	115	25	36	96	224	210
C. lorenzianus	—	—	—	10	—	—	48	—	20	12	—	16	—
C. pseudocurvisetus	15	—	—	30	80	—	—	—	25	—	200	—	—
C. spp.	—	20	10.5	—	—	—	—	—	—	—	—	—	—
Corethron hystrix	—	—	—	10	16	—	—	—	—	—	—	8	10
Coscinodiscus radiatus	—	—	—	—	—	—	—	—	—	6	—	8	—
Dactyliosollen mediterraneus	—	5	—	—	—	—	—	5	—	4	—	—	20
Ditylum brightwellii	—	—	—	25	—	—	16	—	10	—	16	8	—
Eucampia zoodiacus	—	—	—	5	64	—	—	20	—	6	8	—	—
Guinardia flaccida	—	—	—	10	—	—	—	—	—	4	—	24	—
Hemiaulus hauckii	—	10	—	—	16	20	8	—	—	—	16	—	—

Lauderia borealis	—	—	—	—	48	—	8	—	—	4	24	—	—
Leptocylindrus danicus	—	75	5	5	—	—	32	—	—	16	—	—	—
Nitzschia closterium	—	5	—	—	—	—	—	15	—	—	24	—	—
N. delicatissima	20	25	2.5	30	—	20	32	5	10	—	—	—	—
N. paradoxa	100	—	25	75	—	—	90	—	—	—	—	—	—
N. longissima	—	—	5	15	—	—	16	10	—	—	—	—	—
N. seriata	—	—	5	100	24	—	24	—	10	12	—	—	110
Rhizosolenia alata f. *indica*	—	—	—	—	—	—	—	—	—	—	8	—	10
R. setigera	—	10	—	10	40	—	24	—	5	4	—	32	40
R. stolterfothii	—	5	—	—	16	—	8	—	5	12	8	24	—
Skeletonema costatum	380	740	352.5	1570	1400	2060	3976	2020	710	638	968	1200	4970
Stephanopyxis palmeriana	—	—	—	—	16	—	—	—	—	—	—	40	—
Thalassionema nitzschioides	45	5	2.5	1150	3728	2340	3320	90	65	180	536	1856	3410
Thalassiothrix frauenfeldii	—	—	—	—	—	—	—	—	—	—	56	80	140
Dinoflagellata and Zooplankton Total	10	5	2.5	185	104	40	176	25	30	30	48	840	620
Peridinium sp.	—	—	—	—	—	—	—	—	—	—	—	8	—
Gymnodinium sp.	—	—	—	—	—	—	—	5	10	—	—	—	—
Ceratium furca	—	—	—	—	—	—	—	5	—	2	—	—	—
C. fusus	—	—	—	5	—	—	—	—	5	2	—	56	—
Amphorella amphora	—	—	—	—	—	—	—	—	—	—	16	—	—
Dadayiella ganymedes	—	—	—	—	—	—	—	—	5	—	—	—	10
Metacylis arurifera	—	—	—	—	16	—	—	—	5	10	—	16	—
Tintinnopsis cylindrica	—	—	—	15	8	—	—	—	—	—	8	8	—
T. lindenii	—	—	—	—	—	—	—	5	—	2	8	—	—
Tintinnus lusus undae	—	—	—	—	—	—	—	—	—	4	—	—	—
Dictiocha fibula	—	—	—	160	40	40	152	10	5	10	16	720	610
Mesocena polymorpha	—	—	—	—	8	—	—	—	—	—	—	—	—
Paracalanus parvus	—	—	—	—	—	—	—	—	—	—	—	24	—
Copepoda Nauplius	10	5	2.5	5	32	—	24	—	—	—	—	8	—

Koshika-ura, Ago Bay. September 18, 1960. cells/100cc

Station	A							B					
Depth (m)	0	1	2	4	6	8	10	0	1	2	3	5	7
Diatomae Total	10075	280	6695	410	1735	2880	4400	340	255	215		575	1575
Achnanthes longepes	15	—	—	—	—	—	—	—	—	—		—	—
Asterionella japonica	125	—	10	—	—	—	—	50	—	—		—	—
Bacteriastrum elongatum	—	—	—	—	—	40	—	—	—	—		—	—
B. comosum	—	30	—	—	35	100	—	—	—	—		—	15
B. varians	5	—	—	—	40	—	—	5	15	10		—	30
Cerataulina bergonii	—	—	—	5	—	—	—	—	—	—		—	—
Chaetoceros danicus	—	—	—	—	5	25	140	—	—	—		15	—
C. eibenii	—	—	—	—	—	—	—	—	—	—		10	—
C. peruvianus	—	—	5	—	20	—	40	—	—	—		—	15
C. pendulus	—	—	—	—	—	10	—	—	—	—		—	—
C. affinis	10	30	85	90	250	270	500	60	20	65		185	155
C. brevis	—	—	—	—	—	—	40	—	—	—		15	—
C. compressus	10	—	—	—	—	—	—	—	—	—		30	—
C. constrictus	—	—	—	—	—	—	—	—	—	—		—	20
C. curvisetus	30	—	—	—	165	60	80	10	—	—		—	30
C. didymus	—	—	30	15	115	405	840	—	—	15		50	265
C. diversus	—	—	—	—	15	55	160	—	—	—		—	15
C. laciniosus	130	15	—	25	25	—	60	—	—	—		—	40
C. lorenzianus	—	—	—	—	30	—	100	25	—	25		—	10
C. spp.	15	—	25	10	—	10	—	—	—	—		—	—
Corethron hystrix	—	—	—	—	—	10	20	—	—	—		5	—
Coscinodiscus marginatus	10	—	—	—	—	—	—	—	—	—		—	—
C. radiatus	—	—	—	—	—	—	—	10	25	—		10	5
Dactyliosollen mediterraneus	5	—	5	—	—	—	—	10	—	—		—	—
Ditylum brightwellii	—	—	5	—	—	—	—	—	—	—		—	—
Eucampia zoodiacus	5	—	—	—	—	—	—	—	—	—		—	—
Guinardia flaccida	—	—	—	—	5	—	—	—	—	—		—	—
Hemiaulus hauckii	—	—	5	—	—	—	—	—	—	—		—	—
Lauderia borealis	—	—	—	—	—	—	—	—	—	—		20	—
Leptocylindrus danicus	60	—	—	40	95	550	460	—	—	—		—	75
Nitzschia closterium	15	5	—	—	5	—	—	—	—	—		—	—
N. delicatissima	—	5	—	—	—	5	20	—	—	—		—	—
N. longissima	15	5	—	—	—	20	40	—	—	—		—	—

N. *seriata*	10	20	30	10	365	600	580	5	—	—		45	665
Rhizosolenia calcar avis	—	—	—	—	—	—	—	—	—	5		—	—
R. *setigera*	5	—	10	—	—	—	20	—	—	5		—	5
R. *stolterfothii*	—	—	—	25	—	150	240	10	—	—		15	—
R. *styliformis*	—	—	10	—	—	5	—	—	—	—		—	—
Skeletonema costatum	9000	120	6380	120	140	305	—	—	—	—		50	160
Thalassionema nitzschioides	610	50	75	70	425	625	1060	155	195	80		125	70
Thalassiothrix frauenfeldii	—	—	20	—	—	—	—	—	—	10		—	—
Dinoflagellata and Zooplankton Total	120	1470	1055	260	855	385	260	540	970	830		350	2185
Cochlodinium spp.	—	—	—	50	—	—	—	—	—	—		—	—
Dinophysis homunculus	—	10	10	—	—	10	—	—	—	10		—	20
D. sp.	—	5	—	—	—	—	—	—	—	—		—	—
Gymnodinium sp.	—	—	—	—	50	5	—	5	—	—		—	—
Peridinium inflatum	—	5	5	—	—	—	—	—	15	—		—	—
Ceratium furca	100	1340	980	175	85	15	20	450	885	765		270	1980
C. *fusus*	—	—	—	—	5	—	—	—	—	—		—	—
C. *inflexum*	—	—	—	—	—	5	—	—	15	—		—	—
C. *pentagonum*	10	—	—	—	—	—	—	—	—	—		—	—
Amphorella amphora	—	—	—	5	—	10	—	—	5	—		—	—
Metacylis anurifera	—	—	—	—	—	—	—	—	5	—		5	5
Salpingella ricta	—	—	5	—	655	175	12	—	5	—		30	120
Tintinnopsis cylindrica	—	—	10	—	10	35	60	—	—	—		—	—
T. *lindeni*	—	10	10	10	5	30	—	—	—	—		5	10
T. *nordguisti*	—	—	—	—	10	—	—	—	—	—		—	—
Tintinnus lusus undae	—	—	—	—	5	5	—	—	—	—		5	5
Dictiocha fibula	—	—	—	20	—	—	—	—	—	—		—	—
Mesocena polymorpha	—	—	—	—	10	70	40	—	—	—		—	—
Paracalanus parvus	—	—	—	—	—	—	—	—	—	—		5	—
Oithona plumifera	—	5	5	—	—	—	—	10	—	—		—	—
O. *similis*	—	—	5	—	—	—	—	—	—	5		—	—
Copepoda Nauplius	10	75	25	—	20	25	20	70	45	50		30	45

Shiraishijima, Inland Sea. August 17-18, 1960. cells/100cc

Station	Takashima						Torinokuchi						
Depth (m)	0	1	2	4	6	7.5	0	1	2	4	6	8	10
Diatomae Total	135210	134600	125000	129350	34090	52900	172300	165750	149780	196700	199700	2200	43750
Asterionella japonica	550	1050	300	3000	3150	2900	3450	4250	180	1450	700	—	2600
Bacteriastrum varians	1300	600	150	—	250	50	850	1150	1350	1350	650	150	150
Biddulphia longicrulis	—	—	—	—	—	—	—	—	—	—	100	—	—
B. sinensis	50	50	—	—	—	—	—	200	—	50	—	—	—
Cerataulina bergonii	150	—	—	50	—	—	—	—	—	—	—	—	—
Chaetoceros danicus	—	—	—	—	—	50	150	50	250	—	—	—	100
C. eibenii	—	—	—	—	400	100	50	100	100	550	100	—	250
C. affinis	2200	700	1850	950	2850	2850	2150	4850	7150	7350	4150	550	4200
C. brevis	—	150	—	—	200	—	—	200	—	—	—	—	—
C. compressus	2300	4350	850	1450	2650	2850	4150	4100	3900	8700	2750	200	1150
C. curvisetus	610	5500	2150	2800	3500	1750	3750	8750	4500	73500	81000	—	2250
C. didymus	300	1000	350	350	200	650	—	850	500	900	1650	—	350
C. diversus	—	—	—	—	—	—	—	—	—	150	—	—	—
C. laciniosus	—	—	—	400	150	1050	—	250	250	4500	400	100	—
C. lorenzianus	1850	1250	400	500	450	400	450	500	1150	1300	1400	—	300
C. pseudocurvisetus	2250	2500	2250	3000	4250	4900	600	1750	5000	1100	1500	—	4550
C. socialis	—	—	—	—	—	—	2000	—	—	300	—	—	400
C. spp.	250	250	—	—	250	—	100	—	—	—	500	—	—
Corethron hystrix	—	—	—	—	—	50	50	50	50	—	50	—	—
Coscinodiscus marginatus	150	100	50	—	—	50	100	—	150	—	100	—	—
C. radiatus	50	—	—	—	—	100	50	100	—	—	—	—	—
Dactyliosollen mediterraneus	100	—	100	—	—	200	200	150	350	400	—	—	150
Ditylum brightwellii	150	50	200	50	—	—	100	300	450	250	200	—	100
Eucampia zoodiacus	—	300	300	—	—	—	—	200	—	200	—	—	—
Guinardia flaccida	500	50	250	300	300	100	—	—	200	—	—	—	—
Hemiaulus hauckii	150	50	200	200	300	200	400	200	100	150	400	—	—
Lauderia borealis	—	—	—	—	—	—	150	—	100	—	—	—	—

Leptocylindrus danicus	—	—	—	150	—	—	—	—	—	400	—	350	—
Melosira sulcata	—	—	—	—	—	150	—	—	—	—	—	—	—
Nitzschia delicatissima	—	—	—	—	—	—	—	—	—	—	—	50	50
N. seriata	1000	200	300	300	300	350	150	150	800	1100	250	100	200
Rhizosolenia alata f. *gracillima*	—	—	—	200	50	—	—	—	—	—	50	—	—
R. calcer avis	—	—	—	—	50	—	—	—	—	—	—	—	—
R. setigera	—	—	50	—	—	—	—	—	50	50	50	—	—
R. styliformis	—	—	—	100	100	—	—	100	—	—	50	—	—
Skeletonema costatum	117200	112200	112500	111700	7240	32700	149100	132200	115200	86600	97700	700	24000
Stephanopyxis palmeriana	—	300	—	100	100	—	—	—	—	—	200	—	—
Thalassionema nitzschioides	3850	3800	2650	3300	7150	1150	4200	5250	7750	6150	5500	—	2950
Thalassiosira rotula	—	—	—	200	100	—	—	50	100	50	150	—	—
T. nordenskioldii	—	—	—	—	—	—	—	—	—	100	—	—	—
Thalassiothrix frauenfeldii	250	150	100	250	100	300	100	—	150	50	100	—	—
Dinoflagellata and Zooplankton Total	450	1050	1200	1200	350	250	400	300	150	0	100	0	150
Gonyaulux sp.	—	50	—	—	—	—	—	50	—	—	—	—	—
Peridinium catenatum	300	700	900	750	50	100	300	—	—	—	—	—	—
Dinophysis ovum	—	—	—	—	—	—	—	50	—	—	—	—	—
Ceratium furca	100	150	250	200	150	—	50	100	100	—	100	—	50
C. fusus	—	50	—	100	—	—	50	50	—	—	—	—	50
Tintinnopsis nordguistii	—	—	—	—	—	50	—	—	—	—	—	—	—
T. lindeni	—	—	—	—	—	50	—	—	—	—	—	—	—
Tintinnus lusus undae	—	—	—	50	50	—	—	—	—	—	—	—	—
Dictiocha fibula	—	50	—	—	50	—	—	—	—	—	—	—	—
Noctiluca scintillans	—	—	—	—	—	—	—	—	50	—	—	—	—
Paracalanus parvus	—	—	—	50	—	—	—	—	—	—	—	—	—
Fritillaria sp.	—	—	—	—	50	—	—	—	—	—	—	—	—
Copepoda Nauplius	—	50	50	50	50	—	—	50	—	—	—	—	50
Gastropoda Veliger	—	50	—	—	—	—	—	—	—	—	—	—	—

真珠の黄色色素の研究*,1)

沢　田　保　夫

国立真珠研究所

真珠の価値を決定する要因のうち色調は最も重要なものである。この真珠の色調を解明する目的で多くの研究がなされているが[1)2)3)]，未だ決定的な報告はみられない。著者は既に真珠や真珠貝貝殻の色調を構成するものと推定される真珠層中の微量無機元素や[4)]ポーフイリン[5)]について研究を行なつたが，いずれも真珠の実態色の主要因ではないことが判明した。またピンク系の色は色素によるものではなく，光の反射や干渉その他の物理的な原因によるものであることを認めた。しかし，クリーム，イエロー等の名で呼ばれている黄色系の真珠には色素の存在が推定されるが，これに関する報告は未だみられない。著者は黄色系の真珠の色素をとり出すことに成功し，ある程度その化学的性質をたしかめ，更にこれが真珠の実態色に関係する主な原因の一つになつていることを認めたのでここに報告する。

実験方法および実験結果

試料として用いた真珠は，国立真珠研究所において養殖された直径 6～7 mm のもので，白色系および黄色系の2種類を選別して，木槌で破壊して核をとりのぞき，真珠層のみを集めて実験に供した。

1．黄色色素の抽出：このようにして得た黄色真珠の真珠層の 100g を 2N HCl - メタノールの等容混合液で真珠層の主成分である炭酸カルシウムを溶解した。液は酸性を保つているうちは黄色を呈しており，不溶の粗コンキオリンが浮遊してくる。真珠層が完全に溶解した後粗コンキオリンを濾別し，濾液を減圧でメタノールおよび HCl を除去すると不溶性の黄色物質が沈澱する。沈澱を遠心分離し再び HCl - メタノールに溶解し，先の操作と同様に減圧でメタノールとHClを除去後生成した沈澱をアルコール，エーテルで乾燥させ，この精製を数回くりかえすと濃褐色の無定形沈澱が得られる。収量は 100g の黄色真珠より精製物 21mg であつた。これと同様の処理を白色系の真珠について行なつても黄色沈澱はほとんど認められないので，この黄色沈澱が黄色系真珠の色素成分であると推定される。また，この物質は水や多くの有機溶媒には不溶であり，HCl 酸性のメタノールのみに溶解する。化学的に非常に安定な物質らしく酸化剤や還元剤によつてもその分光特性には変化をみとめられなかつた。

---

* Yasuo Sawada. Studies on the yellow pigment of the pearl. Bull. Natl. Pearl Res. Lab. 7: 865—869. 1961.

1) 国立真珠研究所業績 No. 88.（国立真珠研究所報告 7: 865—869. 昭和36年7月）

2. 黄色色素の分光特性: 黄色色素を HCl-メタノールに溶解し，その分光特性をみると，紫外部より可視部にかけて全く特異な吸収がみられず，第1図に示したごとくわずかに 320mμ 附近に弱い吸収がみとめられるのみである。またその赤外スペクトルは第2図に示すごとく，NH 伸縮，CH_2 伸縮，アミドⅠ(C=O 伸縮)，アミドⅡ(NH 変角，C-N 伸縮)，CH_2 変角が認められるが，水酸基や燐酸基およびエステル結合は全くみられないので，糖やリピド系物質の結合を予測することができず，ペプタイドではないかと推定される。

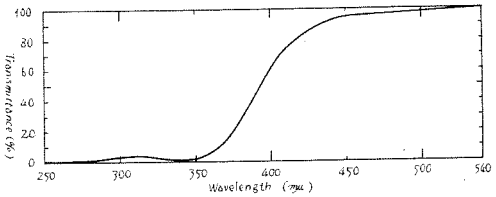

第1図. 真珠より抽出した黄色色素の分光特性（紫外部～可視部）

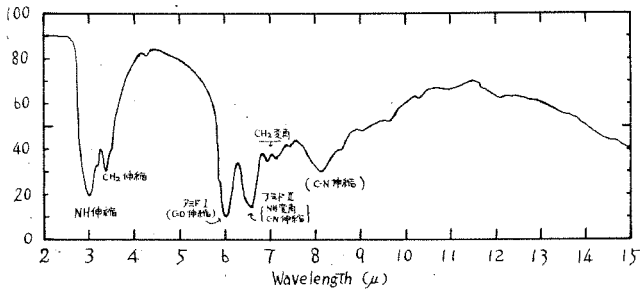

第2図. 真珠より抽出した黄色色素の赤外スペクトル.

3. 黄色色素の加水分解: このようにして赤外スペクトルの結果この色素の構成成分としてペプタイドが期待されたので，加水分解して構成アミノ酸の検出をおこなつた。すなわち色素を封管中で濃塩酸を用いて約40時間加水分解をおこない，減圧下で充分に乾燥し，全く HCl を除去して後少量の水に溶解し，ペーパークロマトグラフイーにかけた。すなわち一次元展開はブタノール・醋酸・水 (4: 1: 2) の混合溶媒を用いておこない，更に二次元はフエノール・水 (8: 2) で展開して後ニンヒドリンで発色させると第3図に示した

第3図. 真珠より抽出した黄色色素のペーパークロマトグラム.

試料: 黄色真珠より抽出した色素の塩酸加水分解物

一次元展開: ブタノール・醋酸・水 (4: 1: 2)

二次元展開: フエノール・水 (8:2)

発色: ニンヒドリン

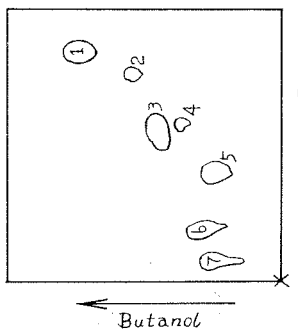

1: Leucine
2: ?
3: Alanine
4: ?
5: Glycine
6: Glutamic acid
7: Asparatic acid

ごとき Rf 値を示すアミノ酸の呈色がみられる。これを標準アミノ酸の Rf 値と比較した結果5個のスポットは，ロイシン，アラニン，グリシン，グルタミン酸，アスパラギン酸に一致するが，他に未確認のスポット2個が認められた。従つて黄色系真珠の色素成分は，これらのアミノ酸で構成された一種のペプタイドであることが認められる。

4．真珠層に含まれる鉄と黄色色素との関係：先に著者[6]は淡水真珠や海産真珠の真珠層中に含有されている Fe や Mn について検討したが，これらの元素は含窒化合物としばしば着色の錯化合物をつくることが知られている。従つて真珠の黄色の色調が前記のペプタイドのみならず含有微量金属元素とも関係をもつと予測されるので，黄色真珠および白色系真珠の真珠層に含まれている微量無機元素について分析をおこなつた。すなわち，真珠層を常法によつて灰化した試料についてロダン塩として比色法により Fe を定量した結果第1表に示したように黄色系の真珠の方が白色系の真珠よりも多く含まれていることを

第1表　白色系および黄色系真珠の成分比較

試　　料	湿　分 %	灰　分 %	灰分中の含有率 Fe	灰分中の含有率 P_2O_5 %
			p.p.m.	
白色系真珠	0.3	96.2	21.6	0.7
黄色系真珠	0.3	96.0	34.2	0.6
黄色系真珠の黄色色素			* 0.5	

*　黄色色素中に0.5%含むことを示す。

認めた。また，前記の黄色色素について同一の方法で Fe の含量を測定すると 0.5% という多量の Fe の存在が認められ，この含有率は色素の溶解沈澱をくりかえして精製をおこなつてもほとんど変化しなかつた。この事実は黄色色素がペプタイドと Fe の錯化合物であることを示唆する。何となれば，アミノ酸や分子量の特に大きくないペプタイドは水溶性であり，且つその水溶液は無色であるのが通性であるにかかわらず，真珠の黄色色素は酸性の水にのみ溶解して，且つ強い黄色を呈するからである。

黄色色素がペプタイドの錯化合物であるとの推定を確かめる一つの手段として，アミノ酸およびペプタイドの水溶液に一定分子比の鉄塩を添加した場合におこる分光特性と溶解度の変化をしらべた。種々の第一および第二鉄塩を黄色色素の構成アミノ酸の水溶液のいずれかと共に加温すると，直ちに発色して茶褐色となり，更に長時間加温を続けるとついに茶褐色の沈澱を生ずる。鉄塩のうち $Fe_2(SO_4)_3$ のごとき第二鉄塩は最も反応性が大きく冷時においても直ちに茶褐色の溶液となる。第4図より第8図に示したものは，種々のアミノ酸に重量比 1:1 で $Fe_2(SO_4)_3$ を混じたものの分光特性を $Fe_2(SO_4)_3$ 自体のものと対比したものであるが，アミノ酸の重量比が増加すると次第に発色が強くなる。その発色の強さはグリシン，アラニン，グルタミン酸，アスパラギン酸，ロイシンの順に低下している。またグリシル・グリシン，グリシル・グリシル・グリシン，アラニル・アラニン，アラニル・ロイシン，グリシル・ロイシンの水溶液について同様の処理をおこなうと，直ちに茶褐色の沈澱を生じ，水溶液は無色となり，また塩酸酸性とすると沈澱は溶解して黄色溶液となる。これらの性質は真珠より得られた黄色色素の挙動と酷似している。この実験結果は黄色色素がペプタイドと Fe の錯化合物であることを支持するものである。

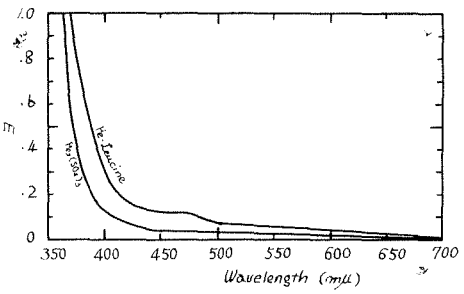

第4図. Fe-Leucine の分光特性.

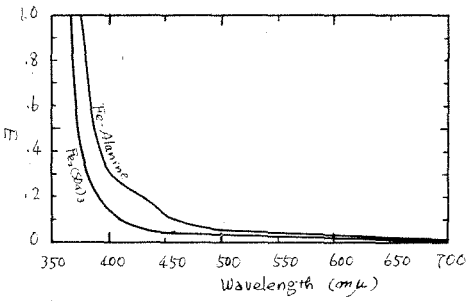

第5図. Fe-Alanine の分光特性.

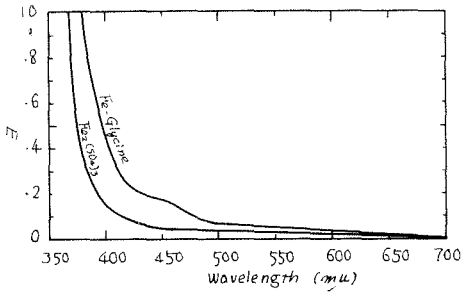

第6図. Fe-Glycine の分光特性.

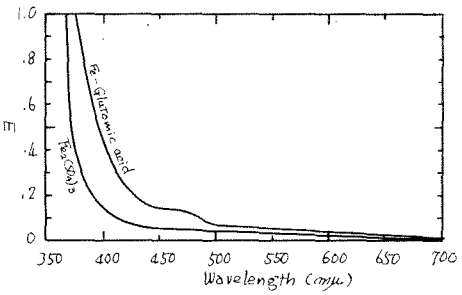

第7図. Fe-Glutamic acid の分光特性.

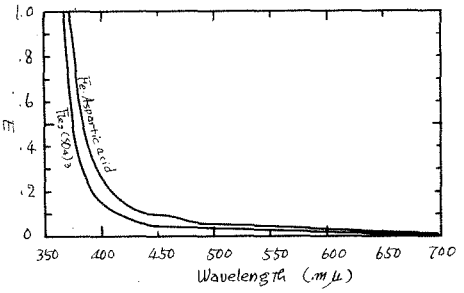

第8図. Fe-Asparatic acid の分光特性.

考　　察

以上の実験結果を綜合すると，真珠の黄色色素は Fe とペプタイドとの錯化合物と推定される新しい色素であり，その構成成分よりみて真珠や貝殻の成分であるコンキオリンと密接な関係にあるものと考えられる。この黄色色素の真珠中における分布は真珠層に均一に存在しており，また白色系の真珠でも色彩測定器で測色すると[7]，淡黄色を帯びていることを示すので，この新しい Fe-ペプタイドが真珠の実態色の主因の一つであると思われる。

終りに当り，この研究に終始御指導をいたゞいた京都大学田中正三教授および国立真珠研究所高山活夫所長に深く感謝する。

要　　約

1. 真珠より黄色色素を抽出し，これがロイシン，アラニン，グリシン，グルタミン酸，アスパラギン酸等のアミノ酸より構成されたペプタイドと Fe との錯化合物であるとの結論に達した。

2. 更にこの黄色色素は真珠の実態色の主因の一つであると推定した。

文　　献

1) 内田洋一・上田正康　1947. 真珠の層状構造と iridescence に就て. 生理生態 1: 171.
2) 大森啓一　1947. 真珠の色とつや. 科学朝日 7: 34.
3) 神前武和　1947. 真珠中ポルフィリン体に就て. 生理生態 1: 247—250.
4) 沢田保夫　1957. アコヤガイ貝殻及び真珠の無機成分に関する研究. 国立真珠研報 2: 68—73.
5) ———— 1958. 真珠貝の生化学的研究，真珠貝の色素. 国立真珠研報 4: 335—339.
6) ———— 1959. 放射線による真珠及び真珠貝貝殻の変化に関する研究. 国立真珠研報 5: 395—406.
7) ———— 1957. 自記分光光度計による真珠の色の測定. 国立真珠研報 3: 175—185.

昭和36年7月25日　印刷
昭和36年7月31日　発行

三重県志摩郡阿児町賢島
発行所　国立真珠研究所

発行者　高山活夫

印刷者　笹気直三

大阪市東淀川区十三南之町二丁目六五番地
印刷所　笹気出版印刷

国立真珠研究所報告 7 (1961)

◇

内　　容

国立真珠研究所
三重県志摩郡阿児町賢島

National Pearl Research Laboratory
Kashikojima, Ago-cho, Shima-gun,
Mie Prefecture, Japan